Biochemical characterization of chitinolytic enzymes and evaluation of chitooligosaccharides generated by a chitosanase of plant growth promoting *Paenibacillus elgii*

Thesis submitted for the degree of
DOCTOR OF PHILOSOPHY

by

Subha Narayan Das

(Regd. No. 10LPPH07)

Department of Plant Sciences
School of Life Sciences
University of Hyderabad
Hyderabad – 500 046
INDIA

March, 2016

University of Hyderabad
(A Central University established in 1974 by an act of parliament)
HYDERABAD – 500 046, INDIA

CERTIFICATE

This is to certify that Mr. SUBHA NARAYAN DAS has carried out the research work embodied in the present thesis under the supervision and guidance of Prof. Appa Rao Podile for a full period prescribed under the Ph.D. ordinances of this University. We recommend his thesis **"Biochemical characterization of chitinolytic enzymes and evaluation of chitooligosaccharides generated by a chitosanase of plant growth promoting *Paenibacillus elgii*"** for submission for the degree of Doctor of Philosophy of the University.

Prof. Appa Rao Podile
(Research Supervisor)

Head,
Department of Plant Sciences

Dean,
School of Life Sciences

University of Hyderabad
(A Central University established in 1974 by an act of parliament)
HYDERABAD – 500 046, INDIA

DECLARATION

This is to declare that the work embodied in this thesis entitled **"Biochemical characterization of chitinolytic enzymes and evaluation of chitooligosaccharides generated by a chitosanase of plant growth promoting *Paenibacillus elgii*"** has been carried out by me under the supervision of Prof. Appa Rao Podile, Department of Plant Sciences, School of Life Sciences. The work presented in this thesis is a bonafide research work and has not been submitted for any degree or diploma in any other University or Institute. A report on plagiarism statistics from the University Librarian is enclosed.

Subha Narayan Das

Prof. Appa Rao Podile
(Research Supervisor)

University of Hyderabad
Department of Plant Sciences
School of Life Sciences

(A Central University established in 1974 by an act of parliament)
HYDERABAD – 500 046, INDIA

CERTIFICATE

This is to certify that Mr. SUBHA NARAYAN DAS has carried out the research work embodied in the present thesis under the supervision and guidance of Prof. Appa Rao Podile for a full period prescribed under the Ph.D. ordinances of this University. We recommend his thesis entitled **"Biochemical characterization of chitinolytic enzymes and evaluation of chitooligosaccharides generated by a chitosanase of plant growth promoting *Paenibacillus elgii*"** for submission for the degree of Doctor of Philosophy of the University. This work was done in part in the laboratory of Prof. Dr. Bruno Moerschbacher at the University of Muenster, Germany in the framework of International Research Training Group in Molecular and Cellular Glycosciences (IRTG-MCGS). I declare to the best of my knowledge that this work has not been submitted earlier for the award of degree or diploma from any other University or Institution.

Prof. Appa Rao Podile
(Research Supervisor)

ACKNOWLEDGEMENTS

I would like to take this opportunity to extend my gratitude to my supervisor Prof. Appa Rao Podile for his unrelenting encouragement and constant support, without whom, this endeavour would not have been possible. Working under him gave me a true sense of freedom, broadened my scientific outlook, and inculcated a spirit of positive attitude in me. I am deeply indebted of his unfailing support in every scientific aspect like writing, communication, presentation skills, which enabled me towards the successful completion of this Ph.D. programme. Above all, I can't forget his care and help showed towards me at difficult times during the entire tenure of my doctoral research.

My special thanks to Prof. Bruno Maria Moerschbacher for his guidance, support and encouragement during my stay at the University of Muenster, Germany. Also I would like to thank Dr. Dominique Gilletet, Mahatani Chitosan Pvt Ltd, Veraval, Gujarat, for chitinous substrates.

I thank the former Deans, Prof. M. Ramanadham, Prof. R. P. Sharma, Prof. Aparna Dutta Gupta, Prof. A. S. Raghavendra and the present Dean Prof. P. Reddanna, School of Life Sciences and former Heads, Prof. Appa Rao Podile, Prof. A. R. Reddy and the present Head, Prof Ch. Venkata Ramana, Dept. of Plant Sciences, for their support in all possible ways.

I thank Prof. M. J. Swamy from School of Chemistry for allowing me to work in collaboration with his group for conducting ITC and DSC experiments.

I thank my doctoral committee members Dr. K. Gopinath and Prof. S. Dayananda for their suggestions during my work. I also thank them for allowing me to use their lab facilities.

My special thanks to Prof. Ch. Venkata Ramana for his suggestions in identification and phylogenetic analysis of bacteria and his students for timely help.

I would like to thank Prof. N. Siva Kumar, the coordinator of IRTG-MCGS programme for selecting me as a student of MCGS and also DFG for the research fellowship.

I gratefully acknowledge the DST, CSIR-DSRF, UOH-BBL, and EU for research fellowship. I thank DST-SERB travel grant for financial support to attend the ICCC/EUCHIS 2015 conference held at Muenster, Germany. I would like to acknowledge the infrastructural support provided by UGC-SAP and DST-FIST and DBT-CREBB to the Dept. of Plant Sciences and School of Life Sciences.

My special thanks to Dr. Martin, Dr. Ratna, Sven, Stefan, and Shoa from Prof. Moerschbacher's lab, Dr. Pavan from Prof. Swami's lab and Ramana from Dr. Balamurugan's lab for their valuable suggestions and timely help during my Ph.D.

I wish to thank my previous lab members, Dr. Sashidhar, Dr. Vasudev, Dr. Debashish, Dr. Purushotham, Dr. Ch. Neeraja, Dr. Anil, Dr. Praveen, Dr. Anil Singh, Dr. Swarnalee, Dr. Narayana Rao, Dr. Suma, Dr. Uma, Dr. Swaroopa, Nanda Kishore, Dr. Madhuprakash, Dr. Manjeet and Rambabu (late) for their suggestions and help.

I thank all my present lab mates, Dr. Sadaf, Dr. Anjali, Dr. Ramakrishna, Sharma, Papa Rao, Sravani, Sandhya, Bhuvana, Mohan, Rajesh, Anirban, Danteswari for their cooperation and maintaining camaraderie atmosphere in the lab.

I would like to thank my friends, Dr. Naveen, Dr. Anirudh, Dr. Dillip, Dr. Shukla, Dr. Mahesh, Dr. Ahan, Dr. Abhay, Abhaypratap, Deepankar, Ishrar, Rakesh, Sumit, Kapil, Satya from UoH and Dr. Devendra from NEHU, for their support.

I thank Narasimha, Devaiah, Sita Ram and Malla Reddy for their assistance in the lab and in maintaining plants in greenhouse.

Words fail to express my heartfelt gratitude for my parents and my brother, and all my family members to whom I'm forever indebted for their love, unconditional support, endless patience, without their cooperation I would not have come so far.

I am immensely grateful to all those individuals who have helped me in making this endeavour possible.

Above all, I thank God Almighty for eternal love, blessings, and providing enough strength in every moment of my life.

Subha Narayan Das

Dedicated to my

Beloved Parents

Contents

Abbreviations and symbols

AA10	Auxiliary Activity family 10
AMAC	2-aminoacridone
A-unit	Acetylated unit (GlcNAc)
BLAST	Basic Local Alignment Search Tool
bp	Base pair
CAZy	Carbohydrate Active Enzyme
CBM	Carbohydrate Binding Module
CBP	Chitin Binding Protein
ChBD	Chitin Binding Domain
COS	Chitin/Chitosan oligosaccharides
CD	Circular Dichroism
C-terminal	Carboxy terminal
°C	Degree centigrade/degree Celsius
DA or F_A	Degree of Acetylation or Fraction of Acetylation
DP	Degree of Polymerization
D-unit	Deacetylated unit (GlcN)
EDTA	Ethylene Diamine Tetra Acetic acid
FN3	Fibronectin type-3
g	Gram
GH	Glycoside hydrolase
GlcN	Glucosamine
GlcNAc	*N*-acetyl glucosamine
h	hour (s)
HPLC	High Performance Liquid Chromatography
HPTLC	High Performance Thin Layer Chromatography
ITC	Isothermal Titration Calorimetry
IPTG	Isopropyl β-D-thiogalactoside
kb	kilobase
kDa	kilo Dalton
l	litre
LB	Luria-Bertani
M	Molar
MALDI-ToF	Matrix Assisted Laser Desorption/ionization–Time of Flight
mg	milligram
min	minute

ml	milliliter
mM	millimolar
M_w	Molecular weight
NCBI	National Centre For Biotechnological Information
N-terminal	amino terminal
OD	Optical Density
PA	Pattern of Acetylation
PAGE	Polyacrylamide Gel Electrophoresis
PCR	Polymerase Chain Reaction
PDB	Protein Data Bank
PKD	Polycystic Kidney Disease
rpm	revolutions per minute
SDS	Sodium Dodecyl Sulphate
SEC	Size Exclusion Chromatography
s	Second (s)
TG	Transglycosylation
TIM	Triosephosphate Isomerase
TLC	Thin Layer Chromatography
UHPLC-ELSD-ESI-MS	Ultra-High Performance Liquid Chromatography-Evaporative Light-Scattering Detection-Electrospray Ionisation Mass Spectrometry
T_m	Transition temperature
µg	microgram
µM	micromolar
ΔH	calorimetric enthalpy
ΔG	Gibbs free energy
ΔS	Entropy

List of Tables

List of Figures

Chapter I

Introduction

1.1. Chitin and Chitosan

1.1.1 Chemical structure

Chitin is the second most abundant natural carbohydrate polymer consisting of (1→4) linked units of 2-acetamido-2-deoxy-β-D-glucopyranose (*N*-acetylglucosamine/ GlcNAc/A-unit). The consecutive sugar units in chitin are rotated 180° relative to each other (Fig. 1.1). Depending on the arrangement of the individual chitin chains, three different crystalline forms (α, β and γ) of chitin are found. In α-chitin, the chains are arranged alternatively in an antiparallel fashion (↑↓) with the involvement of both inter- and intra-molecular hydrogen bonding between the chains. This explains why the chains are densely packed in α-chitin making it the most rigid structure with the inability to swell in water (Minke & Blackwell, 1978). In β-chitin, the chains are arranged in a parallel way (↑↑) (Gardner & Blackwell, 1975), giving a looser packing, and soft chitinous structures. Detailed analysis showed that γ-chitin is a variant of α family (Atkins, 1985) and consists of two parallel strands which alternate with a single antiparallel strand (↑↑↓) (Rudall, 2011).

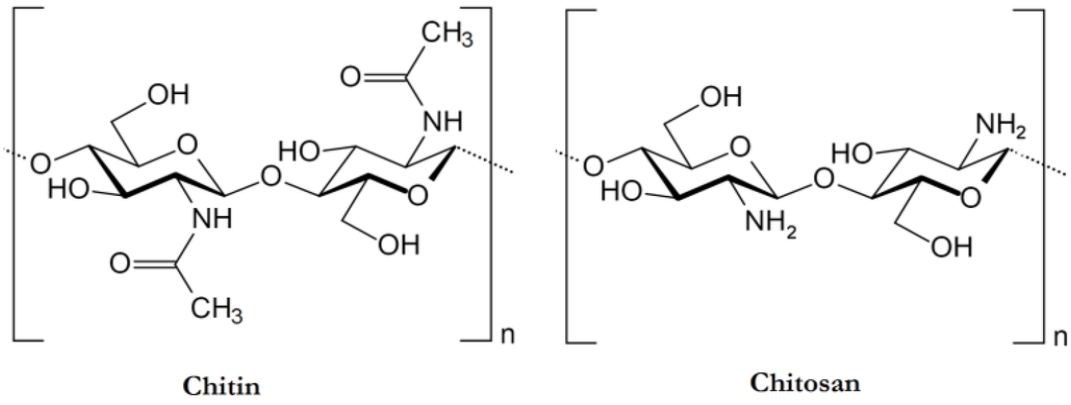

Fig. 1.1: Chemical structures of chitin and chitosan.

Chitosans are the linear varied deacetylated forms of chitin, water soluble and consist of (1→4) linked units of 2-amido-2-deoxy-β-D-glucopyranose (Glucosamine/GlcN/D-unit) and A-unit. Chitosans can be described and classified

according to the degree of *N*-acetylation (DA) or fraction of *N*-acetylated residues (F_A), the degree of polymerisation (DP) or the molecular weight (M_W), the molecular weight distribution (PD, for PolyDispersity), and the pattern of *N*-acetylation (PA) or sequence (Aam et al., 2010). Chitosans with a pKa-value of around 6.5 (Strand et al., 2001) possess positive charge at pH-values below 6.5. Chitosan exhibits anarray of attractive physicochemical and biological properties in combination with its non-toxicity, biocompatibility, and biodegradability, making chitosans applicable in agriculture, cosmetics, water treatment and medicine (Kim & Rajapakse, 2005; Neeraja et al., 2010).

1.1.2 Natural occurrence

Chitin is widely distributed across diverse environments as a constituent of quite a lot of organisms, including exoskeletons of insects, the shells of crustaceans, fungal cell wallsand the microfilarial sheath of nematodes (Gooday, 1990; Ruiz-Herrera & Martines-Espínoza, 1999). The annual worldwide production of chitin is around 100 billion tons (Tharanathan & Kittur, 2003).

In nature, chitosan is present in the cell walls of a limited group of fungi belonging to the order Mucorales. For an example, the mycelia of the fungi *Mucor rouxii* can have chitosan of varying amount, ranging from 8.9 to 35% of the cell wall dry weight (Peberdy, 1990; Synowiecki & Al-Khateeb, 2003). The chitosan of fungal cell wall was reported to be 5-10% acetylated (White et al., 1979). Some biotrophic plant pathogenic fungi also contain chitosan in their cell wall during endophytic development as part of their pathogenic mechanism (El Gueddari et al., 2002).

1.2. Chitin/chitosan oligosaccharides (COS)

Chitin and chitosan oligosaccharides together referred to as chitooligosaccharides (COS) are oligomers produced either by partial depolymerisation of the chitin and chitosan or by oligomerisation of the primary monosaccharide building blocks GlcNAc and GlcN. Oligomerisation of GlcNAc and GlcN can be achieved either by chemical or enzymatic means. Chemical synthesis of COS has been based on polycondensation,

ring-opening polymerisation, and stepwise elongation, and requires series of protection and de-protection steps (Barroca-Aubry et al., 2010; Hansen & Skrydstrup, 2007). Today, it is not a routine procedure. An alternative biotechnological approach towards the production of COS makes use of enzymes from the microbial source, namely chitin hydrolases or a combination of chitin synthases and chitin deacetylases (Samain et al., 1997; Cottaz & Samain, 2005). A combination of glycoside hydrolases and chitin deacetylases can be used for the enzymatic synthesis of various structurally different COS as illustrated in figure 1.2. The limitation of the biological approach is

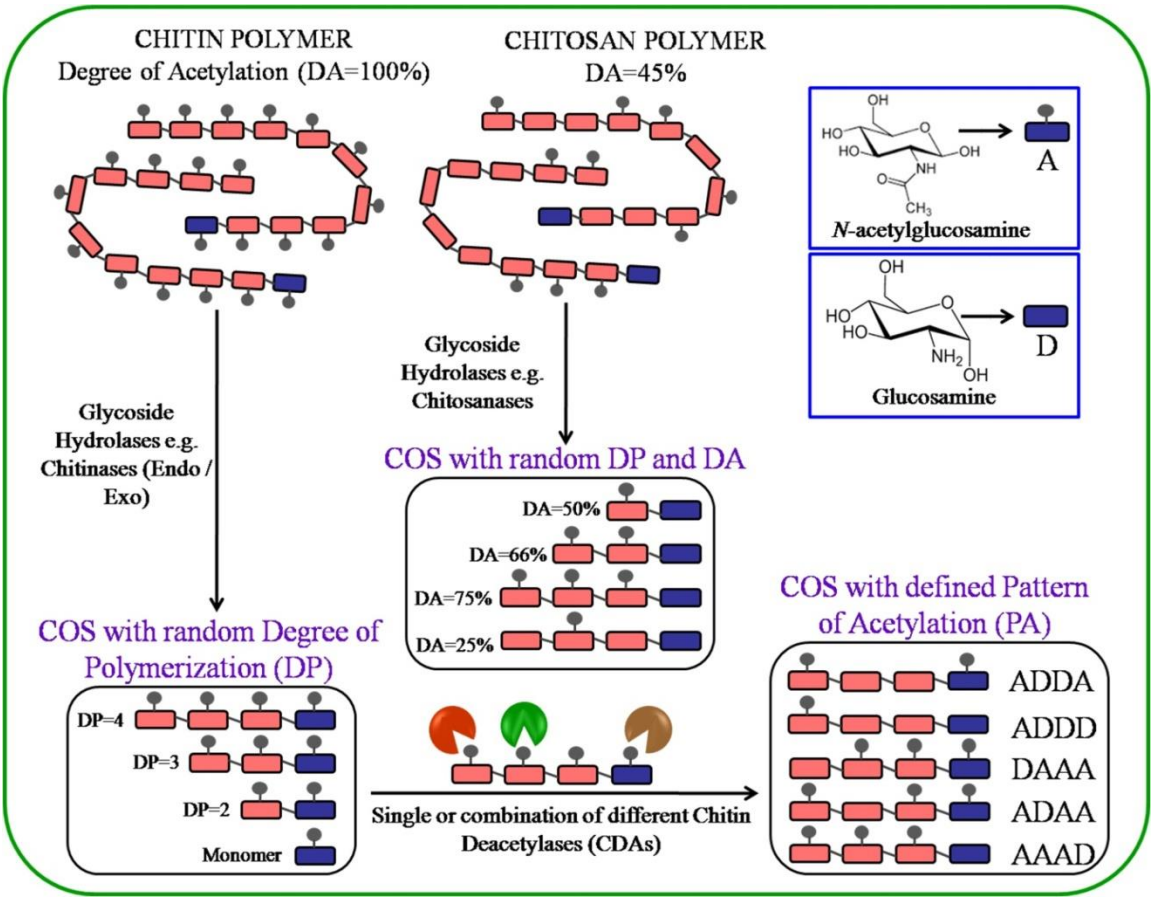

Fig. 1.2: Diagrammatic presentation of enzymatic synthesis of COS with diverse molecular structure. Chitin and chitosan polymers can be cleaved by random-acting glycoside hydrolases such as endochitinases, exochitinases and chitosanases to produce mixture of oligomers with varying degree of polymerization (DP) and degree of acetylation (DA). Chitin oligomers can further be deacetylated in a sequence specific manner to generate defined pattern of acetylated (PA) oligomers by using different chitin deacetylases (CDAs).

the availability of suitable enzymes, leading to a very limited selection of COS that can be produced. Therefore, partial depolymerisation of a vast amount of readily available chitin/chitosan to COS by both chemical and enzymatic means appears to be the choice.

1.2.1 Chemical methods of partial depolymerisation

Chemical methods have been used to produce COS at the industrial level (Sakai et al., 1990). The polymeric chitin or chitosan is subjected to partial hydrolysis using concentrated hydrochloric acid followed by column chromatographic fractionation. Treatment of chitin with acids may cause deacetylation which can be prevented by careful selection of appropriate conditions (Einbu & Vårum, 2008). Chemical hydrolysis mostly gives low DP COS, up to hexamer, and often results in rather low yields of COS and high amount of *N*-acetyl glucosamine (Uchida et al., 1989). Defaye et al. (1994) showed that solvolysis of chitin in anhydrous hydrogen fluoride results in a quantitative yield of COS (DP 2–9), but again with low DP oligomers as primary products. The combination of mild acid degradation and sonolysis under ultrasound irradiation has the potential for the preparation of COS with higher DP (Takahashi et al., 1995). Such methods for the preparation of longer chain COS require time-consuming purification methods and result in low yields with random PA and, therefore, are not preferable for large-scale production. Moreover, the possible contamination of toxic chemicals with the prepared COS, thus, is not ideally suited as bioactive materials. Enzymatic hydrolysis of chitin/chitosan, therefore, might be a preferred method for the generation of bioactive COS with non-random PA (Kohlhoff et al., 2009).

1.2.2 Enzymatic methods of partial depolymerisation

Enzyme methods may provide an opportunity to produce COS with specific DP and PA and, thus, desired bio-activity. Several industrial non-specific enzymes such as cellulases, lipases, pectinases and lysozymes have been used for COS production from chitosan (Vishukumar et al., 2005; Lee et al., 2008). The low specificity of these biocatalysts typically led to the production of low DP COS, with few exceptions.

Clearly, use of chitin/chitosan specific enzymes would be a great step forward towards the reliable synthesis of COS mixture with defined chemical composition and desired biological activities. A great diversity of chitin and chitosan degrading enzymes exist, including endo- and exo-acting chitinases, endo-chitosanases, and glycosidases, such as GlcNase and GlcNAcase (El Gueddari et al., 2007).

1.2.3 Purification and characterization of COS by chromatography and mass spectrometry

Both chemical and enzymatic depolymerisation or synthesis used in COS production invariably yield mixture of COS. These methods are time consuming and involve cumbersome separation and purification steps to produce the desired longer chain bioactive COS. Long chain COS are essential for the establishment of detailed structure/function relationships, and also for the development of reliable agricultural applications. Presently, chromatographic techniques such as gel filtration, ion exchange and metal affinity are used for separation and purification (Sørbotten et al., 2005; Haebel et al., 2007; Le Dévédec et al., 2008). A combination of these techniques is required to obtain more or less homogeneous COS. In a first step, separation of oligomers is typically achieved based on size, i.e. on DP. Sørbotten et al. (2005) separated individual oligomers up to DP 20 by size exclusion chromatography using SuperdexTM 30 columns. Further, by using cation exchange chromatography, COS of identical DP can be separated based on the number of deacetylated residues (Haebel et al., 2007), i.e. according to DA. No method has yet been developed to separate isobaric COS, i.e. COS with identical DP and DA, according to their PA. Mass spectrometry (MS) and nuclear magnetic resonance (NMR) spectroscopy have been applied in characterizing COS in terms of DP, DA, and, to a limited extent the PA (Younes & Rinaudo, 2015). NMR has long been the method of choice, but requires comparatively large amounts of sample. It gives only average values for DP and DA in COS mixtures, while DP and DA even of complex mixtures of COS can easily be determined using MS, where both matrix-assisted laser desorption ionization and electrospray ionization based methods have been employed (Tømmeraas et al., 2001; Trombotto et al., 2008).

One advantage of NMR is that it gives information on the acetylation state of the reducing end unit, and to some extent also of the non-reducing and penultimate units (Heggset et al., 2012). However, Bahrke et al. (2002) developed a method based on a reducing end tagging by using 2-aminoacridone, for sequencing of COS up to DP 12 using MS, and advanced MS-based sequencing methods are currently being developed (Haebel et al., 2007, B. M. Moerschbacher lab, unpublished).

1.3. Applications of chitin, chitosan and their COS

Chitin, chitosans and COS are known independently to have different biological activities (Younes & Rinaudo, 2015). Chitosans being cationic in nature are used in numerous applications such as in agriculture (fungus control agents and seed coating), cosmetics industry, the food industry (packaging films, fish feed additive and dietary fibre), and water treatment (Tharanathan & Kittur, 2003; Kurita, 2006; Prashanth & Tharanathan, 2007; Karlsen et al., 2010). Both chitin and chitosan are also promising molecules in biomedical, and pharmaceutical applications like wound dressings (act as antimicrobial and antifungal agents) (Xia et al., 2011), gene and drug delivery vehicles (Schipper et al., 1996; Köping-Höggård et al., 2001) and chitosan gels (Kumar et al., 2004). COS have inhibitory effects on tumor growth and metastasis of lung cancer in mice (Shen et al., 2009). COS are also reported to induce production of interleukins and, consequently, help to improve the function of macrophages, natural killers, cytotoxic T cells, and polymorphonuclear leukocytes as defense mechanisms (Wang et al., 2008).

In agriculture, COS are desirable because of their ability to boost immunity in plants (Das et al., 2015). The DP, DA, and concentration of the COS strongly influence their plant strengthening activities (Hadwiger, 1999; Yamada et al., 1993; Day et al., 2001, dos Santos et al., 2008). COS-mediated protection also varies depending on the plant type under study. In all cases, however, the biological activity of COS increases with an increase in DP, as long as the COS remains soluble. The Highest activity was reported for hexamers to nonamers (DP≥6–9) and little or no activity for small oligomers (DP ≤ 5) in suspension-cultured Arabidopsis cells (Cabrera et al.,

2006). Long chitin oligomers (DP = 6–8) were more effective in inducing chitin-responsive genes than smaller chitin oligomers (DP = 4–5) (Zhang et al., 2002). The DA of COS also affects the elicitor activity. In most cases, the fully acetylated COS, i.e. chitin oligomers, induce a broad-spectrum defense responses while fully deacetylated COS tend to be inactive as an elicitor (Vander et al., 1998; Wei et al., 2004). The elicitor activity of partially acetylated COS has rarely been studied, but they may in some cases be more potent than their fully acetylated counterparts (dos Santos et al., 2008).

Detailed analyses of structure/function relationships of bioactive COS as well as recent progress towards understanding the mechanism of COS sensing in plants through the identification and characterization of their cognate receptors have generated fresh impetus for approaches that would induce innate immunity in plants. COS are recognized as pathogen associated molecular patterns (PAMPs) either by lysine motif (LysM) receptor-like kinases (LYKs) or LysM receptor like proteins in plants (LYPs) (Fig. 1.3). The first identified receptor of COS, chitin elicitor binding protein (CEBiP), was from rice (Kaku et al., 2006). Subsequently, chitin elicitor receptor kinase 1 (OsCERK1; an LYK), OsLYP4 and OsLYP6 were identified in rice and their roles in chitin perception have been elucidated (Shimizu et al., 2010; Liu et al., 2012). In *Arabidopsis thaliana*, while AtCERK1 was essential for chitin-triggered immunity (Miya et al., 2007; Wan et al., 2008), an auxiliary role of AtLYK4 also contributes to chitin-triggered immunity (Wan et al., 2012). In addition to rice, other crop plants such as maize and sorghum have homologs of OsCEBiP (Fliegmann et al., 2011). In barley, a homolog of OsCEBiP was functionally shown to contribute to fungal resistance (Tanaka et al., 2010).

1.4. Glycoside hydrolase (GH)

Glycoside hydrolases (GHs) are a group of enzymes which hydrolyse the glycosidic bond between two sugars or between a carbohydrate and a non-carbohydrate moiety. GHs are classified into several families based on the similarity in primary amino acid sequence and 3-D structure (Henrissat, 1991; Henrissat & Davies, 1997). By 2015, 135

GH families have been described in the Carbohydrate-Active Enzymes database (CAZy; www.cazy.org).

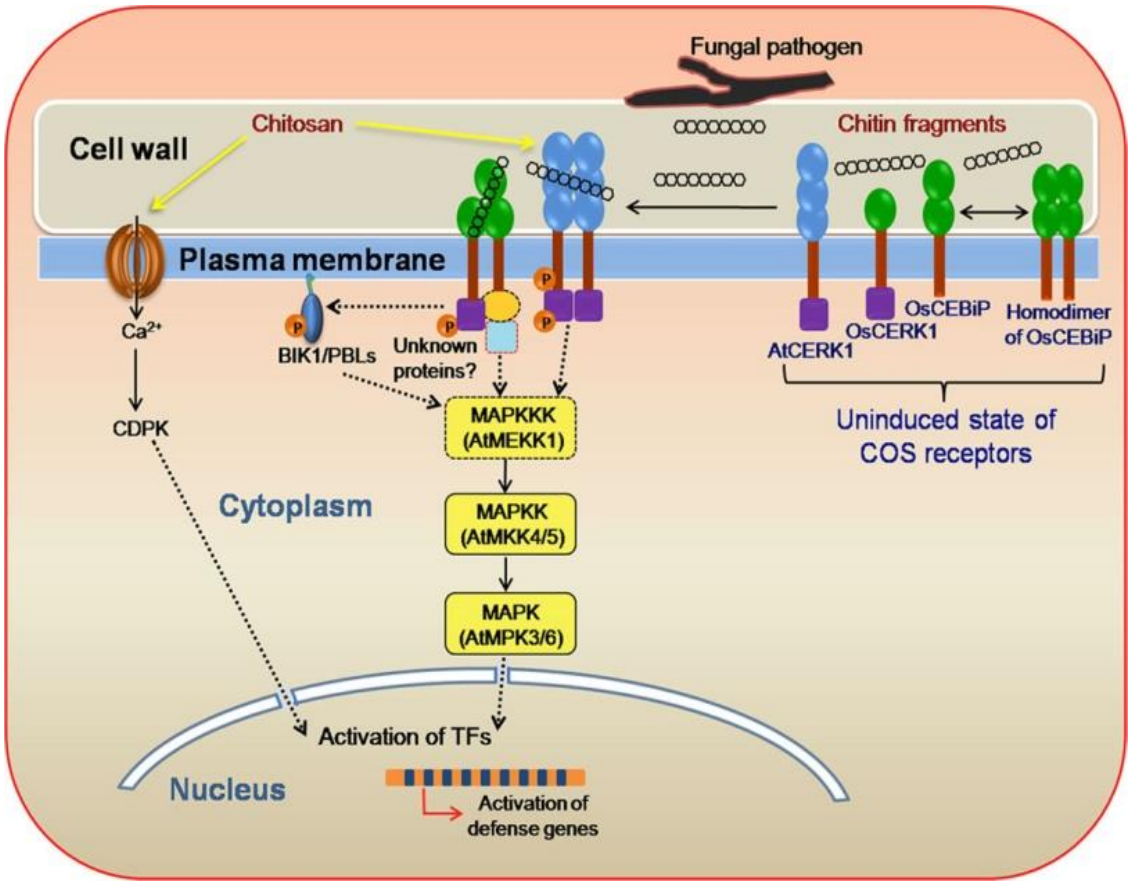

Fig. 1.3: A model for COS-induced activation of chitin receptors and subsequent COS-signaling pathway in plants (Das et al., 2015). During fungal infection, COS released from the fungal cell wall bind to membrane receptors: AtCERK1 in Arabidopsis and OsCEBiP in rice harboring LysM domains. Binding of the ligands induces homodimerization of AtCERK1 in Arabidopsis and hetero-oligomerization of OsCEBiP and OsCERK1 by the interaction of their ectodomain in rice. The latter could form a protein complex by yet unknown proteins. Cytoplasmic receptor-like kinases, such as BIK1, could be a partner of the complex. Upon phosphorylation the BIK1 may get detached from the complex and activate other cytoplasmic proteins in a way similar to the flg22-mediated signaling (Zhang & Zhou, 2010). Activation of the complex leads to activation of a MAPK cascade which in turn phosphorylate transcription factors that regulate chitin-responsive genes. Partially deacetylated chitosan can bind to AtCERK1 and activate the defense genes in addition to their effect on membrane destabilization. Dotted arrow and dotted circle/square denote unknown physical interaction and unidentified hypothetical molecules, respectively. Abbreviations: CDPK, calcium-dependent protein kinase; BIK1, Botrytis-induced kinase 1.

1.4.1 Mechanism of hydrolysis by GHs

A nucleophilic substitution at the anomeric carbon during the hydrolysis of the glycosidic linkage can lead to either inversion or retention of the anomeric configuration (Sinnott, 1990). The hydrolysis reactions in GHs take place through general acid catalysis and need a pair of carboxylic acids at the active site of the enzyme. One of the carboxylic acids acts as a proton acceptor (inverting mechanism) or as a nucleophile (retaining mechanism), and the other carboxylic acid acts as a proton donor (Fig. 1.4).

In the inverting mechanism, also called the single displacement mechanism, is a one-step reaction, where the protonation of the glycosidic oxygen takes place simultaneously with a nucleophilic attack on the anomeric carbon (Aam et al., 2010). The activated water molecule acts as a nucleophile and the reaction proceeds through an oxocarbenium ion transition state. The water molecule is activated by a carboxylic acid, the proton acceptor. The inverting mechanism leads to product formation with an inversion of the anomeric configuration. Chitinases belonging to GH family 19 and chitosanases of GH families 8, 46, 75 and 80 use this inverting mechanism (Davies & Henrissat, 1995; Adachi et al., 2004; Cantarel et al., 2009).

The retaining mechanism also referred to as the double displacement mechanism is a two-step reaction (Fig. 1.4). In the first step, the protonation of the glycosidic oxygen occurs by a catalytic acid with a subsequent nucleophilic attack on the anomeric carbon atom by the second carboxylic acid. This attack leads to breakage of the glycosidic linkage and the formation of an intermediate with a covalent linkage between the anomeric carbon and the catalytic nucleophile (Vocadlo et al., 2001). In the second step, the intermediate is hydrolysed by a water molecule that approaches the anomeric carbon from a position close to that of the original glycosidic oxygen, leading to retention of the anomeric carbon configuration. Both family 18 chitinases and chitosanases belonging to GH family 5 and 7 use this retaining mechanism (Cantarel et al., 2009).

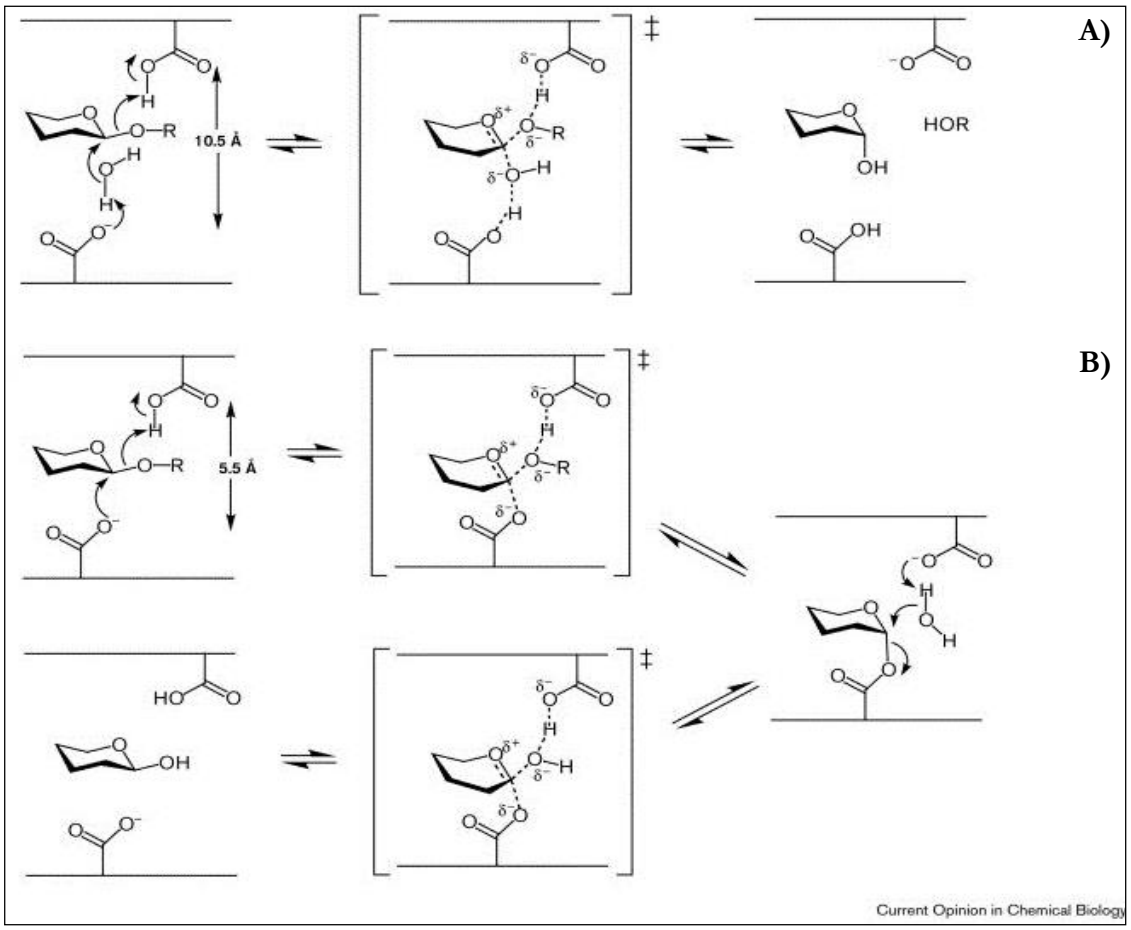

Fig. 1.4: Mechanisms of hydrolysis by glycoside hydrolases. A) the inverting mechanism. **B)** the retaining mechanism (Rye & Withers, 2000).

1.4.2 Mode of action, processivity and substrate binding of GHs

According to various mode of action, GHs are classified as endo- or exo-enzymes. Exo-enzymes degrade the carbohydrate polymers from one of the chain ends while endo-enzymes attack from a random point within the polymer chain. Each of these two mechanisms can take place in combination with a processive mode of action, meaning that the substrate is not released after successful cleavage but glides through the active site for the next hydrolytic event to occur (Robyt & French, 1970). Processivity of GHs when degrading insoluble substrate such as chitin is hard to measure, but can be measured when degrading a soluble substrate such as chitosan

(Eijsink et al., 2008). The active site of non-processive endo-enzymes is comparatively shallow and open which allows random cleavage within the polymer chain followed by the release of the substrate. The substrate binding cleft of exo-enzymes is deep or even tunnel-like when the enzyme hydrolyses the substrate in a processive mode of action (Davies & Henrissat, 1995; Henrissat & Davies, 1997). The role of stacking and hydrophobic interactions by aromatic amino acids in the binding cleft has been explored in many processive GHs (Horn et al., 2006a; Zakariassen et al., 2009). The essential role of polar residues in maintaining processivity is also shown in ChiA of *S. marcescens* (Hamre et al., 2015).

During enzymatic hydrolysis, several amino acid residues of the GHs interact to the substrate in addition to the catalytic residues which execute the catalytic cleavage. The substrate-binding sites distant from the bond undergoing hydrolysis are called subsites, which affect the catalytic activity of GHs (Davies et al., 1997). Such a subsite system not only exists in GHs but also in proteinases and nucleases. Subsites are named from -n to +n (where 'n' is an integer). The '-n' subsites represent the binding of the non-reducing end of the sugar chain and '+n' subsites bind the reducing end of the sugar. Cleavage occurs between the bound sugars in subsites -1 and +1 as shown in figure 1.5. After hydrolysis, the sugar bound in -1 subsite will become the new reducing end while the sugar bound in +1 subsite will be the new non-reducing end.

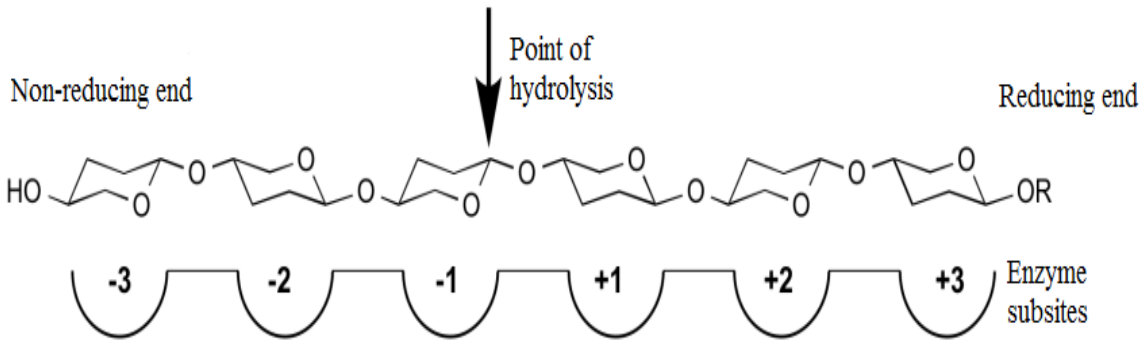

Fig. 1.5: Schematic representation of sugar-binding subsites in GHs. By principle, the non-reducing end of the substrates is drawn on the left and the reducing end on the right.

1.4.3. Chitinases

Chitinases (EC 3.2.1.14) are GHs, which hydrolyse the β-(1→4) glycosidic linkages in chitin. Chitinases hydrolyse the A-A linkage, but not the D-D linkage. Chitinases are found in GH family 18 and 19, except for one chitinase from *Ralstonia* sp. belonging to GH23 (Cantarel et al., 2009; Arimori et al., 2013). Chitinases are found in a wide range of organisms, including bacteria, virus, fungi, plants and animals with different associated physiological roles (Bhattacharya et al., 2007). Bacteria produce chitinases to utilize chitin as a source of carbon and nitrogen for growth, whereas chitinases in fungi and yeasts are important for autolysis, nutritional and morphogenetic functions. Plants use chitinases as a defense against pathogenic fungi and some parasites by disrupting their cell walls, whereas viral chitinases are involved in the pathogenesis of host cells. Animal chitinases are involved in dietary uptake processes. Human chitinases are particularly associated with anti-inflammatory effects against T-helper-2-driven diseases, such as allergic asthma.

1.4.3.1 Structure and catalytic mechanism of chitinases

As of January 2016, family 18 chitinases contain ~60 structural entries in the CAZy database and are found in bacteria, fungi, insects, plants, mammals, archaea and viruses (www.cazy.org). The catalytic domains of family 18 chitinases have a (α/β)8 (TIM-barrel)-fold and are characterized by several conserved sequence motifs. The most prominent of these motifs is the D*X*D*X*E motif that spans strand 4 of the TIM barrel and includes the Glu that acts as the catalytic acid. The active site grooves of these chitinases are lined with aromatic amino acids that contribute to substrate binding (Synstad et al., 2004). The mode of action of the chitinases is based on the aspartic acid residues lying in the core of the active site groove. Structural studies have provided information on the binding modes and specificity of chitinase inhibitors, as well as elucidating the mechanism of the hydrolysis reaction (Dixon et al., 2006; Schüttelkopf et al., 2006; Andersen et al., 2008).

In family 18 chitinases, the core sugar binding subsites are termed -2, -1, +1, +2, where cleavage occurs between subsites -1 and +1. Chitin binds to the active site

groove of family 18 chitinases with the GlcNAc units stacking on the solvent exposed tryptophans, with the -1 sugar assuming a boat conformation. Furthermore, chitin binding results in a reorientation of the middle Asp side chain (in the D*X*D*X*E motif), leading to its interaction with the C2-acetamido group of the -1 sugar. Nucleophilic attack of the carbonyl oxygen of the acetamido group on the anomeric C1 carbon of the same pyranose ring occurs concurrently with protonation of the glycosidic oxygen by the catalytic acid, generating the leaving group from the reducing end of chitin as well as an oxazolinium ion intermediate. This step differs from the classical retaining mechanism of glycoside hydrolases such as lysozyme, cellulase, xylanase, and endo-1,3-1,4-β-D-glucan-4-glucanohydrolase that use a carboxylate side chain as the nucleophile (Vaaje-Kolstad et al., 2013). This particular variant of the double displacement mechanism is referred as the substrate-assisted double displacement mechanism. Because of the involvement of the *N*-acetyl group in catalysis, productive substrate-binding of chitosan and chitosan oligomers to family 18 chitinases requires a GlcNAc bound in the -1 subsite.

By January 2016, ~15 structural entries of family 19 chitinases are reported in the CAZy database and are mainly found in plants; some bacteria and viruses also possess GH 19 chitinases (www.cazy.org). A chitinase (ChiC) from *Streptomyces griseus* HUT6037 was the first bacterial family 19 chitinase to be identified (Ohno et al., 1996) whose crystal structure was solved by Kezuka et al. (2006). The structures of most of the family 19 chitinases of the plant are composed of two lobes rich in α-helical content. The substrate binding groove is a deep cleft formed between the two lobes (Hart et al., 1995; Monzingo et al., 1996; Fukamizo, 2000). Crystal structure of two family 19 chitinases from *Streptomyces griseus* HUT6037 and *Streptomyces coelicolor* A3(2) revealed that the bacterial GH 19 chitinases lack loops (Hoell et al., 2006; Kezuka et al., 2006).

The family 19 chitinases degrade chitin/chitosan substrates in an inverting mechanism, producing α-anomeric hydrolysis products from β-anomeric substrates (Davies & Henrissat, 1995). The three amino acid residues i.e. Glu, Glu, and Ser are

almost conserved in GH19 chitinases, and are involved in the catalysis (Hoell et al., 2006; Ohnuma et al., 2013; Ohnuma et al., 2014). Family 19 chitinases also lack stacking interactions provided by aromatic residues in the catalytic cleft, compared to GH18 chitinases and cellulases (Ubhayasekera, 2011).

1.4.3.2 Transglycosylation (TG) by GH18 chitinases

In addition to the hydrolytic ability, some of the GH18 family chitinases show inherent TG activity. GH18 family chitinases showing TG are known in bacteria, fungi, cycads, and plants. Details of TG chitinases with the ability to synthesize longer chain COS are given in Table 1.1.TG is the process through which the transfer of a glycosyl unit to

Table 1.1: Details of chitinases showing TG from different biological sources.

Enzyme	Source organism	Maximum length of TG product obtained	Duration of formation (min)	Substrate concentration (mM)	References
CrChi-A	*Cycas revolute*	DP9	30	1.0[a]	Taira et al. (2009)
NtChiV	*Nicotiana tabacum*	DP8	10	5.0[a]	Ohnuma et al. (2011b)
AtChiC	*Arabidopsis thaliana*	DP8	10	4.6[a]	Ohnuma et al. (2011a)
AcMNPV chitinase	*Autographa californica* multiple polyhedran virus	DP8	10	4.6–5.0[a]	Fukamizo et al. (2011)
SpChiD	*Serratia proteamaculans* 568	DP13	45	3.5[a]	Purushotham & Podile (2012)
Chitinase A	*Vibrio carchariae*	DP8	30	1.0[b]	Suginta et al. (2005)
Chitotriosidase	Human macrophages	DP9	40	5.0[b]	Aguilera et al. (2003)

[a]DP6, [b]DP5, [c]DP4, [d]DP3

another glycoside bearing an –OH group happens. The TG occurs through a double-displacement mechanism (Ly & Withers, 1999) with the formation of an intermediate that decomposes with different possible outcomes. Hydrolysis is attained by the attack

of a water molecule on the glycosyl-enzyme intermediate that is assisted by the conjugated base of the catalytic acid residue leading to the release of a hydrolyzed sugar. Alternatively, TG may occur if the water molecule is outcompeted by another acceptor, such as a carbohydrate or an alcohol (Zakariassen et al., 2011). Thus, the amino acid residues responsible for acceptor binding seem to be important for TG activity (Martinez et al., 2012). Since TG is a kinetically controlled reaction, efficient TG requires an enzyme with an active site architecture that disfavors correct positioning of the hydrolytic water molecule and/or favors binding of incoming carbohydrate molecules, through strong interactions in the glycon subsites (Williams & Withers, 2000).The TG property of chitinases has immense potential in synthesizing longer chain COS. But, lack of availability of suitable enzymes with higher TG activity limits such application. TG depends on the substrate concentration, solvent system and even the type of enzyme used, which are often manipulated for COS synthesis. The enzyme modifications would need to aim at reducing hydrolytic activity while increasing binding strength for the glycosyl donor in the glycon subsites (Jahn et al., 2003). Two family 18 chitinases ChiA and ChiB from *Serratia marcescens* have very little inherent TG on DP4 COS. The mutants of ChiA and ChiB i.e. ChiA-D313N, ChiA-D313N-F396W and ChiB-D142N showed increased TG by forming COS with longer DP up to 8 (Zakariassen et al., 2011). TG reaction, however, generates a mixture of long chain COS and may even synthesize large, water insoluble COS. To overcome such problems, recently, Martinez et al. (2012) evaluated mutations in the catalytic amino acids of two family GH 18 chitinases, *Bacillus circulans* WL-12 chitinase A1 (*Bc*ChiA1) and *Trichoderma harzanium* chitinase 42 (*Th*Chit42). These mutated chitinases, where the catalytic machinery was disrupted enough to abolish hydrolytic activities, but still operational for TG reaction by providing oxazoline activated donor for the synthesis of desired artificial COS, can be considered as novel "glycosynthases". Alteration of amino acid residues in the catalytic center, in the substrate-binding groove, and in solvent accessible regions of ChiD from *S. proteamaculans* substantially improved the TG activity concerning in increasing the quantity of TG products and in extending the duration of TG activity (Madhuprakash et al., 2012).

1.4.4. Chitosanases

Chitosanases (EC 3.2.1.132) are enzymes that hydrolyze the β-(1→4) linkages in chitosan. They have been found in GH families 3, 5, 7, 8, 46, 75 and 80 and are characterized from bacteria, fungi, cyanobacteria and plants (Cantarel et al., 2009Gupta et al., 2012). The family GH46, GH75, and GH80 exclusively contain chitosanases. GH3 and GH5 contain a variety of enzymatic activities, including β-glucosidase, xylanases, chitosanases, cellulases, licheninases and mannanase. Chitosanase activity has been detected in only a few cases, e.g. a GH3 chitosanase from *Anabaena fertilissima* RPAN1 (Gupta et al., 2010) and a GH5 chitosanase II from *S. griseus* HUT6037 (Tanabe et al., 2003). The GH7 is primarily a cellulase family and in a few cases, chitosanase activity has been detected as a subordinate activity (Ike et al., 2007; Xia et al., 2008). In GH8, a few true chitosanases have been reported e.g. ChoK from *Bacillus* sp. K17 (Adachi et al., 2004) and a chitosanase from *Bacillus* sp. No.7M (Vårum et al., 1996).

Chitosanases belonging to different GH families have shown different mechanisms of hydrolysis. Family 3, 5 and 7 chitosanases are retaining (Wang et al., 1993; Divne et al., 1994), while chitosanases from family 8, 46 and 75 use the inverting mechanism (Fukamizo et al., 1995; Adachi et al., 2004; Cheng et al., 2006). The mechanism of family 80 chitosanase is not yet known, but can be inferred to be inverting mechanism (www.cazy.org). Based on the specificity towards chitosan substrate, chitosanases are classified into three subclasses (I-III) (Fukamizo et al., 1994). The subclass II exclusively cleaves the linkage between two D-units. In addition to hydrolysis of the glycosidic linkage between two D-units, chitosanases belonging to subclass I and III can cleave the linkage between A-D and D-A, respectively (Mitsutomi et al., 1996).

The best-studied chitosanases, regarding their three-dimensional structures, are those belonging to family 8 and 46 (Marcotte et al., 1996; Saito et al., 1999; Adachi et al., 2004; Lyu et al. 2014). By January 2016, the GH8 and GH46 have one and four crystal structure entries, respectively in the CAZy database (www.cazy.org). The ChoK,

a GH8 chitosanase from *Bacillus* sp. K17 has a catalytic site constructed on the scaffold of a double-α6/α6-barrel formed by six repeating helix-loop-helix motifs. In ChoK, the E122 acts as a proton donor and E309 acts as the proton acceptor during catalysis.

The structure GH46 is quite different from the chitosanase of GH8. The structure of CsnN174, a GH46 chitosanase from *Streptomyces* sp. N174 consists of two globular domains with a high α-helical content. In between the two lobes a large substrate binding and catalytic cleft is formed (Marcotte et al., 1996). This structural core is similar for all the members of the family GH46. Site-directed mutagenesis identified that E22 and D40 of Csn174 are essential for catalytic activity. The CsnN174 has a substrate binding cleft consisting of six subsites (from -3 to +3) with cleavage occurring in the middle (Fukamizo et al., 1995; Tremblay et al., 2001).

1.5. Role of accessory domains in chitinases and chitosanases

GHs have evolved special strategies to ensure efficient degradation of crystalline and inaccessible polymeric substrates like chitin and cellulose. In addition to their catalytic domains, GHs often have one or multiple accessory/auxiliary domains. These accessory domains are found in different combinations and different arrangements with respect to the position of the catalytic domain (Henrissat & Davies, 2000). Among these auxiliary domains CBMs are frequently found in GHs and by January 2016, CBMs belonging to 72 different families have been documented in CAZy database.

Carbohydrate-binding modules (CBMs) are distinct structural folds of a stretch of amino acids within carbohydrate-active enzymes having carbohydrate-binding activity. CBMs increase the activity of endo-acting enzymes, several folds, by increasing the concentration of appended enzymes in the vicinity of insoluble substrates and providing specificity to the enzymes (Boraston et al., 2004 & Cuskin et al., 2012). Based on the nature of binding, inferred from structural and functional data, CBMs are classified into A, B and C types (Boraston et al., 2004; Gilbert et al., 2013). CBMs of type A have a planar binding surface that is rich in aromatic amino acids, and bind to surfaces of crystalline chitin or cellulose. Binding sites of B type show extended clefts

or grooves that bind internally on glycan chains and accommodate longer sugar chains, whereas type C CBMs bind to the termini of glycans with a less defined binding pocket.

The multi-domain chitinases often consist of auxiliary domains like CBMs (cellulose binding domain, CBD or chitin binding domain, ChBD), fibronectin type III (FN3) or polycystic kidney disease (PKD) domains. The CBMs found in chitinases belong to family CBM5 and CBM12 which are modules of 40–60 amino acid residues. In chitinases, the primary role of the auxiliary domains (ChBD, PKD, and FN3) is to potentiate catalytic activity by disrupting the substrate, at times without even promoting the enzyme-substrate binding. The presence of PKD domain is an added advantage for chitinase-mediated crystalline chitin hydrolysis. This domain has a β-sandwich fold and the sequence 'WDFGDG' is highly conserved in the domain. The role of PKD was experimentally proved in the case of chitinase A from *Alteromonas* sp. strain O-7 (AlChiA). Mutational studies proved that W30 and W67 in PKD domain of AlChiA play an important role in the efficient hydrolysis of powdered chitin (Orikoshi et al., 2005a). FN3 domain did not affect chitin-binding but strongly reduced chitin hydrolysing activity when deleted from ChiA1 of *B. circulans* (Watanabe et al., 1994). So far, well studied potential functions of CBMs include, correct positioning of the catalytic domain on to crystalline substrates and their contributions to the processive mode of action, and perhaps even local decrystalization of the substrate (Eijsink et al., 2008). CBMs are characterized by the presence of conserved exposed tryptophans that interact and increase affinity with the substrate (Uni et al., 2012).

Among all the CBM families, members grouped under CBM family 32 are more diverse, prevalent in the GHs of bacteria and bind to a variety of carbohydrate ligands (Abbott et al., 2008). A few bacterial family 32 CBMs have been functionally characterized for their ligand specificities. CBMs of a GH89 from *Clostridium perfringens* binds to galactose, GalNAc and GlcNAc-α-1,4-Gal whereas CBM32 from an *N*-acetyl-β-hexosaminidase GH84C (Ficko-Blean et al., 2012) binds preferentially to β-D-galactosyl-1,4-β-D-N-acetylglucosamine (LacNAc) and lactose (Ficko-Blean et al.,

2009). CBM32 of sialidase from *Micromonospora viridifaciens* recognized galactose and lactose (Newstead et al., 2005). Two CBM32s present tandemly in a GH8 from *Paenibacillus fukuinensis* bind chitosan oligomers (Shinya et al., 2013). Cocrystalization of CBMs with their preferable substrates showed differences in the residues in the loop region of their binding sites. A subtle variation in the substitution of amino acids leads to change in the pattern of molecular interaction of CBMs with their ligands (Ficko-Blean et al., 2009). Multiple CBMs of family 32 appended to a single enzyme had different ligand specificities and were phylogenetically distinct, suggesting that enzymes containing multiple copies possess complex mechanisms of ligand recognition (Ficko-Blean et al., 2012). Irrespective of high sequence identity (>70%), members of CBM32 display greater variability in binding affinity (Shinya et al., 2013). Even members of CBM32 with low sequence identity (20%) recognize one type of sugar moiety (Grondin et al., 2014), suggesting the inability to predict the binding specificity and affinity from the primary structure. The diversity and different ligand binding specificity, and perhaps the potential biotechnological applications reinforce the necessity to study CBM32-carbohydrate interactions, in particular, to unravel their specificities, and binding mechanisms.

1.6. Objectives of this study

One of the major difficulties in using the chitin, chitosan and COS for large scale applications has been the variations in their biological activity, mostly due to poorly characterized molecules with the differences in their DP, DA, and PA. Therefore, it is highly desirable to generate COS with defined DP, DA, and if possible, also the defined PA using enzymatic approaches. Furthermore, the degradation of chitosan by chitosanases is not fully understood due to a lack of well-defined chitosan substrates in terms of their DA and PA. The amorphous nature of chitosan also suggests that the binding of CBMs would differ from their counterparts in chitinases and cellulases.

Considering the importance of enzymatic hydrolysis of chitin/chitosan to convert low-value chitin/chitosan polymer into high-value bioactive COS for specific biological applications, the following objectives are pursued:

1. Exploration of the chitinolytic bacterial diversity from chitin-rich soil and selection of potential plant growth promoting rhizobacteria (PGPR).
2. Characterization of chitinases from *Paenibacillus elgii* and improvement of transglycosylation (TG) by site-directed mutagenesis.
3. Degradation of chitosan by a multi-domain chitosanase from *P. elgii* and role of its CBM32 in chitosan binding.
4. Production and plant strengthening activities of bioactive chitosan oligosaccharides generated by a chitosanase from *P. elgii*.

Chapter II

Materials and methods

2.1 Chemicals

Regular laboratory chemicals and routine media components for bacterial culture were obtained from Merck or HiMedia Laboratories, India unless otherwise stated. Isopropyl-β-D-thiogalactoside (IPTG), X-Gal, phenol solution Tris equilibrated and agarose were purchased from Sigma-Aldrich (USA). Luminol and potassium hexacyanoferrate(III) for oxidative burst experiments and 3-Methyl-2-benzothiazolinone hydrazone hydrochloride hydrate (MBTH) for reducing end assay were purchased from Sigma-Aldrich. Antibiotics were purchased from Calbiochem (Darmstadt, Germany). Polymeric substrates such as α- chitin, β-chitin and polymeric chitosan substrates with a DA of 10 and 25% were kindly provided by Dr. Dominique Gillet, Mahatani Chitosan Pvt. Ltd. (Veraval, India). Chitosans with different DAs were prepared by partial re-*N*-acetylation using acetic anhydride in 1,2-propanediol (Vachoud et al., 1997) and the resulting chitosan polymers were analysed by ^{1}H-nuclear magnetic resonance (NMR) spectroscopy (Hirai et al., 1991). Chitosan monomer (D1), dimer (D2), trimer (D3), tetramer (D4), pentamer (D5), hexamer (D6), chitin monomer (A1), dimer (A2), trimer (A3), tetramer (A4), pentamer (A5), and hexamer (A6) were obtained either from Megazyme (Wicklow, Ireland) or Seikagaku Corporation (Tokyo, Japan). Cellobiose was purchased from Sigma-Aldrich.

2.2 Kits

DNeasy Blood & Tissue Kit (Qiagen, Germany) was used for genomic DNA isolation. For plasmid isolation and PCR clean up, NucleoSpin Plasmid kit and NucleoSpin Gel and PCR Clean-up (Macherey-Nagel, Germany) were used, respectively. Gibson Assembly Cloning Kit (NEB) was used for restriction enzyme free cloning. All the kits were used as per the manufacturers' instructions.

2.3 Enzymes

High-Fidelity Q5 DNA Polymerase (NEB), Phusion Hot Start II High Fidelity proof reading DNA Polymerase (Thermo Scientific) were used for PCR amplification, and restriction enzymes and T4 DNA ligase were used for cloning from MBI Fermentas

(Ontario, Canada). All enzymes were used as per the manufacturers' instructions.

2.4 Soil collection site for isolation of chitinolytic bacteria

Soil samples were collected from the dump yards of a chitin/chitosan producing company, Mahatani Chitosan Pvt. Ltd., Gujarat, India and also from a mushroom production firm, S. M. Agritech Pvt. Ltd., Hyderabad, India.

2.5 Bacterial strains

Paenibacillus elgii SMA-1-SDCH02 was isolated from the soil sample collected from mushroom production firm, S. M. Agritech Pvt. Ltd., Hyderabad, India. For general cloning, *E. coli* DH5α (NEB) was used, whereas Rosetta 2 (DE3) [pLysSRARE2] and BL21 (DE3) (Novagen, Germany) were used for protein expression. The plasmid pET-22b (Novagen, Darmstadt, Germany) including a StrepII tag sequence upstream of the multiple cloning site (MCS) and pET-28a (Novagen, Madison, WI) with His6 tag were used for protein expression.

2.6 Primers and plasmid constructs

The primers used in this study for making plasmid constructs of *P. elgii* chitinases and single/double mutants of *Pe*Chi1 (Table 2.1) were procured from MWG Biotech Pvt. Ltd. (Bangalore, India) and IDT, USA. The primers used for making plasmid constructs of *Pe*Csn truncations, eGFP fusions and *Pe*CBM32 mutants (Table 2.2) were procured from MWG Biotech Pvt. Ltd. (Germany).

2.7. Media used

2.7.1 Luria-Bertani (LB) medium

LB medium-10 g tryptone, 10 g NaCl, 5 g yeast extract and 15 g agar were added to 900 ml of water and pH was adjusted to 7.2. Final volume was made up to 1 liter.

2.7.2 Chitin agar medium

Colloidal chitin-10 g, Na_2HPO_4-0.065 g, KH_2PO_4-1.5 g, NaCl-0.25 g, NH_4Cl-0.5 g,$MgSO_4$- 0.12 g, $CaCl_2$-0.005 g and agar-15 g. The pH was adjusted to 7.0, and volume was madeup to 1 liter.

Table 2.1: Details of primers used and plasmid constructs generated for *Pe* chitinases. Sequences underlined represent restriction sites. Bold and italicised sequence encodes altered amino acid. 5'-PHO stands for 5' phosphorylated primers.

Primer name	Primer sequence	Restriction site	Plasmid construct	Protein product
*Pe*Chi1-for	5'-CTCAGAATTCATATACTTCTACGTCCAGCAG-3'	*Eco* RI	pET-28a-*Pe*Chi1-His6	*Pe*Chi1
*Pe*Chi1-rev	5'-ATAAACTCGAGCATTTGCAGCTGCTCCGAAAG-3'	*Xho* I		
*Pe*Chi3-for	5'-TAATAGAATTCTCCCCTCTCCCCTCTGCC-3'	*Eco* RI	pET-22b-*Pe*Chi3-His6	*Pe*Chi3
*Pe*Chi3-rev	5'-ATAACTCGAGCTTCAGCTGCCACAGCGCC-3'	*Xho* I		
*Pe*Chi4-for	5'-TAATACCATGGTGTTCGCCGCTGCGGCTTGG-3'	*Nco I*	pET-22b-*Pe*Chi4-His6	*Pe*Chi4
*Pe*Chi4-rev	5'-AATCACTCGAGCGGATTCAGACCGTTTTTCACG-3'	*Xho* I		
*Pe*Chi5-for	5'-CAAGGATCCGTGCTCAAGCTGCGGGACGTC-3'	*Bam* HI	pET-28a-*Pe*Chi5-His6	*Pe*Chi5
*Pe*Chi5-rev	5'-GCATACTCGAGTTTCAGGCCGTCCAAGAACGG-3'	*Xho* I		
*Pe*Chi1-G103W-rev	5'-PHO-***CCA***TACGCCTAGCACAAGATTCG-3'	-	pET-28a-*Pe*Chi1-G103W	*Pe*Chi1-G103W
*Pe*Chi1-Y105W-rev	5'-PHO-***CCA***ACCGCCTACGCCTAGCAC-3'	-	pET-28a-*Pe*Chi1-Y105W	*Pe*Chi1-Y105W
*Pe*Chi1-D141N-for	5'-PHO-***AAT***TGGGAGTACCCGGCTTC-3'	-	pET-28a-*Pe*Chi1-D141N	*Pe*Chi1-D141N
*Pe*Chi1-Y105W/G103W-rev	5'-PHO-***CCA***ACC***CCA***TACGCCTAGCACAAGATTCG-3'	-	pET-28a-*Pe*Chi1-Y105W/G103W	*Pe*Chi1-Y105W/G103W
*Pe*Chi1-Y105W/F62W-rev	5'-PHO-TTCGC***CCA***AGCGATAAAGGCG-3'	-	pET-28a-*Pe*Chi1-Y105W/F62W	*Pe*Chi1-Y105W/F62W
*Pe*Chi1-Y105W/G101S-rev	5'-PHO-CCAACCGCCTAC***GCT***TAGCAC-3'	-	pET-28a-*Pe*Chi1-Y105W/G101S	*Pe*Chi1-Y105W/G101S
*Pe*Chi1-Y105W/G104S-rev	5'-PHO-CCA***GCT***GCCTACGCCTAGCAC-3'	-	pET-28a-*Pe*Chi1-Y105W/G104S	*Pe*Chi1-Y105W/G104S
*Pe*Chi1-Y105W/M216A-for	5'-PHO-***GCG***AGCTATGACCTAACTG-3'	-	pET-28a-*Pe*Chi1-Y105W/M216A	*Pe*Chi1-Y105W/M216A
*Pe*Chi1-Y105W/Y218A-for	5'-PHO-ATGAGC***GCG***GACCTAACTGG-3'	-	pET-28a-*Pe*Chi1-Y105W/Y218A	*Pe*Chi1-Y105W/Y218A

Table 2.2: Details of primers used and plasmid constructs generated for *PeCsn*. Bold and italicised sequences encode altered amino acid. 5'-PHO stands for 5' phosphorylated.

Primer name	Primer sequence	Plasmid construct	Protein product
*Pe*Csn-for	5'-TAATACCATGGTGGCCGGAGAAATGAAACCGTTC-3'	pET-28a-*Pe*csn-His6	*Pe*Csn
*Pe*Csn-rev	5'-AATCACTCGAGATTGCTCGGGCCGTATACTTC-3'		
*Pe*GH8FN3-for	5'-PHO-GAGCTCCGTCGACAATGG-3'	pET-22b-GH8FN3-StrepII	GH8FN3
*Pe*GH8FN3-rev	5'-PHO-GGCGGTATTGCTGTTCGCC-3'		
*Pe*GH8-for	5'-PHO-CGGAATCCACCAGTTGCC-3'	pET-22b-GH8-StrepII	GH8
*Pe*GH8-rev	5'-PHO-GGCGGTATTGCTGTTCGCC-3'		
*Pe*CBM32-for	5'-PHO-CATATGTATATCTCCTTCTTAAAGTTAAACAAAATTATTTCTAGAG-3'	pET-22b-*Pe*CBM32-StrepII	*Pe*CBM32
*Pe*CBM32-rev	5'-PHO-AGCGCCACGACGACCGAC-3'		
eGFP-for	5'-AAGTATACGGCCCGAGCAATTTAAAGCTTGTGAGCAAGGG-3'	pET-22b-StrepIIC-*Pe*CBM32-eGFP-His6	*Pe*CBM32-eGFP
eGFP-rev	5'-CCGTCGGTCGTCGTGGCGCTCGAATTCGGATCCGAATTAATTCC-3'		
CBM32-for	5'-AGCGCCACGACGACCGAC-3'		
CBM32-rev	5'-ATTGCTCGGGCCGTATACTTCG-3'		
*Pe*CBM32-E16A-for	5'-PHO-AG***GCG***GGAAGCGGCTACG-3'	pET-28a-*Pe*CBM32-E16A-His6	*Pe*CBM32-E16A
*Pe*CBM32-S18A-for	5'-PHO-CAGGAAGGA***GCC***GGCTACG-3'	pET-28a-*Pe*CBM32-S18A-His6	*Pe*CBM32-S18A
*Pe*CBM32-E38A-rev	5'-PHO-GCTTCC***CGC***CTTGCTCG-3'	pET-28a-*Pe*CBM32-E38A-His6	*Pe*CBM32-E38A
*Pe*CBM32-E38F-for	5'-PHO-GCGAGCAAG***TTT***GGAAGCGAC-3'	pET-28a-*Pe*CBM32-E38F-His6	*Pe*CBM32-E38F

2.7.3 Potato dextrose agar (PDA)

Potato infusion-200 g, dextrose-20 g and agar 20 g were added to 900 ml of water and pH was adjusted to 5.6. The final volume was made up to 1 liter.

2.8. Culturable diversity of chitinolytic bacteria

2.8.1 Isolation

Soil suspensions were prepared by mixing 10 g of soil to 100 ml of sterile DDW. Ten-fold dilutions of soil suspensions were plated on LB agar. For enrichment of

chitinolytic bacteria, M9 media supplemented with colloidal chitin as the sole source of carbon was used as described by Kishore et al. (2005a). The bacterial isolates were spot-inoculated and incubated at 30°C for 24-96 h. Colonies showing zones of clearance were considered as chitinase-producers and restreaked until pure cultures were obtained.

2.8.2 Identification

Bacterial isolates were identified based on the morphological and biochemical tests described by Benson (1990) and further confirmed by 16S rRNA gene sequence analysis. Genomic DNA of individual isolates was used as the template for amplification of the 16S rRNA gene using universal primers: forward primer 27F (5'-GTTTGATCCTGGCTCAG-3') and reverse primer 1489R (5'-TACCTTGTTACGACTTCA-3'). The obtained partial sequences were matched with the nucleotide sequences available at Gen Bank, using BLAST tool in NCBI and in EzTaxon database (http://www.ezbiocloud.net/eztaxon). Phylogenetic analysis of the all 27 chitinolytic isolates was done by using MEGA version 4 (Kumar et al., 2008).

2.9. Evaluation of PGPR activity of *P. elgii* in groundnut and tobacco

2.9.1 Seed bacterization

To test *P. elgii* as a potent PGP bacterium in groundnut under greenhouse condition, cells of *P. elgii* with and without chitosan (90% DDA) were used as described by Kishore et al. (2005b) with minor modifications. For inoculum preparation, *P. elgii* was grown in 50 ml of LB broth for 24-48 h at 30°C, and the cell pellet was collected by centrifugation at 4600×*g* for 10 min. The cell pellet was washed twice with buffer containing 20 mM glucose and 20 mM of potassium phosphate and finally suspended in the same buffer. Surface-sterilized groundnut seeds cv. JL 24 soaked with chitosan (1%) were suspended in bacterial cell suspension for 30 min and dried overnight under a flow of sterile air, resulting in 1×10^6 to 1×10^7CFU/seed. Seed treatments with *P. elgii* alone, *P. elgii* with chitosan, and chitosan alone were compared with sterile water treatment.

2.9.2 Growth promotion in groundnut

Plastic pots of 30 cm diameter filled with red soil, black soil, and manure (2:2:1) were used for sowing bacterized groundnut seeds (3 seeds/pot). The pots were watered daily and kept in the greenhouse and maintained at a temperature of 28 ± 2°C. To determine the root length, shoot height, fresh weight and total chlorophyll content, plants were uprooted at 25 days after sowing (DAS). The dry weight of the plants was also measured after drying in an oven at 80°C for 24 h. The emergence of seedlings was recorded 6 DAS. Total leaf chlorophyll content was estimated according to Graan and Ort (1984). For each treatment, five replicates with two repetitions were evaluated in a completely randomized block design.

2.9.3 Growth promotion in tobacco under gnotobiotic condition

Growth promotion in tobacco under gnotobiotic condition was studied by designing a setup as shown in Fig. 2.1. The system consisted of two chambers; the upper chamber

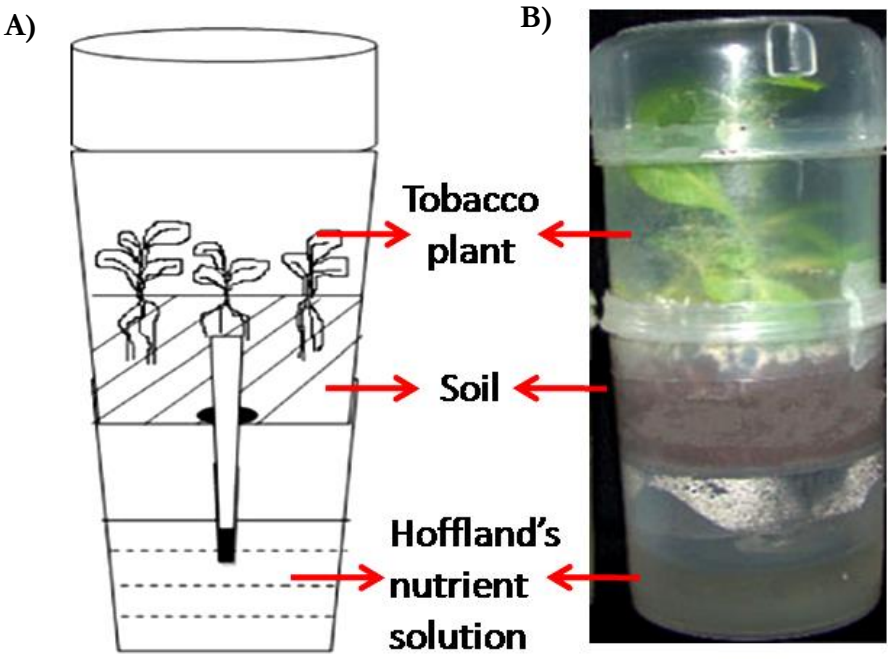

Fig. 2.1: Growth promotion study of tobacco plant in gnotobiotic setup. Gnotobiotic setup was designed using toothpick bottles. **A)** Assembled setup and **B)** grown tobacco plants in the gnotobiotic setup.

was filled with 30 g of sand with a hole in the bottom through which a 200 µl pipette tip was inserted. The bottom of the micropipette tip was clogged with cotton and connected the upper chamber with the lower chamber containing Hoffland's plant nutrient solution (PNS). Components of PNS are 5 mM $Ca(NO_3)_2$, 5 mM KNO_3, 2 mM $MgSO_4$, 1mM KH_2PO_4, and micronutrients ($g.l^{-1}$ of $MnSO_4$, 0.61; $ZnSO_4.7H_2O$, 0.1; H_3BO_3, 1.27; $Na_2MoO_4.2H_2O$, 0.40; and $CuSO_4$, 0.04). After autoclaving the unit, surface sterilised tobacco seeds (1% sodium hypochlorite solution for 30 s) were immersed in *P. elgii* suspension of 1×10^7 $CFU.ml^{-1}$ for 30 min and dried for 1 h and placed in the chamber containing sand. Treatment with sterile water served as control. After 30 days of growth, the shoot height, root length and dry weight of the plants were recorded. For each treatment, six replicates with three repetitions were evaluated in a completely randomized block design.

2.10. Cloning and heterologous expression

Draft genome sequence information of *P. elgii* B69, a soil isolate having broad-spectrum antimicrobial activity (Ding et al., 2011) was used for designing primers to amplify chitinase/chitosanase genes of *P. elgii* SMA-1-SDCH02. For PCR, restriction digestion, ligation, competent cell preparation, transformation and agarose gel electrophoresis, standard molecular biology protocols were followed as described by Sambrook and Russell (2001).

2.10.1 Chitinases from *P. elgii*SMA-1-SDCH02 (*Pe* chitinases)

Primers were designed excluding the predicted signal peptide sequence of chitinases for the amplification of *Pechi1*, *Pechi3*, *Pechi4* and *Pechi5* from the gDNA of *P. elgii* SMA-1-SDCH02. Amplified fragments of *Pechi1* and *Pechi5* were cloned at *Eco* RI/*Xho* Iand *Bam* HI/*Xho* I restriction sitesof pET-28a, respectively. *Pechi3* and *Pechi4*amplicons were cloned at *Eco* RI/*Xho* Iand *Nco* I/*Xho* I sitesof pET-22b, respectively. The resultant plasmid constructs were designated as pET-28a-*Pe*Chi1-His6, pET-28a-*Pe*Chi5-His6, pET-22b-*Pe*Chi3-His6 and pET-22b-*Pe*Chi4-His6 (Table 2.1).

2.10.2 Chitosanase from *P. elgii*SMA-1-SDCH02 (*Pe*Csn)

Using gene-specific forward and reverse primers (Table 2.2), chitosanase of *P. elgii* (*Pecsn*)was amplified without signal peptide sequence and cloned into pET-28a-His6 at *Nco* I and *Xho* I sites to make pET-28a-*Pe*Csn-His6 construct. *Pecsn* gene was also cloned into pET-22b-StrepII by Gibson assembly kit method giving rise to pET-22b-*Pe*Csn-StrepII.

2.10.3. Protein expression, isolation and purification

2.10.3.1 Heterologous expression

E. coli BL21 and *E. coli* Rosetta 2 (DE3) [pLysSRARE2] expression hosts were used for expression of chitinases and chitosanase. Expression host harbouring pET28a and pET22b constructs were grown in LB medium containing 50 μg.ml^{-1} kanamycin and 100 μg.ml^{-1} ampicillin, respectively. Additionally, 25 μg.ml^{-1} chloramphenicol was added for growing *E. coli* Rosetta 2 (DE3) [pLysSRARE2] cells. The overnight grown culture was used as starter culture for bulk expression of the required protein. In auto-induction media, cells were grown at 37ºC for 3 h and then at 26ºC for 20 h. For IPTG induction, bacterial cells were grown at 37ºC until the optical density reached a value of 0.6. Then IPTG at a final concentration of 0.1 mM was added and the cells were grown at 18ºC for 20 h.

2.10.3.2 Protein isolation and purification

All the heterologously expressed proteins were isolated from respective cell pellets by whole cell lysate using sonicator. The cell pellets were resuspended in Ni-NTA equilibration buffer (50 mM NaH_2PO_4, 100 mM NaCl and 10 mM imidazole pH 8.0) and were lysed by sonication at 35% amplitude with 10 s on and 15 s off pulses for 6 cycles on ice with a Vibra Cell Ultrasonic Processor, converter model CV33, equipped with a 3 mm probe (Sonics, Newtown, CT, USA). The lysed cells were centrifuged at 40,000×*g*for 40 min at 4°C to remove the insoluble cell debris. The supernatant with cleared lysate of His-tagged proteins was applied to 4 ml Ni-NTA agarose resin (Clonetech, USA) packed in a 10 ml syringe and purified by gravity flow method. Expressed recombinant proteins were eluted with four column volumes of elution

buffers with different concentrations of imidazole i.e. 50 mM, 100 mM and 250 mM in 50 mM NaH_2PO_4+100 mM NaCl, pH 8.0.

Cell pellets with StrepII-tag expressed proteins were resuspended in lysis buffer (40 mM TEA, 400 mM NaCl, pH 8.0). Proteins fused to C-terminal StrepII-tag were purified by using ÄKTA™prime 4.01 fast protein liquid chromatography system (GE Healthcare, Germany) fitted with a 1 ml Strep-Tactin Superflow Plus Cartridge (Qiagen, Germany).The column was washed with wash buffer (20 mM TEA, 400 mM NaCl, pH 8.0) before loading the sample with a flow rate of 2.0 ml min^{-1}. Proteins were eluted atthe same flow rate using wash buffer supplemented with 2.5 mM D-desthiobiotin. All buffers for FPLC were filtered before use. The pure fraction containing desired proteins was collected, concentrated, and buffer exchanged with 50 mM of suitable buffer of pH 5.0-6.0 using Vivaspin 20 centrifugal concentrators (MWCO 10 kDa, Sartorius).

2.10.3.3 Protein measurement

Concentrated and buffer exchanged purified proteins were quantified using Pierce BCA protein assay kit (Thermo Scientific, USA). Samples were measured in appropriate dilution series according to the kit manual. Using different concentrations of bovine serum albumin (BSA), the slope from the standard calibration curve was obtained as per the instructions given in the kit.

2.10.4 SDS-PAGE analysis

The protein samples were separated by SDS-PAGE on vertical slab gels according to Laemmli (1970). The stacking gel contained 4.5 % polyacrylamide in 0.125 M Tris-HCl, pH 6.8 and the resolving gel contained 12% polyacrylamide in 0.375 M Tris-HCl, pH 8.8. Electrode buffer contained 0.025 M Tris-HCl, 0.192 M glycine and 0.1% (w/v) SDS of pH 8.5. The samples were boiled at 100°C for 5 min in sample buffer [1% SDS (w/v) and 12% glycerol (v/v), in 0.063 M Tris-HCl, pH 6.8] and electrophoresis was carried out at 50V in stacking gel and at 100V in resolving gel. The gels were stained in a solution containing 0.5% (w/v) Coomassie brilliant blue G-250, 30% (v/v) methanol

and 10% (v/v) glacial acetic acid, and destained in a solution containing 30% (v/v) methanol and 10% (v/v) glacial acetic acid till the protein bands were visible.

2.11. Characterization of *Pe* chitinases

2.11.1 Zymogram analysis

The activity of purified recombinant chitinases was qualitatively determined by dot blot assay. An acrylamide gel supplemented with 0.1% glycol chitin without SDS was prepared. Chitinases (5 µg) were spotted on to the gel and placed in humid chamber at 37°C for overnight. The gel was stained with 0.01% calcofluor white M2R in 0.5 M Tris-HCl pH 8.9 for 10 min at 4°C. The gel was washed thoroughly with distilled water for 10 min at 4°C to remove the brightner. Lytic zones were visualized by placing the gels under UV light in a gel doc.

2.11.2 Reducing end assay to measure activity

Chitinase activity was measured by a modified Schales' procedure using colloidal chitin as the substrate (Imoto & Yagishita, 1971). All the reaction was performed in triplicate in 200 µl reaction volume consisting of appropriate amount of enzyme and colloidal chitin in 50 mM suitable buffer at 40°C for 1-2 h with constant shaking at 190 rpm. The reaction was centrifuged at 16,100×*g* at 4°C for 15 min, and 40 µl supernatant was transferred to pre-cooled eppendorf. To this 40 µl reaction containing reducing sugars, 300 µl of freshly prepared colour reagent (0.5 M sodium carbonate, 0.05% potassium ferricyanide) was added and boiled in dark for 15 min at 100°C. After cooling to room temperature, 200 µl of each reaction was taken in 96 well microtiter plate and the absorbancy was taken at 420 nm using microtiter plate reader (Multiscan, Labsystems, Finland).

2.11.3 Optimum pH

The optimum pH for *Pe* chitinases was determined by incubating enzymes (*Pe*Chi1: 20 µg, *Pe*Chi3 and *Pe*Chi4: 5 µg, and *Pe*Chi5: 40 µg) and colloidal chitin (20 $mg.ml^{-1}$) in different buffers at different pH (2.0-12.0) for 1 h at 40°C. The buffers used were 50 mM sodium citrate buffer (pH 2.0-5.0), 50 mM sodium acetate buffer (pH 5.0-6.0), 50

mM sodium phosphate buffer (pH 6.0-8.0), and 50 mM glycine-NaOH buffer (pH 8.0-10.0) and 50 mM NaH_2PO_4-NaOH (pH 10.0-12.0). The relative activity (%) was determined by considering the maximum observed activity as 100% under standard assay conditions.

2.11.4 Optimum temperature

The optimum temperature for activity *Pe* chitinases was determined by incubating enzymes (*Pe*Chi1: 20 µg, *Pe*Chi3 and *Pe*Chi4: 5 µg and *Pe*Chi5: 40 µg) and colloidal chitin (20 $mg.ml^{-1}$) in 50 mM of suitable buffers at optimum pH for 1 h at different temperatures ranging from 20-100°C. The relative activity (%) was determined by considering maximum observed activity as 100% under standard assay conditions.

2.11.5 Kinetic analyses

Kinetic parameters of *Pe* chitinases were determined by incubating a constant amount of each enzyme (*Pe*Chi1: 20 µg, *Pe*Chi3 and *Pe*Chi4: 5 µg, and *Pe*Chi5: 40 µg) with varying concentration of colloidal chitin ranging from 0.5-75 $mg.ml^{-1}$ at optimum pH and temperature of respective enzyme. Buffer, enzyme and substrate alone were taken as control for reducing end assay as described in the section 2.11.2. Enzyme activity was defined as the release of one micromole of *N*-acetyl glucosamine (NAG) per sec under standard experimental conditions, and specific activity was expressed in $\mu mol.sec^{-1}.mg^{-1}$ of protein. Kinetic parameters were obtained by fitting values of two independent experiments to the Michaelis-Menten equation by nonlinear regression function available in GraphPad Prism version 5.01 (GraphPad Software Inc., San Diego, CA).

2.11.6 Determination substrate specificity

The substrate specificity of purified *Pe* chitinases on chitin derived substrates namely α-chitin, β-chitin, colloidal chitin, glycol chitin and chitosan with 90% DDA was tested. The reaction mixture containing enzymes (*Pe*Chi1: 20 µg, *Pe*Chi3 and *Pe*Chi4: 5 µg, and *Pe*Chi5: 40 µg) and different polymeric substrates (1% w/v) were incubated in 50 mMsuitable buffer at optimum pH and temperature for 1 h. Chitinase activity was

assayed under standard conditions.

2.11.7. Analysis of degradation/transglycosylated products by high performance liquid chromatography (HPLC)

2.11.7.1 Analysis of hydrolysed product generated from colloidal chitin

Degradation/transglycosylated products were analysed by HPLC. The hydrolysis of colloidal chitin by *Pe* chitinases was performed by incubating enzymes (*Pe*Chi1: 0.7 µM, *Pe*Chi3 and *Pe*Chi4: 0.3 µM, and *Pe*Chi5: 2.7 µM) with colloidal chitin (20 $mg.m^{-1}l$) in 50 mM of suitable buffer. Reaction mixtures for different chitinases were incubated at their respective optimum temperature and 1000 rpm in a thermomixer. A reaction volume of 25 µl was removed at different time points starting from 0, 2, 5, 10, 30, 60, 120, 240 and 720 min and was transferred to an eppendorf tube containing 25 µl of 70% acetonitrile to stop the reaction. The reaction mixtures were centrifuged at 16,100×*g* for 15 min at 4°C to remove undigested colloidal chitin. The reaction mixture (20 µl) from each fraction was injected into HPLC connected to SHODEX Amino-P50 4E column (4.6 ID×250 mm, Showa Denko K. K, USA). Chitin oligomers were eluted under isocratic condition with ACN:H_2O in 70:30 with a flow rate of 0.7 $ml.min^{-1}$. Elution of COS was monitored at 210 nm. Quantification of COS was done by comparing peak areas of the products with peak areas obtained from a known concentration of the COS. A mixture containing the equal weight of COS ranging from A1-A6 was used for standard graph preparation. A linear correlation between peak area and concentration of COS in standard samples was established for quantification of reaction products up to A6. Standard calibration curves for individual COS were constructed separately. These data points yielded a linear curve for each standard sugar with the R^2 values of 0.997–1.0 allowing molar concentration of COS to be determined with confidence.

2.11.7.2 Analysis of hydrolysed/transglycosylated products generated from oligomeric substrates (A3-A6)

To determine the mode of action of chitinases on COS and to detect formation of TG

products, isocratic HPLC was performed. The reaction mixture containing 3 mM of each oligomer (A3-A6) was incubated separately with individual chitinases (600 nM *Pe*Chi1-Chi5 and 40 nM *Pe*Chi3 and *Pe*Chi4) in 50 mM sodium acetate buffer pH 6.0. A reaction volume of 20 µl was removed at different time points and monitored by HPLC as described in the section 2.11.7.1.

2.12. Generation of *Pe*Chi1 mutants and their characterization

2.12.1 Molecular docking of *Pe*Chi1 with chitin pentamer (A5)

Molecular docking for *Pe*Chi1 with A5 was performed by Autodock 4.2. Homology modeled *Pe*Chi1 structure was used as a receptor molecule. Polar hydrogens and atomic charges by the Kollman method were added to the modeled receptor molecule by Auto Dock Tools (ADT) graphical user interface. Torsion and rotatable bonds were defined, and Gasteiger charges were added to the ligand molecule using ADT graphical user interface. The ligand was allowed to dock to the receptor within a grid box space of 56×66×70 grid points along X, Y and Z axes with 0.46 Å grid spacing. The centre of the grid was set to -7.405, -14.449 and -8.849 on XYZ coordinates. Docking was employed by using the Lamarckian Genetic Algorithm (LGA) available in Autodock 4.2 with parameters set to LGA population size: 150; GA runs: 10 and a maximum number of energy evolutions: 250,00,000. During docking, a maximum number of top 10 conformers were considered, and the root-mean-square (RMS) cluster tolerance was set to 0.2 nm. Amongst the docked conformations of all ten ligands, the conformation with the lowest binding energy was visualized for detailed interactions in PyMol Molecular Graphics System 1.3 and Discover Studio 4.0.

2.12.2 Selection of amino acid residues for point mutations

The amino acid residues that might influence hydrolytic and TG activities of *Pe*Chi1 were selected based on the sequence alignment of well-characterized chitinases with emphasis for looking the hydrophobic aromatic residues that are known to have a role in catalytic interactions with chitin. By considering the information generated from both sequence alignment and docking study, a few amino acid residues were selected

for point mutations.

2.12.3 Generation of *Pe*Chi1 mutants and their characterization

To make *Pe*Chi1 mutants pET-28a-*Pe*Chi1-His6 construct was used as a template for amplifying the entire plasmid by 5' phosphorylated back to back mutagenic primers. Details of primers used for creating point mutations are listed in table 2.1. Amplicons were ligated at 22°C for 30 min and inserted mutations were confirmed by automated DNA sequencing. All the mutant proteins of *Pe*Chi1 were expressed in *E. coli* BL21 and purified as described in 2.10.3. Characterization of mutants was done as per the protocol described in the section 2.11.2 and 2.11.7.2.

2.13. Characterization of chitosanase (*Pe*Csn)

2.13.1 Estimation of reducing group by MBTH assay

Reducing ends of COS generated by chitosanase were measured by 3-methyl-2-benzothiazolinone hydrazone (MBTH) method as described earlier (Horn & Eijsink, 2004). All the reactions were performed in triplicate in 40 µl reaction volume consisting of appropriate amount of enzyme and chitosan substrates of different DAs in 50 mM suitable buffer at 60°C for 10 min with constant shaking at 400 rpm. To this 40 µl reaction containing reducing sugars, 40 µl 0.5 N NaOH was added to inactivate the enzyme followed by addition of 20 µl (3 $mg.ml^{-1}$) MBTH and 20 µl (1 $mg.ml^{-1}$) DTT. The reaction mixture was incubated for 15 min at 80°C. Immediately after heating, 80 µl colour reagent [0.5% (w/v) $FeNH_4(SO_4)_3$+0.5% (w/v) H_3NSO_3+0.25 M HCl] was added and cooled to room temperature. The entire reaction (200 µl) was taken in 96 well microtiter plate, and the absorbance was measured at 620 nm using microtiter plate reader.

2.13.2 Optimum pH

The optimum pH of *Pe*Csn was determined by incubating 100 nM enzyme and 0% DA chitosan (1.0 $mg.ml^{-1}$) in a buffer (40 mM ammonium formate+20 mM TEA+20 mM KH_2PO_4+20 mM Na_2HPO_4) at different pH (3.0-10.0) for 10 min at 40°C. The relative activity (%) was determined by considering the maximum observed activity as

100% under standard assay conditions.

2.13.3 Optimum temperature

The optimum temperature of *Pe*Csn was determined by incubating 100 nM enzyme and 0% DA chitosan (1.0 $mg.ml^{-1}$) in an appropriate buffer at optimum pH for 10 min at different temperatures ranging from 4-80°C. The relative activity (%) was determined by considering maximum observed activity as 100% under standard assay conditions.

2.13.4 Kinetic analysis

Kinetic parameters of *Pe*Csn were determined by incubating 100 nM enzyme with varying concentration of 0% DA chitosan ranging from 0.01-1.5 $mg.ml^{-1}$ at optimum pH and temperature. Buffer, enzyme and substrate alone were taken as control for reducing end assay as described in the section 2.13.1. Enzyme activity was defined as the release of one micromole of glucosamine per sec under standard experimental conditions, and specific activity was expressed in $\mu mol.sec^{-1}.mg^{-1}$ of protein. Kinetic parameters were obtained by fitting values of two independent experiments to the Michaelis-Menten equation by nonlinear regression function available in GraphPad Prism version 5.01 (GraphPad Software Inc., San Diego, CA).

2.13.5 High performance thin layer chromatography (HPTLC)

Separation of COS based on the DP was performed by TLC. Approximately 20 µg chitosan oligomers/polymers in a total volume of 10 µl were sprayed to the TLC-plates (HPTLC Silica gel 60 F_{254}, Merck Co., Germany). The eluent consisted of butanol, methanol, ammonia (25%; w/v) and water at a ratio of 5:4:2:1. The samples were run until solvent front reaches about 1 cm below the upper limit of the plate. To improve the separation, this process canbe repeated after the plate is dried. The detection of COS was made by spraying the TLC plate with 30% (w/v) ammonium bisulphate and baking the plate to above 180°C using a hot air gun. The DP and the distinction between chitosan oligomers were determined by comparing with chitin (A1-A6) and chitosan standards (D1-D6).

2.13.6. Determination of substrate specificity of *Pe*Csn on polymeric substrate analysed by UHPLC-ELSD-ESI-MS

2.13.6.1 Preparation of *Pe*Csn hydrolysate

Chitosan polymer substrate of DA 37% (300 µg) was incubated with 100 nM *Pe*Csn in 50 mM ammonium acetate buffer (pH 6.0) at 60°C. The reaction was stopped after 2, 20 and 720 min by adding an equal volume of 10% ammonium hydroxide and subsequent heating at 98°C for 5 min. The sample was vacuum drying to remove ammonium acetate buffer and was dissolved in 300 µl of water. Reducing end assay by MBTH method was performed to quantify the amount hydrolysate produced by chitosan polymer digestion at each time point.

2.13.6.2 Acetylation of *Pe*Csn hydrolysate for quantitative MS analysis

*Pe*Csn hydrolysate contains a mixture of COS with different DP and DA. The deacetylated (D) residues in the COS mixture were acetylated by a modified protocol of Haebel et al. (2007). The acetylation was done by heavy isotopic acetic anhydride $^{2}H_{6}$ giving rise to 2 extra mass to COS for each acetylation which makes the distinction of existing acetylated (A) unit with that of new acetylated residue. For acetylation, 2.5 µl of acetic anhydride $^{2}H_{6}$ was added to ~30 µg of *Pe*Csn hydrolysate dissolved in 1:1 methanol:50 mM Na_2HCO_3. The Addition of acetic anhydride was done stepwise; each time with 0.5 µl followed by 15 min incubation at 30°C and 1200 rpm to make sure of complete acetylation of free amino groups of D units in COS. The reaction mixture was vacuum dried and dissolved in 70 µl water followed by freeze drying to remove remaining volatile compounds.

Quantification of different oligomers varying in DP and DA was done by using double isotopic labeled internal standards (R*1-6). The internal standards were prepared by acetylation of chitosan oligomers (D1-6) by labeled acetic anhydride ($^{2}H_{6}$ $^{13}C_{4}$) by following the protocol described above.

2.13.6.3 ^{18}O-labeling to determine sequence of oligomers by MS/MS

Determination of the sequence of oligomers for identifying different PA by MS/MS

requires a distinction between fragments deriving from reducing or nonreducing ends. ^{18}O labeling of oligomers was done to distinguish the fragments derived from the reducing and nonreducing end by a modified protocol of Körner et al. (1999). The acetylated oligomers derived from *Pe*Csn hydrolysate (~5 µg) as described in 2.13.6.2 were dissolved in 5 µl $H_2{}^{18}O$ (Eurisotop) containing 0.1 % formic acid. The sample was incubated at 70°C for 16 h for the exchange of ^{18}O at the reducing end.

2.13.6.4 UHPLC-ELSD-ESI-MS analysis of COS

The applied UPLC-ELSD-ESI-MS method was followed based on the methods described by Hamer et al. (2015) with minor modifications. Aliquots of 2 µl were analysed by UHPLC-ELSD-ESI-MS. In brief, an Acquity UPLC BEH Amide column was used to separate chitosan oligomers by hydrophilic interaction chromatography (HILIC). Samples were run at a flow rate of 0.4 $ml.min^{-1}$ in isocratic conditions with the following eluent: 80:20 acetonitrile:water, 10 mM NH_4HCO_2 and 0.1% (v/v) formic acid. Mass spectra were acquired over a scan range from m/z 50–2000 in positive scan mode. Internal standards (D1-D6) of known concentration were injected for quantification of oligomers generated from the polymer. Data were analysed using Data Analysis 4.1 software (Bruker, Bremen, Germany).

2.13.7. Determination of substrate specificity of *Pe*Csn by using defined PA chitosan tetramer

Tetramer of different DAs and PAs (A-D-A-A, A-D-D-A, D-D-A-A, A-D-D-D, D-A-D-D and D-D-D-A) were used for determining the specificity of *Pe*Csn. By using individual or combination of different CDAs, the above mentioned tetrameric substrates were enzymatically synthesised from chitin tetramer (1 $mg.ml^{-1}$). The CDAs used for this purpose were COD from *Vibrio cholerae*, NodB from *Rhizobium* sp., CDA2 from *Pestalotiopsis* sp. and Pgt from *Puccinia graminis* f.sp. *tritici*. The freeze dried tetramers of different PAs were dissolved in 15 µl of ammonium acetate buffer pH 6.0 and treated with 1.4 µM *Pe*Csn. The reaction was incubated at 60°C for 2h. All products were analysed by UHPLC-ELSD-ESI- MS.

2.14. Role of a CBM32 in *Pe*Csn

2.14.1 Generation of deletion and fusion constructs, and site-directed mutagenesis

To make truncated genes of *Pecsn* lacking the CBM32 (designated as *Pe*CBM32 from now onwards) and FN3, pET-22b-*Pe*Csn-StrepII construct was used as a template for amplification by 5' phosphorylated primers. Similarly, the pET-28a-*Pe*CBM32-His6 construct was made and used as a template to create mutations in the *Pe*CBM32 domain using 5' phosphorylated mutagenic primers. To fuse enhanced green fluorescent protein (eGFP) to *Pe*CBM32, the plasmids pET-22b-StrepII-CSN-eGFP-His6 (Nampally et al., 2012) and pET-22b-*Pe*Csn-StrepII (this study) were used to amplify the respective two fragments using a set of overlapping primers as per Gibson assembly manual. Finally, the fragments were assembled yielding the pET-22b-StrepII-*Pe*CBM32-eGFP-His6 construct. The details of plasmid constructs used in this study are given in table 2.2. Protein expression, isolation and purification were done as described in the section 2.10.3.

2.14.2 Binding specificity of *Pe*CBM32 determined by dot blot

In order to determine the binding specificity to polymeric substrates, chitosans with a DA of 0%, 10%, 20%, 40% and 60%, and glycol-chitin were spotted at two different concentrations, i.e. 1.0 µg and 0.2 µg onto a nitrocellulose membrane. The membrane was incubated at 70°C for 30 min to allow the chitosans and glycol chitin to stick to the membrane. To block the membrane, 3% biotin-free milk powder in 1x Tris-buffered saline (TBS) was used and incubated for 1 h at 25°C. The membrane was washed with TBS for 15 min and incubated with 100 µg.ml^{-1}*Pe*CBM32 containing 3% milk powder in TBS for 1 h. After washing with 1x TBS containing 0.05% (v/v) of both Tween 20 and Triton X-100 (twice for 15 min each), the membrane was incubated with Strep-Tactin antibodies conjugated with horseradish peroxidase (HRP). In a parallel independent experiment, instead of adding protein and antibody, the membrane was stained with Ponceau stain to confirm that the chitosan substrates were

bound to the membrane. The signal was detected by chemiluminescence.

2.14.3 Circular dichroism (CD) measurements for studying thermal unfolding

CD measurements were recorded on a Jasco-J810 spectropolarimeter. A change in thermal stability of *Pe*CBM32 was monitored using the ellipticity changes at 218 nm by increasing the temperature at a rate of 1°C.min^{-1}. To verify the influence of chitosans on thermal unfolding, different DAs of polymeric chitosan substrates (1 mg.ml^{-1}) were used, and the final concentration of protein was 35 µM. The ellipticity values were normalized between 0 (native) and 1 (fully unfolded). The fraction of unfolded protein at each temperature was calculated from the CD value by linearly extrapolating pre- and post-transition baselines into the transition zone and plotted against the temperature.

2.14.4 Isothermal titration calorimetry (ITC)

The binding affinity and stoichiometry of *Pe*CBM32 and its variants towards chitosan oligomers and other carbohydrates were quantified by ITC. Titrations were performed on a VP-ITC isothermal titration calorimeter from MicroCal (Northampton, MA, USA). All purified proteins used in ITC measurements were dialysed extensively in a surplus of 50 mM sodium acetate buffer (pH 5.6). The buffer from the final dialysate was filtered through a 4 µm filter and used to dissolve ligands and also for titrations at 25°C. *Pe*CBM32 and chitosan oligosaccharide solutions were degassed under vacuum. The reaction cell contained *Pe*CBM32 at 80-340 µM and the syringe contained the chitosan oligosaccharide at a concentration of 2-15 mM. A constant stirring speed of 300 rpm was maintained. The data were analyzed using MicroCal Origin ITC software. Thermodynamic parameters such as change in enthalpy (ΔH), association constant (K_b) and binding stoichiometry (n) were obtained by nonlinear least-squares fitting of experimental data using the *one set sites* binding model in the MicroCal Origin software provided by the ITC manufacturer (Narahari et al., 2011).

2.14.5 Chemical synthesis of chitobioside derivatives (GlcNAc-GlcN and GlcN-GlcNAc)

Chitobioside derivatives GlcNAc-GlcN and GlcN-GlcNAc were synthesized using phenyl 3,4,6-tri-O-acetyl-2-deoxy-2-phthalimido-1-thio-*β*-D-glucopyranoside and *tert*-butyldimethylsilyl 3,6-di-O-benzyl-2-deoxy-2-azido-*β*-D-glucopyranoside monomer building blocks. The glycosylation of 4-free azido sugar derivative with phthalimido N-protected glucosamine derivative yielded *tert*-butyldimethylsilyl 3,4,6-tri-O-acetyl-2-deoxy-2-phthalimido-*β*-D-glucopyranosyl-(1→4)-3,6-di-O-benzyl-2-deoxy-2-azido-*β*-D- glucopyranoside. The thioglycoside donor was activated under the NIS-TfOH reagent system to get protected disaccharide. Selective deprotection of two different N-protecting groups viz. phthalimide and azide at the C2 positon followed by global deprotection were carried out sequentially to obtain 2-acetamido-2-deoxy-*β*-D-glucopyranosyl-(1→4)-2-amino-2-deoxy-D-glucopyranose and 2-amino-2-deoxy-*β*-D-glucopyranosyl-(1→4)-2-acetamido-2-deoxy-D-glucopyranose. The structure of the disaccharides produced was assigned by ^{1}H-NMR and MALDI-MS analysis and by comparing the results obtained with literature (Tokuyasu et al., 1999).

2.14.6 Molecular docking of *Pe*CBM32 with D2 and D4

Amino acid sequence homology search by BLAST against the protein databank (PDB) was performed to identify 3D structures that could share high sequence homology. The 3D structure of the *Pe*CBM32 was generated using the MODELLER v9.12 (Sali and Blundell, 1993) and validated by performing Verify_3D and Ramachandran plot generated by PROCHECK analysis (Liithy et al. 1992). D2 and D4 ligands were extracted from the crystal structure of the LysM effector protein of *Cladosporium fulvum* (4B8V), using Discovery Studio 4.0. Molecular docking for *Pe*CBM32 with D2 and D4 was performed by Autodock 4.2 (Morris et al., 2009) as described in the section 2.12.1.

2.14.7 *In situ* staining of chitosan in the fungal cell wall by *Pe*CBM32-GFP

Urediniospores of the wheat stem rust fungus *Puccinia graminis* f. sp. *tritici* (Eriks. & E. Henn) were used for induction of infection structures as described by Nampally et al. (2012). For differentiation of infection structures, spores were sown in poly-styrene petri dishes containing 5 ml of sterile milliQ water and incubated for 50-60 min at 23°C

followed by a mild heat shock (30°C) for 2 h and finally spores were incubated at 23°C overnight for the development of infection structures. After the differentiation of infection structures, checked using a light microscope, germlings were incubated with 2% (wt/v) BSA in 1x phosphate-buffered saline (PBS) for 2 h followed by repeated washing in 1x PBS containing 0.05% (v/v) Tween 20. Subsequently, spores were incubated with 0.1 mg.ml^{-1} *Pe*CBM32-eGFP and wheat germ agglutinin (WGA) conjugated with Texas Red in TBS containing 5% BSA for 1 h at 25°C. After washing with 1x PBS containing Tween 20, spores were observed under confocal laser scanning microscope. The excitation/emission wavelengths for eGFP and Texas Red were 488/595 nm and 500 to 545/608 to 700 nm, respectively.

2.15. Elicitor and priming activity of COS produced by *Pe*Csn

2.15.1 Preparation of COS

To obtain COS, 150 mg chitosan polymer (38% DA) was homogeneously dissolved at 37°C in 30 ml sodium acetate buffer (50 mM, pH 5.6) and then hydrolyzed by 75 µg of *Pe*Csn at 37°C for 48 h. An aliquot of hydrolysates was lyophilized and dissolved in sterile MilliQ water to a final concentration of 1 mg.ml^{-1} for MALDI-TOF-MS analysis. To separate COS based on their DP, the entire filtered hydrolysate was loaded on to a set of 3 HiLoad™ 26/60 Superdex™ 30 prep grade columns of SECcurity GPC System (PSS Polymer Standards Service, Mainz) with a refractive index detector (Agilent 1200 series RID®). Prior to loading the hydrolysate, columns were equilibrated with filtered and degassed elution buffer (150 mM ammonium acetate, pH 4.5). Flow rate of elution was maintained at 0.7 ml.min^{-1} for 22 h. Fractions containing COS of same DP were pooled together and were freeze dried twice to remove any undesired volatile substance.

2.15.2 Chemical characterization of COS

Purified COS were characterized by using HPTLC and UHPLC-ELSD-ESI-MS. Samples containing 5 to 20 µg COS were concentrated to a total volume of 10 µl by spinning in a vacuum centrifuge at 45°C. COS were separated and detected as

described in the section 2.13.5. In order to know the composition of COS in terms of their DA in each fraction belonging to a particular DP, MS analysis was done by injecting 2 µl (2 µg) of each sample as described in the section 2.13.6.4.

2.15.3 Maintenance of rice and tobacco cell suspension system

Suspension cultured rice (*Oryza sativa* L.) and tobacco (*Nicotiana tabacum* Petit Havanna SR1) cells were grown in MS medium (Murashige & Skoog, 1962) supplemented with sucrose (30 $g.l^{-1}$) and 2,4-dichlorophenoxyacetic acid (1 $mg.l^{-1}$). For tobacco suspension cells, additionally kinetin (0.1 $mg.l^{-1}$) was added. Suspension cultures were sub-cultured at intervals of 7 days in 20 ml of fresh medium and were maintained at 26°C in the dark under continuous agitation on a rotary shaker (120 rpm).

2.15.4 Determination of oxidative burst

Determination of oxidative burst was performed based on chemiluminescence of luminol as described by Warm and Laties (1982) using a luminometer (Lumat LB 9501/16 Berthold, Wildbad, Germany). After 4 days of sub-cultivation, the medium was gently removed from cells by using a glass pipette under sterile conditions. Then 300 mg of cells were suspended in 5 ml of oxidative burst medium [10 mM MES with 5% (v/v) culture medium pH 5.8 and 3% (w/v) sucrose] and incubated at 26°C in the dark under agitation. After eliciting or priming the cells by COS, 200 µl culture was mixed with 700 µl of potassium phosphate buffer (50 mM, pH 7.9) in a test tube. To this 100 µl of 1.2 mM luminol and 100 µl of 14 mM potassium hexacyanoferrate(III) were added and the chemiluminescence was measured by using luminometer. The chemiluminescence was measured as relative light units (RLU) which were proportional to the amount of H_2O_2 released from cells after stimulation. A schematic representation of oxidative burst measurement for both elicitation and priming is shown in Fig. 2.2.

2.15.5 Elicitor activity

For testing elicitor activity of COS, 5 h pre-incubated cells were treated with COS before the start of measurement. For tobacco cells 10 $\mu g.ml^{-1}$ ulvan and rice cells 10

µg.ml^{-1} HF chitosan were used as positive controls. At different time points, 200 µl of the sample were taken for measurement.

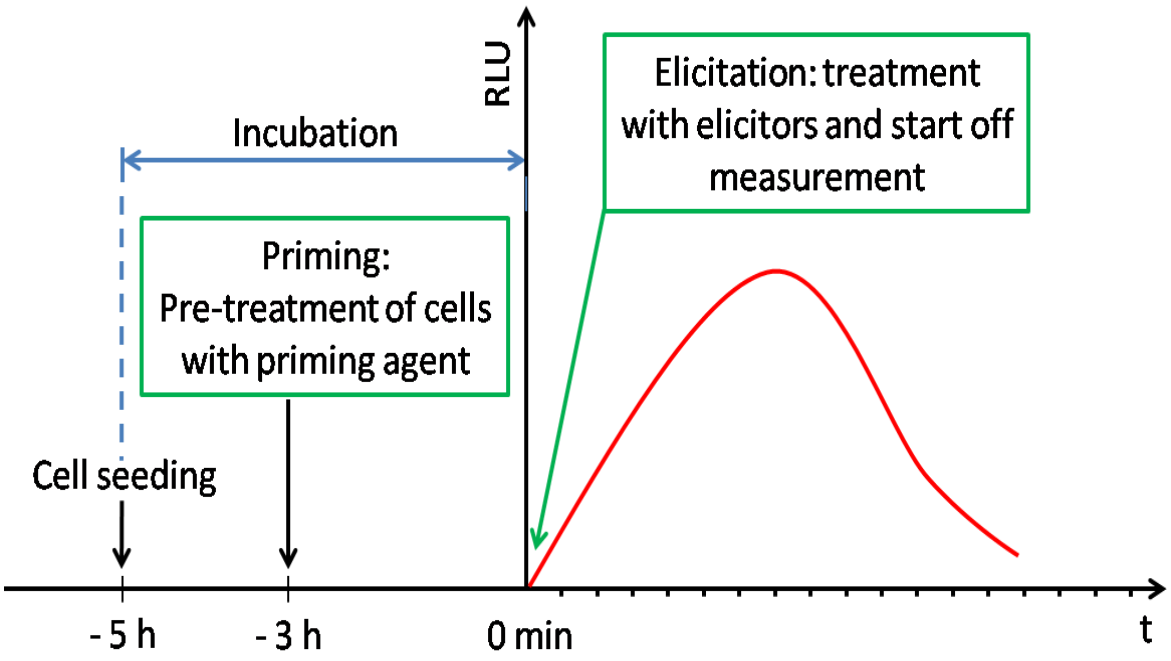

Fig. 2.2: A schematic diagram showing oxidative measurements performed using rice and tobacco cell suspension cultures.

2.15.6 Priming activity

For testing priming activity, 2 h pre-incubated cells were treated with COS and were incubated in the dark at 26°C with shaking. Pre-treated cells were incubated for another 3 h at the same condition before elicitation was triggered by adding 10 µg.ml^{-1} ulvan and 10 µg.ml^{-1} HF chitosan to tobacco and rice cells, respectively. Immediately after adding elicitors, 200 µl of the sample were taken for measurement at different time points. Salicylic acid (SA) at a concentration of 5 µg.ml^{-1} and ulvan (10 µg.ml^{-1}) were used as positive control for tobacco and rice cells, respectively. Appropriate volumes of deionized water were used as negative control.

Chapter III

Exploration of the chitinolytic bacterial diversity from chitin-rich soil and selection of potential plant growth promoting rhizobacteria (PGPR)

3.1. Introduction

Bacteria and fungi are important decomposers of chitin and thereby contribute to the recycling of carbon and nitrogen resources in soil ecosystems. Bacteria produce chitinases to degrade and utilise chitin as carbon and nitrogen source. A large number of chitinolytic soil bacteria were isolated from soil (Wang et al., 1997), garden and park waste compost (Poulsen et al., 2008), shellfish waste (Wang & Hwang, 2001), shrimp shell-enriched soil (Zhu et al., 2007) and vermicompost (Yasir et al., 2009). Phytospheres, such as rhizosphere and phylloplane, are also important habitats for chitin-degrading bacteria (Gonzalez-Franco et al., 2003; Kishore et al., 2005a).

There is a considerable interest in chitinolytic bacteria for efficient bioconversion of chitinaceous waste based on the exploitation of chitinases. Soil bacteria are promising sources of chitinases and could be used for catabolic conversion of chitinaceous biomass into useful bioactive molecules for application in agriculture, biotechnology and medicine (Kishore et al., 2005b; Bhattacharya et al., 2007). Bacteria from genera like *Bacillu*s, *Serratia*, *Pseudomonas*, *Streptomyces*, *Aeromonas* etc., frequently occur in soil and are potentially suitable sources of enzymes for the recycling of chitin wastes.

Chitin is abundantly present in the cell walls of the majority of fungi. The β-(1→4) glycosidic bonds in the chitin are responsible for the cell wall integrity and therefore, become a sensitive target for chitin-degrading enzymes. Chitin-degradation is an essential attribute for several of the successful microbial agents used in biological control of fungal pathogens. The chitinolytic biocontrol strains and the partially purified chitinases caused extensive damage to major fungal pathogens of groundnut (Podile &Prakash, 1996; Manjula et al., 2004; Manjula & Podile, 2005). The chitinolytic potential of the biocontrol PGPR strains was also exploited to improve both the shelf life and effectiveness of the formulations (Manjula & Podile, 2001, 2005; Kishore et al., 2005 a,b). The chitinolytic bacterial strains isolated from phylloplane of groundnut were capable as PGPR when applied on to the seeds (Kishore et al., 2005c).

Despite the rich diversity of chitinolytic bacteria, there could also be several unexplored culturable resources for novel chitinases with useful properties. Isolation of chitinolytic bacteria from chitin-rich soil sources, therefore, would be a powerful approach for selecting bacteria with high chitinolytic activity and to explore the vast diversity of chitin- degrading/modifying enzymes from soil bacteria. The identification of diverse novel bacteria with chitinolytic potential would also be an added benefit to screen them as biocontrol PGPR. So, the focus of this chapter is on the following objectives:

1. To isolate and study the chitinolytic bacterial diversity in chitin-rich soil.
2. To identify an efficient chitin-degrading bacterial strain with diverse chitin- degrading/modifying enzymes.
3. To screen and identify PGPR from soil rich in chitin.

To pursue these objectives, in this chapter, soils from dump yards of ten years history of industrial chitin production were selected to isolate and identify the chitinolytic bacteria. Diversity analysis and grouping of the isolates basing on 16S rDNA were carried out to identify the predominant species. The plant growth promoting (PGP) activity of *Paenibacillus elgii*, selected through a screening process, was tested in peanut under greenhouse and in tobacco under gnotobiotic condition.

3.2. Results

3.2.1. Culturable diversity of chitinolytic bacteria

3.2.1.1 Isolation of chitinolytic bacteria

Soil collected from waste dump yards of the Mahatani Chitosan Pvt. Ltd. (MC) and S. M. Agritech (SMA) had ten years history of enrichment with chitin wastes generated daily during processing of chitin-rich substances such as shrimps and mushrooms. A total of six chitin-rich soil samples were collected from various sites of MC and SMA. Soil samples were dark brownish to light black in colour and sticky in texture. MC soil was slightly acidic in nature of pH 6.4 and SMA soil was slightly alkaline in nature ofpH 7.5.

A total of 140 pure culture isolates of culturable bacteria were isolated from the soil samples collected from MC and SMA. Twenty one (out of 100 bacterial isolates) from MC soils and six out of 40 isolates from SMA showed chitinolytic zone of 2-7 mm on colloidal chitin agar plates indicative of extracellular chitinase activity. MC soil showed moderately higher proportion (21%) of chitinolytic isolates in comparison to SMA (15%). Out of 27 chitinolytic isolates, only 10 isolates showed a zone of clearance of ≥4 mm as shown in Fig. 3.1.

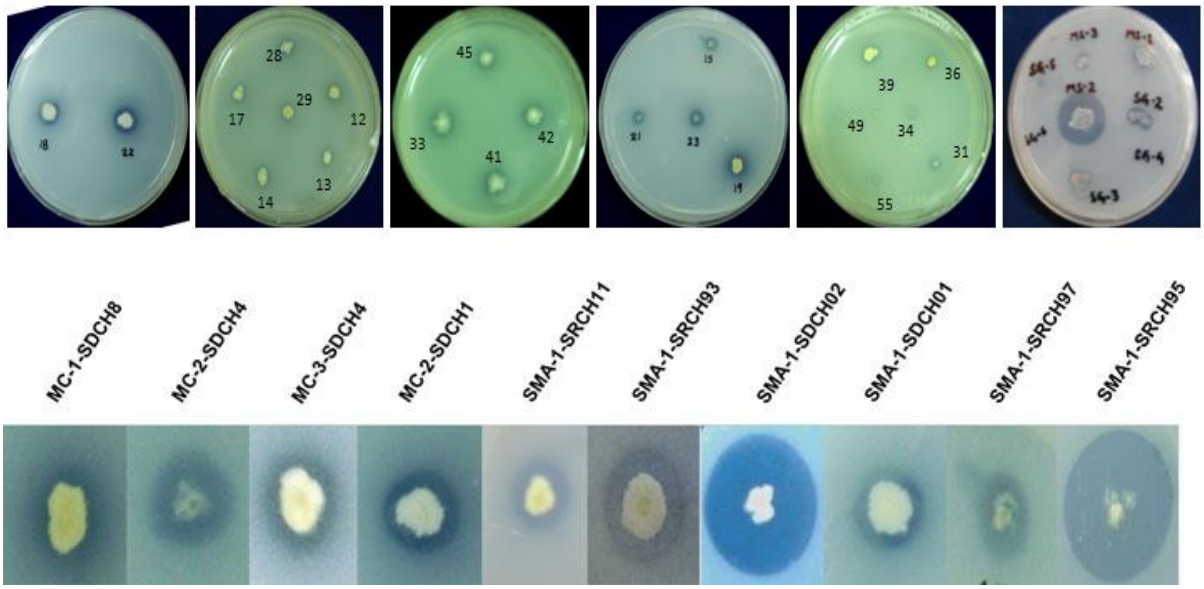

Fig. 3.1: Screening of chitinolytic bacteria. Bacterial cultures were grown on M9 medium agar plates containing colloidal chitin and zone of clearance were recorded after 5-7 days of incubation at 30°C.

The population densities of culturable chitinolytic bacteria were expressed in terms of colony forming unit per gram of soil (CFU.g^{-1}). The chitinolytic bacterial abundance of MC soil varied from 1.2 to 2.9×10^{5} CFU.g^{-1} soil and was higher in comparison to SMA soil, which showed chitinase-degrading bacteria ranged from 1.8 to 2.8×10^{4} CFU.g^{-1} soil (Fig. 3.2). The differences between chitinolytic bacterial counts in MC and SMA soils were statistically significant ($P_{0.001}$).

3.2.1.2 Identification of chitinolytic bacteria and phylogenetic analysis based on16S rDNA

Morphologically, bacterial isolates appeared white to yellow in colour, irregular to round shaped colony, and small to medium-sized colony on nutrient agar. Microscopic observation revealed that all the isolates were rod-shaped, and out of 27 chitinolytic isolates 11 were Gram-positive and 16 were Gram-negative. The results presented in Table 3.1 were matched with those presented in Bergey's Manual of Determinative Bacteriology (Holt et al., 1994). These characteristics suggest that isolates tentatively belong to genera *Stenotrophomonas*, *Pseudomonas* and *Bacillus*. All the strains were negative for indole and positive for catalase production. Apart from producing extracellular chitinases, isolates such as MC1SDCH5, MC1SDCH7, MC2SDCH1, MC2SDCH5, MC2SDCH7, MC3SDCH4, MC3SDCH5, SMA-1-SDCH01, SMA-1-SDCH02, and SMA-1-SRCH95 were positive for starch hydrolysis (Table 3.1).

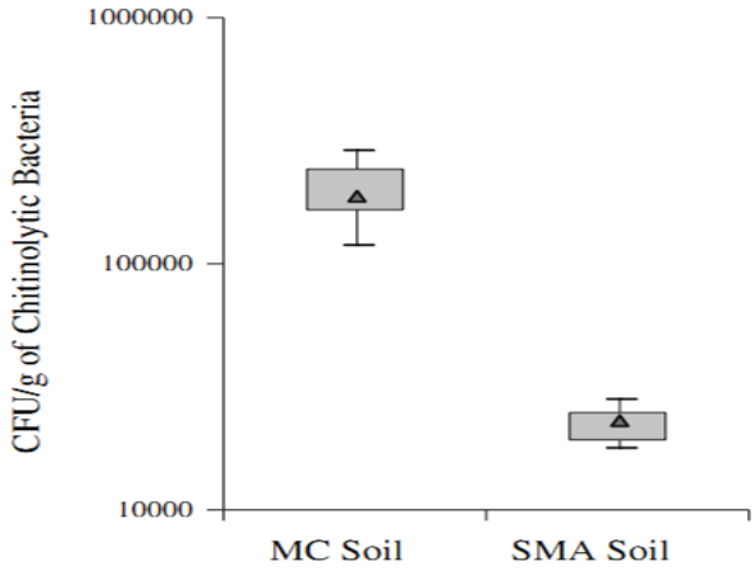

Fig. 3.2: Comparison of chitinolytic bacteria counts in MC and SMA soil. The data are presented as box plot diagrams, with the box comprising the range of values from 25th percentile (lower bar) and the 75th percentile (upper bar). The symbol 'triangle' within the box represents the median and the vertical lines below and above the box means the minimum and maximum values, respectively.

Molecular characterization based on 16S rRNA gene sequences (Fig. 3.3) showed that out of 27 isolates, 10 isolates showed 16S rDNA similarity with genus *Bacillus*, 6 with *Pseudomonas*, 10 with *Stenotrophomonas* and one with genus *Paenibacillus*, with more than 97% sequence similarity. The 16S rDNA sequences of ten isolates showing zone of clearance of ≥4 mm on colloidal chitin-containing agar plates were deposited in GenBank database with accession numbers GQ985501-GQ985504, GU187965-GU187968, GQ262777 and GQ266393.

The phylogenetic tree (Fig. 3.4) was constructed to determine the affiliation of chitinolytic bacterial isolates. Out of the 27 chitinolytic isolates, 16 Gram-negative isolates belonged to the class *Gammaproteobacteria* and 11 Gram-positive isolates belonged to class *Bacilli*. Among the *Gammaproteobacteria*, species of *Stenotrophomonas* appeared to be the most predominant genus followed by *Pseudomonas* (Table 3.1). Genus *Bacillus* was the predominant among the class *Bacilli* and was represented by species like *B. cereus*, *B. thuringiensis*, *B. licheniformis* and *Paenibacillus elgii* (Table 3.1).

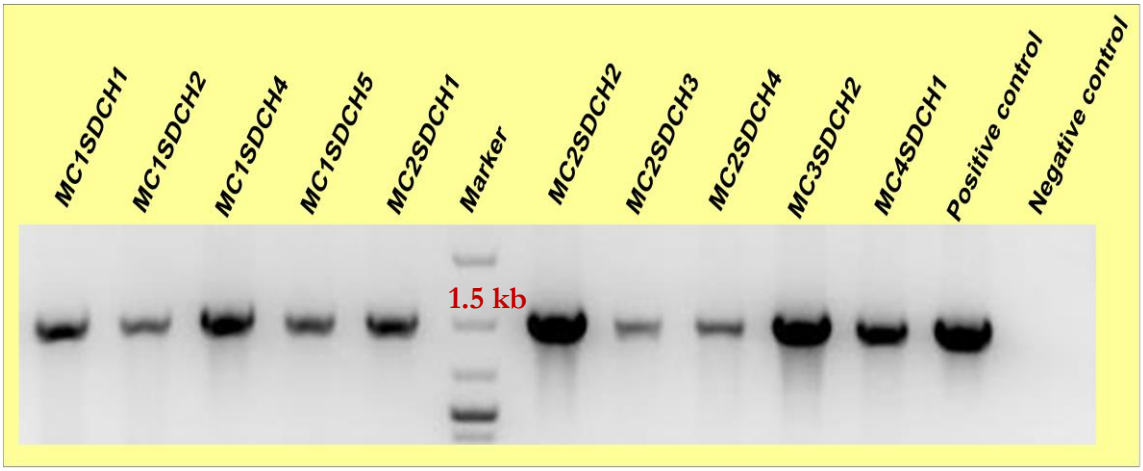

Fig. 3.3: PCR amplification of 16S rDNA of a few representative chitinolytic isolates.

Table 3.1: Morphological, biochemical and molecular characteristics of chitinolytic bacteria.

Sl. No.	Designation of chitinolytic Isolate	Source of soil sample	16S rDNA seq. similarity	Gram Staining	Shape	Indole test	Methyl red test	Voges Proskauer test	Citrate test	Catalase test	Starch hydrolysis
1	MC1SDCH1	Mahatani Chitosan	*Pseudomonas pseudoalkaligens*	-	Rod	-	+	-	+	+	-
2	MC1SDCH2	"	*Stenotrophomonas maltophila*	-	Rod	-	-	+	-	+	-
3	MC1SDCH4	"	"	-	Rod	-	-	+	-	+	-
4	MC1SDCH5	"	*Bacillus cereus*	+	Rod	-	+	+	+	+	+
5	MC2SDCH1	"	*Bacillus* sp.	+	Rod	-	+	+	+	+	+
6	MC2SDCH2	"	*Pseudomonas* sp.	-	Rod	-	+	-	+	+	-
7	MC2SDCH3	"	*P. pseudoalkaligens*	-	Rod	-	+	-	+	+	-
8	MC2SDCH4	"	"	-	Rod	-	+	ND	+	+	-
9	MC3SDCH2	"	*Stenotrophomonas* sp.	-	Rod	-	-	+	+	+	-
10	MC4SDCH1	"	"	-	Rod	-	-	+	+	+	-
11	MC1SDCH6	"	*Stenotrophomonas maltophila*	-	Rod	-	-	+	-	+	-
12	MC3SDCH3	"	"	-	Rod	-	-	+	-	+	-
13	MC3SDCH4	"	*Bacillus megaterium*	+	Rod	-	+	+	+	+	+
14	MC1SDCH7	"	*Bacillus* sp.	+	Rod	-	+	+	+	+	+
15	MC2SDCH5	"	"	+	Rod	-	+	+	+	+	+
16	MC3SDCH5	"	*Bacillus cereus*	+	Rod	-	+	+	+	+	+
17	MC2SDCH6	"	*S. maltophila*	-	Rod	-	-	+	-	+	-
18	MC1SDCH8	"	"	-	Rod	-	-	+	-	+	-
19	MC1SDCH9	"	*Stenotrophomonas* sp.	-	Rod	-	-	+	-	+	-
20	MC1SDCH10	"	"	-	Rod	-	-	+	-	+	-
21	MC2SDCH7	"	*Bacillus cereus*	+	Rod	-		+	+	+	+
22	SMA-1-SDCH01	S. M. Agritech	*Bacillus licheniformis*	+	Rod	-	-	+	+	+	+
23	SMA-1-SDCH02	"	*Paenibacillus elgii*	+	Rod	-	+	+	+	+	+
24	SMA-1-SRCH11	"	*Bacillus* sp.	+	Rod	-	+	ND	+	+	-
25	SMA-1-SRCH93	"	*Pseudomonas putida*	-	Rod	-	+	-	+	+	-
26	SMA-1-SRCH95	"	*Bacillus pumilus*	+	Rod	-	+	+	+	+	+
27	SMA-1-SRCH97	"	*Pseudomonas.sp*	-	Rod	-	+	-	+	+	-

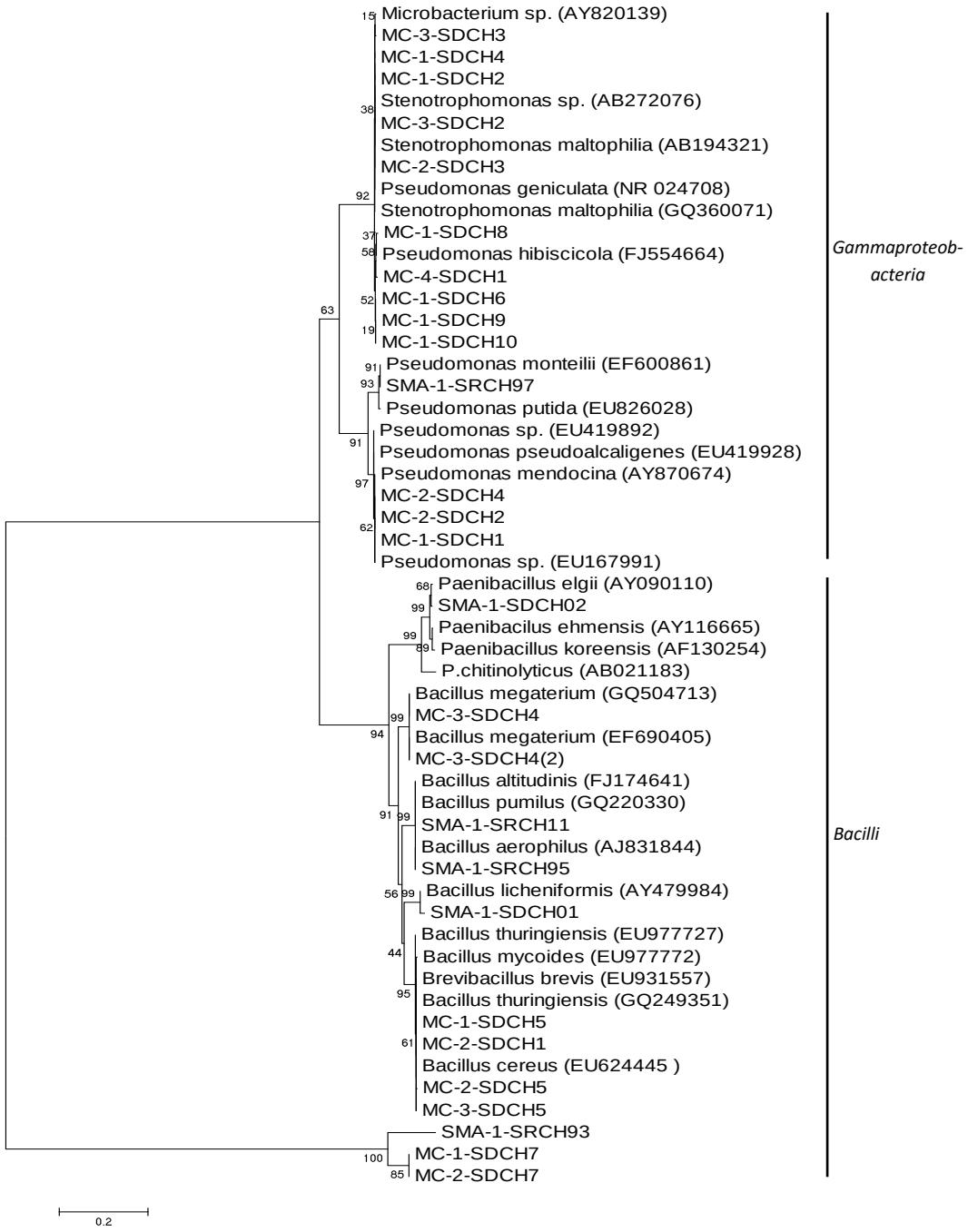

Fig. 3.4: Relationship of the chitinolytic isolates and selected reference strains based on the partial 16S rRNA gene sequences. The bacterial isolates from chitin-rich soils were designated by sampling site symbols (Table 3.1) and the selected reference strain sequences by species names followed by accession numbers. The tree was constructed by using MEGA 4. The numbers at the nodes indicate levels of bootstrap support based on neighbor-joining analysis of 1000 resampled data sets. Horizontal bar represents the number of nucleotide substitutions per site.

3.2.1.3 Identification of isolate SMA-1-SDCH02 based on full 16S rDNAsequence

BLAST results of the 16S rRNA gene sequence of SMA-1-SDCH02 showed maximum identity to the genus *Paenibacillus*. Based on sequence comparison and phylogenetic analysis of the 16S rDNA sequence of SMA-1-SDCH02 with 30 sequences of the nearest type species retrieved from EzTaxon (http://www.ezbiocloud.net/eztaxon), in addition to morphological and biochemical characteristics, it was concluded that the test strain was *Paenibacillus elgii* (Fig. 3.5).

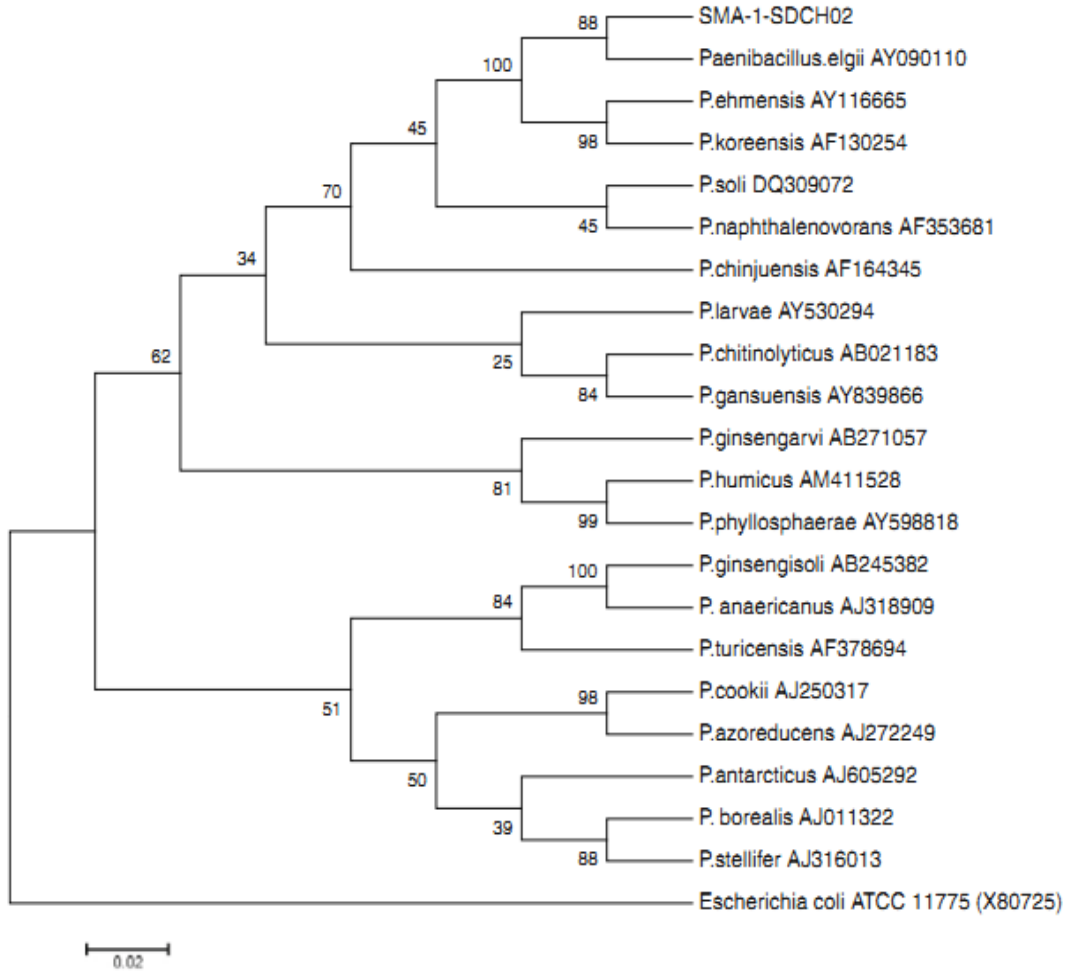

Fig. 3.5: Identification of isolate SMA-1-SDCH02. Phylogenetic tree, constructed using MEGA version 4, showing the position of isolate SMA-1-SDCH02 with other species of the genus *Paenibacillus* based on 16S rDNA full sequences. Bar, 0.02 accumulated changes per nucleotide. *E. coli* 16S rDNA sequence was used as an out group.

3.2.2 Evaluation of PGP activity of *P. elgii* SMA-1-SDCH02

Chitinolytic bacterial isolates showing a zone of clearance ≥3 mm were tested for their PGP traits *in vitro* (Table 3.2). The isolate SMA-1-SDCH02 was chitinolytic and antifungal apart from solubilising mineral phosphate, whereas SMA-1-SDCH01, although showed chitinolytic and antifungal activities, did not solubilize inorganic phosphate. SMA-1-SDCH03 solubilized mineral phosphate, besides being chitinolytic, but lacked antifungal activity. Therefore, we selected *P. elgii* SMA-1-SDCH02 to test for PGP activity.

Table 3.2: PGP-like traits of different bacterial isolates from two different sites. [a]Chitinolytic activity of the bacterial isolates, 3 mm or greater of the zone of clearance on M9 medium containing colloidal chitin after 5-6 days of incubation. [b]Antifungal activity by dual culture plate measured as zone of inhibition after 96 h of incubation at 27 ± 2°C. [c]Mineral phosphate solubilization (MPS) of the bacterial isolates was measured as zone of clearance on NBRIP medium after incubation for 7 days at 30°C. + = showing activity; - = showing no activity.

Designation of bacterial isolates	Source of soil sample	Chitinolytic activity[a]	Antifungal activity[b]	Mineral phosphate solubilization[c]
MC-1-SDCH6	Mahatani Chitosan	+	−	−
MC-3-SDCH10	"	+	−	−
MC-1-SDCH7	"	+	−	−
MC-2-SDCH8	"	+	−	−
MC-3-SDCH12	"	+	−	−
MC-3-SDCH14	"	+	−	−
MC-2-SDCH9	"	+	−	−
MC-1-SDCH8	"	+	−	−
MC-1-SDCH9	"	+	−	−
MC-1-SDCH11	"	+	−	−
SMA-1-SDCH01	S. M. Agritech	+	+	−
SMA-1-SDCH02	"	+	+	+
SMA-1-SDCH03	"	+	−	+

3.2.3 Evaluation of growth promotion in groundnut under greenhouse

Seed bacterization with *P. elgii* SMA-1-SDCH02 significantly improved the germination (Fig. 3.6) of groundnut seeds, both individually (72.30%) and in combination with

chitosan (75%) 6 DAS. Only chitosan-treated groundnut seeds also showed an increase in the germination (52.38%). The combined effect of chitosan and *P. elgii* was significant (P<0.05) but not remarkable.

The data presented in Fig. 3.6 suggested that both treatments - *P. elgii* alone and in combination with chitosan - significantly enhanced the growth of groundnut compared to control and chitosan-treated seeds. The greatest increase in root length (31.75%), fresh weight (31.75%), and total chlorophyll content (7.87%) was seen in plants treated with *P. elgii* with chitosan followed by *P. elgii* alone. The maximum increases in shoot height and dry weight (25.33 and 61.32%, respectively) were also recorded in seedlings treated with *P. elgii* and chitosan; however, they were not significantly different from those of *P. elgii* treated seedlings.

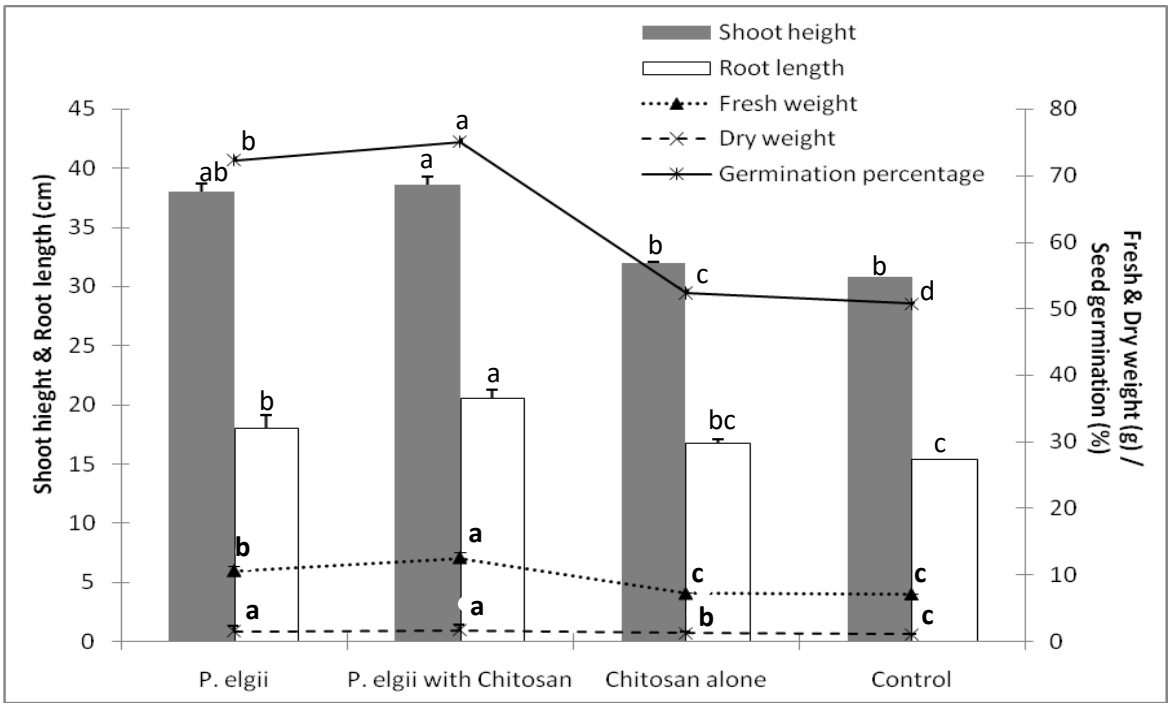

Fig. 3.6: Effect of *P. elgii* with or chitosan on germination and growth of groundnut seeds. Seed germination percentage was recorded 6 DAS. Shoot height and root length were measured in cm while fresh weight and dry weight were measured in terms of g 25 DAS. Groundnut seeds bacterized with *P. elgii* with or without chitosan were raised in plastic pots filled with soil in green house. Treatments consisted of five replicate pots containing three seeds each and were repeated twice. Data represent the mean (±SD, n = 15) of the two independent experiments. Different letter on each bar represents values that are statistically different ($P_{0.05}$). The vertical bars indicate standard error.

3.2.4 Evaluation of growth promotion in tobacco under gnotobiotic condition

The growth of tobacco seeds bacterized with *P. elgii* SMA-1-SDCH02 was highly significant under gnotobiotic conditions after 25 days of growth. An increase in shoot height (55.90%), root length (72.17%), and dry weight (91.52%) over control was observed (Fig. 3.7).

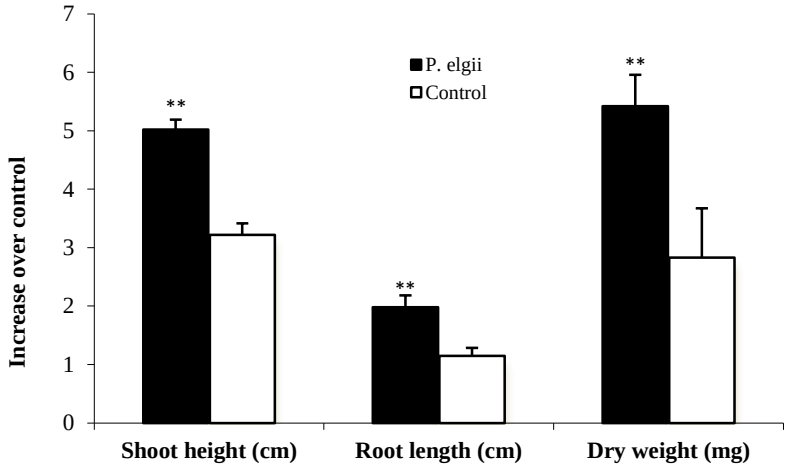

Fig. 3.7: Effect of *P. elgii* on tobacco seedlings after 25 days. Shoot height and root length were measured in cm while dry weight was measured in terms of g. Tobacco seeds bacterized with *P. elgii* were grown in gnotobiotic set-up. Treatments consisted of six replicates and were repeated thrice. Data represent the mean (±SD, $n = 18$) of the three independent experiments. '**' denotes statistically highly significant at $t_{0.01}$.

3.3. Discussion

Characterization of extracellular microbial enzymes including chitinases has received increased attention because of their wide range of applications (Bhattacharya et al., 2007). Chitin-containing organisms like fungi and insects produce chitinases for their growth and development, whereas bacteria produce chitinases in their saprophytic phase to derive carbon and nitrogen from chitin. A requirement for efficient bioconversion of chitin into useful products led to the identification of chitinolytic microorganisms from different habitats including soil.

Soil composition and type is the primary determinant of the composition of total and active bacterial communities in soils (Girvan et al., 2003). We have isolated several chitinolytic bacterial strains from soil collected from waste dump yards of the chitin and mushroom production industries, which had, at least, ten years of production history. Soil collected sites were dumped with daily waste usually containing with some amount of chitin, which enriched these soils for chitinolytic microorganisms. Chitinolytic bacterial counts of MC soil were more than SMA soil (Fig. 3.2). The observed difference could be attributed to the amount of chitin and their diverse forms in MC soil, which was exposed to different type of crustaceans containing a higher amount of chitin in their shells (Kurita, 2006). We have also observed bacteria that were able to degrade chitin comprised 21 and 15% of a total number of culturable bacteria of the MC and SMA soil, respectively. Kamil et al. (2007) observed only 5% of chitinolytic bacteria out of 400 culturable bacteria isolated from rhizosphere soil of maize and wheat. Our observation of a higher percentage of chitinolytic bacteria in MC and SMA soils could be attributed to the chitin enrichment. Poulsen et al. (2008) also reported that soils amended with chitin affected the chitinolytic bacterial population and also increased chitinase activity in soil.

Since chitinases can diffuse through agar, assays to identify chitinolytic bacteria producing chitin-degrading enzymes were performed by monitoring the degradation of polymeric chitin incorporated into an agar medium (Howard et al., 2003). The larger and clear zone of chitin hydrolysis was attributed to the chitinolytic ability of the bacteria. Even though the plate method was considered to be a preliminary quantitative test, with limited sensitivity, still it represents a widely acceptable, straightforward and inexpensive method that would selectively differentiate the chitinolytic bacteria from the pool of bacterial diversity. In the present study, a total of 140 bacterial cultures were isolated from both MC and SMA soil, among which only 27 isolates showed chitinolytic ability *in vitro* on chitinase detection agar medium (Fig. 3.1). Cody (1989) used a similar method for detection of chitinolytic bacteria representing species of *Bacillus* that were chitinolytic. Microorganisms isolated from phytosphere of peanut

plants and Kimchi juice were also selected for their chitinolytic ability based on the clear zone on the colloidal chitin plate (Kishore et al., 2005a; Kim et al., 2007).

The analysis of 16S rRNA gene sequences of the bacterial cultures isolated from both MC and SMA soil revealed that a majority of the isolated chitinolytic microorganisms belonged to the genus *Bacillus* and *Stenotrophomonas*. This was expected since members of the genus *Bacillus* were frequently recovered during enrichment of chitin-degrading microorganisms from soil (Cody et al., 1989; Nishimura et al., 2005). The chitinolytic bacterial community of such soils was clearly dominated by the class *Gammaproteobacteria* though *Bacillus* was found to be one of the dominant genera, as observed earlier by Smit et al. (2001) that the soil with a high content of readily available nutrients showed positive selection for *Alpha* and *Gammaproteobacteria*.

A collection of diverse types of chitinolytic strains would help in the selection of highly efficient chitinolytic strains having several biotechnological applications. Results in the present study showed that soils dumped with chitin wastes were dominated by chitinolytic *Bacillus*, *Stenotrophomonas* and *Pseudomonas* species. These chitinolytic microbes and enzymes associated with chitinolysis might play a role in the de novo generation of bioactive molecules having industrial importance. Furthermore, to our knowledge this study is the first report on assessing the chitinolytic bacterial diversity of soils from chitin production industries.

The ability of PGPR, isolated from the rhizosphere of crop plants, to promote plant growth and induce resistance in various crops is known (Podile & Kishore, 2006). The bacteria isolated from sources other than rhizosphere also hold potential for improving plant growth when applied as seed treatments (Kishore et al., 2005c). Of the 27 chitinolytic bacterial strains isolated from chitin-rich soil, the isolate *Paenibacilluselgii* SMA-1-SDCH02showed highly significant growth enhancement in groundnut in terms of shoot height, root length, fresh and dry weight besides increasing the total chlorophyll content in the leaves (Fig. 3.6).The growth promoting effect of *P. elgii* was confirmed in tobacco under gnotobiotic condition (Fig. 3.7). *P. elgii*

isolate SMA-1-SDCH02 solubilized mineral phosphate apart from chitinolytic and antifungal activities.

Phosphorous is one of the major nutrients present in soil in the form of insoluble phosphates which the plants are unable to utilize as such. PGPR solubilize precipitated phosphates and enhance phosphate availability to different crops that represent a possible mechanism of plant growth promotion under field conditions (Verma et al., 2001). *P. elgii* selected through the screening process displayed MPS activity and also showed antifungal activity (Table 3.1), which will enhance the application as a biocontrol PGPR.

Most of the bacterial strains from chitin-rich soils showed considerable chitinolytic activity. The extracellular chitinolytic enzymes produced by the biocontrol agents lyse chitin (Podile & Prakash, 1996), a major constituent of fungal cell walls, thereby playing a significant role in the management of phytopathogenic fungi indirectly improving growth of crop plants. The chitinolytic potential of bacterial inoculants would help in developing formulations with longer shelf life and more effective when used in combination with chitin/chitosan.

Although *P. elgii* SMA-1-SDCH02 was not isolated from plant parts, it had tremendous potential in plant growth promotion and antifungal activities similar to other reported PGPR strains. This provides ample scope of utilizing bacterial strains from unconventional sources, especially chitin-rich soils (with an added quality of chitinolysis), to facilitate plant growth directly or indirectly. Bacteria, including *Bacillus* and *Paenibacillus*, isolated from soils used as rhizosphere inoculum and successfully improved plant growth besides controlling diseases (von der Weid et al., 2003). The efficiency of *P. elgii* in this study demonstrated that the unconventional sources harbour potential PGP bacteria to develop bioformulations to increase crop yields and reduce disease.

Chapter IV

Characterization of chitinases from *Paenibacillus elgii* and improvement of transglycosylation (TG) by site-directed

4.1. Introduction

Bacterial chitinolysis, the process of degradation of chitin by enzymatic hydrolysis, is important in recycling the vast amounts of chitin waste in the environment. The chitinous waste, which poses environmental problems, could be converted to useful products for several biotechnological applications by adopting enzymatic methods. The chitinolytic enzymes associated with chitinolysis could be used as powerful tools to utilize the chitin biomass to generate products that have commercial importance. Therefore, chitinolytic bacteria and their chitinases are of considerable economic and environmental significance.

In addition to the hydrolytic ability, some of the GH18 family chitinases show inherent TG activity. The TG property of chitinases has immense potential in synthesising longer chain COS. But, lack of availability of suitable enzymes with higher TG activity limits such application. Although chemical synthesis of long chain COS is feasible, it requires selective protection and subsequent manipulation of various monosaccharide donors and acceptors making the process cumbersome and costly (Kanie et al., 1994; Aly et al., 2001). Therefore, enzymatic synthesis employing the TG activity of chitinases may be exploited as a better biological tool for a large-scale production of bioactive compounds from chitin.

GH18 family chitinases with TG ability were reported in bacteria (Neeraja et al., 2010; Purushotham & Podile, 2012), fungi (Lü et al., 2009), cycads (Taira et al., 2009) and plants (Ohnuma et al., 2011a; Ohnuma et al., 2011b). Chitotriosidase from human macrophages generated TG products up to DP6–9from a DP5 substrate (Aguilera et al., 2003).The main drawback in using chitinases with meager inherent TG was that the product of the TG reaction unavoidably serves as a substrate for the enzyme, which can result in reduced yield of longer chain COS. To overcome the problem of lower yield of longer COS, targeted mutagenesis of TG chitinases that would have reduced hydrolytic activity may be employed. Till today, only one chitinase from *S. proteamaculans* (*Sp*ChiD) belonging to GH18 was reported to be a hyper-TG chitinase (Purushotham & Podile, 2012).

There is a need to explore the chitinolytic potential and to identify novel chitinases from microbes for better utilisation of chitin/chitosan. Further, understanding the mechanism of action of chitinases might provide novel tools to improve substrate accessibility. This, in turn, would help to design a more efficient enzymatic process for the better exploitation of the second most abundant biopolymer to generate bioactive COS. The chitinolytic machinery of *P. elgii* SMA-1-SDCH02 seems to be complex with seven different chitin/chitosan degrading enzymes with diverse domain architecture (Fig. 4.1).

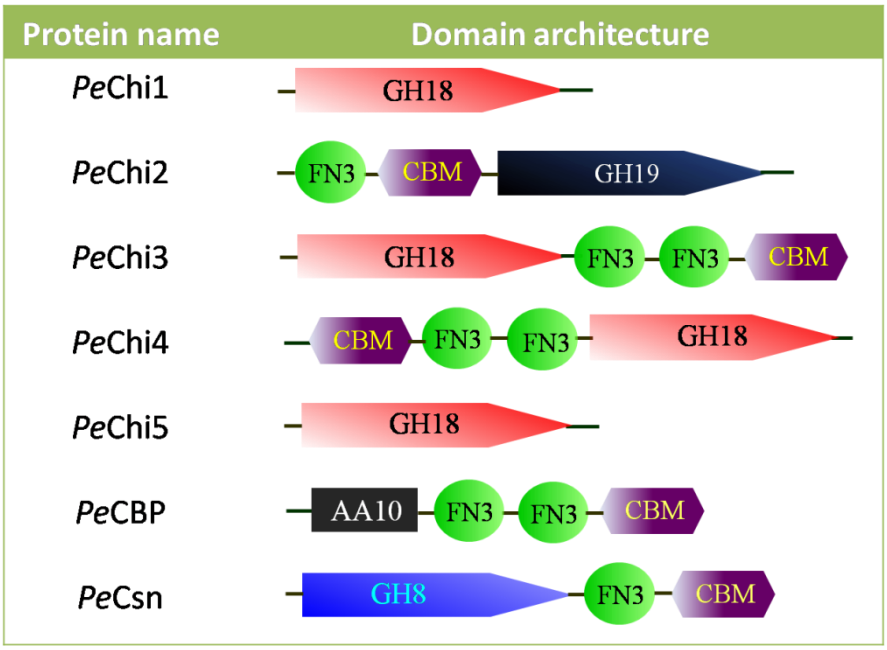

Fig. 4.1: The chitinolytic machinery of *P. elgii* SMA-1-SDCH02. Domain search of the deduced amino acid sequence obtained after sequencing of the cloned chitin/chitosan degrading genes showing diverse domain architecture. *P. elgii* SMA-1-SDCH02 possesses four GH18 and one GH19 chitinases, a GH8 chitosanase and a chitin binding protein (CBP) classified as Auxiliary Activity family 10 (AA10).

This chapter describes the efforts made towards understanding several aspects of *P. elgii* chitinases to address the following questions:

1. Do the chitinases of *P. elgii* differ in their mode of action?

2. What is the structural and functional difference in *P.elgii* chitinases with respect to the degradation of chitin/chitosan substrates?
3. Do the chitinases of *P. elgii* have TG activity?

To determine the mode of action and to identify chitinases withTG ability for longer chain COS synthesis, characterization offour GH18 chitinases (*Pe*Chi1, *Pe*Chi3, *Pe*Chi4, and Chi5) was carried out (Studies on chitinase belonging to GH19 (*Pe*Chi2) and CBP are not part of the thesis). As *Pe*Chi1 showed a weak TG activity, an attempt was also made to improve the TG activity both in terms of increasing the quantity of TG products and in extending the duration of TG activity by site-directed mutagenesis.

4.2. Results

4.2.1 Cloning, expression and purification of *Pe* chitinases

P. elgii chitinases (*Pe*Chi1, *Pe*Chi3, *Pe*Chi4 and *Pe*Chi5) were amplified using gene specific primers with *Pe* gDNA as template. Three of the chitinase genes, except *Pechi5*, were predicted (http://www.cbs.dtu.dk/services/SignalP/) to contain N-terminal leader peptide-encoding nucleotide sequences.All four genes were cloned without the signal peptide-encoding nucleotides (*Pechi1*: 57 bp, *Pechi3*: 99 bp and *Pechi4*: 72 bp). The amplicons, 1.1 kb of *Pechi1* and 0.9 kb of *Pechi5*were cloned in pET-28a(Fig. 4.2A).The amplicons, 1.8 kb of *Pechi3*and 2.2 kb of *Pechi4* were cloned in pET-22b(Fig. 4.2A). The clones were confirmed by double digestion with appropriate restriction enzymes (Fig. 4.2B).The insert sequence was confirmed by automated DNA sequencing. Protein BLAST at NCBI for the deduced amino acid sequences of *Pe*Chi1, *Pe*Chi3, *Pe*Chi4 and *Pe*Chi5 displayed 95%, 96%, 97% and 98% identity, respectively to chitinases of *P.elgii* B69 (Ding et al., 2011).

All the four *P. elgii* chitinase genes were over expressed with C-terminal His-tag in *E. coli*. The expressed chitinases were obtained in soluble form from whole celllysate. The proteins were purified using Ni-NTA agarose chromatography. SDS-PAGE analysis (Fig. 4.3) of purified chitinases revealed a molecular mass of 44, 63, 70 and 37 kDa which correspond to *Pe*Chi1, *Pe*Chi3, *Pe*Chi4 and *Pe*Chi5, respectively.

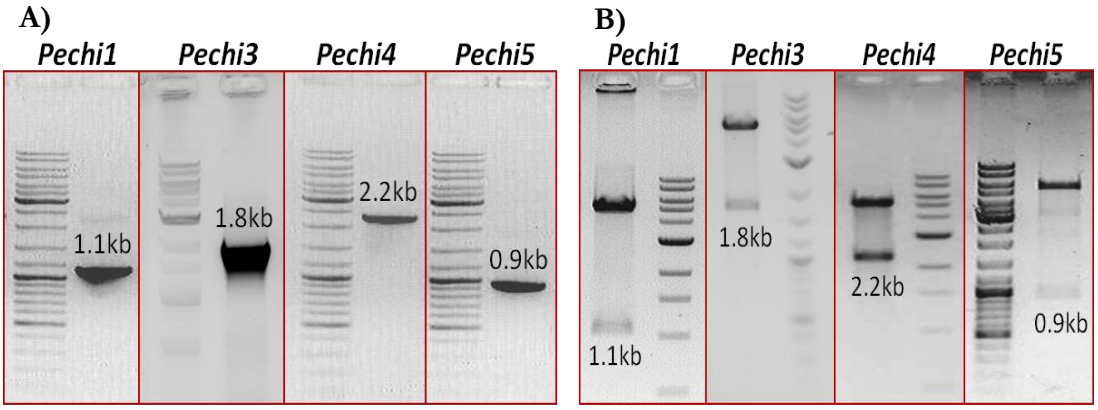

Fig. 4.2: Amplification and cloning of chitinases from *P. elgii* SMA-1-SDCH02. Chitinases of *P. elgii* (*Pechi1, Pechi3, Pechi4* and *Pechi5*) were PCR-amplified with gene specific primers using gDNA as a template and resolved on a 1% agarose gel **(A)**. The presence of insert was confirmed by double digestion with *Eco* RI and *Xho* I for *Pechi1* and *Pechi3*, *Nco* I and *Xho* I for *Pechi4*, and *Bam* H1 and *Xho* I for *Pechi5* **(B)**. The molecular weight marker was DNA ladder mix from Fermentas (100 bp-10 kb) and 1 kb DNA ladder (0.5 kb-10 kb) from NEB.

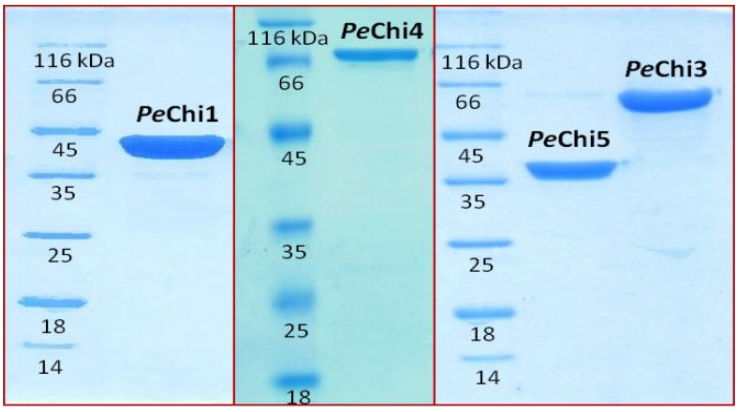

Fig. 4.3: Purification of *P. elgii* chitinases. Recombinant *Pe*Chi1, *Pe*Chi3, *Pe*Chi4 and *Pe*Chi5 were purified using Ni-NTA agarose chromatography. Elution buffer containing 250 mM imidazole was used to elute chitinases from the column and loaded on 12% SDS-PAGE followed by staining with Coomassie brilliant blue G-250. The molecular weight (Mw) of the protein markers is indicated in kDa.

4.2.2. Characterization of *Pe* chitinases

4.2.2.1 Effect of pH

Enzyme assay with different pH range buffers showed that *Pe*Chi1, *Pe*Chi3 and *Pe*Chi5 had optimum activity in sodium phosphate buffer pH 6.0 while *Pe*Chi4 had optimum

activity in sodium acetate buffer pH 5.0 (Fig. 4.4). *Pe*Chi1 was active over a broad pHrange between 5.0-9.0, and the activity was less than half maximum below pH 5.0. *Pe*Chi3 retained above 60% of its activity between pH 5.0 to10.0 and lost activity at pH ≤ 4.0.*Pe*Chi4 was active over the pH range between 3.0-8.0 with negligible activity at pH 9.0 and 10.0. *Pe*Chi5 showed 50% of its maximum activity between pH 5.0 to 9.0 and completely lost activity at pH 2.0.

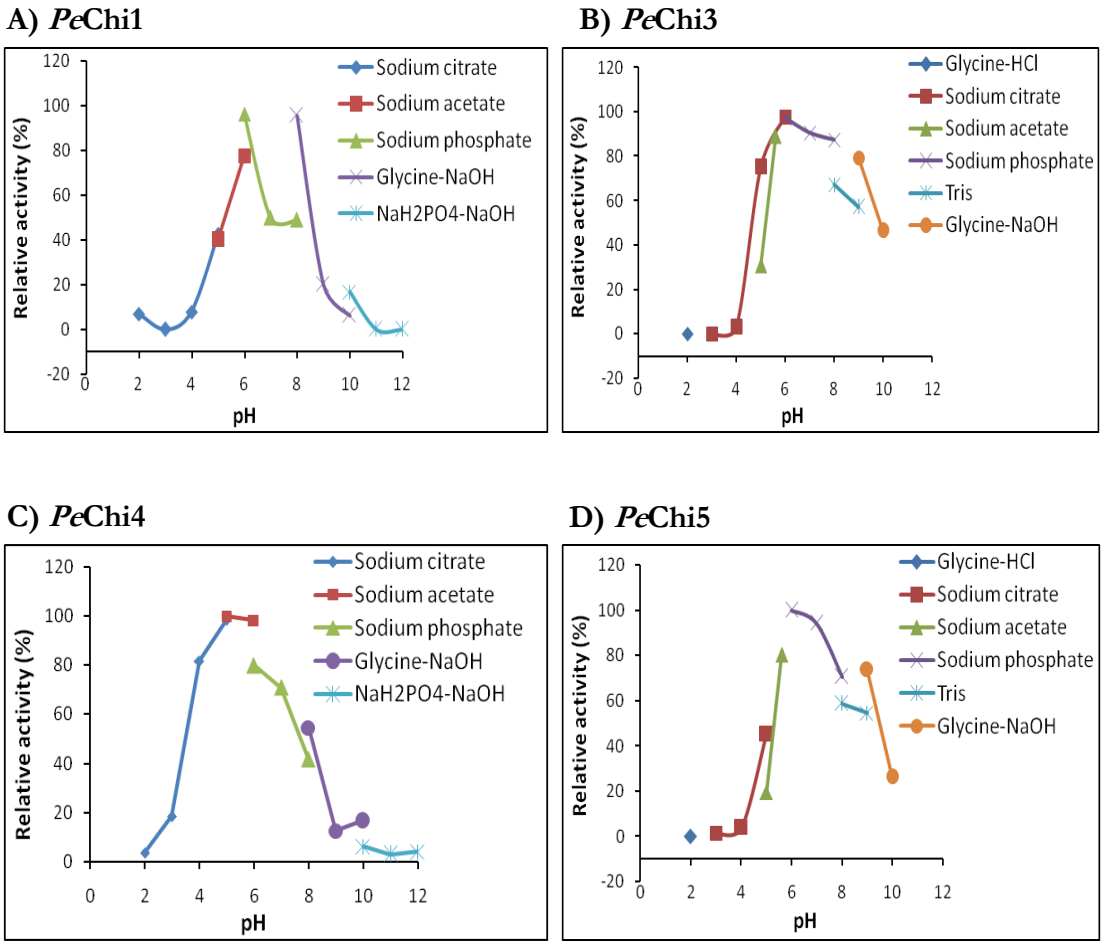

Fig. 4.4: Optimum pH for activity of *Pe* chitinases. The optimal pH of *Pe* chitinases was determined by incubating the enzymes (*Pe*Chi1: 20 µg, *Pe*Chi3-*Pe*Chi4: 5 µg and *Pe*Chi5: 40 µg) with colloidal chitin (20 mg.ml^{-1}) at 40°C for 1 h in 50 mM of different buffers pH ranging from 2-12 and the relative activity (%) was determined under standard assay condition. **A-D:** pH optima for *Pe*Chi1, *Pe*Chi3, *Pe*Chi4, *Pe*Chi5.

4.2.2.2 Effect of temperature

The *Pe* chitinases were incubated with colloidal chitin at different temperatures (20-

80°C) to determine the optimum temperature. *Pe*Chi1 and *Pe*Chi5 had temperature optima at 40 and 50°C, respectively, whereas *Pe*Chi3 and *Pe*Chi4 showed maximum activity at 60°C (Fig. 4.5). The activity of all four enzymes decreased by nearly half of the maximum activity at temperature above 60°C. *Pe*Chi3 retained more than 80% activity over a broad temperature range of 20-60°C and retained more than 50% activity at 70°C. All the four chitinases showed below 20% activity at 80°C.

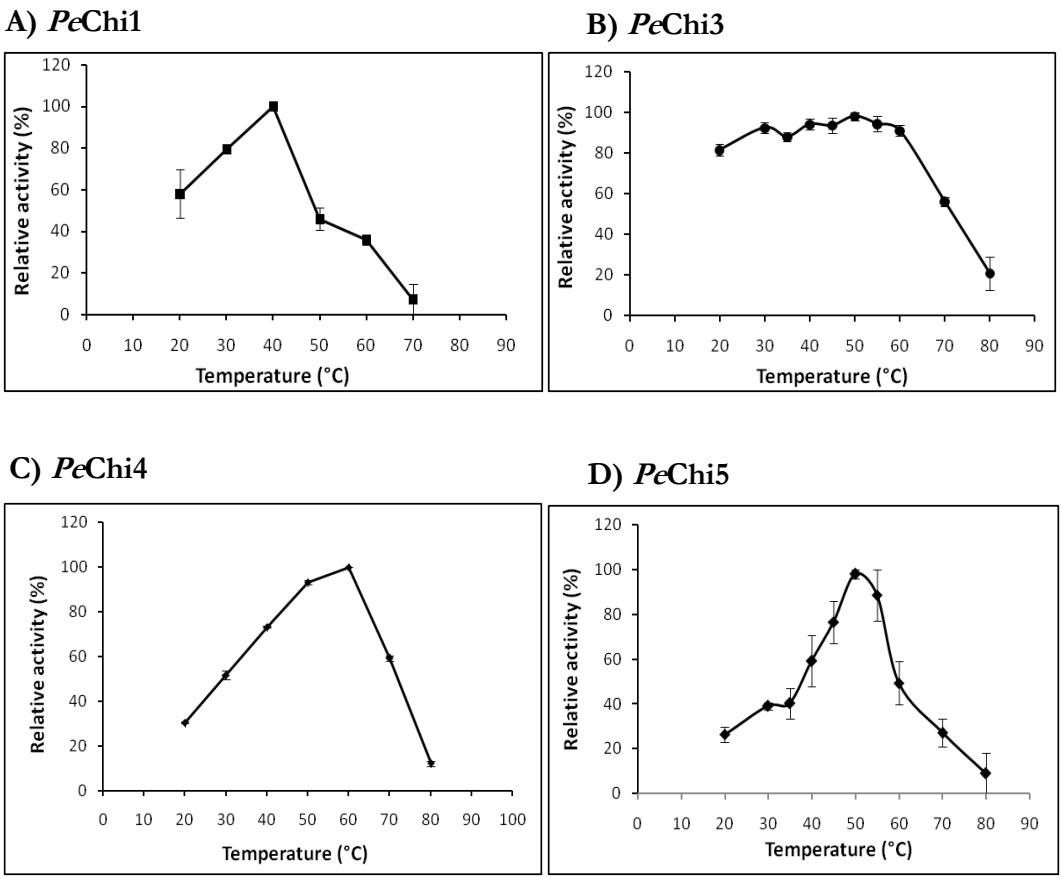

Fig. 4.5: Optimum temperature for activity of *Pe* chitinases. The optimum temperature for *Pe* chitinases was obtained by incubating the enzymes (*Pe*Chi1: 20 µg, *Pe*Chi3-*Pe*Chi4: 5 µg and *Pe*Chi5: 40 µg) with colloidal chitin (20 mg.ml^{-1}) in 50 mM buffers at optimum pH for 1 h at different temperatures ranging from 20-80°C. Relative activity (%) was determined under standard assay condition. Vertical bars represent the standard deviation of triplicate experiments. **A-D:** temperature optima for *Pe*Chi1, *Pe*Chi3, *Pe*Chi4, *Pe*Chi5.

4.2.2.3 Steady state kinetics analysis

The activity of chitinases (µmoles.min^{-1}) obtained by reducing end assay and the varying substrate concentration (mg.ml^{-1}) were fitted to the Michaelis-Menten equation

(Fig. 4.6 and Table 4.1). The curve fitting for the enzymes showed highest V_{max} value for *Pe*Chi3 (3.377×10^{-2}) followed by *Pe*Chi4 (2.142×10^{-2}), *Pe*Chi1 (0.4301×10^{-2}) and *Pe*Chi5 (0.2358×10^{-2}). The K_m for *Pe*Chi4 (0.726) was the lowest in comparison to *Pe*Chi3 (29.26), *Pe*Chi5 (45.14) and *Pe*Chi1 (84.58) indicating the substrate-binding affinity of *Pe*Chi4 was the highest among the three chitinases.*Pe*Chi4 had the highest (412.887) overall catalytic efficiency (k_{cat}/K_m) when compared to *Pe*Chi1 (0.109), *Pe*Chi3 (15.003) and *Pe*Chi5 (0.045).

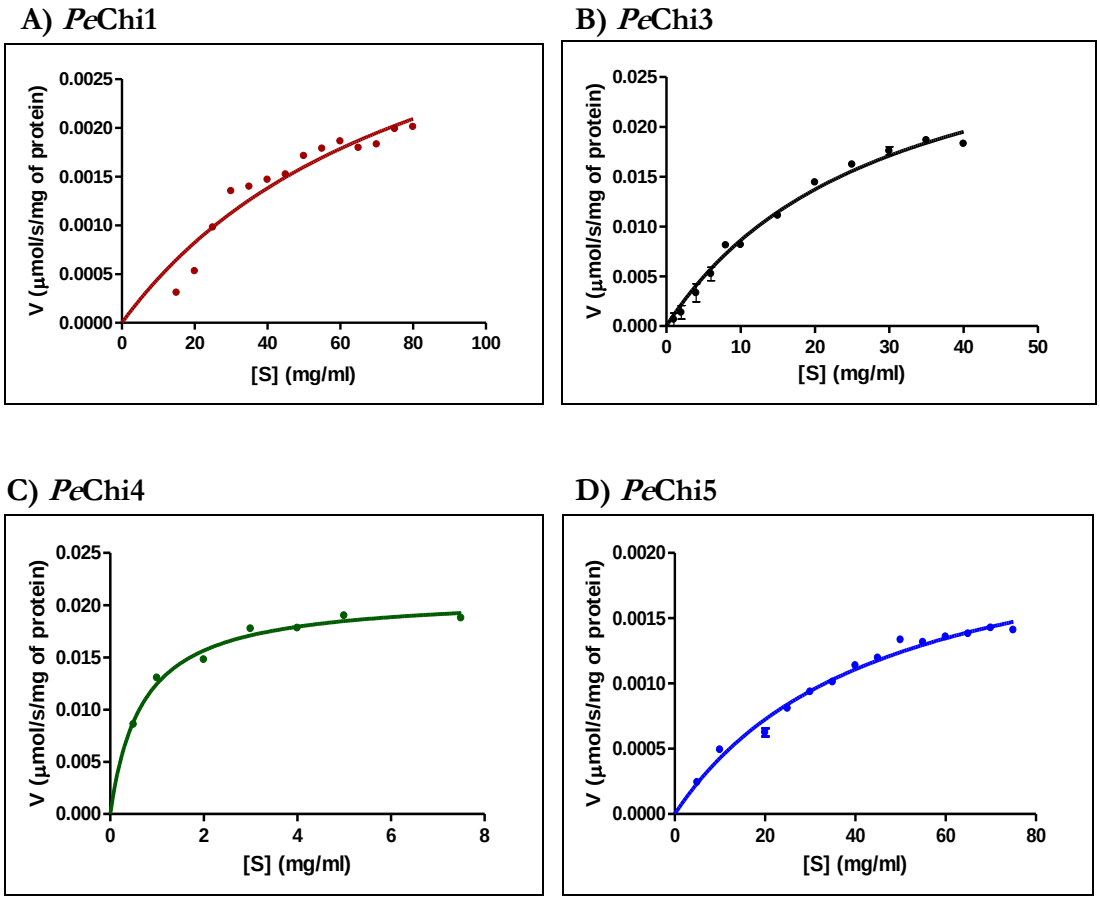

Fig. 4.6: Kinetic analyses of *Pe* chitinases. Kinetic studies of *Pe* chitinases were done by estimating reducing sugars generated from colloidal chitin. Varying concentration of substrate (*Pe*Chi1 and *Pe*Chi5: 5-80 mg.ml^{-1}, and *Pe*Chi3 and *Pe*Chi4: 1-40 mg.ml^{-1}) was incubated with *Pe* chitinases (Chi1: 20 µg, Chi3: 3 µg, Chi4: 5 µg and Chi5: 40 µg) in 50 mM buffer with respective controls in triplicates at optimum pH and temperature for 2 h at 190 rpm. Specific activity in µmol.sec^{-1}.mg^{-1} of protein was calculated and plotted against substrate concentration. The data was fitted to the Michaelis-Menten equation by nonlinear regression function using GraphPad Prism software version 5.0 to construct the kinetic graph and derive kinetic parameters. **A-D:** Curve fitting for *Pe*Chi1, *Pe*Chi3, *Pe*Chi4, *Pe*Chi5.

Table 4.1: Kinetic parameters of colloidal chitin hydrolysis by *Pe* chitinases.

Enzyme	V_{max} (μmol.s^{-1}.mg^{-1})	K_m (mg.ml^{-1})	k_{cat} (s^{-1})	k_{cat}/K_m (mg^{-1}.ml.s^{-1})
*Pe*Chi1	0.4301×10^{-2}	84.58	9.24	0.109
*Pe*Chi3	3.377×10^{-2}	29.26	439.01	15.003
*Pe*Chi4	2.142×10^{-2}	0.726	299.88	412.887
*Pe*Chi5	0.2358×10^{-2}	45.14	2.06	0.045

3.2.2.4 Hydrolytic activity on polymeric substrates

To find the substrate specificities of *Pe* chitinases, the hydrolytic activity with different polymeric substrates was compared. Purified *Pe*Chi1, *Pe*Chi4 and *Pe*Chi5hydrolysed colloidal chitin more efficiently among the other polymeric substrates, while *Pe*Chi3 showed nearly equal activity on both colloidal chitin and chitosan with 90% DDA (Fig. 4.7). The *Pe*Chi1 and *Pe*Chi4 preferred β-chitin as substrate, next to colloidal chitin while *Pe*Chi5 showed second preference to chitosan with 90% DDA. *Pe*Chi1 had no activity towards chitosan with 90% DDA. Among all the polymeric substrates used, *Pe*Chi4 had the lowest activity towards chitosan. The α-chitin was the least preferred substrate by the four *Pe* chitinases. With α-chitin, *Pe*Chi4 had the highest activity followed by *Pe*Chi3, *Pe*Chi1. *Pe*Chi5 displayed no activity on α-chitin.The order of the substrate preferences for the four *Pe* chitinases was as follows: *Pe*Chi1: colloidal chitin>β-chitin>glycol chitin>α-chitin. *Pe*Chi3: colloidal chitin>chitosan>β-chitin>glycol chitin>α-chitin. *Pe*Chi4: colloidal chitin>β-chitin>glycol chitin>α-chitin>chitosan.*Pe*Chi5: colloidal chitin>chitosan>glycol chitin>β-chitin.

4.2.2.5 Hydrolytic activity on colloidal chitin

To assess the ability and effectiveness in hydrolysing the natural substrates and to get insight into the mode of action, the hydrolytic products generated by *Pe* chitinases were analyzed using HPLC. The hydrolytic activity of *Pe* chitinases was studied using colloidal chitin as substrate at various incubation times. HPLC profiles suggested that all the four *Pe* chitinases released DP2 as predominant product at the end of the

reaction (Fig. 4.8). In the initial reaction period, the DP2 and DP3 were detected for all four chitinases, but DP4 was also detectedfor*Pe*Chi1 and *Pe*Chi5. During the reaction time course, DP4 intermediate products generated by *Pe*Chi1 and *Pe*Chi5 were further hydrolyzed into DP2, whereas DP3 intermediates were converted to DP2 and DP1 by *Pe*Chi3, *Pe*Chi4 and *Pe*Chi5 (Fig. 4.9). The formation of DP1 was the highest for *Pe*Chi4. In case of *Pe*Chi1, formation of both DP2 and DP3 gradually increased till 720 min and DP4 remained till 720 min.

4.2.2.6. Hydrolytic activity of *Pe* chitinases on oligomeric chitin substrates

The ability and efficiency of *Pe* chitinases to degrade oligomeric substrates were assessed analysing the hydrolytic products formed in the course of their action (Fig. 4.10A-D). Up to 720 min of incubation with *Pe*Chi1, there was no hydrolytic product detected in reaction mixtures with DP3 substrate. DP3 was hydrolysed completely into DP2and DP1 by *Pe*Chi3 and *Pe*Chi4, whereas DP3 hydrolysis was incomplete even at 720 min by *Pe*Chi5. *Pe*Chi3 had rapid hydrolytic rate on DP3 and degraded DP3 completely within 10 min. With DP4 substrate, DP2 was detected as sole major end product from *Pe*Chi1-Chi5 enzymes. Degradation rate of DP4 by *Pe* chitinases was in the order of *Pe*Chi3>*Pe*Chi4>*Pe*Chi5>*Pe*Chi1.

When DP5 was used as substrate, *Pe*Chi3, *Pe*Chi4 and *Pe*Chi5 released DP2 as majour end product, while *Pe*Chi1 released both DP2 and DP3 (Fig. 4.10A-D). *Pe*Chi3, *Pe*Chi4 and *Pe*Chi5 released DP3 as intermediate product, which was present 120, 60 and 120 min, respectively and further hydrolyzed into DP2 and DP1. On the other hand, *Pe*Chi1 also released intermediate hydrolytic products (DP2-DP4) and longer chain (DP7) transglycosylation (TG) products. Degradation rate of DP5 by *Pe* chitinases was in the order of *Pe*Chi3>*Pe*Chi4>*Pe*Chi1≥*Pe*Chi5. The hydrolysis of DP6 by all the *Pe* chitinases yielded DP2, DP3 and DP4 as intermediate products and resulted in DP2 as major end product. Substrate degradation rate was in the following order: *Pe*Chi3>*Pe*Chi4≥*Pe*Chi1>*Pe*Chi5.

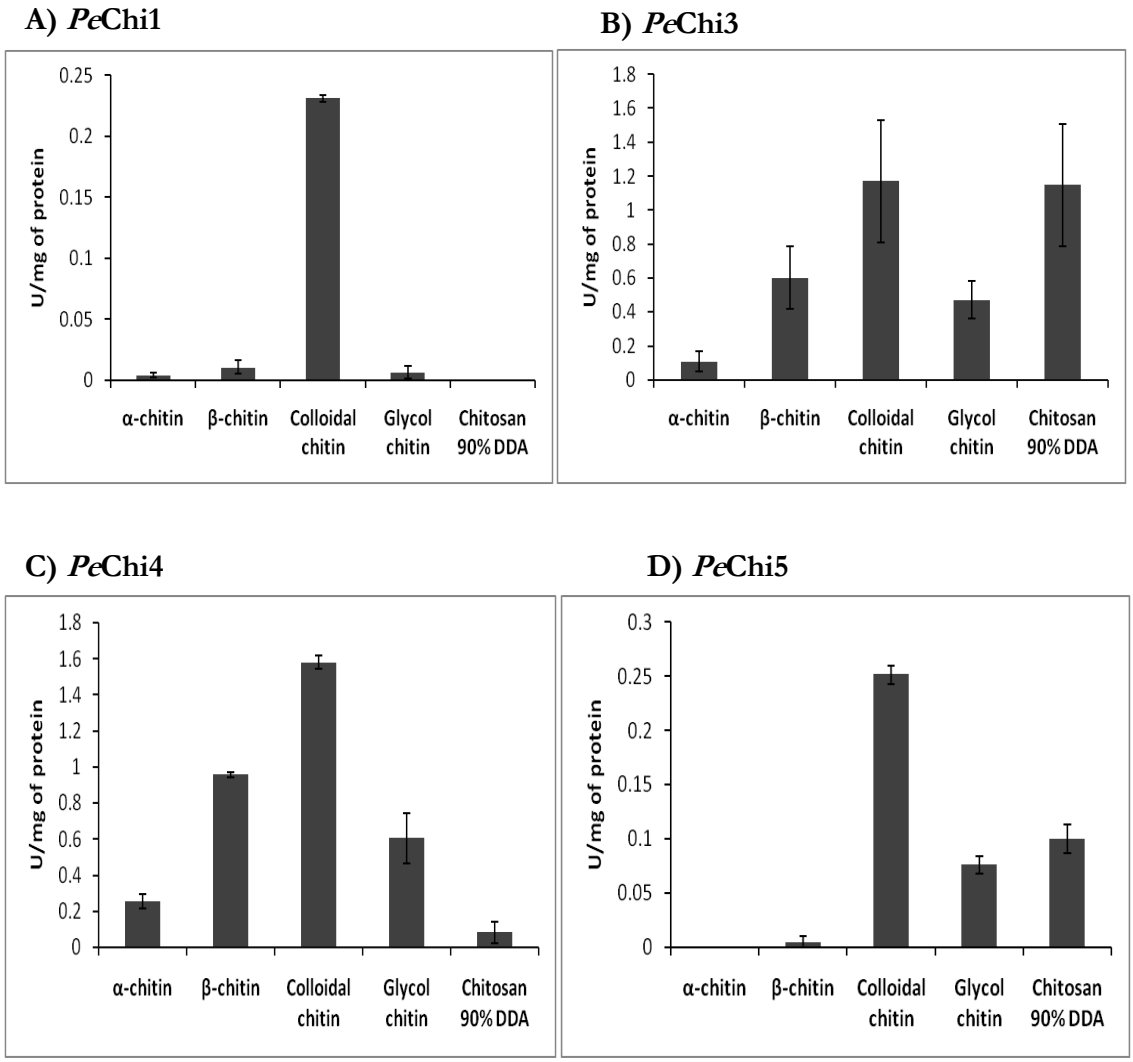

Fig. 4.7: Substrate specificity of *Pe* chitinases. The reaction mixture containing *Pe* chitinases (Chi1: 20 µg, Chi3 and Chi4: 5 µg and Chi5: 40 µg) and indicated polymeric substrates (2 %, w/v) were incubated in 50 mM buffer at optimum temperature for 1 h. The reaction was monitored by reducing sugar estimation. One unit of chitinase activity was defined as the amount of enzyme that produces 1 µmol of reducing sugar per minute. Vertical bars represent standard deviation of triplicate experiments. **A-D:** Substrate specificity for *Pe*Chi1, *Pe*Chi3, *Pe*Chi4, *Pe*Chi5.

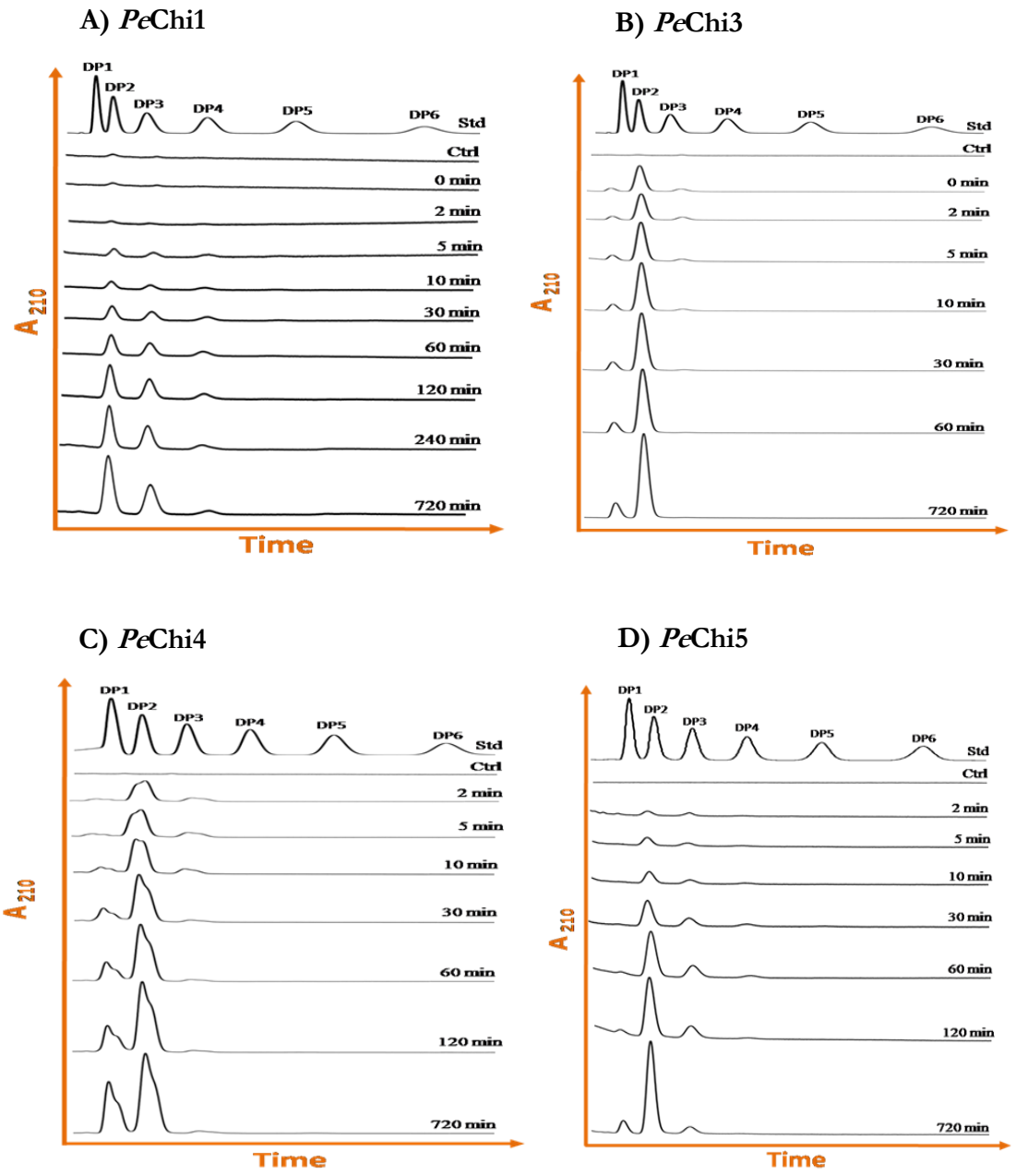

Fig. 4.8: Time course of colloidal chitin hydrolysis by *Pe* chitinases. The reaction mixture (1 ml) containing colloidal chitin (20 mg.ml^{-1}) in 50 mM buffer was incubated with *Pe* chitinases (*Pe*Chi1: 450 nM, *Pe*Chi3 and *Pe*Chi4: 300 nM, *Pe*Chi5: 2.7 µM) for different time periods starting from 0-720 min. Each time point, 20 µl of reaction mixtures were withdrawn and equal amount of 70% acetonitrile was added to stop the reaction. The reaction mixtures (40 µl each) were centrifuged, and 20 µl of supernatant was analyzed by isocratic HPLC using Shodex Asahipack NH_2P-50 4E column and eluted COS were monitored by recording absorption at 210 nm. The top most profile shows a standard mixture of COS ranging from DP1-DP6. The other profiles indicate the reaction proceeding (incubation times indicated). **A-D:** HPLC product profile of *Pe*Chi1, *Pe*Chi3, *Pe*Chi4, *Pe*Chi5.

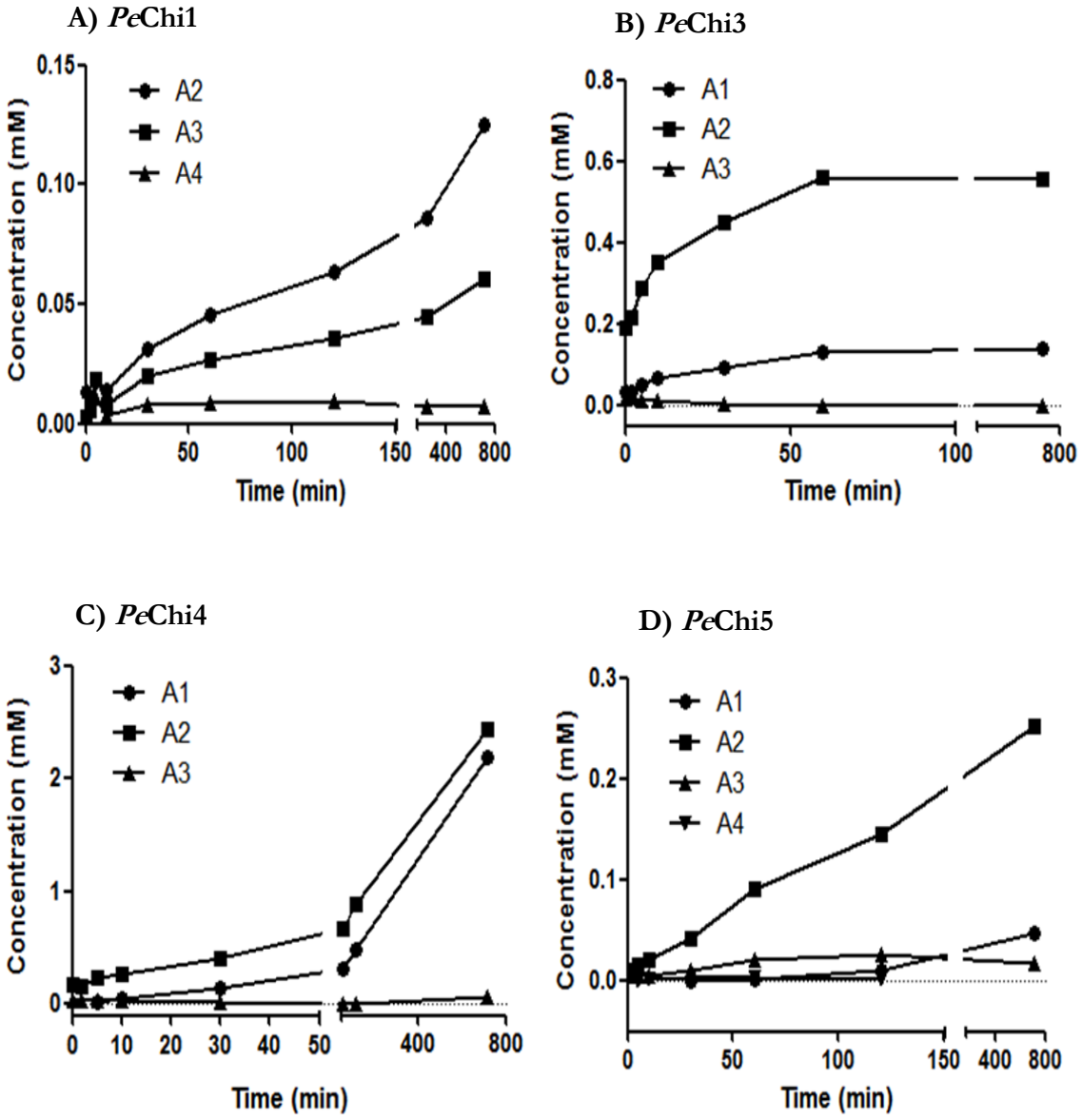

Fig. 4.9: Concentrations of COS products generated during reaction time course of colloidal chitin hydrolysis by *Pe* chitinases. The generated COS by *Pe* chitinases were quantified from respective peak areas of products by using standard calibration curves of COS ranging from DP1-DP6. **A-D:** Quantification profile for *Pe*Chi1, *Pe*Chi3, *Pe*Chi3, *Pe*Chi5.

4.2.3. Sequence and structural analysis of *Pe* chitinases

The protein sequence of catalytic domains of *Pe*Chi1, *Pe*Chi3, *Pe*Chi4 and *Pe*Chi5 were aligned with the structurally and functionally well characterised chitinases of *S. marcescens* (*Sm*ChiA, *Sm*ChiB and *Sm*ChiC). Sequence analysis showed that the catalytic module of *Pe*Chi3 and *Pe*Chi5 like *Sm*ChiC lacks an α + β-fold insertion between β-sheets 7 and 8 of the TIM-barrel fold, while it was present in *Pe*Chi1 and *Pe*Chi4 (Fig. 4.11). The catalytic sequence motifs (S*X*GG and D*X*D*X*E) were conserved among three *Pe* chitinases except in *Pe*Chi1 where Ser was substituted by Gly. The *Pe*Chi1, *Pe*Chi3, *Pe*Chi4 and *Pe*Chi5 sequences were submitted to BLASTP in NCBI and searched for suitable templates for homology modeling. The *Pe*Chi1 and *Pe*Chi4 displayed 21% and 69% sequence identity to chtinase of *B. circulans* (1ITX), respectively. *Pe*Chi3 and *Pe*Chi5displayed 52% and 62% sequence identity to chitinase of *B. cereus* NCTU2 (3N11), respectively. Surface exposed aromatic amino acids in *Pe*Chi1 (Phe62, Tyr105, Tyr218, Trp224, Tyr270, Trp359) (Fig. 4.12A), *Pe*Chi3 (Phe22, Phe45, Tyr62, Phe124, Phe174, Phe216, Trp320) (Fig. 4.12B), *Pe*Chi4 (Trp255, Tyr277, Trp323, Trp335, Trp365, Tyr459, Trp486, Tyr536, Trp631) (Fig. 4.12C) and *Pe*Chi5 (Phe18, Phe34, Tyr147, Tyr181, Trp286) (Fig. 4.12D) were also identified in the models. A closer assessment of these structures showed that *Pe*Chi1 and *Pe*Chi4had deep, almost tunnel-like substrate-binding cleft (Fig. 4.12A, C). Whereas, *Pe*Chi3 and *Pe*Chi5 had shallower substrate binding cleft with lesser aromatic residues (Fig. 4.12B, D). The catalytic cleft of *Pe*Chi4 showed a tunnel-like substrate-binding cleft with a closed roof (Fig. 4.12C).

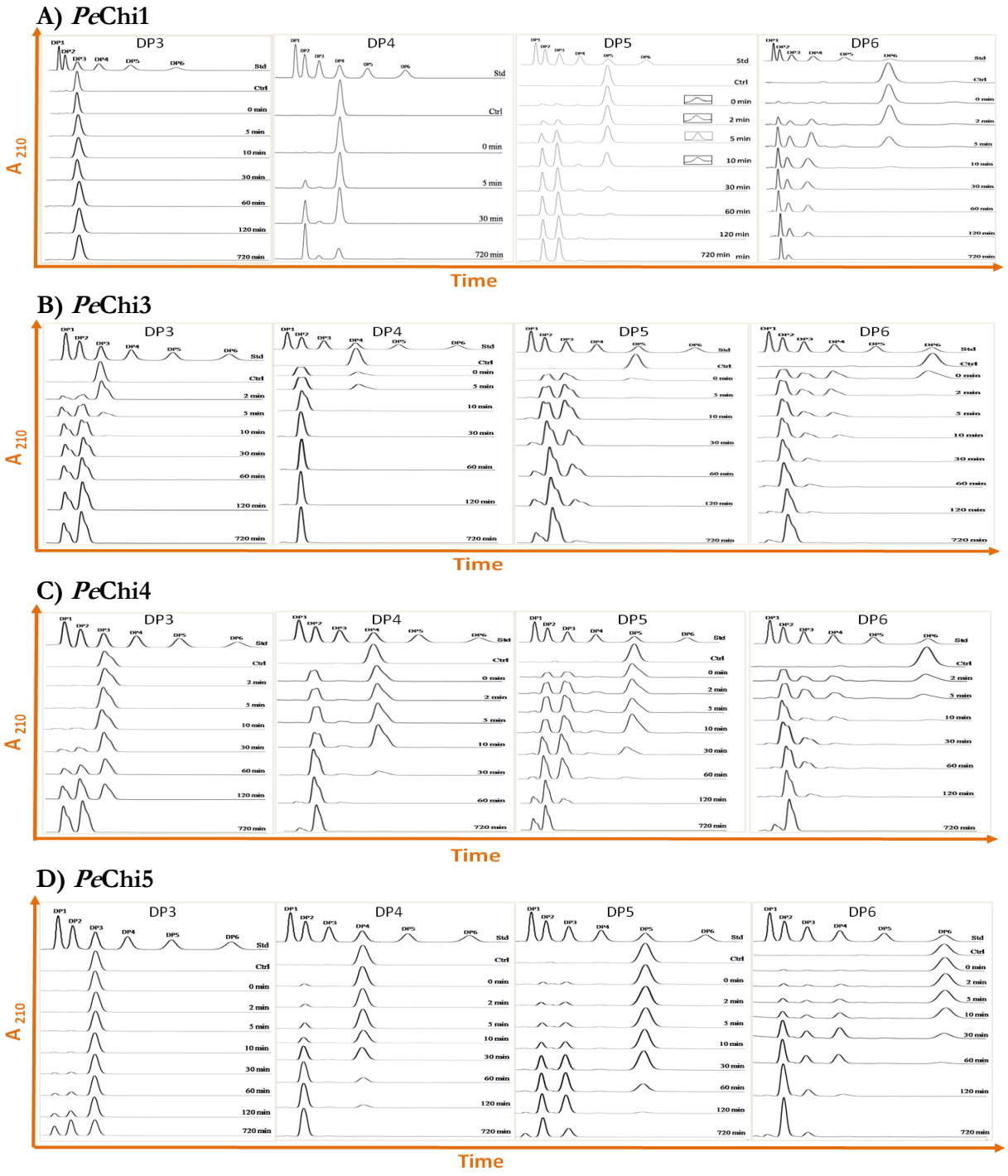

Fig. 4.10: HPLC chromatogram showing time course of DP3, DP4, DP5 and DP6 hydrolysis by *Pe* chitinases. Reaction mixture containing *Pe* chitinases (*Pe*Chi1 and *Pe*Chi5: 500 nM, *Pe*Chi3 and *Pe*Chi4: 40 nM) and 2.0 mM of each oligomer in 50 mM buffer, was incubated at optimum temperature for varied times starting from 0-720 min. After indicated incubation periods (labeled above each chromatogram), 20 µl of reaction mixtures were withdrawn and equal amount of 70% acetonitrile was added to stop the reaction. The reaction solution (20 µl) was analyzed by HPLC and the eluted hydrolysed products were detected at 210 nm. The top most profile shows a standard mixture of COS ranging from DP1-DP6. Insets show the magnified low peak area TG products. **A-D:** HPLC product profile of *Pe*Chi1, *Pe*Chi3, *Pe*Chi4, *Pe*Chi5.

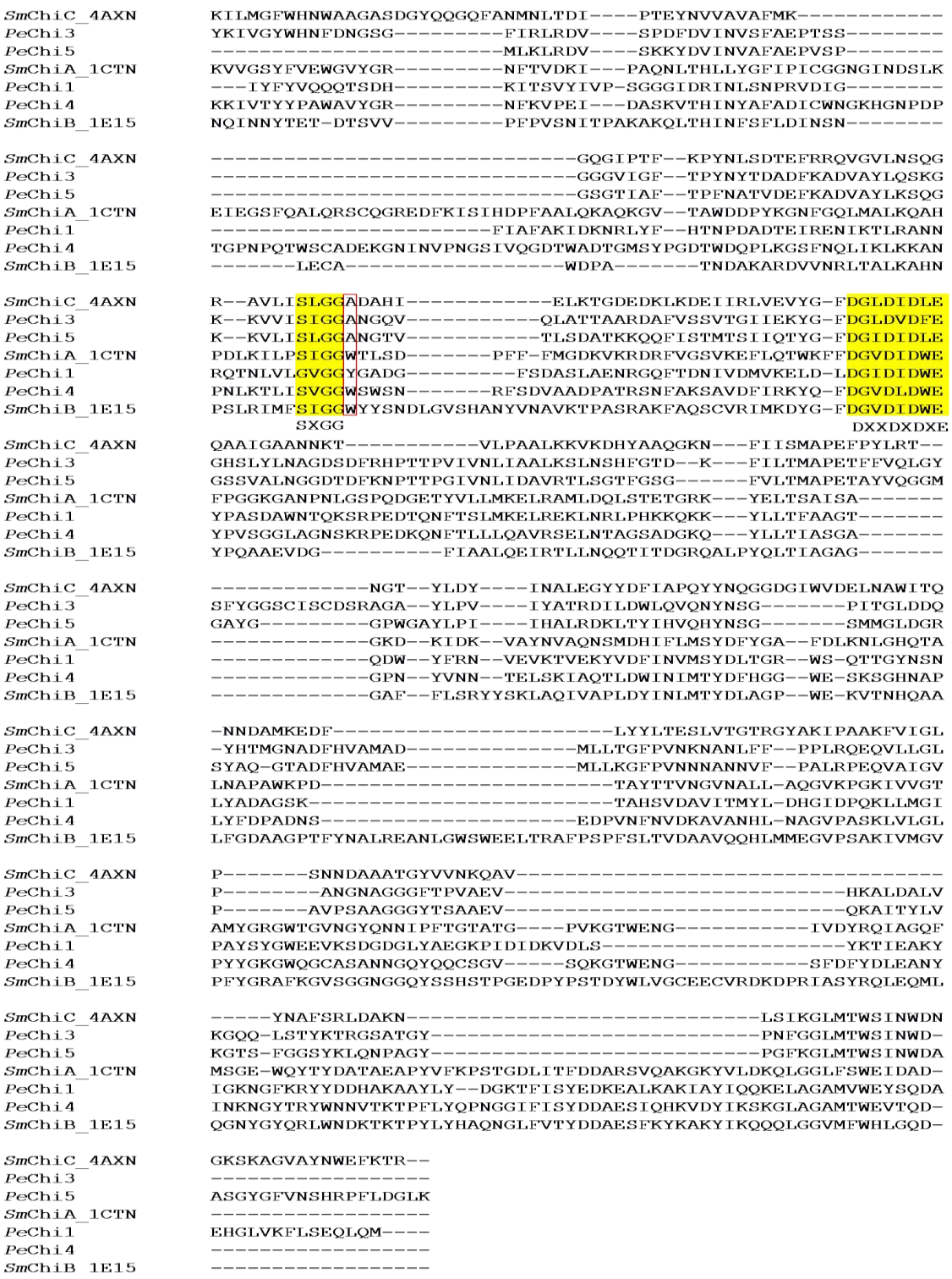

Fig. 4.11: Sequence alignments for *Pe* chitinases. Catalytic domains of *Pe*Chi1, *Pe*Chi2, *Pe*Chi3 and *Pe*Chi4 were aligned with three structurally and functionally well characterised chitinases, *Sm*ChiA, *Sm*ChiB, *Sm*ChiC from *S. marcescens* using clustalw2 (www.ebi.ac.uk/Tools/msa/clustalw2/). Diagnostic sequence motifs containing residues that are crucial for catalysis (S*X*GG and D*X*D*X*E) are shaded in yellow and shown below the alignment. Residues marked within red box are crucial for influencing processivity. Note: In *Pe*Chi1, Ser is replaced with Gly in the S*X*GG motif.

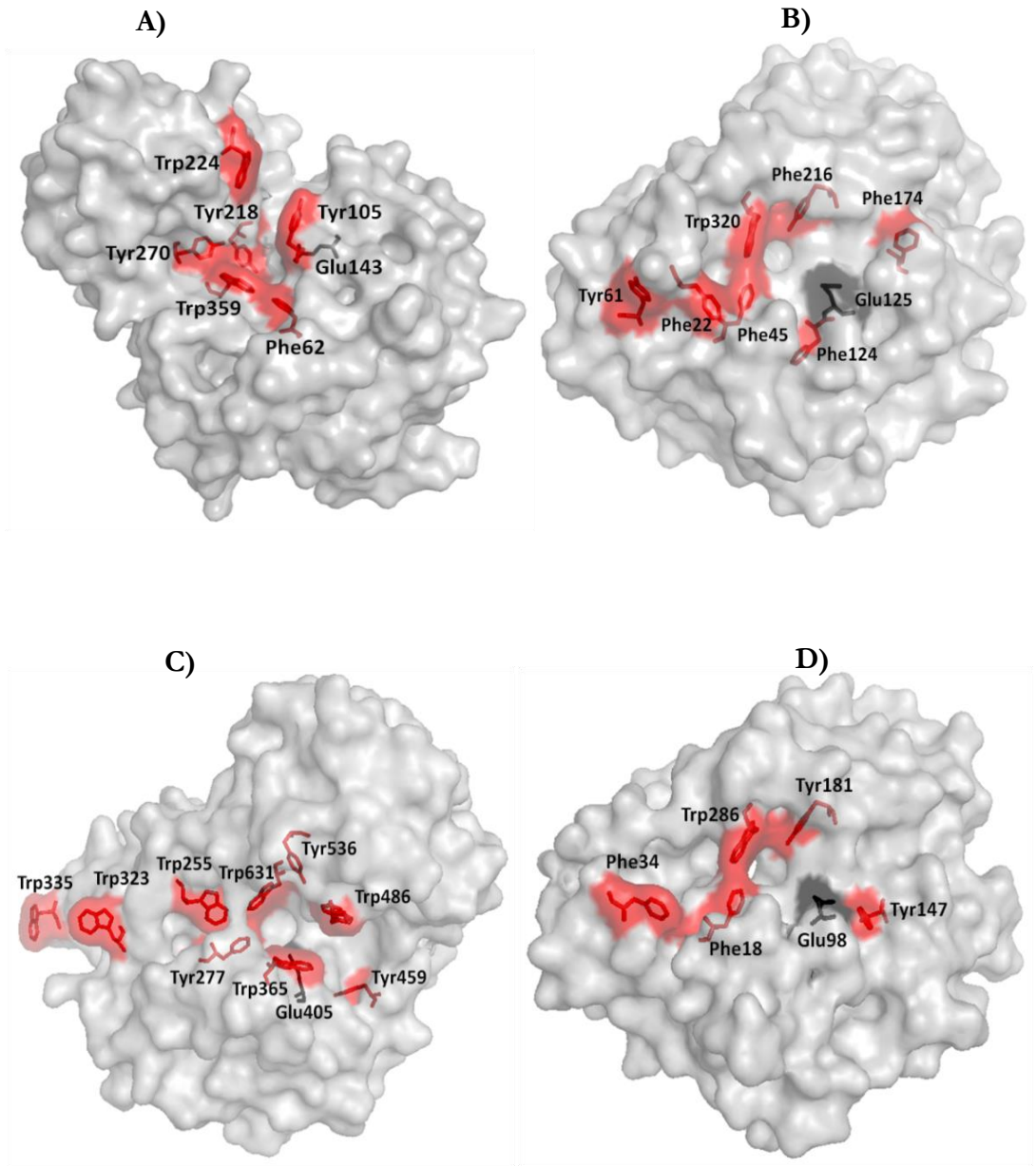

Fig 4.12: Comparison of substrate-binding clefts of the catalytic domain of *Pe* chitinases. Surface representation showing aromatic side chains lining the substrate-binding cleft and the binding surface of *Pe*Chi1 **(A)**, *Pe*Chi3 **(B)**, *Pe*Chi4 **(C)** and *Pe*Chi5 **(D)**. The surface of aromatic residues in the proteins is shown in red and the catalytic Glu is shown in black. Pictures used for representation were made with PyMol (www.pymol.org).

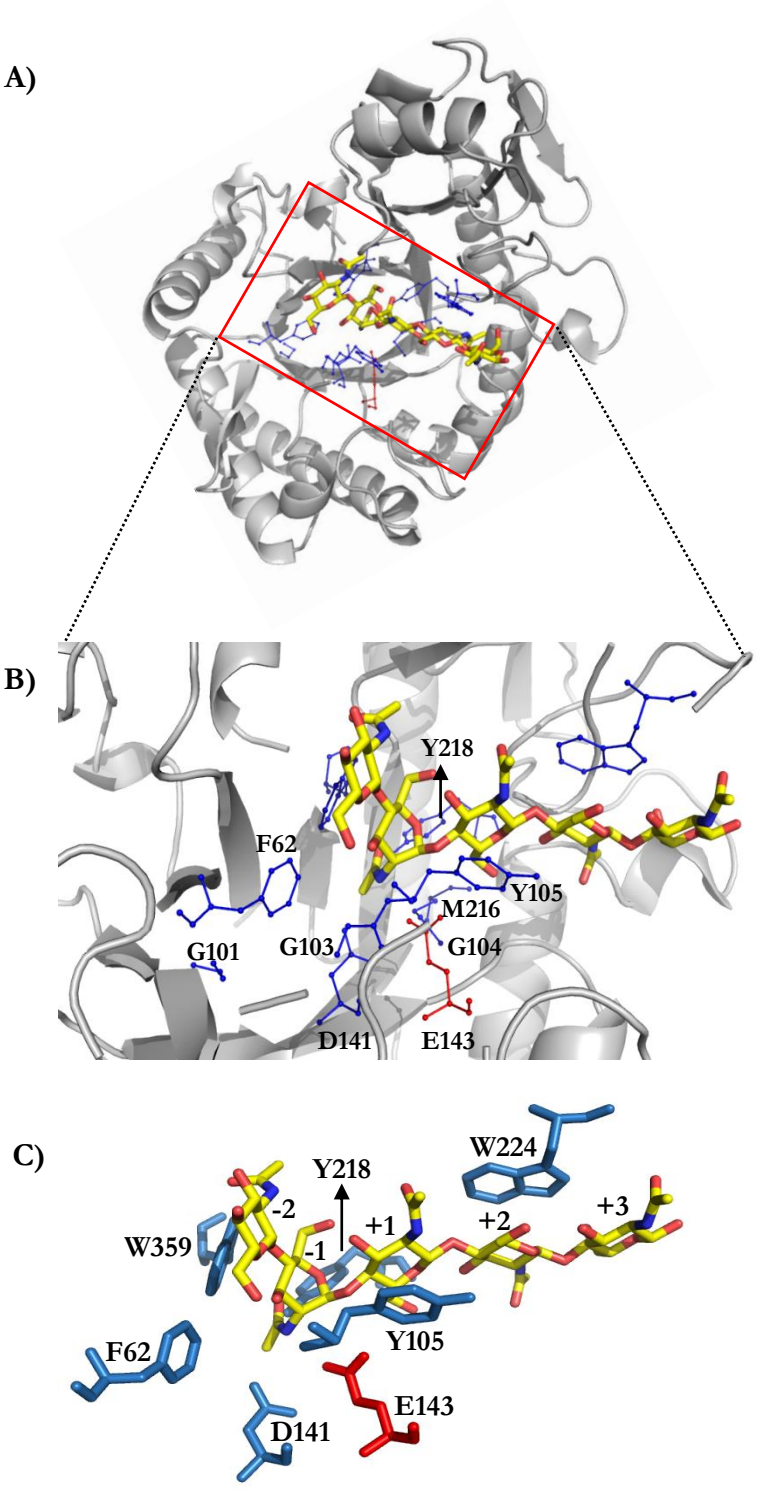

Fig. 4.13: Interacting amino acid residues in the binding cleft of *Pe*Chi1. A) *Pe*Chi1 modeled structure docked with A5 (yellow). **B)** Close view of *Pe*Chi1 showing the residues targeted (shown as blue sticks) for mutation in the catalytic center (M216 and Y218), catalytic groove (F62, G101, G103, G104 and W105) and one residue at the catalytic triad, D141. **C)** Stereo picture showing A5 ligand and aromatic residues near the catalytic center along with two catalytic residues D141 and E143. The catalytic E143 is coloured in red. Pictures used for representation were made with PyMol.

4.2.4. Site directed mutagenesis of *Pe*Chi1 to improve TG

Among the four characterized chitinases, *Pe*Chi1 showed feeble TG activity by generating DP7 from DP5 substrate, in addition to its hydrolytic ability. This finding motivated us to improve the TG activity of *Pe*Chi1 in terms of increasing the quantity and extending the duration of TG products by mutational approach. The amino acid residues in the catalytic center, catalytic groove and in the catalytic triad were selected for mutagenesis (Fig. 4.13). In the catalytic center the residues M216 and Y218 were closer to the catalytic triad D*X*D*X*E (Fig. 4.12B). We have mutated D141 from the catalytic triad and a few residues present in the catalytic groove including F62, G101, G103, G104 and Y105, where the substrate molecules show major interactions.

4.2.4.1 Activity analysis of *Pe*Chi1 mutants

E. coli BL21 cells harbouring the plasmids of *Pe*Chi1 mutants were used for protein expression. Soluble proteins of *Pe*Chi1 variants were passed through Ni-NTA affinity matrix to obtain pure proteins. SDS-PAGE analysis confirmed the purity of collected protein fractions and the mutant protein molecular mass was also ~44 kDa (Fig. 4.14).

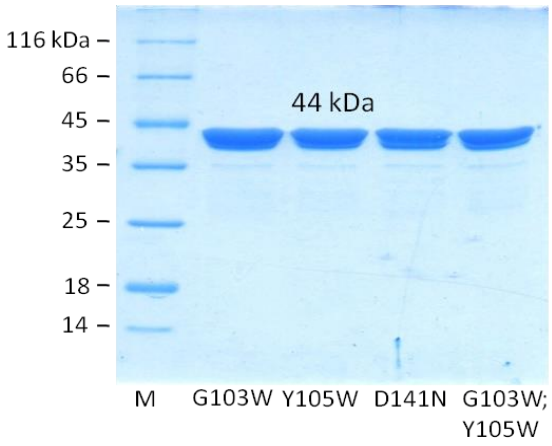

Fig. 4.14: Representative picture showing purified *Pe*Chi1 variants. Recombinant *Pe*Chi1 variants (G103W, Y105W, D141W and G103W/Y105W) were purified by Ni-NTA agarose affinity chromatography using elution buffer containing 50, 100 and 250 mM imidazole. M: Pre-stained protein molecular weight marker and the sizes are indicated in kDa.

The specific activity of *Pe*Chi1 mutant proteins with single/double amino acid substitutions were determined using colloidal chitin as shown in the Fig. 4.15. The mutant G103W completely lost hydrolytic activity. The specific activity decreased for mutants D141N, Y105W/M216A, Y105W/Y218A, Y105W/G103W and Y105W/G104S. The lowest activity was observed in Y105W/Y218A with 300 fold decrease in comparison to the wild type. The mutant Y105W and Y105W/G101S showed 1.5 and 2 fold increase in specific activity, respectively, whereas the mutant Y105W/F62W showed nearly equal activity with that of wild type.

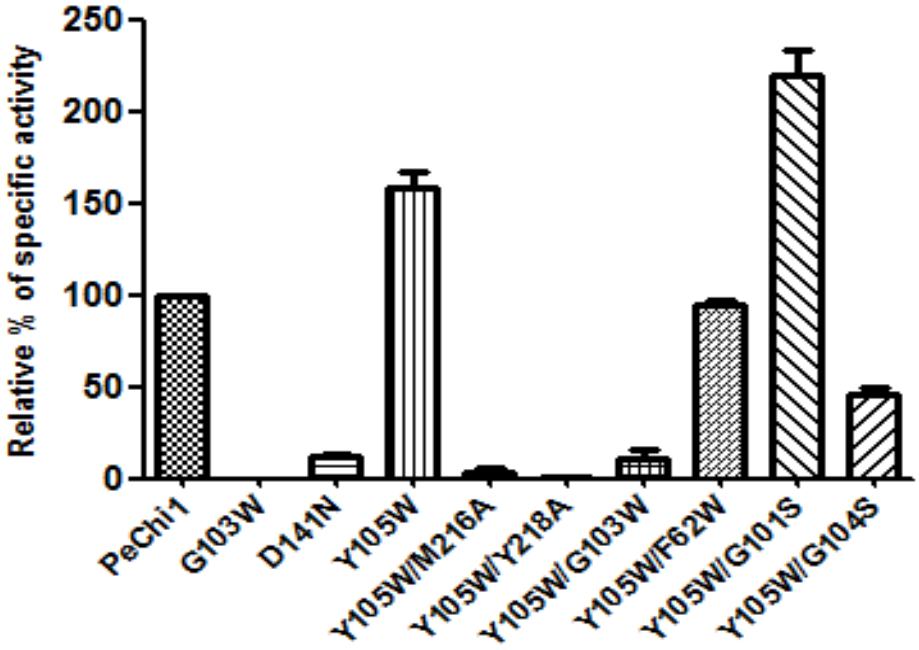

Fig. 4.15: Relative specific activity of *Pe*Chi1 and its mutants towards CC substrate. The reaction mixture containing *Pe*Chi1 (450nM) and polymeric CC substrate (2 mg.ml^{-1}) was incubated in 50 mM sodium acetate buffer at 40°C for 2 h. The reaction was monitored by reducing sugar estimation. Vertical bars represent standard error of triplicate experiments.

4.2.4.2 Effect of single mutations in the catalytic triad and catalytic groove on the hydrolytic and TG activities of *Pe*Chi1

Based on the docking study and sequence analysis, we substituted D141 with Asn in the catalytic triad, G103 with Trp and Y105 with Trp in the catalytic groove. D141N

mutation resulted in loss of both hydrolytic and TG activities leaving the initial amount of DP5 substrate unutilized till the end of 12 h (Fig. 4.15B). Similarly, substitution of G103 to W completely abolished both hydrolytic and TG activities (Fig. 4.15C). Y105Wgenerated more TG products and also differed from the wild type ingenerating DP6 as one of the TG products (Fig. 4.15A, D). At 2 min, the concentration of DP6 product was 2.6%, which decreased to 0.6% by 30 min. Among the TG products, DP6 was detected up to 60 min, and DP7 was observed up to 10 min, when DP5 was used as substrate. This mutant also differed from the wild type in displaying detectable TG activity on DP4 substrate producing DP5 and DP6 (Fig. 4.17). The maximum concentration of DP5 was 1.1% at 60 min, whereas maximum concentration of DP6 was 2.6% at 10 min.

4.2.4.3 Effect of double mutations in the catalytic centre and catalytic groove on the hydrolytic and TG activities of *Pe*Chi1

The mutant Y105W/M216A displayed a low hydrolytic activity with complete loss in TG activity (Fig. 4.18B). Only a trace amount of hydrolytic products, DP2 and DP3 were detected from 1 h that marginally increased up to 12 h leaving 75% DP5 substrate at the end of reaction. The proportion of DP2 and DP3 generated by Y105W/M216A mutant was 9.7% and 12.8%, respectively at the end of 12 h. Complete abolition of both hydrolysis and TG was displayed by Y105W/Y218A mutant (Fig. 4.18C). The mutant Y105W/G101S was unique as it retained TG activity for a shorter time even when the hydrolytic activity increased drastically on DP5 substrate (Fig. 4.18D). Only 2.5% of DP5 remained at 10 min with simultaneous increase in DP2 and DP3 products. Y105W/G101S displayed TG activity up to 5 min. At 2 min, the concentration of DP6 was 1.6% and decreased to 0.8% by 5 min. Y105W/G104S mutation resulted in significant loss of hydrolytic activity leaving 72% of DP5 substrate at the end of 12 h with complete loss of TG activity (Fig. 4.18E).Only a trace amount of hydrolytic products DP1, DP2 and DP3 were detected even after 6 h. The proportion of DP2and DP3 hydrolytic products generated by Y105W/G104S mutant was 5.2%and 10.1% at the end of 12 h.

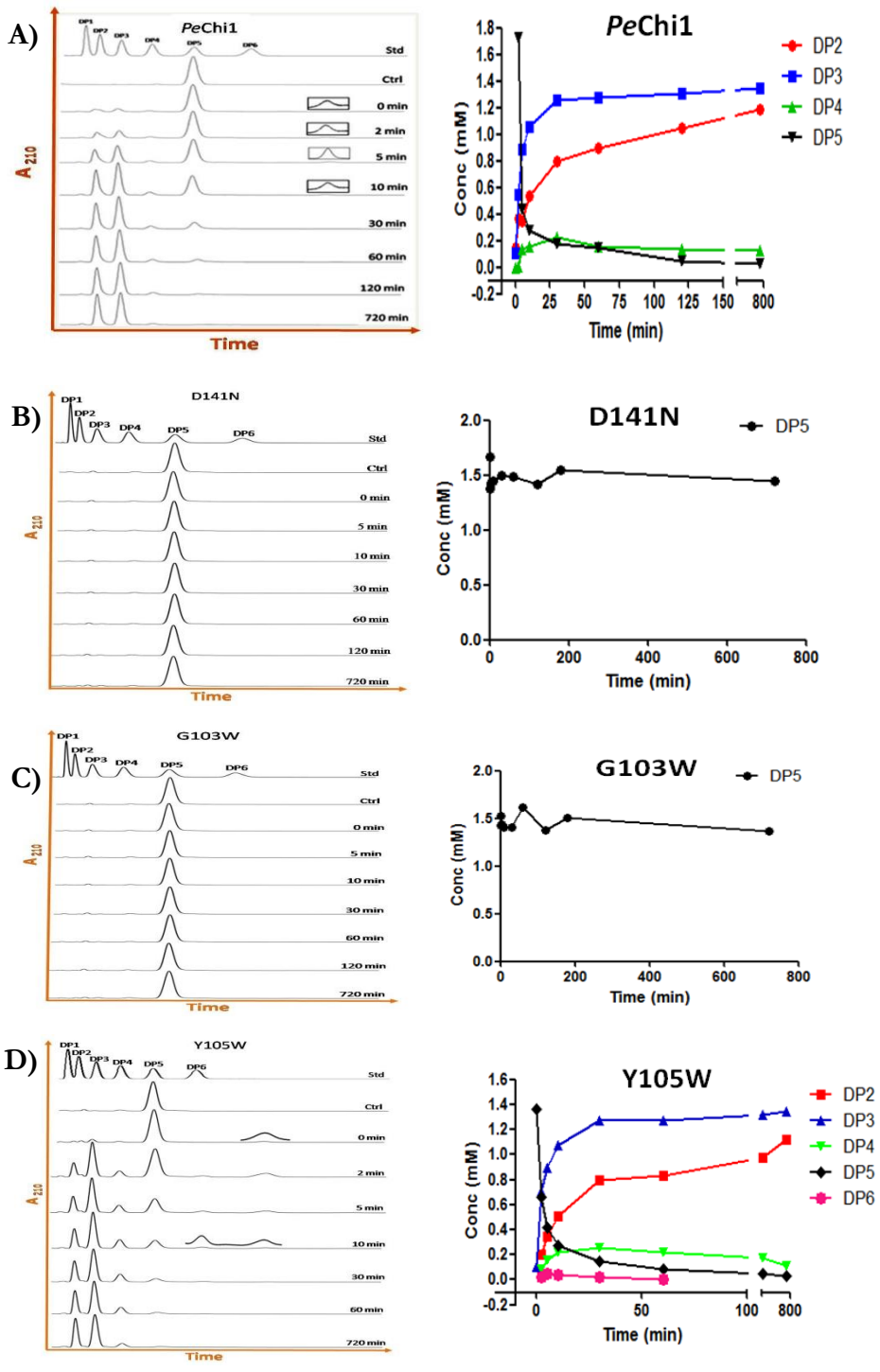

Fig. 4.16: Product profiles of the single mutants targeted at the catalytic triad and catalytic groove. Left column shows HPLC chromatograms of *Pe*Chi1 **(A)** and the single mutants **(B-D)**. Insets show the magnified view of the low peak area products. Individual quantification graph represents all the hydrolytic (DP2-DP4) and TG (DP6) products accumulated during the course of reaction with 3 mM DP5 substrate. **Note:** 20 µl reaction mixture (10 µl hydrolysate + 10 µl of 70% acetonitrile) was analysed by HPLC, making the actual injected concentration of DP5 to 1.5 mM.

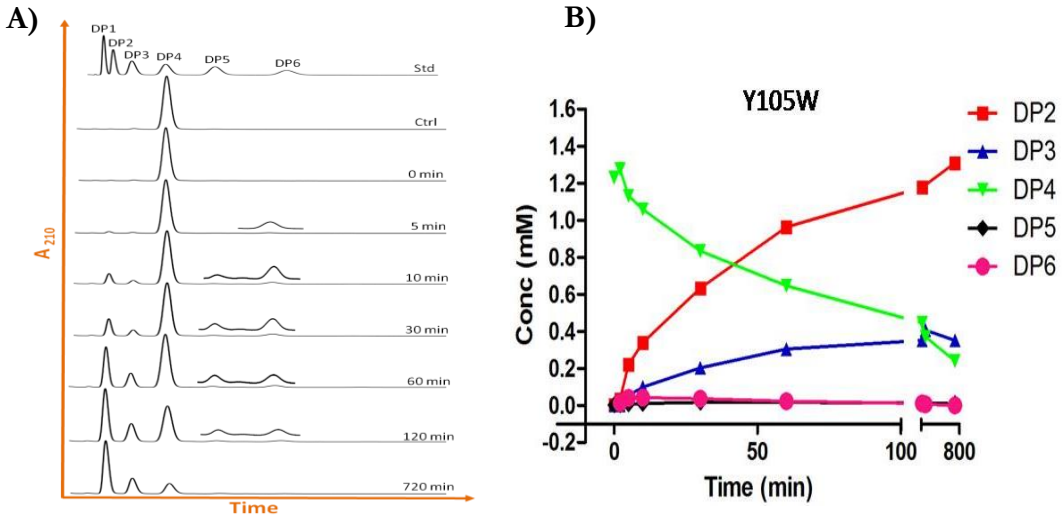

Fig. 4.17: HPLC chromatogram and quantification profile of Y105W mutant on DP4 substrate. HPLC chromatograms **(A)** and quantification **(B)** of Y105W mutant. Insets show the magnified view of the low peak area products. The quantification graph represents the hydrolytic (DP2 and DP3) and TG (DP5 and DP6) products accumulated during the course of reaction with 3 mM DP4 substrate.

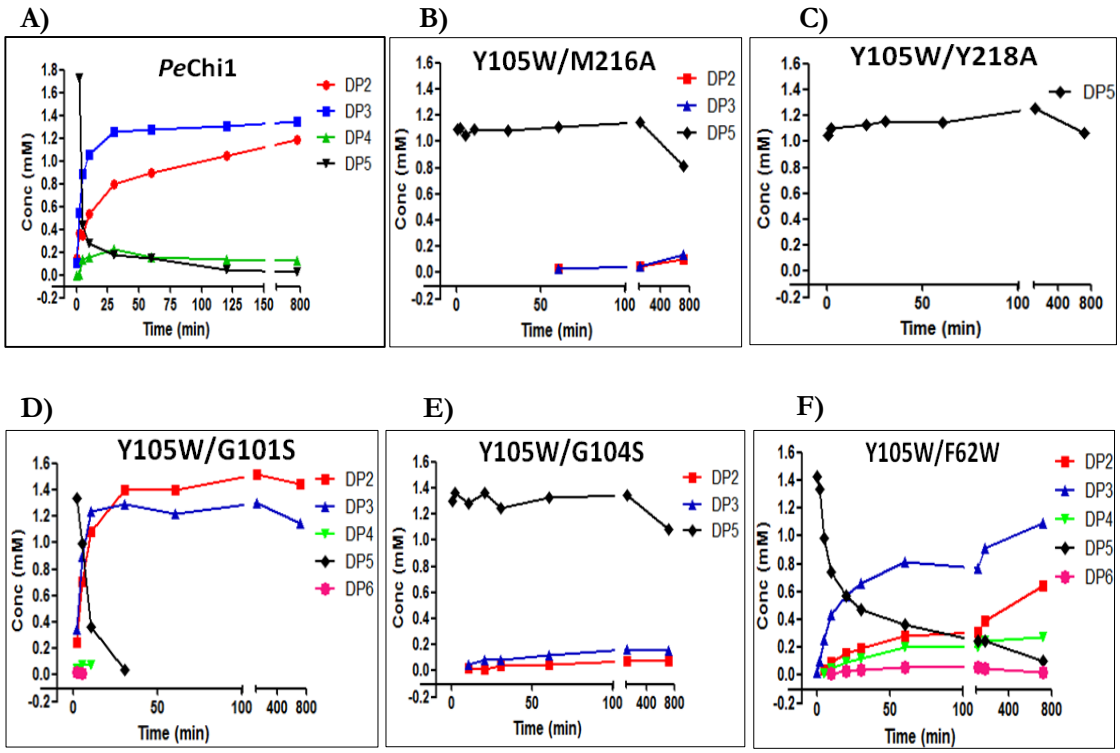

Fig. 4.18: HPLC quantification profiles of the double mutants (B-F). Quantification profiles of the double mutants on DP5 substrate were obtained by a linear correlation between peak area and concentration of oligosaccharides in standard. Individual quantification graph represents all the hydrolytic (DP2-DP4) and TG (DP6) products accumulated during the course of reaction with 3 mM DP5 substrate.

When Y105W was coupled with F62W, the double mutant Y105W/F62W showed similar hydrolytic activity with that of *Pe*Chi1, but the hydrolytic activity reduced by nearly 37% in comparison to Y105W single mutant (Fig. 4.18F). The production of DP6 product by Y105W/F62W was as efficient as Y105W, which remained up to the end of 12 h. The production of DP7 by the double mutant was also similar to the Y105W, but the duration of TG product formation by Y105W/F62W increased up to 180 min (Fig. 4.19A, B).

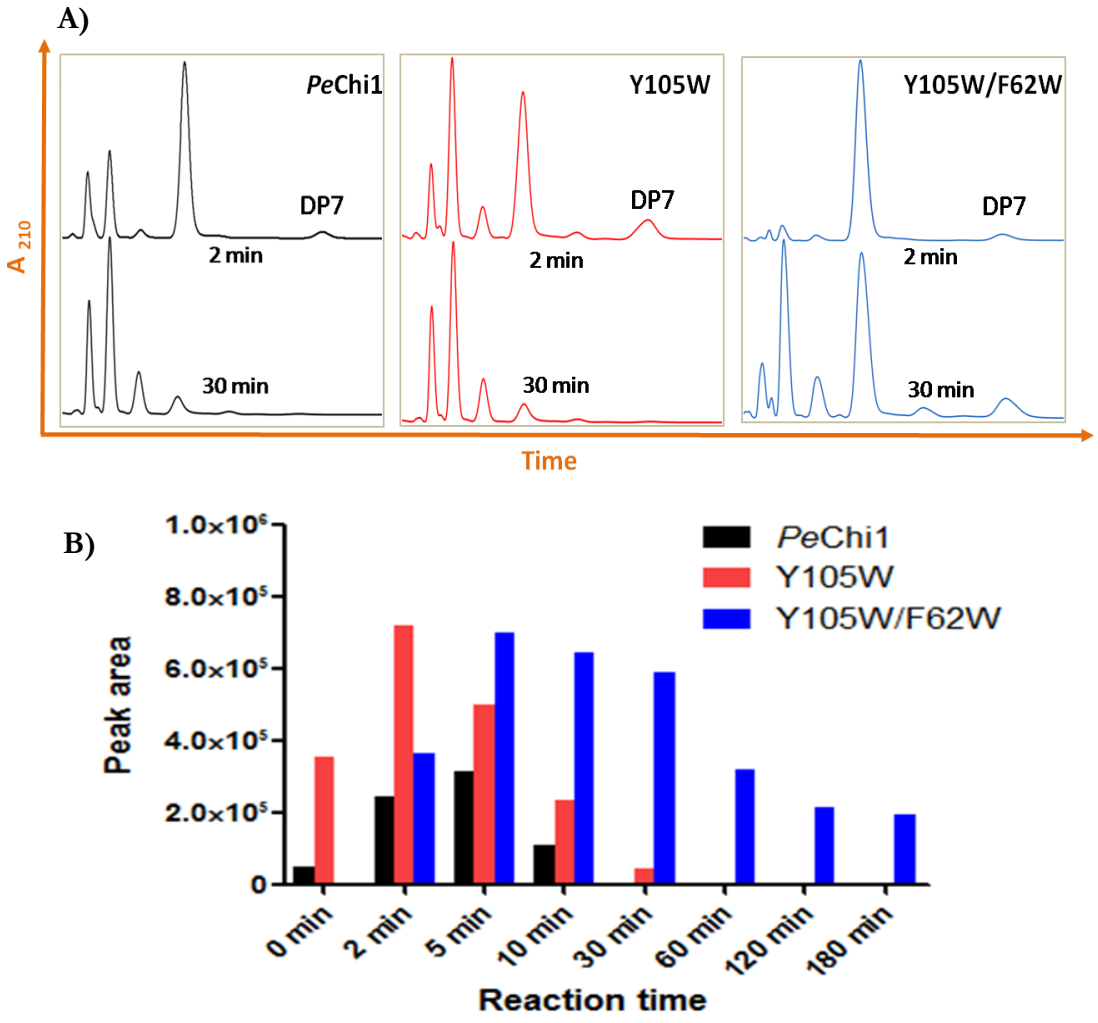

Fig. 4.19: A representative figure showing DP7 formation as a TG product from DP5 substrate. **A)** HPLC chromatograms of *Pe*Chi1, Y105W and Y105W/F62W showing the difference in their hydrolytic and TG activity on DP5 substrate. **B)** The difference in the quantity of DP7 formation over time between the wild type and mutants in terms of peak area. **Note:** Peak areas were considered for comparison due to unavailability of DP7 standard.

4.3. Discussion

4.3.1 Chitinolytic machinery of *P. elgii* is complex with chitinases of various domain arrangements

Bacteria evolved a variety of chitinases, mostly belonging to GH18, to utilize the chitinous substrates during their saprophytic and pathogenic phases. Catalytic GH18 domain is an essential domain and is known to function even in the absence of accessory domains suggesting that domains can have either independent function or contribute to the function of a multi-domain protein in cooperation with other domains.

The presence of five different chitinases belonging to two GH families i.e. GH18 and 19, a chitosanase (GH8) and a CBP (AA10) indicated that the chitinolytic machinery of *P. elgii*SMA-1-SDCH02 was complex with the ability to degrade chitin efficiently. The deduced amino acid sequences of chitinases were tested for functional domains or motifs using SMART data base. Both *Pe*Chi1 and *Pe*Chi5 had the only catalytic domain, whereas *Pe*Chi2 had N-terminal chitin binding domain (ChBD) and a C-terminal GH18 domain linked by FN3 domain. *Pe*Chi3 composed of an N-terminal GH18 and C-terminal ChBD linked by two FN3 domain and the domain arrangement of *Pe*Chi4 was in the reverse orientation of *Pe*Chi3 with similar domains. The presence of different accessory domains with complex domain arrangements was indicative of a complex chitinolytic machinery, probably meant for degradation of different forms of chitin found in nature. Such complex chitinolytic systems were reported in mesophilic soil bacteria like *S. marcescens* (Suzuki et al., 2002), *S. proteamaculans* (Purushotham et al., 2012) and in marine bacteria *Alteromonas* sp. strain O-7 (Orikoshi et al., 2005b) to name a few.

4.3.2 Effect of pH and temperature on the activity of *Pe* chitinases

Bacterial chitinases are active over a wide range of pH and temperature, and the optimum temperature depends on the type of habitat from where they are isolated. All the four *Pe* chitinases were optimally active in slightly acidic to neutral pH (5.0-7.0)

(Fig. 4.4). *Pe*Chi1, *Pe*Chi3 and *Pe*Chi5 were active over a range of pH (5.0-10.0) with an optimum at pH 6.0, similar to chitinases from *Bacillus pumilus* SG2 (Ghasemi et al., 2010), *B. cereus* (Wang et al., 2001) and ChiA from *S. marcescens* 2170 (Suzuki et al., 2002). Among the four chitinases, *Pe*Chi4 was active in more acidic condition ranging from pH 3.0-8.0 with an optimum at pH 5.0, similar to *B. cereus* chitinase which showed stability in the range of pH 2.5 to 8.0 (Wang et al., 2001). Characterization of chitinases from *Bacillus* spp. showed activity in the temperature range of 50–60°C (Barboza-Corona et al., 2003; Huang & Chen, 2005). Unlike mesophilic temperature optima for all chitinases originated from an endophyte (Purushotham et al., 2012), chitinases of *P. elgii* displayed different temperature optima –40°C for *Pe*Chi1, 50°C for *Pe*Chi5, and 60°C for *Pe*Chi3 and *Pe*Chi4 (Fig. 4.5). In view of the wide pH and temperature optima, it is conceivable that *P. elgii* could be an efficient chitin degrader in different environmental conditions.

4.3.3 Catalytic activity

P. elgii chitinases have different domain architectures and the catalytic domain peptide sequences of these four enzymes share very low similarity (>15% and <60%), although these enzymes belong to family 18 chitinases. We, therefore, investigated the kinetics of *Pe* chitinases. Michaelis-Menten kinetic parameters were determined using different concentrations of colloidal chitin as the substrate starting with very low concentration since substrate inhibition was apparent at higher substrate concentration for this type of chitinases (Brurberg et al., 1996; Synstad et al., 2004).

$K_m$value of *Pe*Chi4 (0.76 mg ml^{-1}) was the lowest among the four chitinases with very high overall catalytic efficiency indicating much higher affinity towards colloidal chitin. On a similar kinetic study on colloidal chitin by chitinase from *B. thuringiensis* and *B. licheniformis* showed K_m of 5.4 and 6.9, respectively (Neeraja et al., 2010). Overall, we observed a great difference in kinetic parameters among the four chitinases. The K_m and overall catalytic efficiency were higher for two multi-domain chitinases i. e. *Pe*Chi3 and *Pe*Chi4 in comparison with chitinases comprising of the single catalytic domain (Fig. 4.6). The difference in the kinetic parameters among these chitinases could be due

to a difference in the sequence of catalytic domains in combination with different auxiliary domains. It is conceivable that the primary role of the auxiliary domains (ChBD, PKD and FN3) is to potentiate catalytic activity by disrupting the substrate, without even promoting the enzyme-substrate binding. Watanabe et al. (1994) have shown that deletion of two FN3 domains of ChiA1 from *B. circulans* did not affect chitin-binding but strongly reduced chitin hydrolysing activity. Though the function of PKD domain is so far not clearly understood, the role of ChBD with the involvement of its aromatic residues in binding to chitin is well established (Hashimoto et al., 2000; Akagi et al., 2006). Swapping of ChBD domains was also reported to increase significant improvement in functional stability, conformational stability, and binding ability of chitinases towards insoluble chitinous substrates (Neeraja et al., 2010).

4.3.4 Activity on polymeric carbohydrate substrates

The role of the four *Pe* chitinases in chitin hydrolysis was assessed by considering their hydrolysing activity on different chitinous substrates. All the four chitinases showed maximum activity on colloidal chitin (Fig. 4.7). However, towards crystalline α- and β-chitin, only *Pe*Chi3 and *Pe*Chi4 showed considerable activity suggesting the accessory domain of both these enzymes facilitate in degradation of crystalline chitin substrates. In two independent experiments, it was also shown that ChiA from *S. marcescens* and *Alteromonas* sp. strain O-7 had maximum hydrolytic activity on crystalline α-chitin among the other chitinases produced by these two bacteria. The PKD domain found in the N-terminal region of both these chitinases was implicated for the effective hydrolysis of crystalline α-chitin (Orikoshi et al., 2005a). It seems likely that chitinolytic bacteria produce multiple chitinases with different substrate specificities against a variety of chitinous substrates.

In chitinases of *S. marcescens*, substitution of aromatic amino acid in aglycon site of ChiB and glycon subsite of ChiA by Ala had reduced processivity to crystalline chitin and increased hydrolytic activity more than 20 fold towards chitosan substrate (Horn et al., 2006a; Zakariassen et al., 2009). Among the tested polymeric substrates, chitosan was the second most preferred substrate by both *Pe*Chi3 and *Pe*Chi5 (Fig. 4.7).

Although *Pe*Chi4 showed feeble activity, chitosan was the least preferred substrate in comparison with the other tested polymers. Amino acid sequence comparison of *Pe* chitinases with *Sm*ChiA, *Sm*ChiB revealed that *Pe*Chi3 and *Pe*Chi5 have Ala (A89 and A62 in *Pe*Chi3 and *Pe*Ch5, respectively) in place of Trp in the +1 aglycon subsite (Fig. 4.11). In *Sm*ChiB, although W97 was required for processivity, it reduced the hydrolytic activity towards chitosan substrate (Horn et al., 2006a). Therefore, we assume that the absence of Trp in the +1 aglycon subsite increased chitosan activity in *Pe*Chi3 and *Pe*Chi5. Further experiments on mutational analysis will be required to prove this assumption. In future, it would also be interesting to investigate the role of auxiliary ChBD of *Pe*Chi3 on amorphous chitosan binding and degradation.

4.3.5 Diverse mode of action by *P. elgii* chitinases

Enzymatic degradation of carbohydrate polymers occurs either from one of the chain ends (exo-mechanism) or from a random point within the polymer chain (endo-mechanism). Each of these two mechanisms can take place in combination with a processive mode of action, meaning that the substrate is not released after successful cleavage but glides through the active site for the next hydrolytic event to occur. Hydrolysis of colloidal chitin with *Pe*Chi1 and *Pe*Chi5at the early phase of degradation yielded DP2, DP3 and DP4 indicating endo-mode of action (Fig. 4.8A, D). The appearance of monomeric sugars with *Pe*Chi5 hydrolytic activity suggests that the intermediate trimer product can be degraded into monomer and dimer which was confirmed by using a trimer as substrate (Fig. 4.10D). Slower degradation rate on soluble chitin oligomers was also indicative of endo-action by *Pe*Chi1 and *Pe*Chi5. In the initial phase (2 min) of degradation, *Pe*Chi3 and *Pe*Chi4 generated DP2 as predominant hydrolysis product with meagre DP3 formation suggesting the exo-mode of action by *Pe*Chi3 and *Pe*Chi4. The consecutive sugars in chitin are rotated by 180°, with the consequence that only every second GlcNAc will have a productive configuration when the polymer is threaded through the active site of an enzyme (Zakariassen et al., 2009). This could be the reason for *Pe* chitinases releasing DP2 as a major end product, as most of the chitinases release DP2 as major end product.

The processive action of chitinases on chitin also yields a higher amount of dimers, while trimers can only be produced by an exo-chitinase in the first hydrolytic step depending on the initial binding preference. Therefore, processivity may be assessed by studying the DP2/DP3ratios in product mixtures (Teeri et al., 1998; Medve et al., 1998). Interestingly, the four enzymes showed clear differences in their DP2/DP3 ratios (Table 4.2). The well characterised processive exo-chitinases, *Sm*ChiA and *Sm*ChiB with a deep substrate-binding cleft showed DP2/DP3 ratios of 7.3 and 12.6, respectively on β-chitin (Horn et al., 2006b), while the nonprocessive endochitinase *Sm*ChiC with a shallow substrate-binding cleft showed DP2/DP3 ratios of 4.1. For *Pe*Chi5, the DP2/DP3 ratio was below 2, suggesting the nonprocessive mode action which is supported by the fact that *Pe*Chi5 has very shallow and open substrate binding cleft characteristic of an endo-nonprocessive chitinase (Horn et al., 2006b). The lower D2/D3 ratio (1.7) for *Pe*Chi1 was inconsistent with the modeled 3-D structure analysis of *Pe*Chi1, which showed a deep tunnel-like substrate binding cleft characteristic of a processive enzyme (Fig. 4.12). The lower D2/D3 ratio may occur due to either the endo-mode of action and/or the ability of *Pe*Chi1 to release trimer in the first cleavage step (Horn et al., 2006b). Hydrolysis of chitin oligomers showed *Pe*Chi1 acts in an endo-mode and had the ability to release trimers from DP6 substrate explaining why we observed low DP2/DP3 for *Pe*Chi1. Therefore, it is conceivable that *Pe*Chi1 is an endo- and processive chitinase. The DP2/DP3 ratio of 5.4 and a deep substrate-binding cleft with a closed roof suggested that *Pe*Chi4 was a processive enzyme, further supported by the presence of Trp (has a crucial role in processivity) after S*X*GG motif. *Pe*Chi3 produced the highest DP2/DP3 ratio of 11.41 indicating a processive exo-chitinase. The structure of *Pe*Chi3 showed similar to a *B. cereus* NCTU2 without any comparable deep substrate binding cleft but yet can degrade in an exo- and processive mode with a novel substrate binding mechanism (Hsieh et al., 2010).

4.3.6 *Pe*Chi1 had feeble inherent TG activity

Chitinases from Gram-positive bacteria have not been studied extensively for TG activities, except one GH18 chitinase from *B. circulans* WL-12 (chitinase A1). In our

study, among the four chitinases from *P. elgii*, we observed a weak TG activity by *Pe*Chi1 with a potential to synthesize DP7 from DP5 substrate (Fig. 4.10A, Table 4.3). The presence of DP3 hydrolysed product, when DP4 was used as a natural substrate (*Pe*Chi1 had no ability to degrade DP4 into DP3 and DP1), provided indirect evidence of TG activity on DP4 substrate. DP3 product can only be a hydrolysis product from DP6 intermediate formed as a result of TG activity, as observed in *Sm*ChiB (Zakariassen et al., 2011). The inherent feeble TG activity by *Pe*Chi1 remained only up to 10 min, enticing the scope to improve TG by the mutational approach.

Table 4.2: Molar ratio of DP2 to DP3 as a measure of processivity.

Enzyme	DP2 (mM)	DP3 (mM)	DP2/DP3
*Pe*Chi1	0.010689	0.006124	1.745541
*Pe*Chi3	0.217699	0.019072	11.41428
*Pe*Chi4	0.163061	0.029654	5.498854
*Pe*Chi5	0.010227	0.005214	1.961409

4.3.7 Targeted mutagenesis of *Pe*Chi1 to improve TG activity

The main difficulty in using GH with meagre inherent TG was that the generated COS of the TG reaction will necessarily be a substrate for the enzyme, which can result in the poor yield of longer chain COS. Although the TG products are kinetically controlled, monitoring of the reaction would be quite difficult due to lack of temporal difference between the hydrolytic and TG activities.TG could be enhanced by decreasing the effective concentration of water molecule in the catalytic cleft and/or the addition of large excesses of the acceptor molecule (Williams & Withers, 2000). Targeted mutagenesis of chitinases yielding modified enzymes with reduced hydrolytic activity appears to be a suitable strategy for improving TG reaction. Therefore, we employed a mutational approach to alter the substrate interaction in the catalytic cleft of *Pe*Chi1 for improving TG.

Table 4.3: Summary of products generated from oligosaccharide and polymer substrates catalysed by *Pe* chitinases. Brackets represent the major end products.

Enzyme	Products generated from oligosaccharide and polymer substrates					Substrate -binding cleft	Mode of action
	Chitooligosaccharides				Polymer (Colloidal chitin)		
	DP3	DP4	DP5	DP6			
*Pe*Chi1	-	DP2, DP3 (DP2)	DP2-DP7 (DP2)	DP2-DP5 (DP2)	DP2-DP4 (DP2)	Deep tunnel	Endo, processive
*Pe*Chi3	DP1, DP2	DP2	DP1-DP3 (DP2)	DP1-DP4 (DP2)	DP1-DP3 (DP2)	Open and shallow	Exo, processive
*Pe*Chi4	DP1, DP2	DP1-DP3 (DP2)	DP1-DP4 (DP2)	DP1-DP4 (DP2)	DP1-DP3 (DP2)	Deep tunnel with closed roof	Exo, processive
*Pe*Chi5	DP1, DP2	DP2	DP1-DP3 (DP2)	DP1-DP4 (DP2)	DP1-DP4 (DP2)	Open and shallow	Endo, nonprocessive

Chitinases belonging to family 18 are retaining glycoside hydrolases and are characterised by the presence of D*X*D*X*E catalytic motif. The positioning and nucleophilicity of the acetamido group are heavily influenced by residues in the catalytic cleft, in particular by a conserved middle Asp residue. In ChiB from *S. marcescens*, it has been suggested that rotation of D142 with concomitant dynamic changes in the accompanying catalytic residues play an essential role in catalysis (Synstad et al., 2004; van Aalten et al., 2001). In the present study, the middle D141of *Pe*Chi1 was mutated to Asn, which resulted in the substantial loss in hydrolysis on colloidal chitin (Fig. 4.15) and completely lost both hydrolysis and TG on DP5 substrate (Fig. 4.16B). This observation suggested that the middle D141 was an essential residue for catalysis in *Pe*Chi1. Substitution to Asn could alter the active site electrostatic interactions in a way which affected the stability of the oxazolinium ion

and the reactivity of the catalytic water. As hydrolysis and TG are coupled reaction, loss of hydrolysis on DP5 substrate led to a loss in TG. However, in a study on *Sm*ChiA and ChiB by Zakariassen et al. (2011), the substitution of middle Asp in D*X*D*X*E motif to Asn led to increase in TG with the concomitant decrease in hydrolysis.

The docking study of *Pe*Chi1 with A5 revealed the residues G103 and Y105 were present very close to the catalytic center (Fig. 4.13B). G103 is the last residue of the S*X*GG motif. This conserved motif is usually followed by a Trp in processive chitinases (in *Sm*ChiA and ChiB: SIGGW), which is essential for processivity and efficient degradation of insoluble chitin (Zakariassen et al., 2009). Trp in many GH18 chitinases is thought to maintain the architecture of the catalytic groove with its bulky side chain. Substitution of W97 to Ala in *Sm*ChiB and W114 to Ala in *Sp*ChiD resulted in the loss of TG activity (Zakariassen et al., 2011, Madhuprakash et al., 2012). However, in *Pe*Chi1, we found Y105 in place of Trp. Docking of A5 revealed that G103 and Y105 residues in *Pe*Chi1 seem to be involved in threading of the chitin molecules towards the catalytic center. Hence, point mutations were planned to increase TG and also to recognise the key residue for TG. Both G103 and Y105 were mutated to Trp. The mutant G103W completely lost hydrolytic activity towards colloidal chitin (Fig. 4.15) and DP5 (Fig. 4.16C), and thus the concomitant loss in TG on DP5 substrate. The introduction of bulkier amino acid residue in G103W presumably provided stronger interaction with the substrate in the catalytic tunnel and not allowed the substrate to enter into the catalytic center. A similar observation was made in *Sp*ChiD, where substitution of G113 to Trp lost both hydrolytic and TG activities to a greater extent. A further detailed study by MD simulation also showed the introduction of Trp blocked the tunnel entrance in *Sp*ChiD (Madhuprakash et al., 2014).

The mutant Y105W resulted in the formation of nearly 2 fold DP7 as a TG product, when DP5 was used as the substrate, suggesting the crucial role of bulkier aromatic residue in the +1 subsite (Fig. 4.19). It is conceivable that the bulkier side

chain of Trp facilitated increase number of interactions with the incoming substrate and hence increased TG. The mutant Y105W was also unique in showing higher TG activity irrespective of increased hydrolysis in comparison to the wild type, suggesting the faster deglycosylation step in *Pe*Chi1-Y105W due to a higher rate of formation of TG products as observed in *Sm*ChiA-D313 N/F396W (Zakariassen et al., 2011).

Among the generated single mutants, Y105W showed enhancement in TG on DP5 substrate and also showed the detectable quantity of TG products on DP4 substrate. To further enhance the TG in *Pe*Chi1, double mutants were created on *Pe*Chi1-Y105W by selecting residues at the catalytic center and groove. The residues M216 and Y218 with their side chains close to the catalytic triad D*X*D*X*E are likely to interact with the sugar molecule during catalysis (Fig. 4.13). The residueM216may not be directly involved in catalysis, but seems an essential supporting residue for catalytic activity. The mutant Y105W/M216A displayed a strong decrease in hydrolytic activity and lost TG activity (Fig. 4.18B), suggesting the reduced hydrophobic interaction probably destabilise the oxazolinium intermediate needed for the usual pace of reaction. The Y105W/Y218A completely lost hydrolytic and TG activity (Fig. 4.18C). The residue Y218 is conserved in many chitinases and may involve in stabilising the transition state (Synstad et al., 2004). The loss of hydrolytic activity in Y105W/Y218A could be due to destabilization of the transition state.

In GH18 chitinases, the S*X*GG (residue 101-104 in *Pe*Chi1) followed by a Trp in processive chitinases is much conserved and plays a role in substrate binding in the catalytic groove. These residues directly involve in threading of chitin molecules, and alteration of these residues in this region has been shown to affect substrate interaction leading to either improvement or loss in catalysis or TG (Madhuprakash et al., 2012). Based on this observation, we planned point mutations in this motif along with Y105W substitution to improve TG. In *Pe*Chi1, G101 is present in place of Ser (first residue in S*X*GG). Therefore, we changed G101 to Ser in combination with Y105W. The Y105W/G101S displayed more than two-fold hydrolytic activity both on colloidal chitin (Fig. 4.14) and DP5 (Fig. 4.18D) substrates with a remarkable decrease in TG

activity. The introduction of S101 presumably changed the active site electrostatic interactions favouring the incoming water molecule needed for catalysis. Although the hydrolytic activity of the double mutant Y105W/G104S decreased, there was no increase in TG (Fig. 4.18E). Our result indicates substitution of Ser to Gly in the S*X*GG motif could be an efficient target for improving TG in chitinases. This was further supported by the observation that substitution of S116 in *Sp*ChiD to Gly resulted in improved TG (Madhupraksh et al., 2012).

The amino acid F62 is located at -2 subsite and its substitution with Trp along with Y105W displayed TG activity similar to the Y105W, but increased the duration of formation of TG product (Fig. 4.18F & Fig. 4.19). Though both Phe and Trp residues confer aromaticity, the bulkier side chain of Trp with increased surface area facilitates more interactions with the sugars. The retention of sugar donor due to stronger interaction at the glycon subsite presumably slowed down the hydrolytic activity without affecting TG. Therefore, the introduction of bulkier aromatic amino acid at -2 and +1 subsites i.e. F62W/Y105W resulted in increased TG both in quantity and duration of accumulation of TG products.

Chapter V

Degradation of chitosan by a multi-domain chitosanase from *P. elgii* and role of its CBM32 in chitosan binding

5.1. Introduction

The biological activities of COS primarily depend on properties like DP, DA, and most likely also on the PA. Depending on the type of enzymes and chitosan substrates, COS of varied length and chemical composition can be obtained. The subsite specificity of an enzyme will have the greatest influence on the composition of COS generated. Enzymes of broad subsite specificities have the potential to produce larger variations in COS. However, use of enzyme with higher subsite specificity can yield less complex COS mixtures. Several chitinases belonging to family GH18 (Horn et al., 2006a; Horn et al., 2006b; Sikorski et al., 2005 & 2006) and a GH19 chitinase (Heggset et al., 2009) were examined to gain in-depth insight into enzyme function using chitosans as substrates. Analysis of the hydrolysed products provided information on subsite specificities (for acetylated, A, or deacetylated, D, sugars) in the active site of the enzyme. So far, subsite specificies of a few chitosanases belonging to families GH46 (Heggset et al., 2010) and GH75 (Heggset et al., 2012) were only studied. There was no detailed information on the subsite specificity of GH8 family chitosanases based on the analysis of the generated hydrolysed products.

Chitosanases are found in seven different GH families. But, the mechanism of chitosan binding and degradation by chitosanases, in comparison to chitin and cellulose degradation, is not fully understood due to lack of well-defined chitosan substrates concerning their DA and PA. Further, the amorphous nature of chitosan suggests the substrate binding mechanism of chitosanases would differ from chitinases and cellulases. Chitosanases often have a single catalytic domain without any auxiliary domains, unlike chitinases and cellulases which are frequently associated with CBMs. The chitosanase of *P. elgii* (*Pe*Csn) is a multi-domain protein with an N-terminal GH8 catalytic domain and a C-terminal CBM32 (*Pe*CBM32) linked by an FN3 domain. Therefore, we attempted to address the questions listed below:

1. What is the mode of action of a muti-domain chitosanase, *Pe*Csn?
2. What is the subsite specificity of *Pe*Csn?

3. How does *Pe*CBM32 influence the amorphous chitosan substrate degradation?
4. What is the specificity of *Pe*CBM32 in binding to different carbohydrate molecules?

To address these questions, we have initially characterized *Pe*Csn in terms of their temperature and pH optima, enzyme kinetics and product profile analysis by TLC and MS. By using specific chitosan polymers and oligomers, we have investigated the subsite specificity of *Pe*Csn. The specificities and affinities of CBM32 towards chitosan polymers and oligomers were studied by dot blot assay, CD spectroscopy-based thermal unfolding, and isothermal titration calorimetry. For a better understanding of an apparently specific interaction, we have identified amino acid residues that could be crucial for such interaction using 3D model-guided site-directed mutagenesis. We also show that *Pe*CsnCBM32 of *P. elgii* can be used for *in situ* staining of chitosan of fungal cell wall during the plant-fungal interaction.

5.2. Results

5.2.1 Cloning, expression and purification of *Pe*Csn and its truncations

*Pe*csn gene of *P. elgii* SMA-1-SDCH02 was amplified based on the draft genome sequence information of *Paenibacillus elgii* B69. The amplicon of 1869 bp without the predicted N-terminal signal peptide nucleotide sequence (126 bp) was cloned into pET 22b(+) vector and confirmed by restriction digestion (Fig. 5.1A, B). Sequencing of inserted *PeCsn* gene showed 96.5% identity to *P. elgii* B69 chitosanase gene. Analysis of the deduced polypeptide of 623 amino acid by SMART data base showed that *Pe*Csn is a multi-domain protein with an N-terminal GH8 catalytic domain, and a C-terminal CBM32 linked by FN3 domain (Fig. 5.2). BLASTP analysis of complete *Pe*Csn showed the highest similarity to *P. fukuinensis* chitosanase (71%). *PeCsn* gene was over expressed with C-terminal StrepII-tag in *E. coli*, and the whole cell lysate was extracted in soluble form. SDS-PAGE analysis of purified *Pe*Csn revealed a molecular mass ~69 kDa (Fig. 5.1C, D). The molecular mass of the recombinant truncated proteins – *Pe*CBM32, GH8 and GH8FN3 was 18, 42 and 51 kDa, respectively (Fig. 5.1E).

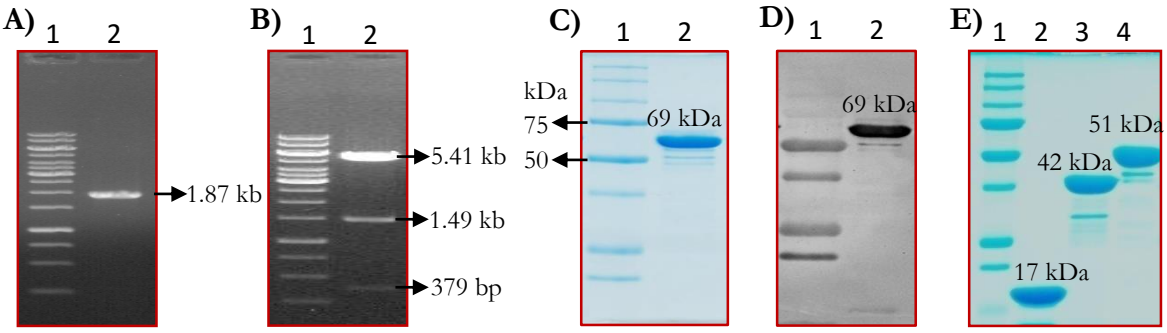

Fig. 5.1: Amplification, cloning and heterologous expression of *Pecsn*. A) *Pecsn* (lane A2) was PCR-amplified with gene specific primers using gDNA as a template and resolved on 1% agarose gel. The molecular weight marker was GeneRuler™ 1 kb DNA ladder mix (250 bp-10 kb; lane A1). **B)** The presence of insert was confirmed by double digestion with *Nde* I and *Sac* I (lane B2). **C)** Recombinant *Pe*Csn was purified using Strep-Tactin column, and the eluted purified protein was loaded on 12% SDS-PAGE followed by staining with Coomassie brilliant blue G-250. The protein marker used was Precision Plus Protein™ Standard (lane C1). **D)** Western blot of *Pe*Csn detected by chemiluminescence after incubation with Strep-Tactin-HRP conjugated antibody. **E)** SDS-PAGE profile of the purified truncated proteins (lane E2 - *Pe*CBM32, lane E3 - GH8, lane E4 - GH8FN3).

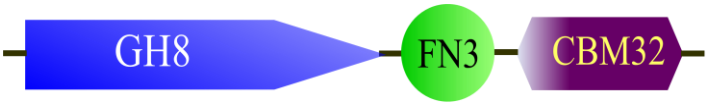

Fig. 5.2: Domain organisation of *Pe*Csn. Multi-domain *Pe*Csn showing an N-terminal glycoside hydrolase 8 (GH8) catalytic domain, fibronectin type III (FN3) domain and a C-terminal carbohydrate binding module belonging to family 32 (CBM32).

5.2.2 Effect of temperature and pH

The optimum temperature of *Pe*Csn was at 60°C and showed activity over a broad range of 30-70°C (Fig. 5.3A). At 70°C, *Pe*Csn retained ~50% of activity. Beyond 70°C, we couldn't measure activity due to precipitation of enzyme. Similarly, enzyme assay using 0% DA chitosan with different pH range buffers revealed that *Pe*Csn was active over a narrow range between pH 5.0-8.0 with optimum activity at pH 6.0 (Fig 5.3B). At pH below 5.0, the activity decreased drastically with complete loss in activity at pH ≤ 4.0.

5.2.3Effect of DA of chitosan on *Pe*Csn

To evaluate the effect of DA on *Pe*Csn, the hydrolytic activity with different DA of

soluble polymeric chitosan substrates was compared. *Pe*Csn preferred chitosans of lower DA as we observed maximum specific activity on 0% DA chitosan i.e. 11.10 $mg.ml^{-1}.min^{-1}$ (Fig. 5.4). With increase in DA, the activity of *Pe*Csn decreased substantially as seen with 60% DA chitosan substrate (0.794 $mg.ml^{-1}.min^{-1}$).

The hydrolytic ability of *Pe*Csn was also analysed using polymeric chitosan substrate after different incubation periods. The TLC profile showed that *Pe*Csn released COS ranging from DP3-DP6 and even longer COS during the initial stages of reaction (Fig. 5.7). At 30 min chitosan polymer was completely degraded into smaller COS, predominantly to DP2, DP3 and DP4. During the reaction time course, intermediate products generated at initial phase were further hydrolysed into DP2 and DP3 as the end products of the reaction.

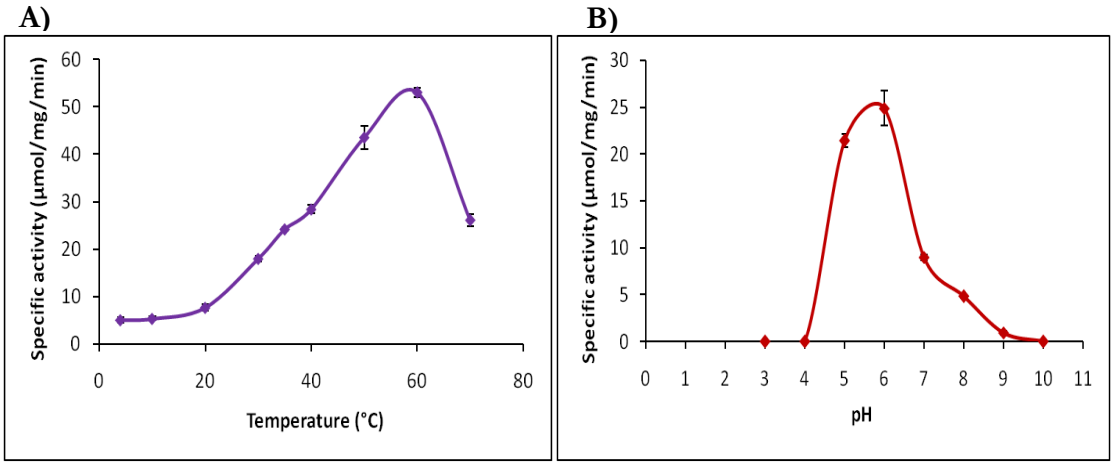

Fig. 5.3: Effect of temperature (A) and pH (B) on the activity of *Pe*Csn. The effect of temperature on *Pe*Csn activity was determined in 50 mM sodium acetate buffer pH 6.0 at different temperatures ranging from 4-70°C. The optimum pH was determined in buffers of different pH from 3-10 (40 mM ammonium formate, 20 mM TEA, 20 mM KH_2PO_4 and 20 mM Na_2HPO_4; pH was adjusted with NaOH). All the reactions were incubated for 5 min using 0% DA chitosan (1 $mg.ml^{-1}$) and 0.3 µg of enzyme and was monitored by reducing sugar determination by MBTH method. Vertical bars represent standard error of triplicate experiments.

5.2.4 Steady state kinetics analysis

The activity of enzyme ($\mu moles.min^{-1}$) obtained by reducing end assay at different substrate concentrations ($mg.ml^{-1}$) was fitted to the Michaelis-Menten equation by

nonlinear regression function of GraphPad Prism version 5.0 software (Fig. 5.5). The curve fitting for *Pe*Csn showed a K_m of 0.543 mg.ml^{-1}, a K_{cat} of 6.58×10^3 min^{-1}, and a K_{cat}/K_m of 1.2×10^4 min^{-1}.mg^{-1}.ml on polymeric chitosan substrate (DA 0%) at optimum pH 6.0 and 60°C.

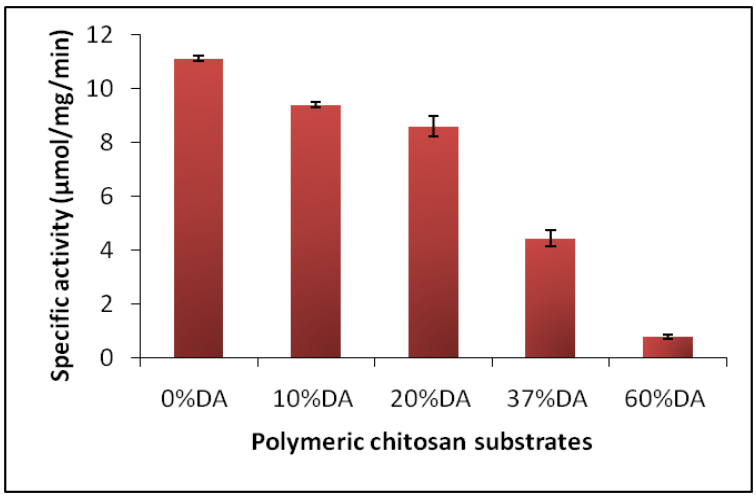

Fig. 5.4: Effect of DA on the activity of *Pe*Csn. The reaction mixture containing *Pe*Csn (1 µg) and polymeric soluble chitosan substrates of different DAs (1 mg.ml^{-1}) were incubated in 50 mM sodium acetate buffer at 60°C for 10 min. The reaction was monitored by reducing sugar determination. Vertical bars represent standard error of triplicate experiments.

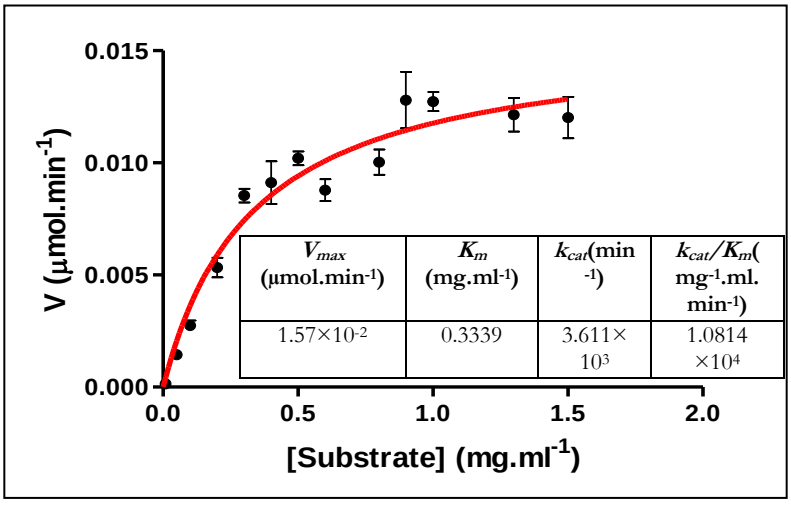

Fig. 5.5: Kinetic analysis of *Pe*Csn. Varying concentration of 0% DA chitosan substrate (0.01-1.5 mg.ml^{-1}) was incubated with *Pe*Csn (0.3µg) in 50 mM sodium acetate buffer with respective controls in triplicates at 60°C for 10 min. The velocity of the reaction was calculated and plotted against substrate concentration. The data was fitted to the Michaelis-Menten equation by nonlinear regression function using GraphPad Prism software version 5.0 to construct the kinetics graph and derive kinetic parameters (inset table).

5.2.5 Hydrolytic product analysis generated by *Pe*Csn from oligomeric and polymeric chitosan substrates

To assess the ability and effectiveness of *Pe*Csn to hydrolyse natural substrates and to get insight into the mode of action, the hydrolytic products were analysed using TLC. The complete hydrolysis of DP6 by *Pe*Csn was observed within 5 min with DP2 as major end product followed by DP3 (Fig. 5.6A). DP6 hydrolysis yielded DP2, DP3

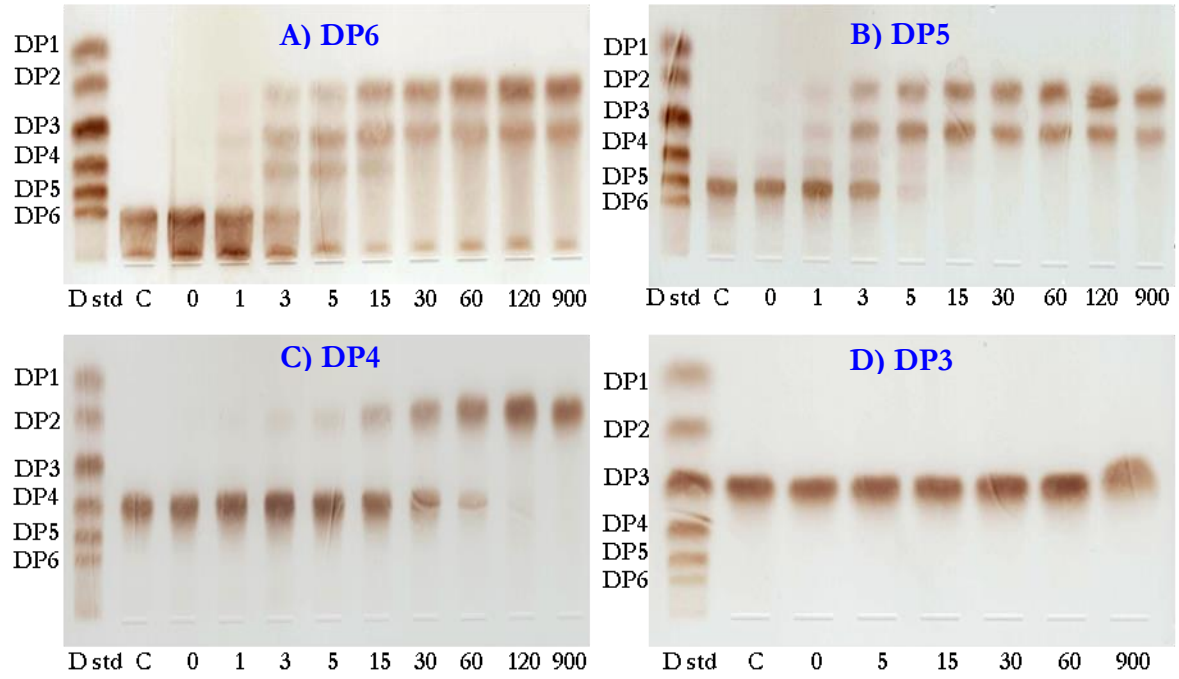

Fig. 5.6: Time course of oligomeric chitosan substrate hydrolysis by *Pe*Csn analysed by TLC. Reaction mixtures containing 1 µg *Pe*Csn and 2 mg.ml^{-1} of each oligomer in 50 mM sodium acetate buffer were incubated for varied times ranging from 0-900 min at 60°C. At various indicated incubation periods, 10 µl of the reaction mixture was withdrawn and directly added to 10 µl of 0.1 N NaOH to stop the reaction. The total reaction solution (20 µl) was vacuum dried and dissolved in 10 µl H_2O, and loaded on to TLC plates. Hydrolysed sugar products were detected with 30% ammonium bisulphate solution. Lane D std: a chitosan standard mix of DP1–DP6, lane C: control substrate without enzyme, lanes 0-900: time (min) at which samples were withdrawn. A-D: TLC profile of DP6, DP5, DP4, DP3 substrate.

and DP4 and subsequently, DP4 degraded into DP2. The product DP4 remained up to 15 min and was converted completely to DP2 from 30 min onwards. On DP5substrate, *Pe*Csn released DP2 and DP3 as primary end products (Fig. 5.6B).

Hydrolysis products formed from 1 min onwards and complete degradation of DP5 was attained at 15 min. With DP4 substrate, the activity of *Pe*Csn was slower in comparison to activity on longer oligomers. Hydrolysis of DP4 by *Pe*Csn generated DP2 as a sole end product, and formation of DP2 started from 3 min with a steady increase in the concentration up to 60 min. The complete hydrolysis of DP4 was attained at 120 min (Fig. 5.6C). When DP3 was used as the substrate, *Pe*Csn couldn't release hydrolysed products (Fig. 5.6D) up to 900 min.

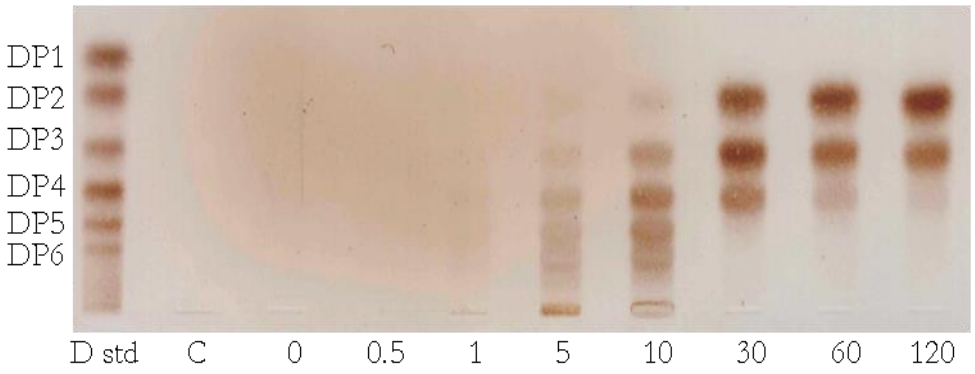

Fig. 5.7: Time course of 0% DA chitosan polymer hydrolysis of *Pe*Csn analysed by TLC. Reaction mixtures containing 1.5 µg *Pe*Csn and 2.5 mg.ml^{-1} of chitosan polymer in 50 mM sodium acetate buffer were incubated for varied times ranging from 0-120 min at 60°C. The total reaction solution (20 µl) was vacuum dried and dissolved in 10 µl H_2O and loaded on to TLC plates. Hydrolysed sugar products were detected with 30% ammonium bisulphate solution. Lane D std: a chitosan standard mix of DP1–DP6, lane C: control substrate without enzyme, lanes 0-120: time (min) at which samples were withdrawn.

5.2.6. Determination of subsite specificity of *Pe*Csn

To analyse the productive binding specificity of *Pe*Csn at different subsites, two approaches were followed. In the first approach, defined PA tetramers were generated by using available CDAs, either individually or in combinations. The tetramers thus generated with defined PA were then used as substrates for *Pe*Csn, and the subsequent hydrolytic products were analysed by UHPLC-ELSD-ESI-MS to decipher cleavage site. In the second approach, the hydrolytic products, generated by *Pe*Csn from DA 37%chitosan polymer, were sequenced and quantified to determine cleavage sites.

5.2.6.1 Subsite determination by using defined PA chitosan tetramers

A chitin tetramer (A4) was selectively deacetylated using chitin deacetylases (CDAs) like NodB, COD, CDA2 and Pgt. NodB deacetylates the first unit and COD deacetylates the second unit of A4 starting from the non-reducing end (Hamer et al., 2015). Similarly, CDA2 deacetylates the penultimate unit from reducing end where as Pgt deacetylates two units from the reducing end (unpublished). Use of these CDAs resulted in synthesis of chitosan tetramer of different PAs i.e., A-D-A-A, A-D-D-A, D-D-A-A, A-D-D-D, D-A-D-D and D-D-D-A (Table 5.1).

To test the ability of *Pe*Csn to cleave different PA chitosan tetramers, enzymatically generated chitosan oligomers were incubated with *Pe*Csn. The products were analysed by UHPLC-ELSD-ESI-MS. The expected cleavage products of chitosan tetramer of different PAs with their molecular weight (M_w) are given in table 5.1.

Table 5.1: Determination of cleavage specificity of *Pe*Csn on different PAs of chitosan tetramer analysed by UHPLC-ELSD-ESI-MS.

Name of CDA used	Generated chitosan tetramers with different PA	M_w of chitosan tetramers	Expected dimers to be generated after hydrolysis by *Pe*Csn with their M_w	m/z obtained after MS analysis
COD	A-D-A-A (DA3)	788.31	A-D-A-A → A-D (382.15)	Not found
			A-D-A-A → A-A (424.16)	Not found
NodB+ CDA2	A-D-D-A (D2A2)	746.30	A-D-D-A → A-D (382.15)	Not found
			A-D-D-A → D-A (382.15)	Not found
COD+ NodB	D-D-A-A (D2A2)	746.30	D-D-A-A → D-D (340.14)	341.15 $[M+H]^+$
			D-D-A-A → A-A (424.16)	Not found
COD+ Pgt	A-D-D-D (D3A)	704.29	A-D-D-D → A-D (382.15)	Not found
			A-D-D-D → D-D (340.14)	Not found
NodB+ Pgt	D-A-D-D (D3A)	704.29	D-A-D-D → D-A (382.15)	Not found
			D-A-D-D → D-D (340.14)	Not found
COD+ NodB+ CDA2	D-D-D-A (D3A)	704.29	D-D-D-A → D-D (340.14)	341.15 $[M+H]^+$
			D-D-D-A → D-A (382.15)	383.18 $[M+H]^+$

Among the tested oligomers, *Pe*Csn cleaved D-D-D-A giving rise to dimers, D-D and D-A of Mw 341.15 and 383.18, respectively (Fig. 5.8). Substrate control of D-D-D-A without enzyme treatment didn't show any peak for D-D and D-A. When D-D-D-A was incubated along with the natural substrate D4, *Pe*Csn cleaved D4 into two molecules of D-D of Mw 341.15 and also cleaved D-D-D-A into D-D (same peak as the degradation product from D4) and D-A with lower intensity as seen in Fig. 5.8, panel III. *Pe*Csn was not active on A-D-A-A, A-D-D-A, D-D-A-A, D-A-D-D and A-D-D-D (Fig. 5.9). Mass search for the cleaved product of D-D-A-A showed peaks for D-D and D-A without any peak for A-A, indicating that the degradation product was not from D-D-A-A. Therefore, it was evident that D-D and D-A were the cleaved product of D-D-D-A which was present as an additional contaminant as seen in the chromatogram of substrate control (Fig. 5.9C).

5.2.6.2 Subsite determination using polymeric chitosan

One of the major challenges in determining subsites using defined PA tetrameric chitosan substrates was to generate appropriate substrates using CDAs. For example, suitable CDA was not available to generate D-D-A-D substrate. Therefore, the subsite preference of *Pe*Csn at +1 position couldn't be determined. To overcome this, we used 37% DA polymeric chitosan to generate hydrolysate with a mixture of oligomers of various PA and DA. The PA of oligomers of chain length DP2 to DP6 was determined and quantified (Fig. 5.10) to find out the binding preferences in different subsites.

Fig. 5.11 showed the COS generated at 2 min were exclusively deacetylated residues (D) at the new reducing and non-reducing ends revealing a clear preference for D-units in the -1 and +1 subsite. At 20 min, less than 5% COS had A-unit at -1 and -2 subsites. Similarly, ~10% of COS had A-unit in +2 subsite; whereas at +1 subsite, the COS having a preference for A-unit was near to 30%. More extensive degradation of chitosan (720 min) generated near to ~60% of COS having A-unit in +1 subsite followed by ~12% of COS showing A-unit in -1 subsite.

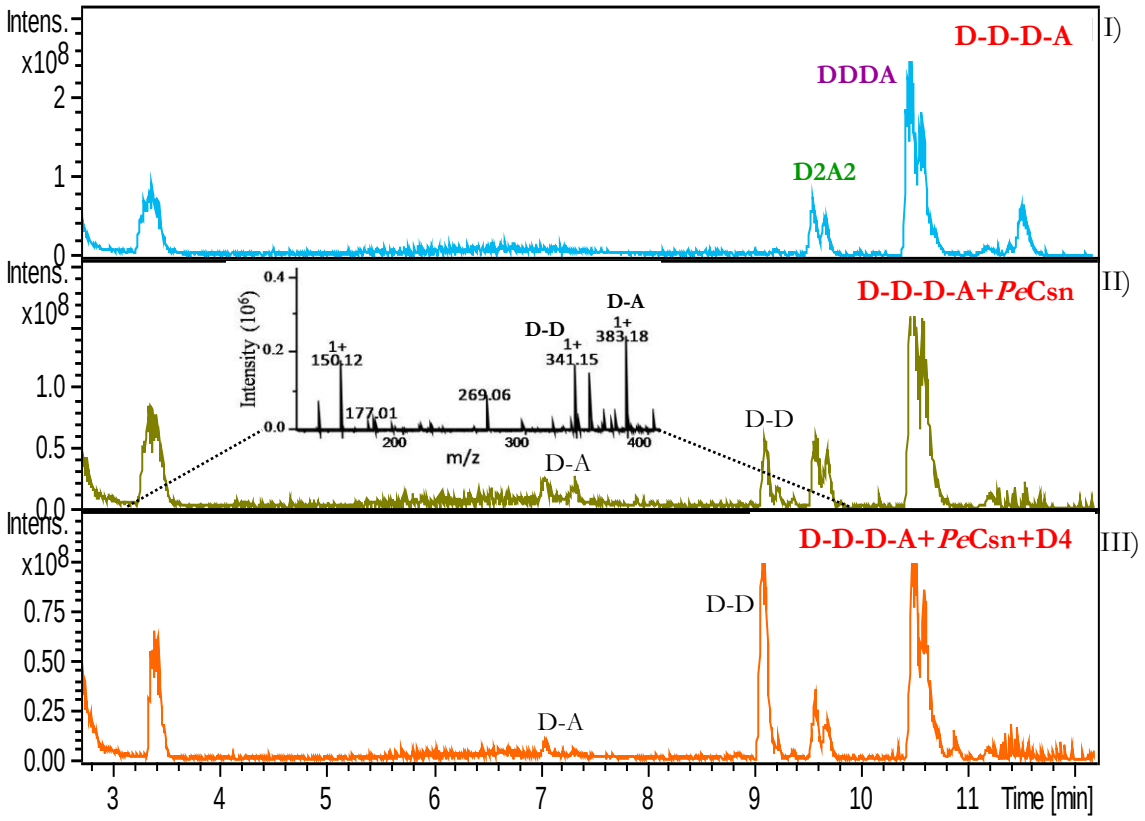

Fig. 5.8: A representative figure showing cleavage specificity of *Pe*Csn analysed by UHPLC-ELSD-ESI-MS. Hydrolysis of D-D-D-A by *Pe*Csn is shown in this figure. Freeze dried D-D-D-A (1mg.ml^{-1}) was dissolved in 15 µl ammonium acetate buffer pH 6.0. The reaction was set up by making three different aliquots each of 5 µl. **I)** The first aliquot was the substrate control (D-D-D-A) without the addition of *Pe*Csn. **II)** The second aliquot was treated with *Pe*Csn (D-D-D-A+*Pe*Csn). **III)** Before adding *Pe*Csn to the third aliquot (D-D-D-A+*Pe*Csn+D4), a commercially available pure D4 (D-D-D-D) was added into the reaction and considered as positive control. Reactions were incubated at 45°C for 2 h. Aliquot of 2 µl each was taken for UHPLC-ELSD-ESI-MS analysis. **Note:** The enzymatically synthesised D-D-D-A used for the experiment (labeled in violet colour) also had other oligomers in a minor fraction; for instance D2A2 labeled in green colour in the panel I.

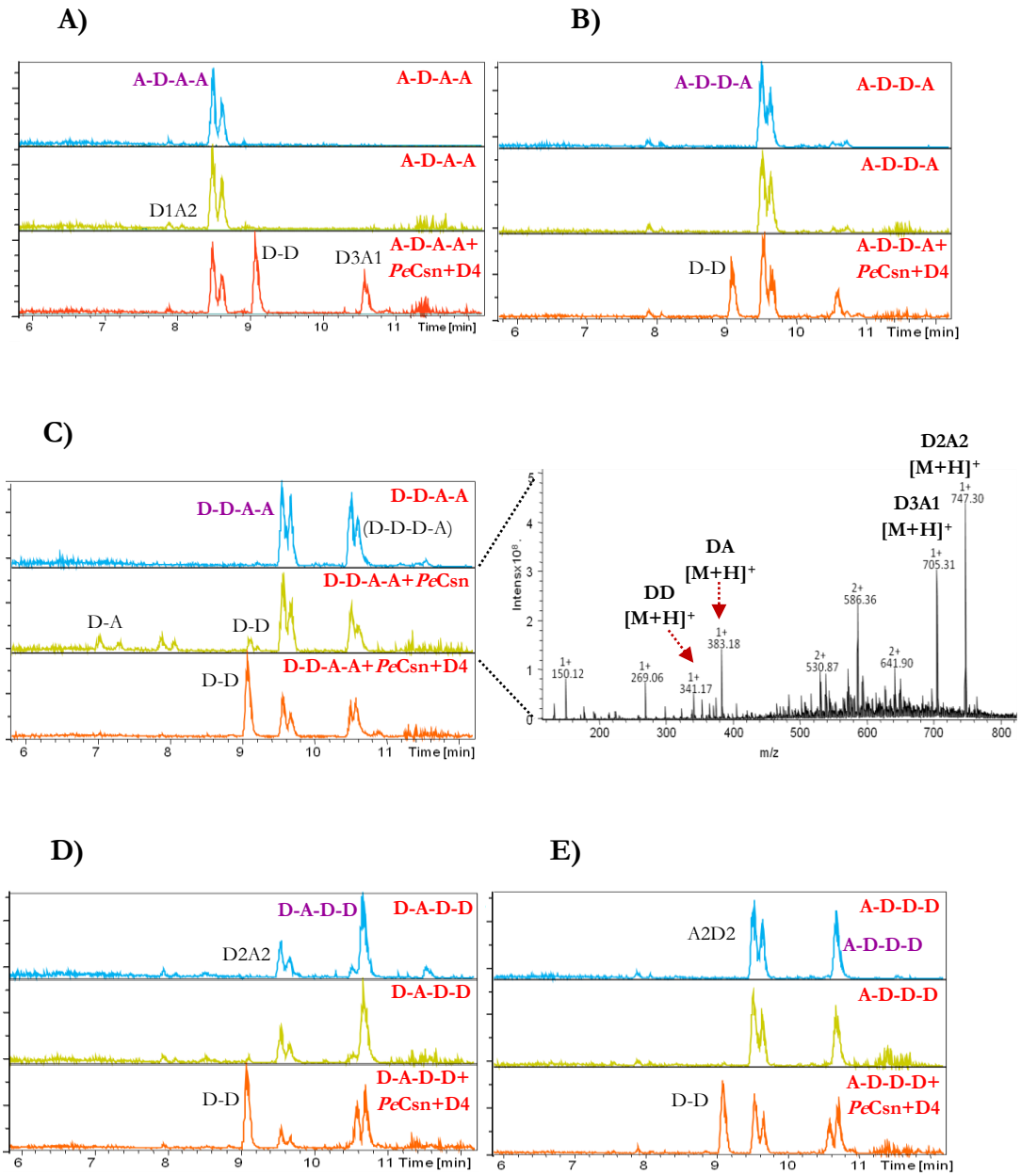

Fig. 5.9: Determination of the cleavage specificity of *Pe*Csn by hydrolysis of various PAs of chitosan oligomers analysed by UHPLC-ELSD-ESI-MS. A) Base peak chromatograph of hydrolysis of A-D-A-A, **B)** base peak chromatograph of hydrolysis of A-D-D-A, **C)** base peak chromatograph and MS analysis of hydrolysis of D-D-A-A, **D)** base peak chromatograph of hydrolysis of D-A-D-D, and **E)** base peak chromatograph of hydrolysis of A-D-D-D. Note: The enzymatically synthesized chitosan oligomers used for the experiment (labelled in violet colour) also had other oligomers in minor fractions.

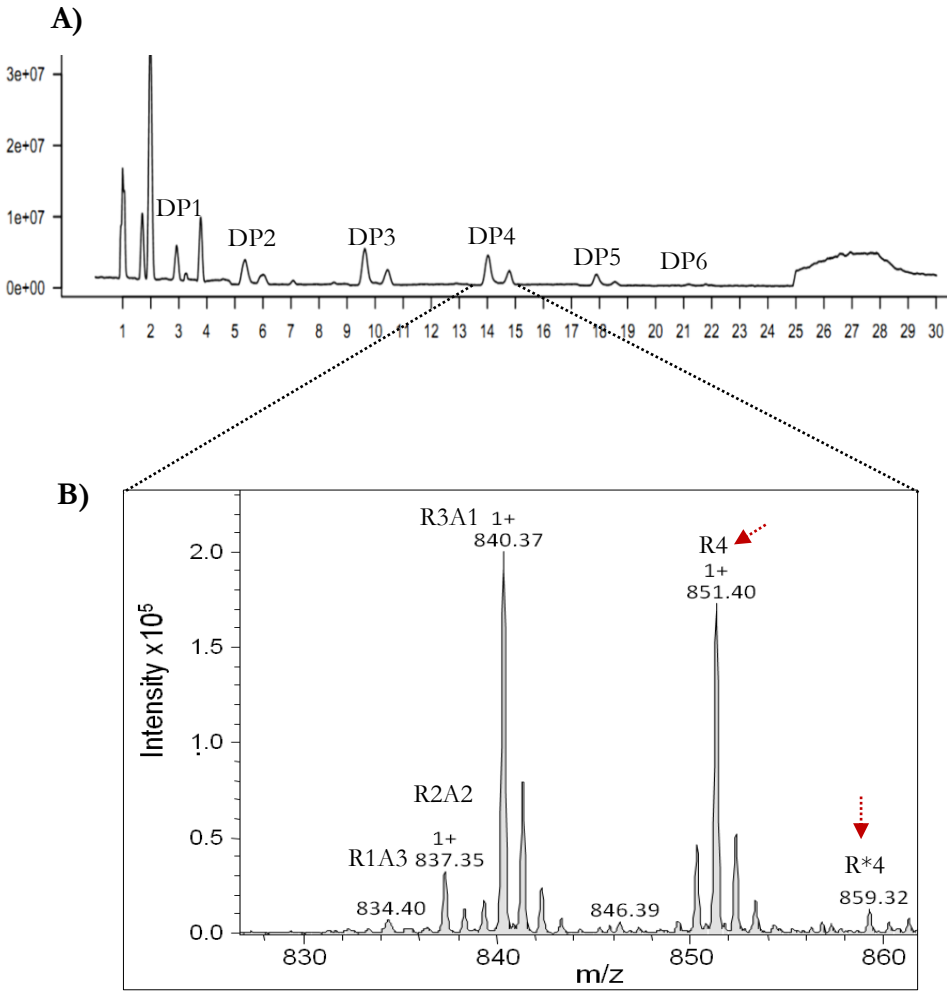

Fig. 5.10: Quantitative analysis of oligosaccharides generated by *Pe*Csn from 37% DA chitosan polymer. Quantitative analysis of COS was done by using an isotopic labeled internal standard in combination with LC-MS^n. The free amino groups of D-glucosamine units (D) in the generated COS were acetylated using acetic anhydride ($^2H_6$). The acetylation resulted in the addition of three ^2H forming a molecule (R) that differs in three unit masses from the existing N-Acetyl-D-glucosamine (A). For pattern analysis, these acetylated COS were incubated with $H_2{}^{18}O$ to label the reducing end for detection of fragmented ions produced from reducing or nonreducing ends by LC-MS^2. On the other hand, the acetylated COS were also mixed with the isotopic labelled internal standard to quantify the COS according to their DP and DA. The internal standard (R*) was produced by reacetylation of D-glucosamine oligomers with a doubly isotopic labelled ($^{13}C_4$-$^2H_6$) acetic anhydride. This acetylation led to the formation of a molecule that had same properties like R but was distinguished by 2 more unit mass. **A)** LC-MS base peak chromatograph showing separation of different COS based on their DP. **B)** As a prototype, MS of DP4 fraction is taken to show the distinction between various molecules depending on their DA. Based on their differences in isotopic masses, R4 and R*4 (red arrow) were differentiated by a unit mass of 8.

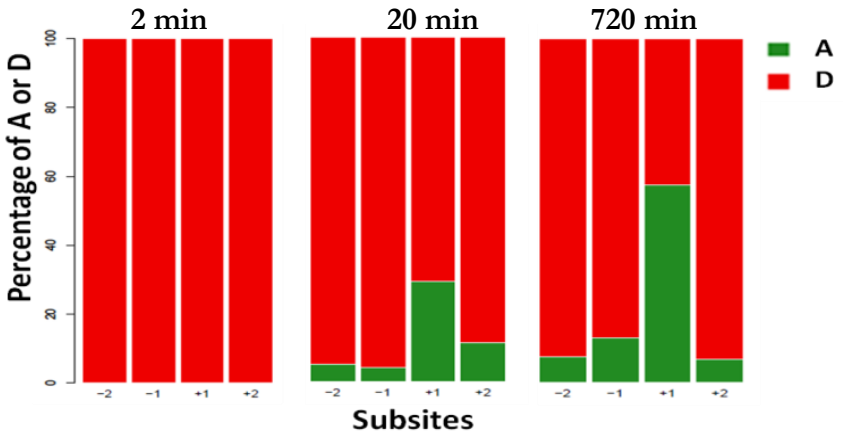

Fig. 5.11: Quantitative estimation of the binding preferences in different subsites. The COS generated by *Pe*Csn at three different time points (2, 20 and 720 min) were quantified as described in Fig. 5.11. Based on the determination of PA of oligomers, the percentage of A or D at various subsites were determined.

5.2.7. Role of *Pe*CBM32 in *Pe*Csn

5.2.7.1 Effect of deletion of *Pe*CBM32 from *Pe*Csn on substrate hydrolysis

To understand the role of *Pe*CBM32 in chitosan degradation, truncated proteins viz. GH8 (lacking FN3 and *Pe*CBM32) and GH8FN3 (lacking *Pe*CBM32) were generated. The calculated molecular mass from the amino acid sequence of the truncated proteins was in reasonable agreement with those assessed by SDS-PAGE (Fig. 5.1E).

The kinetics of hydrolysis of *Pe*Csn and its truncated mutants was determined using 0% DA chitosan as substrate (Fig. 5.12A). The derived kinetic values (K_m, V_{max}, K_{cat} and K_{cat}/K_m) are summarized in Table 5.2. The two truncated protein variants GH8FN3 and GH8 showed a minor increase in the K_m in comparison to the wild type. The overall catalytic efficiency (K_{cat}/K_m) of *Pe*Csn, GH8FN3 and GH8 remained the same suggesting no remarkable influence of *Pe*CBM32 on the activity when soluble chitosan (0% DA) was the substrate (Table 5.2). The hydrolytic activity of both *Pe*Csn and GH8 towards the solubilised chitosan polymers of different DAs decreased substantially when the DA of substrate increased. However, no significant difference in activity was observed between the wild type and the truncated protein (Fig. 5.12B).

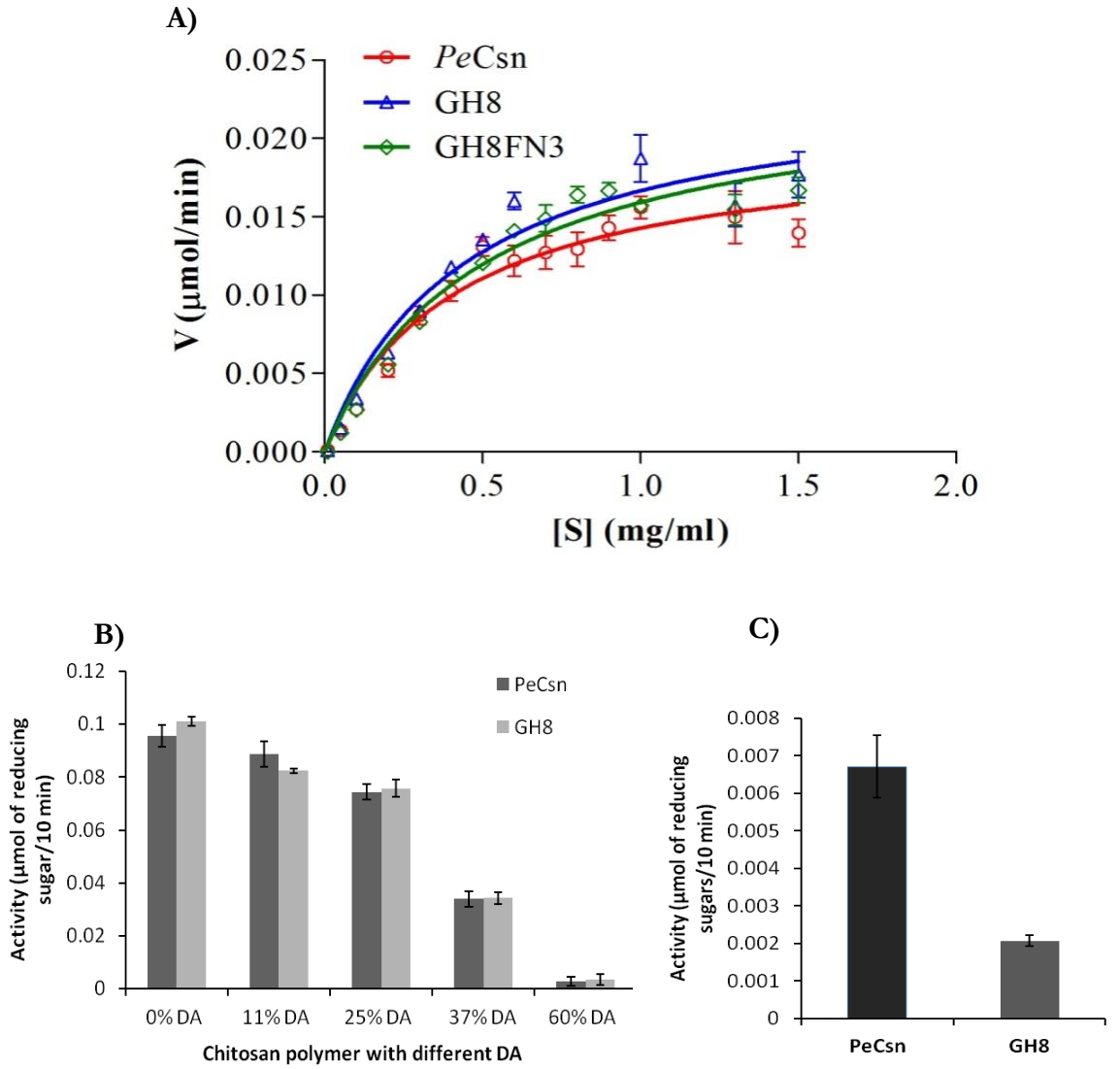

Fig. 5.12: Comparison of hydrolytic activity of *Pe*Csn and its truncated mutants. **A)** Kinetic analysis of *Pe*Csn and its truncated mutants performed on 0% DA chitosan substrate. Equimolar concentration (110nM) of *Pe*Csn, GH8 and GH8FN3 were used, and the hydrolytic activity was measured as µmol of sugar generated per min. The data was fitted to the Michaelis-Menten equation by nonlinear regression function using GraphPad Prism software version 5.0 to get the respective kinetic graphs and parameters. **B)** Chitosan polymers of different DAs were first solubilised and then used as substrates for *Pe*Csn and GH8.**C)** Hydrolytic activity of *Pe*Csn and GH8 on 25% DA insoluble chitosan powder. All the reactions were set up in sodium acetate buffer of pH 5.6at 60ºC for 10 min.

Table 5.2. Comparison of kinetic parameters of *Pe*Csn with its truncated proteins.

Protein	V_{max} (µmol min^{-1})	K_m (mg ml^{-1})	K_{cat}(min^{-1})	K_{cat}/K_m(mg^{-1} ml min^{-1})
*Pe*Csn	2.08x10^{-2}	0.4069	4.61x10^{3}	1.13x10^{4}
GH8FN3	2.29x10^{-2}	0.4817	5.31x10^{3}	1.10x10^{4}
GH8	2.39x10^{-2}	0.4388	5.03x10^{3}	1.14x10^{4}

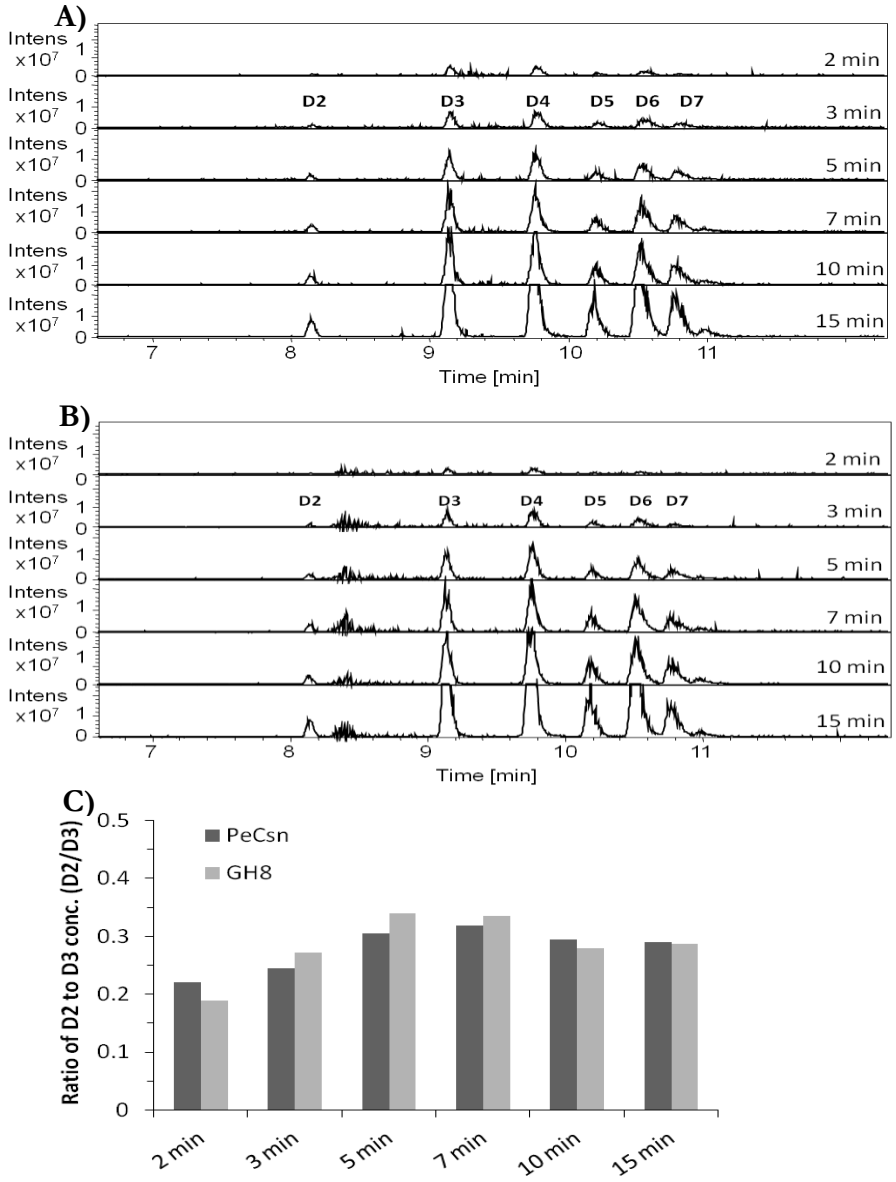

Fig. 5.13: Effect of *Pe*CBM32 on the formation of hydrolysed products. Hydrolysed product analysis of *Pe*Csn **(A)** and GH8 **(B)**. Chitosan of 0%DA was incubated with 5 nM of *Pe*Csn and GH8 in 50mM ammonium acetate pH 5.6 and at 60 °C. At different time points, 10 µl of reaction mixtures were collected and analysed by UHPLC-ELSD-ESI-MS. **C)** Ratio of D2 to D3 concentration analysed by UHPLC-ELSD-ESI-MS at different time points as a measure of processivity.

The activity of GH8 on 25% DA powdered chitosan (without making it soluble) was reduced more than three-fold in comparison to the full length protein (Fig. 5.12C). To discern whether *Pe*CBM32influenced the pattern of product formation, we analysed the hydrolytic products both qualitatively and quantitatively using UHPLC-ELSD-ESI-MS. Hydrolytic products ranging from chitosan dimer to heptamer were observed at the early phase of degradation (Fig. 5.13A, B). With the increase in time, the quantity of all oligomeric products increased progressively both for the wild type and the truncated protein. No noticeable difference in the quantity and pattern of product formation was observed between GH8 and the wild type protein. The ratio of DP2/DP3 for both *Pe*Csn and GH8 was also not affected. Further, the DP2/DP3 ratio for both *Pe*Csn and GH8 was below 0.5 indicating a non-processive mode of degradation (Fig. 5.13C).

5.2.7.2 Binding of *Pe*CBM32 towards polymeric chitosan substrate

The binding specificity of *Pe*CBM32 was detected by a chemiluminescence assay using StrepII antibodies conjugated with HRP. Binding was detected up to 20% DA chitosan with the maximum signal observed for 0% DA chitosan polymer (Fig. 5.14). At a quantity of 0.2 μg, the signal was detected only for 0% DA chitosan polymer. We also clearly observed that the affinity of *Pe*CBM32 decreased with increasing DA. *Pe*CBM32 had no detectable affinity to fully acetylated glycol chitin.

The binding of *Pe*CBM32 to defined DA chitosan polymers was further investigated by measuring the unfolding transition temperature (T_m) using CD spectroscopy at 218 nm as shown in Fig. 5.15. The T_m of *Pe*CBM32 was maximum in the presence of 0% DA chitosan (ΔT_m = 7.2ºC) and 11% DA chitosan (ΔT_m = 7.2). However, elevation of T_m was less for 20% and 60% DA chitosan showing ΔT_m values of 4.5 and 2.9, respectively (Table 5.3). *Pe*CBM32 bound to chitosan polymer with higher affinity where the increase in DA of chitosan polymer resulted in decreased binding.

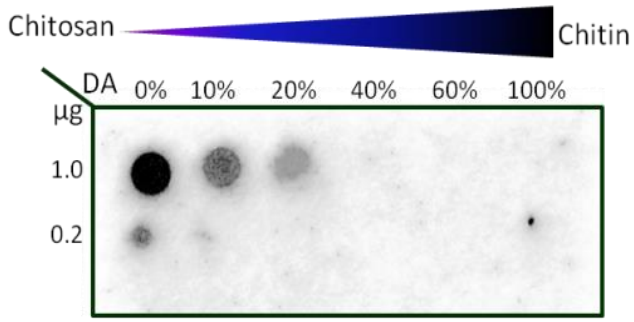

Fig. 5.14: Dot blot assay showing binding specificity of *Pe*CBM32 to polymeric chitosan. Chitosans of different DAs ranging from 0% to 60% and glycol chitin of DA 100% were spotted in a concentration of 1 and 0.2 µg each onto a nitrocellulose membrane. The membrane was blocked with BSA, washed, and incubated with 0.1 mg.ml^{-1} *Pe*CBM32 in TBS containing 5% (wt/vol) BSA for 1 h at 25 °C. Bound *Pe*CBM32 was detected using StrepII antibody.

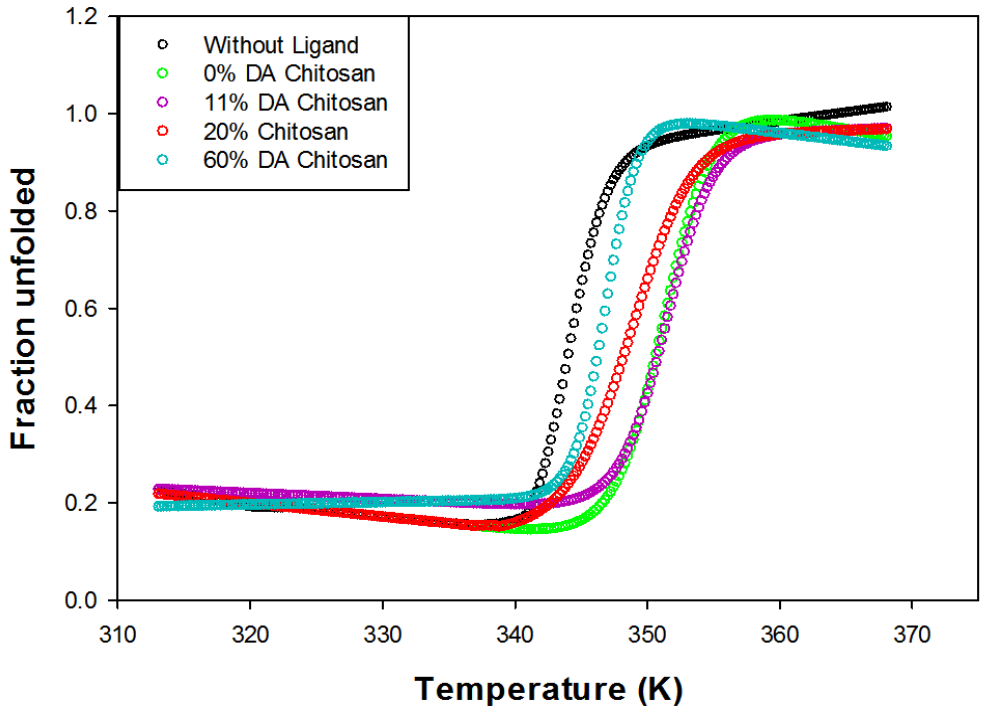

Fig. 5.15: Thermal unfolding of *Pe*CBM32 monitored by CD in the presence of polymeric chitosan. The final concentrations of 35 uM purified *Pe*CBM32 and 1mg.ml^{-1} polymeric chitosans of different DAs in 50mM Na-acetate buffer pH 5.6 were used.

Table 5.3: Thermal unfolding temperatures of *Pe*CBM32 in presence and absence of various chitosan polymers.

Ligands	*T*m (K)	Δ*T*m (°C)
None	344.0418 (70.89°C)	-
0% DA chitosan	351.2988 (78.14°C)	7.25
11% DA chitosan	351.2873 (78.13°C)	7.24
20% DA chitosan	348.5091 (75.35°C)	4.46
60% DA chitosan	346.9553 (73.80°C)	2.91

5.2.7.3 Binding of *Pe*CBM32 towards oligomeric substrates

The binding of D1, D2, D3, D4, A3 and cellobiose was studied using ITC at pH 5.6 and 25°C. Typical ITC thermograms and theoretical fits to the experimental data for D1, D2, D3 and D4 are shown in Fig. 5.16. For D1, the stoichiometry 'n' was 2.01, whereas for D2, D3 and D4 the 'n' value was 1.03, 1.11 and 1.06, respectively (Table 5.4). D1 bound with a K_b of 0.04×10^{-5} and the binding was enthalpy driven ($\Delta H°$ = -6.96 kcal.mol^{-1}) with a very low entropy penalty ($\Delta S°$ = -6.48 cal.mol^{-1}.K^{-1}). For D2 binding, the K_b was 1.37×10^{-5} and the process was also enthalpy driven ($\Delta H°$ = -11.6 kcal.mol^{-1} and $\Delta S°$ = -15.6 cal.mol^{-1}.K^{-1}). When D3 and D4 were used as ligands, similar K_b values of 1.88×10^{-5} and 2.24×10^{-5} were observed. The binding of D3 and D4 exhibited a favourable enthalpic contribution with $\Delta H°$ value equal to -11.43 and -13.5 kcal.mol^{-1}, respectively with a little entropic contribution (Table 5.4). The ITC thermogram for A3 did not provide a complete saturation (Fig. 5.16). However, the K_b value from the theoretical fit was very low (0.09×10^{-5}) suggesting the affinity of *Pe*CBM32 towards A3 was much less in comparison to D3. Similarly, the binding of cellobiose was also low with a K_b of 0.0710^{-5} (Table 5.4).

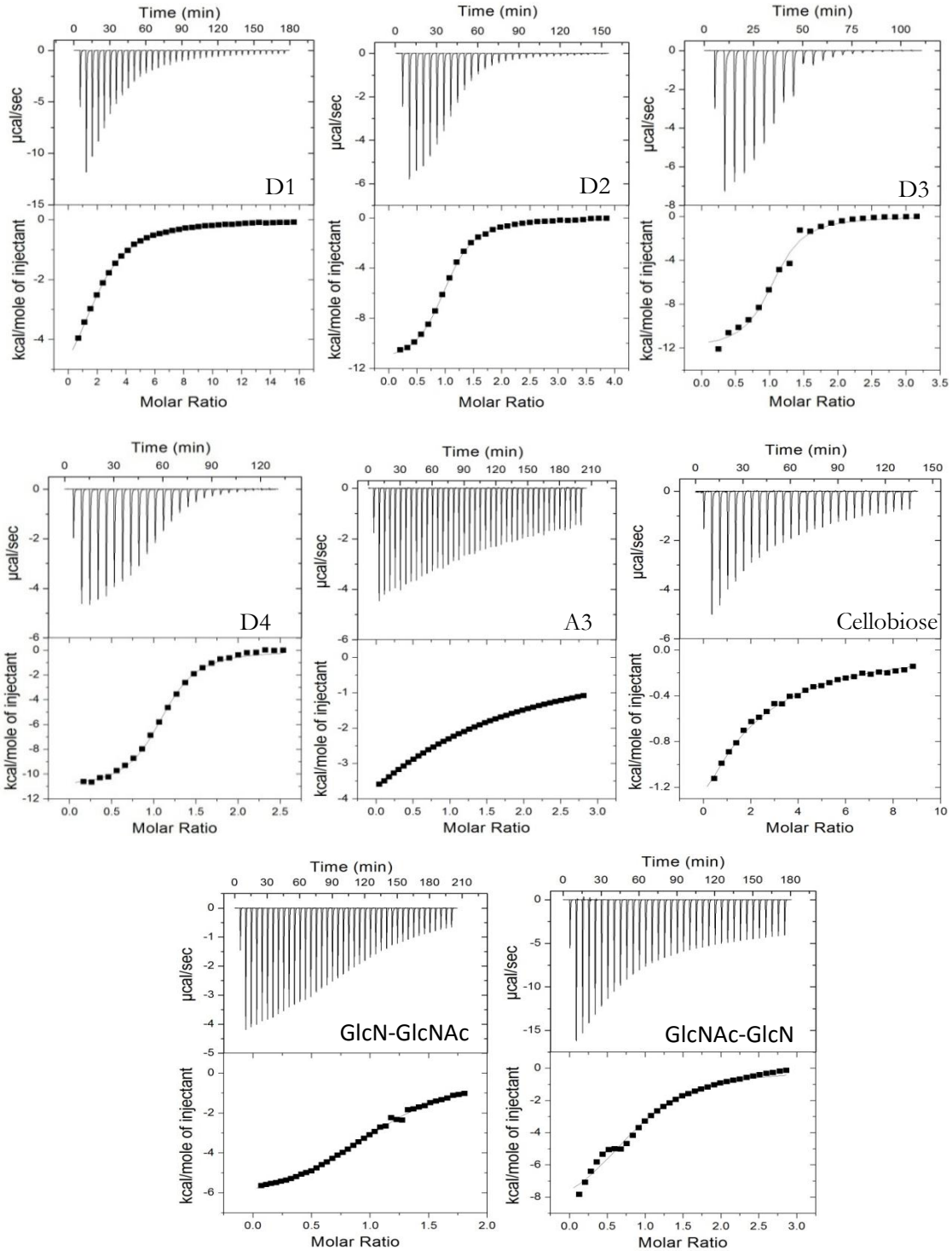

Fig. 5.16: ITC binding studies for *Pe*CBM32. Upper panels show the raw ITC data obtained from successive automatic injections of the ligand from the syringe to the protein in the ITC cell. Lower panels show the integrated heats of binding obtained from raw data shown in the upper panels together with binding isotherms to *one set of sites* binding model. Results are shown for the binding of chitosan monomer (D1) and oligomers (D2, D3, D4), chitin trimer (A3), cellobiose, and chitosan dimer of different pattern of acetylation (GlcN-GlcNAc, GlcNAc-GlcN) to *Pe*CBM32. Titrations were performed at 25ºC and pH 5.6 using a MicroCal VP-ITC System (Microcal, Northampton, MA, USA).

Table 5.4. Thermodynamic parameters of sugar binding to *Pe*CBM32 derived from ITC.

Ligand	*n*	$K_b \times 10^{-5}$ (M^{-1})	$\Delta G°$ (kcal.mol^{-1})	$\Delta H°$ (kcal.mol^{-1})	$\Delta S°$ (cal.mol^{-1}.K^{-1})
D4	1.06 (±0.02)	2.24 (±0.11)	-7.28	-11.43 (±0.31)	-13.9 (±1.1)
D3	1.11 (±0.09)	1.88 (±0.01)	-6.84	-13.5 (±0.29)	-15.37 (±1.02)
D2	1.03 (±0.05)	1.37 (±0.02)	-6.95	-11.60 (±0.12)	-15.6 (±0.14)
D1	2.01 (±0.03)	0.04 (±0.004)	-5.04	-6.93 (±0.28)	-6.34 (±0.04)
A3	1.00	0.09	-4.03	-14.14	-33.9
Cellobiose	1.00	0.07 (±0.008)	-3.91	-6.22 (±0.15)	-7.73 (±0.49)
GlcNAc-GlcN (A-D)	1.13 (±0.32)	0.11 (±0.03)	-5.50	-8.58 (±1.68)	-10.33 (±5.76)
GlcN-GlcNAc (D-A)	1.01 (±0.10)	0.20 (±0.03)	-6.01	-7.53 (±0.51)	-5.75 (±1.58)

To understand the influence of PA of chitosan oligomer on *Pe*CBM32, we used chemically synthesised pure chitosan dimers having GlcN unit either at non-reducing (GlcN-GlcNAc) or reducing end (GlcNAc-GlcN). The ITC isotherms and theoretical fits to the experimental data for GlcN-GlcNAc and GlcNAc-GlcN are shown in Fig. 5.16. For both these disaccharides, the 'n' value was ~1 indicating a one to one stoichiometry. The dimer GlcN-GlcNAc bound with a K_b of 0.20×10^{-5}, and the binding was enthalpy driven ($\Delta H°$ = -7.53 kcal.mol^{-1}) with a very low entropic penalty ($\Delta S°$ = -5.75 cal.mol^{-1}.K^{-1}). For GlcNAc-GlcN binding, the K_b value (0.11×10^{-5}) was near to half of the K_b of GlcN-GlcNAc, and the reaction was also enthalpy driven ($\Delta H°$ = -8.58 kcal.mol^{-1} and $\Delta S°$ = -10.33 cal.mol^{-1}.K^{-1}). Overall, the affinities of *Pe*CBM32 towards chitosan dimer with different PA was found in the order of GlcN-GlcN > GlcN-GlcNAc > GlcNAc-GlcN.

5.2.7.4. Identification of amino acid residues in *Pe*CBM32 essential for chitosan binding

The binding studies performed by dot blot, CD spectroscopy and ITC confirmed the specific binding of *Pe*CBM32 to both chitosan polymers and oligomers. To further understand the mechanism of interaction, particularly to identify the amino acid residues responsible for specific binding, we generated *Pe*CBM32 variants by SDM and compared their ability to bind to chitosan with that of the wild type.

5.2.7.4.1 Molecular docking of *Pe*CBM32 with D2 and D4

Sequence homology search for *Pe*CBM32 in PDB showed 37% identity to the crystal structure of a lectin binding domain (4GWI) from *Streptococcus mitis*. The modeled structure of the *Pe*CBM32 (Fig. 5.17A) was validated using PROCHECK (91.2% of amino acids in the most favoured regions) and Verify_3D (92.42% of residues had an average 3D-1D score > 0.2). The modeled structure had one α helix and eight β strands connected by loops. Consistent with this, secondary structure analysis by CD spectroscopy revealed the presence of ~65% antiparallel β strands and β turns (Fig. 5.18).Docking of D2 with *Pe*CBM32 revealed that all the ligand conformations were restricted to one shallow binding cleft of the protein. Out of ten, seven ligand conformations were associated with nearly the same binding free energies at one binding site. Among these, one conformation with the lowest binding free energy (ΔG in kcal/mol) value of −5.62 kcal.mol^{-1} was selected and analysed for interactions in PyMol and Discovery studio. The residues forming interactions with ligand were E16 and S18 in the loop between β1 strand and α helix, and W34, S36 and K37 in the loop between the α helix and β2 strand. Carboxyl group (-COOH) of S36 formed a hydrogen bond with a distance of 3 Å with the amino group of reducing end sugar moiety (Fig. 5.17B). The carboxyl group of E16 and hydroxyl group of S18 with 2.5 and 2.7 Å distances, respectively formed hydrogen bonds with the amino group of non-reducing end sugar moiety of the ligand (Fig. 5.17B). The carboxyl group E16 also formed a hydrogen bond with the -OH group of the 3rd carbon of reducing end sugar moiety. The -OH group of 6th carbon of reducing sugar moiety formed hydrogen

bonds with the amino group of W34. Docking studies with D4 also showed the involvement of hydrogen bonds with residues similar to D2 (except S18) with additional accessory residues viz. E38 (loop between α helix and β2 strand), E63, Y66 (loop between β3 and β4 strand) and T119 (loop between β7 and β8).

In addition to docking studies, we also considered the amino acid conservedness in *Pe*CBM32 (Fig. 5.19) in selecting the residues for SDM. *Pe*CBM32 showed 68 and 59% identity to CBM32-1 and CBM32-2 of *P. fukuinensis*, respectively. The interacting residues of *Pe*CBM32 were conserved in CBM32-1 and CBM32-2 of *P. fukuinensis* except one substitution i.e. presence of Tyr at 38 position in CBM32-2 in place of Glu. Further, the interacted residues were different from GlcNAc specific residues found in NagJ from *C. perfringens* (Fig. 5.19). Residues E16, S18, W34, and S36 were substituted by Ala to know their role in binding. Since E38 interacted with the -OH group of 4th carbon of non-reducing sugar of D4, we substituted E38 to either Ala or Phe. The mutants E16A, S18A, E38A and E38F were expressed and purified (Fig. 5.20). For W34 and S36, we couldn't get sufficient protein in a soluble form to perform ITC-based interaction studies.

5.2.7.4.2 ITC for binding study of *Pe*CBM32 variants with D4

The binding of *Pe*CBM32 variants to D4 was investigated using ITC at pH 5.6 and 25°C (Fig. 5.21). For all the mutants, the stoichiometry (n value) was ~1 (Table 5.5). The mutant E16A had a K_b of 0.19×10^{-5}, and the binding was enthalpy driven ($\Delta H°$ = -6.70 kcal.mol^{-1}) with a very low entropy penalty ($\Delta S°$ = -2.89 cal.mol^{-1}.K^{-1}). For E38A binding, the K_b was 0.18×10^{-5} and the process was also enthalpy driven ($\Delta H°$ = -6.96 kcal.mol^{-1} and $\Delta S°$ = -3.85 cal.mol^{-1}.K^{-1}). For the mutant S18A, the binding was similar to the wild type having K_b value of 2.05×10^{-5} with a favourable enthalpy contribution ($\Delta H°$ = -11.85 kcal.mol^{-1} and $\Delta S°$ = -15.47 cal.mol^{-1}.K^{-1}). For E38F, we couldn't obtain a considerable thermogram indicating very weak or no binding.

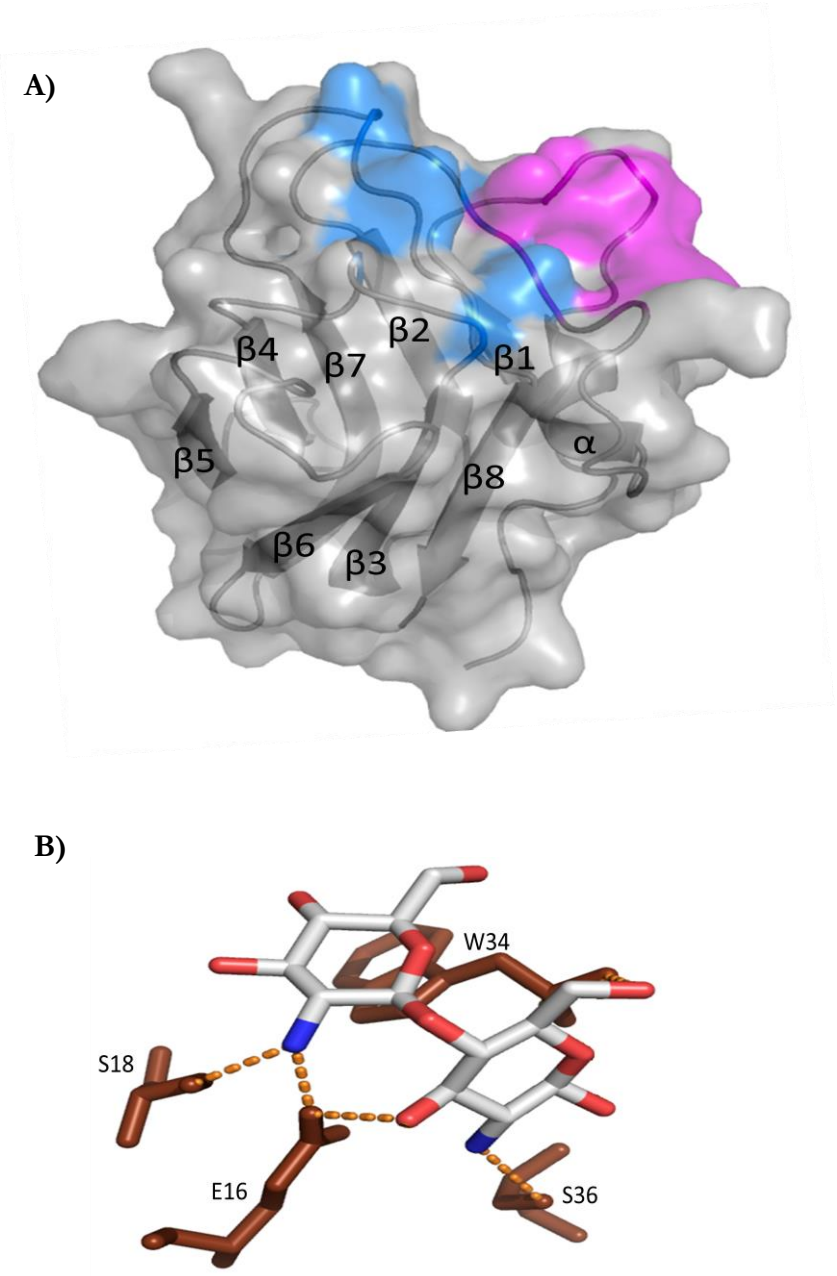

Fig. 5.17: The 3D model of *Pe*CBM32 showing interacting residues. **A)** Modeled CBM32 showed a beta sandwich structure having one alpha helix and eight beta strands connected by loops. The binding site for D2 is shown in magenta, and D4 binds to the region similar to D2 with additional accessory interacting site shown in blue. **B)** Close view of interacting residues targeted for mutation. Pictures used for representation were made with PyMol (www.pymol.org).

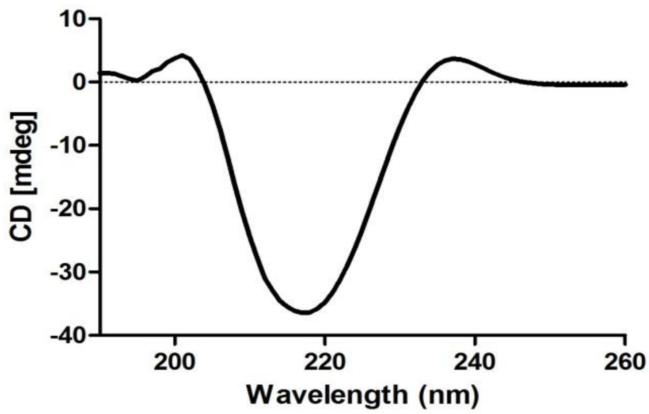

Fig. 5.18: CD spectrum of *Pe*CBM32 recorded at the far-UV region. 35 µM of protein in sodium acetate buffer pH 5.6 was used for the experiment and the spectrum was analysed by CDNN software.

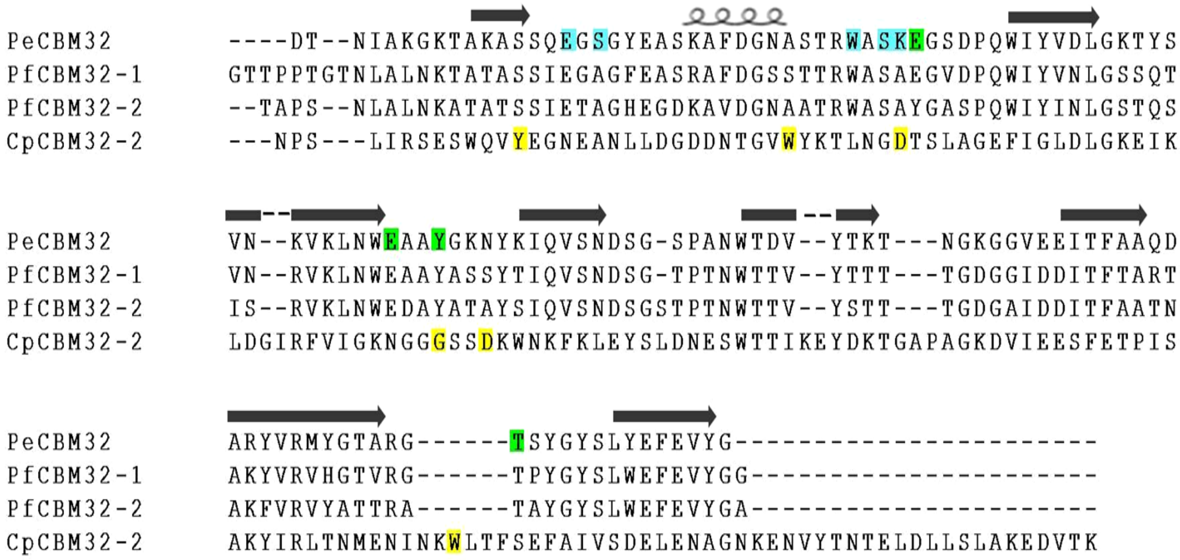

Fig. 5.19: Amino acid sequence alignment of *Pe*CBM32 with related CBM32. Alignment of the *Pe*CBM32 with the CBM32-1 (*Pf*CBM32-1) and CBM32-2 (*Pf*CBM32-2) from *P. fukuinensis*, and CBM32-2 (*Cp*CBM32-2) from *C. perfringens* NagJ specific for GlcNAc. Secondary structure for *Pe*CBM32 is shown above the alignment. Based on docking study, residues in *Pe*CBM32 involved in hydrogen bonds and stacking interactions with the D2 and D4 chitosan are highlighted in cyan and green colour. Residues making hydrogen bonds and van der Waals interactions, based on crystal structure, are highlighted in yellow colour.

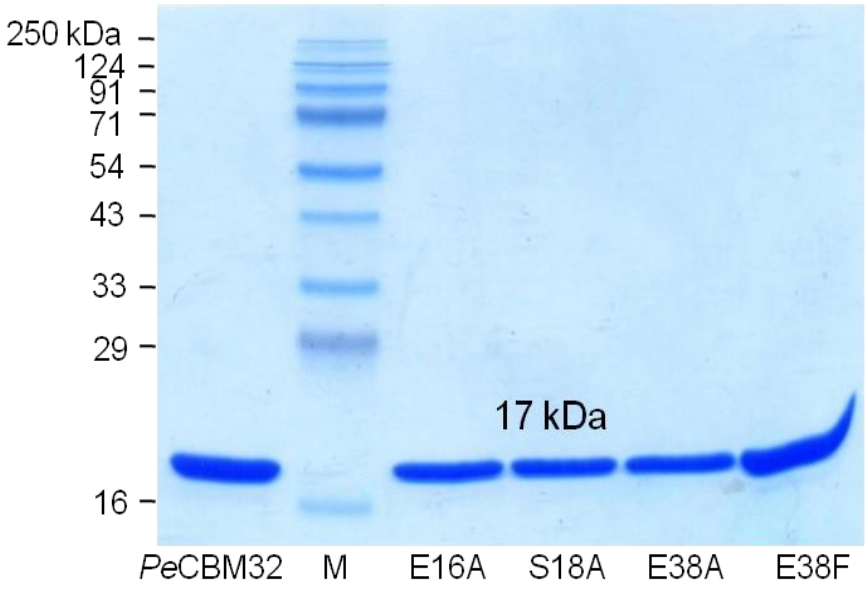

Fig. 5.20: SDS-PAGE profile of the purified *Pe*CBM32 and the variants. The sizes of the standards are indicated in kDa. M: Pre-stained protein molecular weight marker.

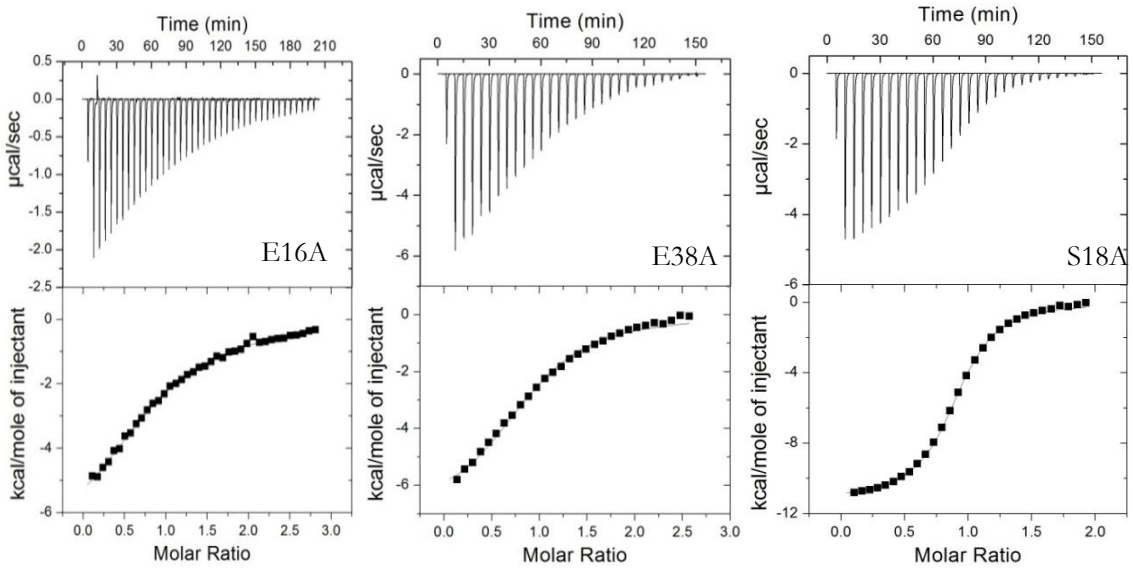

Fig. 5.21: ITC binding studies for *Pe*CBM32 variants with chitosan tetramer (D4). Upper panels show the raw ITC data obtained from successive automatic injections of the ligand from the syringe to the protein in the ITC cell. Lower panels show the integrated heats of binding obtained from raw data shown in the upper panels together with binding isotherms to *one set of sites* binding model. Each isotherm is labelled with the *Pe*CBM32 variant investigated (viz. E16A, E38A and S18A).

Table 5.5: Thermodynamic parameters of chitosan tetramer (D4) binding to *Pe*CBM32 variants obtained from ITC. NB, no binding detected.

***Pe*CBM32 variants**	***n***	K_b **$\times 10^{-5}$ (M^{-1})**	$\Delta G°$ **(kcal.mol^{-1})**	$\Delta H°$ **(kcal.mol^{-1})**	$\Delta S°$ **(cal.mol^{-1}.K^{-1})**
E16A	1.00	0.19	-5.83	-6.70	-2.89
E38A	0.92 (±0.04)	0.18 (±0.13)	-5.81	-6.96 (±0.11)	-3.85 (±0.44)
E38F	NB	NB	NB	NB	NB
S18A	0.85 (±0.05)	2.05 (±0.07)	-7.23	11.85 (±0.95)	-15.47 (±3.25)

5.2.7.5. *In situ* staining of chitosan using *Pe*CBM32-eGFP

A fusion construct *Pe*CBM32-eGFP was made by fusing eGFP downstream of *Pe*CBM32 sequence (Fig. 5.22A). The C-terminal eGFP fused recombinant protein was purified by affinity chromatography. SDS-PAGE analysis (Fig. 5.22B) showed protein at the expected size of 45 kDa.

Differentiation of infection structures was induced by giving mild heat shock to the germinating urediniospores of the wheat stem rust fungus. After induction, urediniospores of wheat rust fungus differentiate into infection structures, namely, germtube, appressorium, substomatal vesicle, and infection hyphae (Fig. 5.23). The germ tube and appressorium expose mainly chitin where as the endophytic structures like substomatal vesicle and infection hyphae expose chitosan on the surface of their cell walls (El Gueddari et al., 2002). Simultaneous staining of germlings with *Pe*CBM32-eGFP and chitin-specific lectin (WGA) coupled to Texas Red showed the binding of *Pe*CBM32-eGFP to substomatal vesicle (green fluorescence) where as WGA bound to appressoria (red fluorescence) as shown in Fig. 5.23. We also observed lower GFP fluorescence signal in the infection hypha.

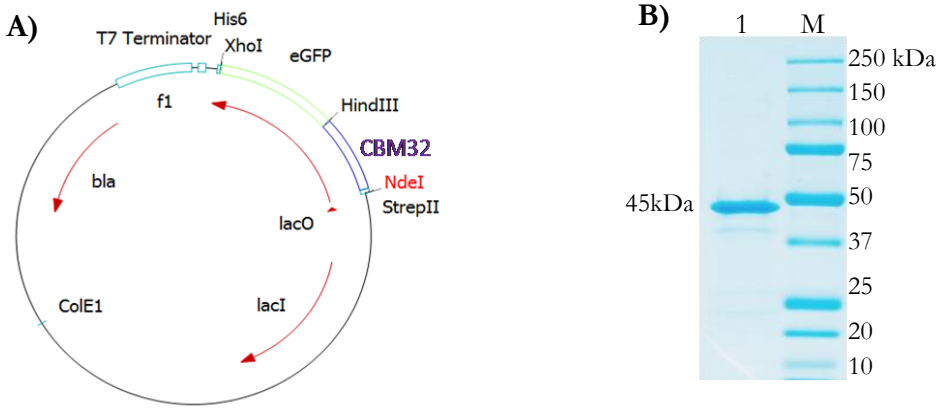

Fig. 5.22: Construction and heterologous expression of *Pe*CBM32-eGFP. A) Schematic representation of the eGFP fusion construct. **B)** SDS-PAGE of the purified *Pe*CBM32-GFP protein purified by affinity chromatography (lane 1) and stained using Coomassie brilliant blue G-250. The band at 45 kDa represents *Pe*CBM32-eGFP. M, molecular mass markers.

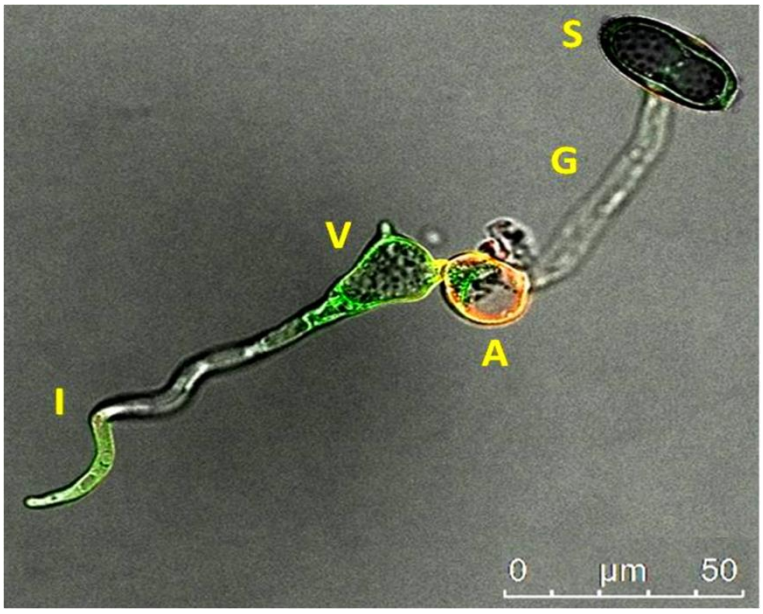

Fig. 5.23: *In situ* staining of fungal cell wall chitosan. Confocal microscope image of *in situ* staining of *in vitro*-induced infection structure of *Puccinia graminis* f. sp. *tritici* using *Pe*CBM32-eGFP and WGA conjugated to Texas Red. Infection structures observed under the microscope were labelled as; S-urediniospore, G-germ tube, A-appressorium, V-substomatal vesicle, I-infection hypha. Green fluorescence coming from substomatal vesicle and infection hypha indicated presence of chitosan, while red fluorescence revealed the presence of chitin in the appressorium.

5.3. Discussion

5.3.1 *Pe*Csn is a multi-domain GH8 chitosanase

Cloning and sequencing of *Pecsn* gene showed 94% identity to *P. elgii* B69 chitosanase, indicating the isolate SMA-1-SDCH02 was different from *P. elgii* B69 whose draft genome sequence is available (Ding et al., 2011). Protein BLAST at NCBI for the deduced amino acid sequence of the GH8 catalytic domain of *Pe*Csn displayed 71% sequence identity to chitosanase-glucanase of *P. fukuinensis* (BAB64835.1), 68% to chitosanase of *B. cereus* (WP_048528534.1) and 70% to a chitosanase of *Bacillus* sp. K17 whose crystal structure is available in PDB (1V5C). Search for functional domains or motifs using SMART data base revealed *Pe*Csn to be a multi-domain protein with a catalytic GH8 domain and a CBM32 domain linked by FN3 domain (Fig. 5.2). To the best of our knowledge, *Pe*Csn is the second multi-domain chitosanase to be functionally characterized.

5.3.2 Temperature, optimum pH and enzyme kinetics

The optimum temperature for activity of chitosanases is found in the range of 30-60°C (Thadathil et al., 2014). *Pe*Csn showed maximum activity at 60°C (Fig. 5.3A) similar to a chitosanase from *B. cereus* (Gao et al., 2008). The activity decreased drastically at 70°C indicating that *Pe*Csn is not a highly thermostable enzyme like a *Paenibacillus* sp. chitosanase displaying optimum activity at around 80°C (Zitouni et al., 2013). *Pe*Csn exhibited maximum activity at pH 6.0 (Fig. 5.3B) suggesting similar acidic pH optima reported by many microbial chitosanases (Thadathil et al., 2014). Many reported microbial chitosanases exhibit optimum pH in the range between 4 to 9. The well characterized chitosanase belonging to family 46 and 75 from *Streptomyces* had optimum activity at pH 5.5 (Heggset et al., 2010; Heggset et al., 2012). The pH range of previously reported *Paenibacillus* chitosanases was also in the range of 4.5-6.5 (Zitouni et al., 2013; Kimoto et al., 2002). Alkaline chitosanases with pH optima of 9.0 and 7.5 were also reported in *B. cereus* and *Anabaena fertilissima*, respectively (Gupta et al., 2012; Goo & Park, 2014).

To evaluate kinetic parameters, the optimal conditions for enzyme activity are required. Activity test of *Pe*Csn on chitosan polymers with varying DA showed the highest activity on 0% chitosan and the activity decreased with increase in DA (Fig. 5.4). Therefore, the kinetic study was done with 0% chitosan substrate at pH 6.0 and 60°C. The low K_m of 0.543 mg.ml^{-1} with high catalytic efficiency indicated that *Pe*Csn has a very high affinity towards 0% DA chitosan substrate (Fig. 5.5). Overall, the derived kinetic values were similar to several other characterized chitosanases, although the substrate preference and optimal enzyme conditions were different. A 45 kDa endochitosanase of *Bacillus* sp. P16 exhibited maximal activity on chitosan of DA 20% with a K_m of 0.52 mg.ml^{-1} (Jo et al., 2003). Another chitosanase from *B. megaterium* P1 had a K_m of 0.8 mg.ml^{-1} for chitosan of DA 19% (Pelletier & Sygusch, 1990), although the optimal temperature of 22°C was quite different.

5.3.3 Mode of action of *Pe*Csn

To determine the end and intermediate products of degradation by *Pe*Csn, the hydrolysed products obtained from various chitosan oligomers (DP3-DP6) were analyzed by TLC. The data clearly showed that *Pe*Csn was not active on DP3, and the hydrolysis was faster for longer COS (DP6>DP5>DP4), indicating an endo-mode of hydrolysis (Fig. 5.6). This was also confirmed by the fact that DP6 hydrolysis released DP4 and DP3 at the initial time points. Degradation of 0% DA chitosan polymer by *Pe*Csn generated longer oligomers starting from DP3-DP6 and even higher in the initial reaction time (Fig. 5.7), further suggesting the endo-mode of action. Homology modeling of *Pe*Csn and docking with D4 and D5 revealed the presence of at least six binding subsites (data not shown). A GH8 chitosanase from *Bacillus* sp. K17 had six subsites as revealed by crystal structure analysis (Adachi et al., 2004). It is conceivable that the binding affinity of *Pe*Csn with shorter oligomers viz. DP3 and DP4 can't be strong because a full occupancy of binding would be satisfied by six sugar moieties, and hence slower activity.

5.3.4 Subsite specificity of *Pe*Csn

In-depth study of the chitosan-degrading ability of family 46 and 75 chitosanases was

reported, providing new insights into the specificity of these enzymes (Heggset et al., 2010; Heggset et al., 2012). However, detailed studies on the subsite specificity of GH8 chitosanase are not yet fully explored because of the assumption that GH8 chitosanase can only cleave GlcN-GlcN linkage, characteristic of type II chitosanase.

Use of defined PA chitosan tetramers revealed that *Pe*Csn had very low hydrolytic activity on D-D-D-A cleaving into D-D and D-A (Fig. 5.8), indicating that A unit could bind productively in +2 subsite in addition to D units. No activity on D-A-D-D and A-D-D-D tetramers suggested that *Pe*Csn has an absolute preference for D unit at -1 and -2 subsites (Table 5.1). The absolute preference for D unit at -1 subsite by *Pe*Csn was different from the GH46 and 75 family chitosanase, where -1 subsite can be productively bind by either D or A units (Heggset et al., 2010; Heggset et al., 2012). Our approach of using defined PA of tetramer clearly revealed the subsite information in both -2 and +2. By ^{1}H and ^{13}C NMR, although it is possible to obtain the information about -2 and +2 subsites, but the assignment of spectra for A or D unit at these subsites are often complicated because of difficulty in deriving sequence information from isolated oligomers with DP > 2 (Heggset et al., 2009; Heggset et al., 2010). Furthermore, when a D unit is productively bound in subsite -1, it is not possible from the proton NMR spectrum to differentiate between the identities of the neighbouring sugar next to the reducing end D (Heggset et al., 2009).

Due to lack of D-D-A-D substrate, we couldn't get information in +1 subsite. Therefore, using MS we sequenced and quantified the hydrolysate generated from chitosan polymer to gain insight about the reducing end of oligomers (Fig. 5.10). At the initial phase of degradation (2 min), an absolute preference for D units was observed in both -1 and +1 subsites (Fig. 5.11). Quantification of COS generated at 20and 720 min showed near to 30 and 60% of COS had 'A' unit in their reducing end, respectively, indicating productive binding of both D and A units in the +1 subsite at a later phase of degradation. Till date, only one variation to the general cleavage pattern of a GH8 chitosanase was reported for a glucanase/chitosanase from *B. circulans* WL-12, which cleaved GlcN-GlcNAc linkage in addition to GlcN-GlcN linkage in chitosan

(Mitsutomi et al., 1998). Our data revealed that *Pe*Csn is a type III chitosanase which can cleave GlcN-GlcNAc linkage in addition to GlcN-GlcN linkage of chitosan (Fig. 5.24), though it prefers GlcN-GlcN linkage at initial degradation phase.

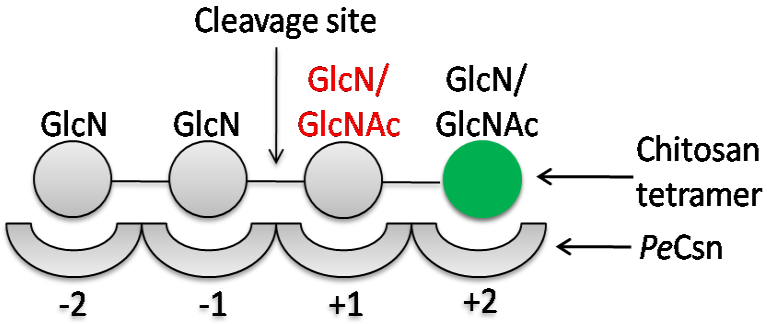

Fig. 5.24: Subsite specificity of *Pe*Csn. Green circle - reducing end.

5.3.5 Role of CBM32 in *Pe*Csn

CBMs play an important role in hydrolytic enzymes that mediate the recycling of carbon and nitrogen in the biosphere. The diversity of CBMs in terms of their sequence, specificity and mechanism of binding with the ligand, offers an attractive model for studying CBM-carbohydrate interaction (Boraston et al., 2004). We have investigated the function of a CBM32 appended to *Pe*Csn using well-defined chitosans. Steady state kinetic data suggested that there was no great difference in the K_m and the overall catalytic efficiency on 0% DA chitosan polymer between the wild type and the truncated mutants, GH8 and GH8FN3 (Table 5.2). However, the activity of *Pe*Csn on insoluble powder chitosan of DA 25% (without making it soluble) was over three-fold higher than GH8 (Fig. 5.12C), indicating the possible contribution of enhanced penetration by *Pe*CBM32 and hence improved catalytic activity. The enhanced binding and penetration may also lead to swelling of chitosan by changing its bulk properties as observed for amorphous cellulose degradation (Reyes-Ortiz et al., 2013). On solubilised chitosan polymers of DA 0, 11, 25, 37 and 60% *Pe*Csn and GH8 showed nearly similar activity (Fig. 5.12B), further supporting the involvement of a penetration mechanism for amorphous chitosan degradation.

CBMs enhance the activity of their cognate enzymes by either disruption and modification of polysaccharide structures (Din et al., 1991) or increasing enzyme concentration in the vicinity of substrate and sometimes by targeting specific carbohydrate molecule in a native biomass containing different polysaccharides (Hervé et al., 2010, Cuskin et al., 2012). Mizutani et al. (2014) showed that a CBM32 appended to a GH5 from *Clostridium thermocellum* directly influenced the mode of catalysis, resulting in a difference in product formation in presence and absence of CBM32. However, comparison of the hydrolysed products generated by *Pe*Csn and GH8 at the very early phase of degradation of 0% DA chitosan didn't show any noticeable difference in the pattern and quantity of product formation (Fig. 5.13). Taken together, the soluble chitosan hydrolysis data suggested that the *Pe*CBM32 neither enhance the hydrolytic activity nor affect the mode of action of *Pe*Csn. It was also possible that the affinity and specificity towards chitosan substrates may permit *Pe*CBM32 to adhere and maintain proximity to chitosan, which occurs along with several other carbohydrate polymers in nature. Therefore, it was paramount for us to study the specificity of *Pe*CBM32 in recognising carbohydrate ligands.

5.3.6 Specificity of *Pe*CBM32

Many ligand molecules like galactose, lactose, sialic acid, LacNAc, chitosan oligomer and mannan oligomer are recognized by CBM32 appended to different enzymes (Abbott et al., 2008; Shinya et al., 2013; Mizutani et al., 2014). We studied the influence of DA of chitosan polymers on the binding of *Pe*CBM32. Both dot blot and thermal denaturation study in the presence of defined DA polymers showed the reduction in affinity or no affinity towards higher DA chitosan (Fig. 5.14 & 5.15), suggesting the specific binding of *Pe*CBM32 to chitosan. *Pe*CBM32 also didn't show detectable binding to laminarin and dextran (data not shown), and the binding to A3 and cellobiose was nearly 20 times weaker than the D3 and D2, respectively (Table 5.4), suggesting the specific binding of *Pe*CBM32 towards chitosan polymers and oligomers. This is the second chitosan specific CBM32 which bound to chitosan polymers and oligomers with greater affinity and is consistent with the general postulation that CBM

specificity matches with the function of the cognate catalytic module. Therefore, it is conceivable that the specificity of *Pe*CBM32 assists in maintaining proximity of *Pe*Csn to the chitosan polymer as observed with other CBMs (Bolam et al., 1998; Hervé et al., 2010).

5.3.7 Binding subsites in *Pe*CBM32

Shinya et al. (2013) showed that the affinity of CBM32 was directed towards chitosan oligomers (D2-D6) using ITC. Here, we report binding of D1 with a stoichiometry of 2 and K_b of 0.4×10^{-4}, clearly indicating the accommodation of two GlcN residues by *Pe*CBM32 (Table 5.4). The binding of D2 with an equimolar stoichiometry confirmed the presence of two primary subsites in *Pe*CBM32. The binding affinities (K_b) increased marginally with the increase in chain length of chitosan oligomers (Table 5.4), indicating the extended part of longer oligomers, beyond the primary interaction site, may be involved in additional, minor interaction with the protein. This was further observed in our docking study, where residues such as E38, E63, Y66, and T119 showed potential interaction with chitin tetramer in addition to the residues that interact with chitosan dimer (Fig. 5.17A). The substitution of Ala in one of these accessory interacting residues, E38A weakly bound to chitosan tetramer (12 times lesser) when compared to the wild type protein (Table 5.5), supporting the involvement of residues other than primary subsites for binding of longer chain chitosan oligomers. In mammalian lectins ERGIC-53 and VIP36, additional secondary binding sites were shown to interact with additional sugar residues, apart from the common primary mannose-binding site (Satoh et al., 2007; Zheng et al., 2013). The extended binding site can also provide specificity for different sugar moieties.

5.3.8 Binding mechanism

Direct hydrogen bond formation in Type A CBMs had little effect in binding towards crystalline polysaccharide ligands (McLean et al., 2000). However, Ala substitution of amino acids, which make direct hydrogen-bonding in B Type and C Type CBMs resulted in a considerable loss of binding affinity towards their respective ligands (Kormos et al., 2000, Notenboom, 2001, Pell et al., 2003). Our results provide

compelling evidence that amino groups of chitosan participate in binding to *Pe*CBM32. Molecular docking of both D2 and D4 substrate revealed that the carboxyl group of E16 formed one hydrogen bond with the amino group of nonreducing end sugar moiety of the ligand (Fig. 5.17B). The substitution of E16 by Ala (E16A) decreased the binding affinity by 11 times suggesting the crucial role of E16 for chitosan binding. However, we didn't observe a reduction in binding affinity in the case of S18A mutant which showed a formation of the hydrogen bond with the amino group of non-reducing sugar of dimer but not with the tetramer. Therefore, we speculate that S18 may not be crucial for longer chain chitosan binding, and needs further structural evidence. The binding affinity for chitosan tetramer was 12 times lesser for E38A, which interacts with the -OH group of 4th carbon of non-reducing end of D4 sugar (Table 5.5). A similar interaction between polar amino acids with the amino groups of GluN was observed in a structural study of a chitosanase from *Bacillus* sp. K7 (Adachi et al., 2004). Substitution of E38 by an aromatic amino acid Phe reduced the binding affinity drastically suggesting the introduction of hydrophobic residues may alter the local conformation in the loop region affecting the binding site. This finding explains why CBM32-2 of *P. fukuinensis* had low binding affinity by two orders of magnitude than CBM32-1 (Shinya et al., 2013), and suggesting that minor subtle changes in the amino acid in loop region may lead change in binding affinity and specificity towards chitosan.

To further substantiate the involvement of amino groups in binding to *Pe*CBM32, we have synthesised well-defined chitosan dimers of two different patterns i.e. GlcNAc at non-reducing end (GlcNAc-GlcN) and at reducing end (GlcN-GlcNAc) for binding studies in ITC (Fig. 5.16). The binding affinities for GlcNAc-GlcN and GlcN-GlcNAc decreased substantially with the K_b lesser than 12 and 7 times in comparison to D2, respectively, indicating the GlcN at non-reducing end is more crucial than at reducing end. The reduction of binding affinity in GlcNAc-GlcN than GlcN-GlcNAc suggests disfavour of the bulkier acetyl group of GlcNAc at the non-reducing end owing to the well-ordered substrate binding site topology specific for chitosan, but not for chitin. For instance, the positioning of acetamido group needs a

hydrophobic pocket of aromatic amino acids for providing substantial van der Waals interactions to select GlcNAc over galactose-based ligands in NagHCBM32-2 (Ficko-Blean et al., 2009).

Binding of all the chitosan oligomers investigated here was exothermic with a very low entropic contribution, suggesting the absence of hydrophobic interaction (Table 5.4 & 5.5). High enthalpic contribution in *Pe*CBM32-chitosan binding was presumably due to an increased number of hydrogen bonds and van der Waals interactions at the ligand-target interface, though the possibility of electrostatic interaction can't be ruled out. Shinya et al. (2013) studied the binding of chitosan hexamer to the CBM32-1 and CBM32-2 of *P. fukuinensis* at pH 5 and 7. At pH 7 (deprotonated state as the p$K_a$value of the amino group of GlcN residue was reported to be 6.4), no decrease in binding of CBM32-1 and CBM32-2 towards either chitosan hexamer or trimer was observed, indicating that electrostatic interactions may play a subordinate role in chitosan binding. In an analogous study on DNA-protein interaction, it was reported that both electrostatic and non-electrostatic forces involve in binding, but the sequence specific binding occurred through non-electrostatic forces driven by enthalpic component (Privalov et al., 2011). Thus, our data on mutation of polar residues to Ala and use of specific pattern chitosan dimers suggested the possible involvement of non-electrostatic forces in providing specificity in *Pe*CBM32-chitosan interaction.

5.3.9 Potential application of *Pe*CBM32

Typically, fungal cell walls contain chitin as a structural element, but some plant-pathogenic fungi produce chitin deacetylase to convert the chitin into chitosan to protect their cell wall as part of their pathogenicity mechanism (El Gueddari et al., 2002). Even a fungal pathogen of human also converts surface exposed chitin to chitosan as a pathogenicity strategy (Baker et al., 2007). The chitosan in the fungal cell wall was mostly detected using chitosan specific polyclonal or monoclonal antibodies (Hartmann et al. 2003, Schubert et al., 2010), or by using gold-labeled chitosanase (Grenier et al., 1991). A catalytically inactive bacterial chitosanase fused to eGFP was

reported to bind specifically to chitosan *in vitro* and *in situ* (Nampally et al., 2012). However, the specificity and binding affinity of chitosan binding proteins may depend on the DA of chitosan present on the fungal cell wall surface, which demands the search for diverse chitosan binding proteins for localization study in pathogenic fungi. To harness the specific binding ability of *Pe*CBM32 to chitosan oligomers and polymers, and being in smaller molecular size, we tested the *in situ* binding of *Pe*CBM32 in localizing chitosan on the fungal cell wall of a biotrophic phytopathogenic fungus i.e. *Puccinia graminis* f. sp. *tritici*. Simultaneous double staining with *Pe*CBM32-eGFP and WGA showed detection of chitosan on the surface of substomatal vesicles and infection hyphae, where as chitin was detected in the appressoria (Fig. 5.23). The observation of stronger GFP signal from chitosan in the substomatal vesicle (strongly deacetylated than the one exposed on the surface of the infection hyphae) was consistent with the findings of Nampally et al. (2012). Our result on simultaneous staining by two binding proteins suggested that *Pe*CBM32-eGFP can be used with other carbohydrate-specific proteins or lectins for localization studies in biological tissues.

Chapter VI

Production and plant strengthening activities of bioactive chitosan oligosaccharides generated by a chitosanase from *P. elgii*

6.1. Introduction

In comparison to branched carbohydrate polymers like pectin, chitosan possesses a rather simple chain structure. However, chitosan polymers and their derivatives (COS) encompass diversity in their structure-related properties that are of high importance in several biotechnological processes. COS generally correspond to chitin/chitosan molecules with a DP between 1 and 10, though this range is not clearly defined and may differ in literature. The influence of structural changes (e.g. DP) on physicochemical properties of COS can be simply illustrated by means of solubility of COS. In contrast to high molecular weight chitosan polymer, COS can be readily dissolved in water of neutral pH, primarily due to their low DP.

As part of induced defence, the early response of plant to elicitors usually accompanied by the production of hydrogen peroxide, H_2O_2 (Lamb & Dixon, 1997; Alvarez et al., 1998). H_2O_2 can either strengthen the cell wall by inducing cross-linking of cell wall associated protein or act as a signal molecule to alter the transcription of genes related to the plant immune system. This immediate induced defence response brought by plants towards elicitors is known as elicitation. In addition to these responses, plants can also attain a 'sensitised defence state' in response to artificial or natural inducer molecules without any visible defence responses. This special adaptive physiological state of the plant is called "priming". In the primed defence state, plants respond with faster and/or stronger immune responses when subsequently challenged by pathogens (Conrath, 2011; Pastor et al., 2013).

The biotechnological exploitation of COS largely depends on properties like DP, DA, and most likely also on the PA (Chatelet et al., 2001; Lamarque et al., 2005; Oliveira et al., 2008; Domard, 2011). Therefore, production of defined COS is of interest not only to food and medicine-related biotechnology industries but also to agriculture (Mourya et al., 2011). In fact, chitosan application by topical means protects a wide range of plants (El Hadrami et al., 2010), including potato tubers against *Erwinia carotovora*, wheat against *Fusarium graminearum*, soybean against *Fusarium solani*, groundnut against the grey mould pathogen *Botrytis cinerea*, cucumber against *B. cinerea*, rice against the

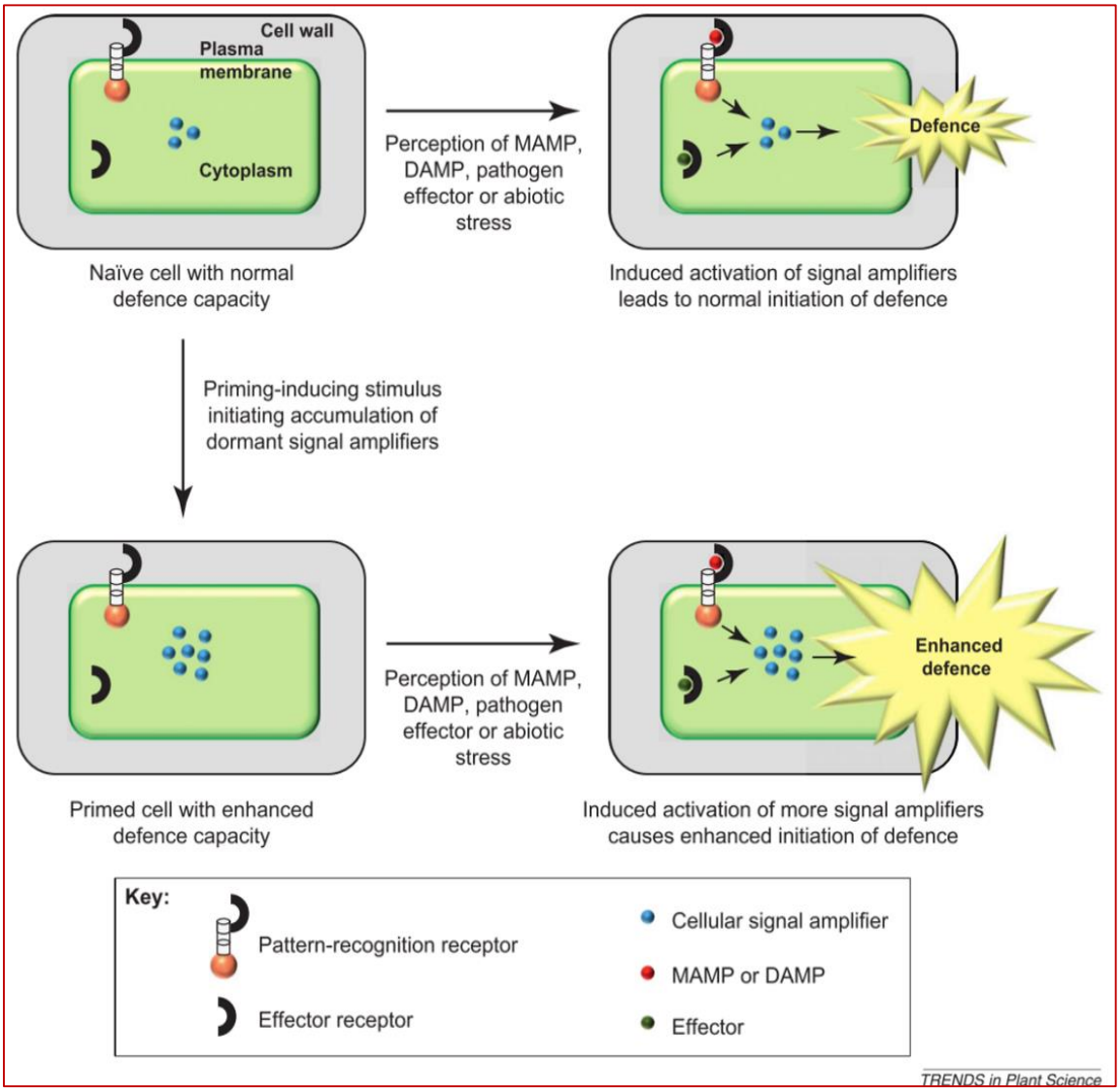

Fig. 6.1: An illustration of the phenomenon of priming in plants (Conrath, 2011). In priming, accumulation of dormant cellular signal amplifiers is a likely mechanism in plants. A priming-inducing stimulus enhances the cellular level of inactive proteins with a role in amplifying cellular signal. Subsequent exposure to MAMPs, DAMPs, pathogen effectors, or abiotic stress stimulates more of these dormant signalling proteins in primed cells than in non-primed cells. It thereby initiates strong signal amplification leading to more rapid and robust activation of defence associated with immunity and stress tolerance.

blast pathogen *Magnoporthe grisea* and wheat against *Bipolaris sorokiniana*. While such reports abound in the literature, the cellular or molecular mode of action has not been elucidated in detail in any one case. One of the major problems in several of these

studies is the use of poorly characterised chitosan/COS, leading to poor reproducibility and an inability to drive conclusions across studies. It is, therefore, of relevance to develop new biotechnological processes for the synthesis of physiologically active COS with defined DP, DA and PA for crop protection. In this chapter, we have attempted to answer a few questions listed below:

1. Will the enzymatic activities of *Pe*Csn provide an option to produce longer chain COS?
2. Will the *Pe*Csn-generated COS show plant strengthening activity?
3. Is there any difference in COS response in tobacco (dicotyledon) and rice (monocotyledon) suspension cells?

Towards addressing the above mentioned queries, we have generated COS of defined DP using a well characterised non-processive endo-enzyme. The composition of each DP COS was also characterised based on their DA by mass spectrometry. Finally, the bioactivity of these well defined COS was tested on tobacco (dicot) and rice (monocot) cell suspension cultures by measuring H_2O_2 as an indicator of a defence response.

6.2. Results

6.2.1. Generation and characterization of COS from chitosan substrate

To choose preferable chitosan substrate for longer chain COS production by *Pe*Csn, we tested 11% and 35% DA chitosan polymers (Fig. 6.2A). Use of 0% DA chitosan showed the generation of oligomers of DP less than or equal to 6, whereas on higher DA chitosan polymer the hydrolysing activity of *Pe*Csn was low (data shown in the previous chapter). Hydrolysate produced from 11% DA chitosan polymer at 300 min was dominated by smaller COS with lesser long chain COS (smear in TLC). However, hydrolysate from 35% DA chitosan (PeCsn35) polymer at 300 min produced a reasonable amount of longer COS (smear seen below D6 std). Further, MALDI-TOF-MS analysis of hydrolysate generated from 35% DA chitosan polymer showed the presence of COS viz. D3, D2A1, D3A1, D4A1, D3A2, D5A1, D4A2, D3A3, D5A2, D4A3, D5A3, D4A4 and D5A4 ranging from chain length of DP 3-9 (Fig. 6.2B).

Therefore, 35% DA chitosan was selected for bulk production of COS.

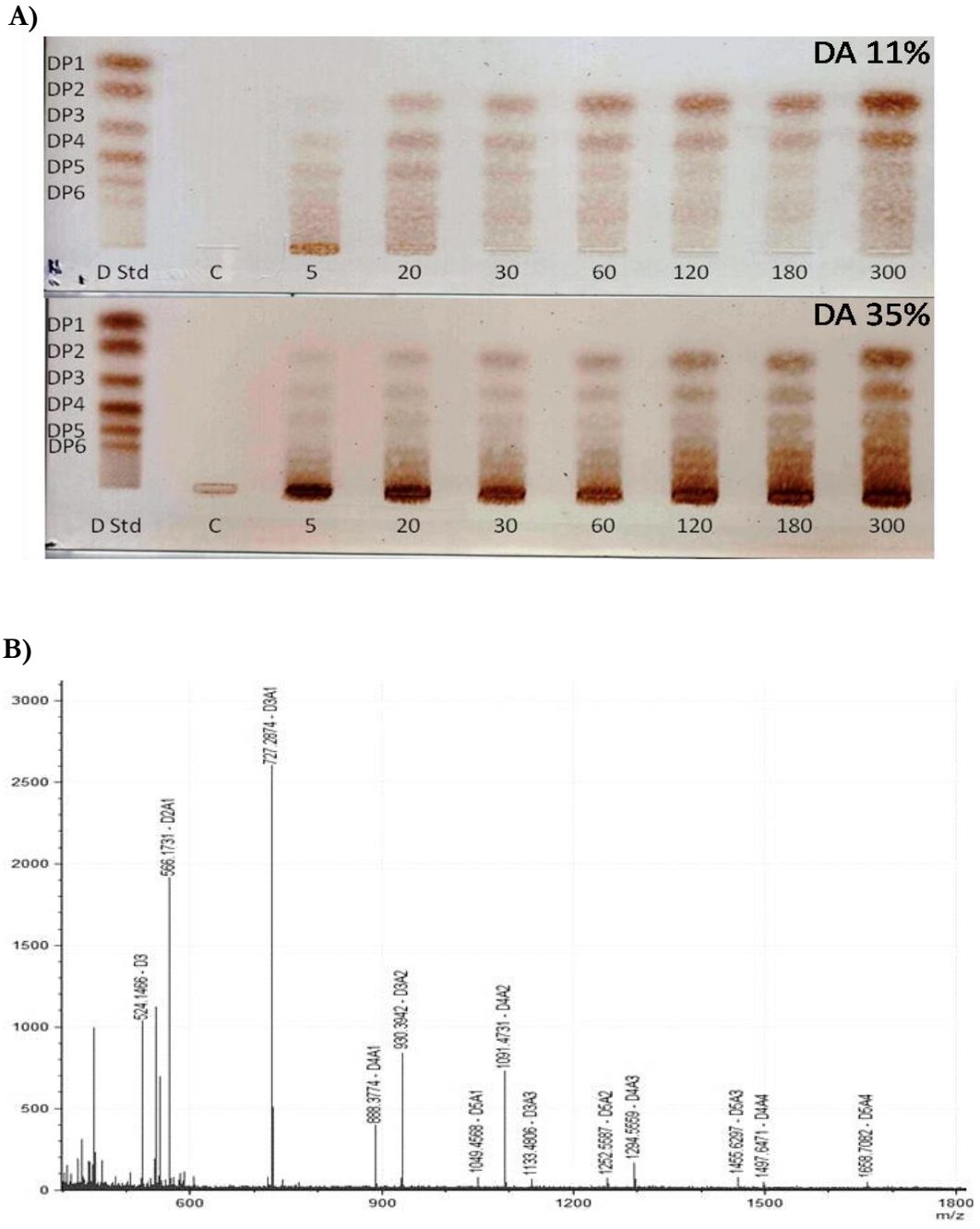

Fig. 6.2: Analysis of chitosan hydrolysates generated using *Pe*Csn. A) HPTLC analysis of hydrolysates generated from 11% and 35% DA chitosans. Fractions collected at different time intervals were loaded on to TLC plates and stained with ammonium bisulphate. D std represents GlcN1-6. **B)** MALDI-ToF-MS analysis of 35% DA chitosan hydrolysate collected at 300 min showing different COS species (Masses shown are with Na adduct).

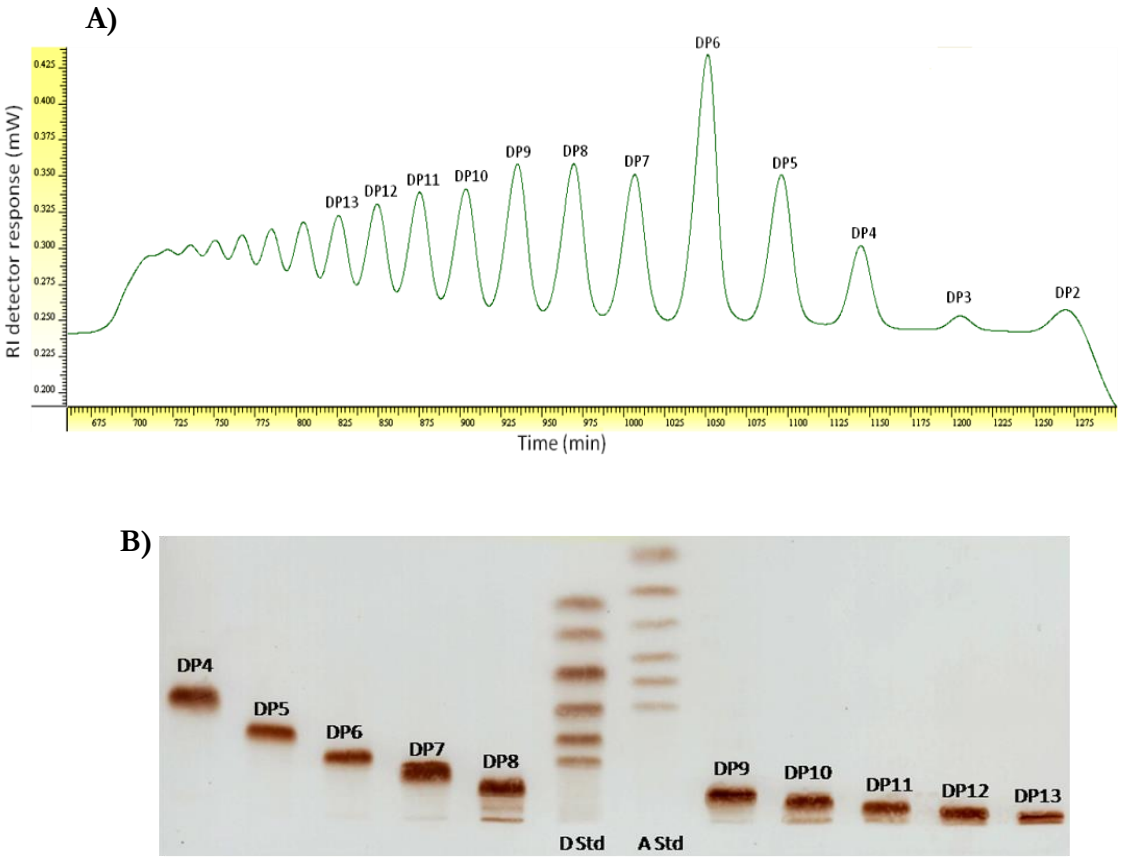

Fig. 6.3: Purification of COS produced by *Pe*Csn. A) SEC purification profile of the crude mixtures of COS generated from 100 mg of 35% DA chitosan. Purification was done using HP-SEC GPC System equipped with a refractive index detector. Individual peaks are labelled by chain length of COS. **B)** HPTLC image showing the purified COS produced. Standard D and A represent GlcN1-6 and GlcNAc1-6, respectively.

Chitosan polymer of DA 35% (100 mg) was hydrolyzed with *Pe*Csn and the hydrolysate was fractionated by SEC resulting in separation of COS based on their chain length (Fig. 6.3A). The size distribution of the oligomers present in the hydrolysate and the corresponding HPTLC data are shown in Fig. 6.3B. The composition of each fraction representing a particular chain length was investigated by UHPLC-ELSD-ESI-MS to identify the structural properties of COS in terms of DA (Table 6.1). With the increase in chain length, we observed presence of higher number

of acetylated COS with varied percentage of acetylation (Fig. 6.4A & B). It is important to note that the COS of a particular DP may have different molecules with varied DA. For instance, COS bearing chain length of 4 (DP4) had D4 component (DA=0%) and D3A1 (DA=25%) component (Table 6.1).

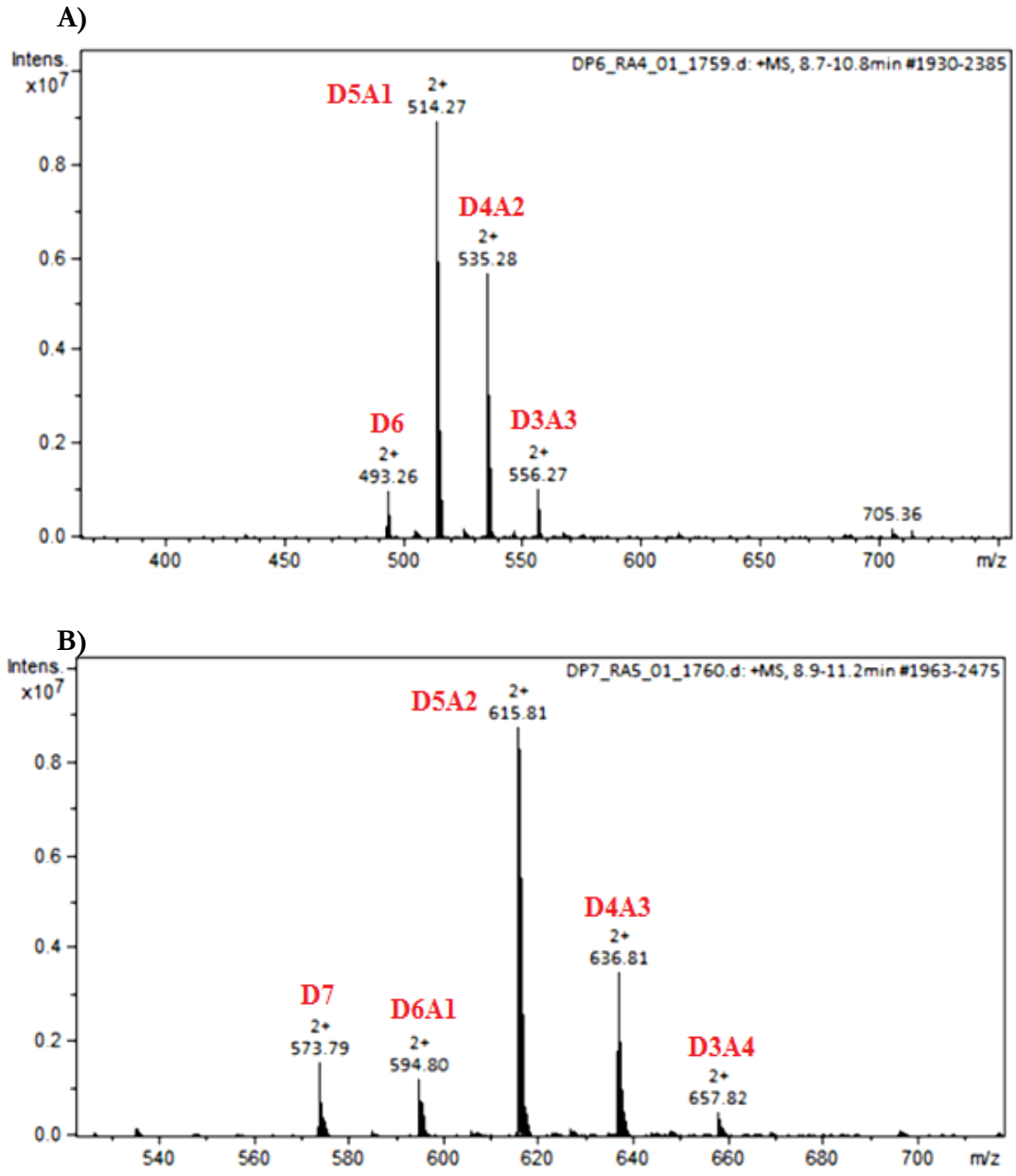

Fig. 6.4: UHPLC-ELSD-ESI-MS analysis of purified COS. A representative figure showing different oligomers of varied DA present in DP6 **(A)** and DP7 fractions **(B)**. Approximately 2 µg of each lyophilized oligomers were taken for MS analysis. Masses shown here for each COS is with H adduct.

Table 6.1: UHPLC-ELSD-ESI-MS analysis of purified COS showing different DA oligomers.

COS (DP)	Components
DP4	D4, D3A1
DP5	D5, D4A1, D3A2
DP6	D6, D5A1, D4A2, D3A3
DP7	D7, D6A1, D5A2, D4A3, D3A4
DP8	D8, D7A1, D6A2, D5A3
DP9	D9, D8A1, D7A2, D6A3, D5A4, D4A4
DP10	D10, D9A1, D8A2, D7A3, D6A4, D5A5
DP11	D10A1, D9A2, D8A3, D7A4, D6A5
DP12	D9A3, D8A4, D7A5, D6A6
DP13	D9A4, D8A5, D7A6, D4A9

6.2.2. Elicitor and priming activity of crude COS mixture (PeCsn35) in tobacco

The cellular oxidative burst response to crude COS mixture was determined by measuring the release of H_2O_2. For elicitation, suspension-cultured cells of tobacco were treated with 10 $\mu g.ml^{-1}$ crude COS mixture right before measuring the production of H_2O_2 (Fig. 6.5A). The crude hydrolysate led to a quite fast and sharp oxidative burst similar to HF chitosan. The maximum response observed at 60 min after treatment of PeCsn35, whereas HF chitosan generated more H_2O_2 and reached a maximum at 90 min. PeCsn35 didn't show priming activity in tobacco cell lines (Fig. 6.5B).

6.2.3. Elicitor and priming activity of purified COS in tobacco and rice

To evaluate the effect of COS on dicotyledon and monocotyledon plants, purified COS in the range between DP4-13 was used for oxidative burst experiments in tobacco and rice cell suspension cultures. In tobacco, COS of different DP showed elicitor activity (Fig. 6.6A) but didn't show priming activity (Fig. 6.6B), corroborating the response observed when the hydrolysate containing mixture of COS of various DP was used. All the tested COS of various chain length (DP4-13) at 20 μM concentration induced weak oxidative burst except DP4, which induced reasonably stronger oxidative burst reaching the maximum at 60 min, similar to HF chitosan. The induction of H_2O_2

started at ~20 min by COS of different DP, whereas a faster response was observed in the case of HF chitosan. There was no clear correlation between the DP of COS and the amount of H_2O_2 production (Fig. 6.6B).

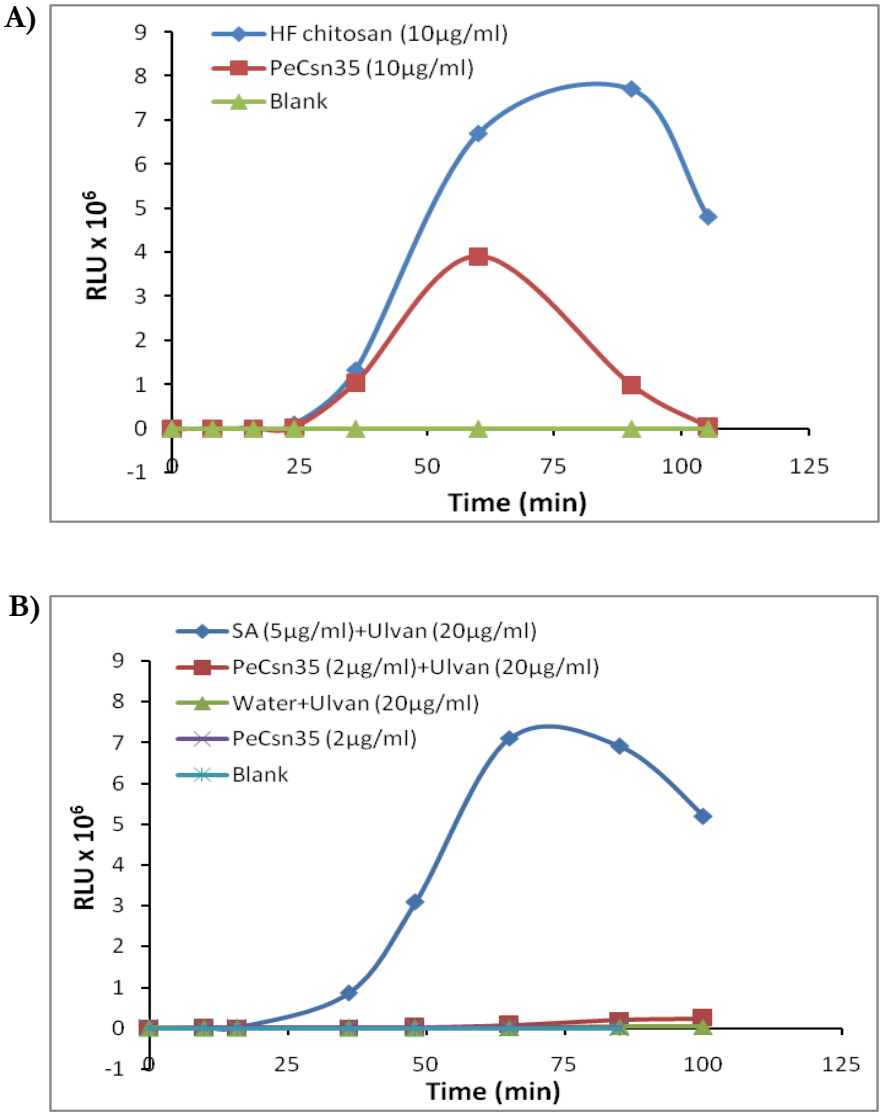

Fig. 6.5: Elicitor and priming response of the crude chitosan hydrolysate in tobacco cells. The crude mixture of *Pe*Csn-generated COS was used for elicitation **(A)** and priming **(B)** in suspension cultured tobacco cells. Released H_2O_2 was detected as relative light unit (RLU) by luminol-dependent chemiluminescence method. For elicitation, 10 µg.ml^{-1} of *Pe*Csn-generated COS mixture (PeCsn35) was used. HF chitosan and sterilized MQ water were used as a positive and negative control, respectively. For priming, 2 µg of PeCsn35 was applied as priming agent followed by treating with ulvan as an elicitor. Salicylic acid (SA) was taken as positive control for priming. Blank represents the basal level H_2O_2 mediated luminescence produced from untreated cells. Data represent one of the three independent experiments with similar results.

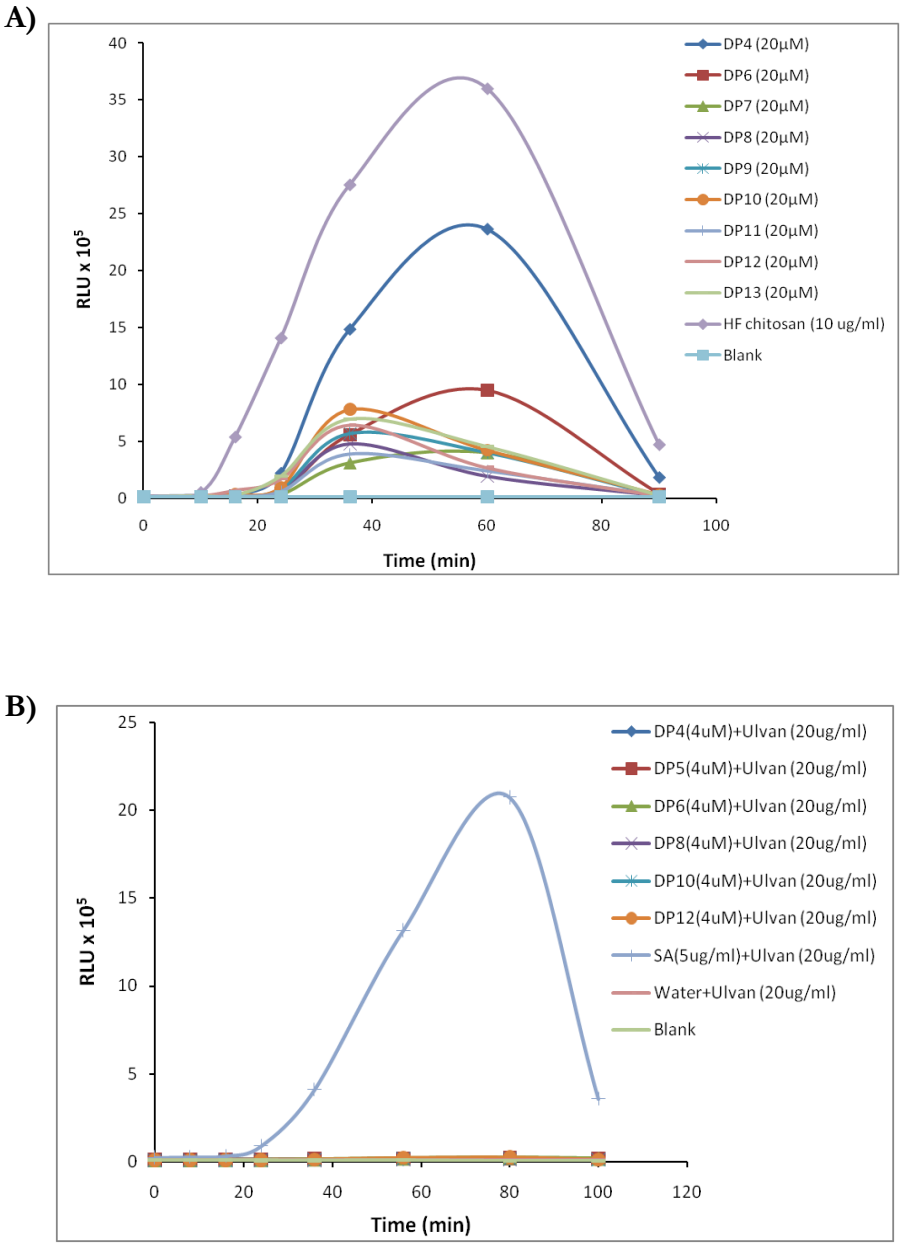

Fig. 6.6: Elicitor and priming response of purified COS in tobacco cells. Purified *Pe*Csn-generated COS were used for elicitation **(A)** and priming **(B)** in suspension cultured tobacco cells. Twenty µM of each purified COS was used for elicitation. HF chitosan and sterilized MQ water were used as a positive and negative control, respectively. For priming, 4 µM of each purified COS was applied as priming agent followed by elicitation of cells using ulvan. Salicylic acid (SA) was taken as positive control for priming. Blank represents the basal level H_2O_2 mediated luminescence produced from untreated cells.

In contrast to the effect seen in tobacco suspension cells, the purified COS didn't show elicitor activity (Fig. 6.7A), but induced strong priming activity (Fig. 6.7B) in rice suspension cells. All the tested oligomers of DP4-13 induced priming-mediated enhancement in H_2O_2 production with the highest response observed for DP13. There was an increase in oxidative burst response with the increase in chain length of the COS ranging from DP8 to DP13. Among the short chain oligomers of DP≤7, DP4 showed the highest oxidative burst response and no distinct correlation between chain length and H_2O_2 production were observed for smaller chain oligomers.

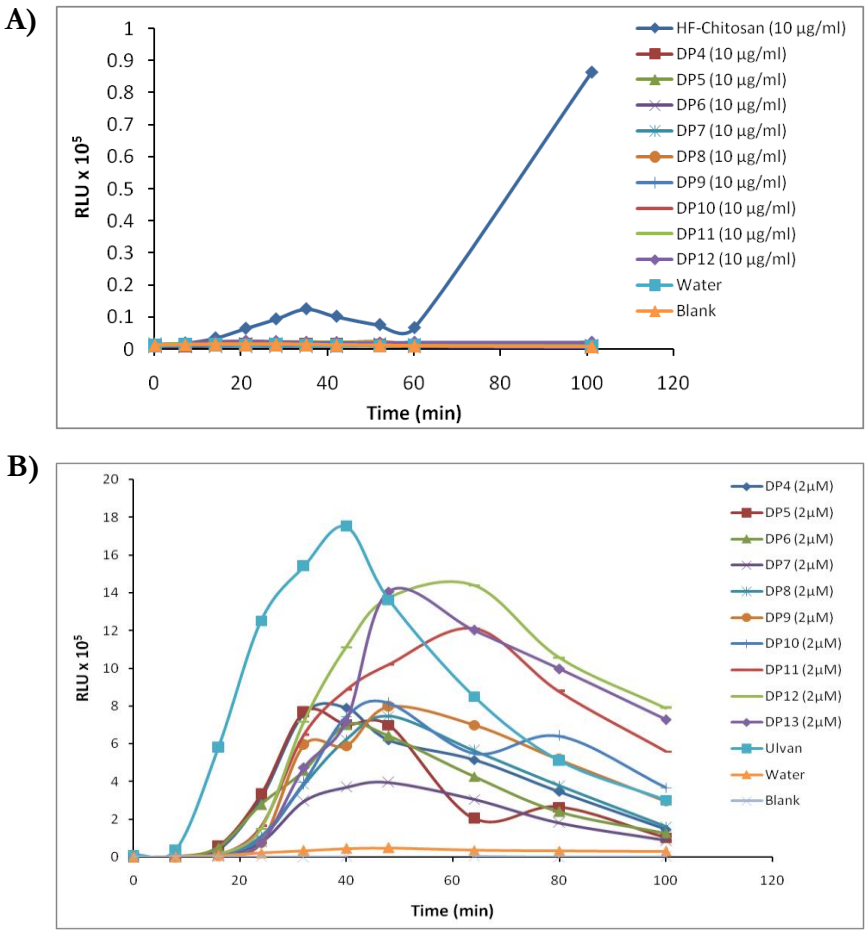

Fig. 6.7: Elicitor and priming response of purified COS in rice cells. Purified *Pe*Csn-generated COS were used for elicitation **(A)** and priming **(B)** in suspension cultured rice cells. Ten µg of each COS was used for elicitation. HF chitosan and sterilized MQ water were used as a positive and negative control, respectively. For priming, 2 µM of each purified COS was applied as priming agent followed by elicitation of cells using HF chitosan. Ulvan was taken as positive control for priming experiments in rice. Blank represents the basal level H_2O_2 mediated luminescence produced from untreated cells.

Between the two tested suspension cell lines, the priming response by purified COS was very strong and consistent in rice suspension cells. Therefore, dose-dependent priming-mediated oxidative burst in rice cell suspension cultures was carried out with pure DP4 (Fig. 6.8A) and DP12 (Fig. 6.8B) COS of various concentrations ranging from 0.001 to 5 µM. DP4 COS induced strong priming-mediated oxidative

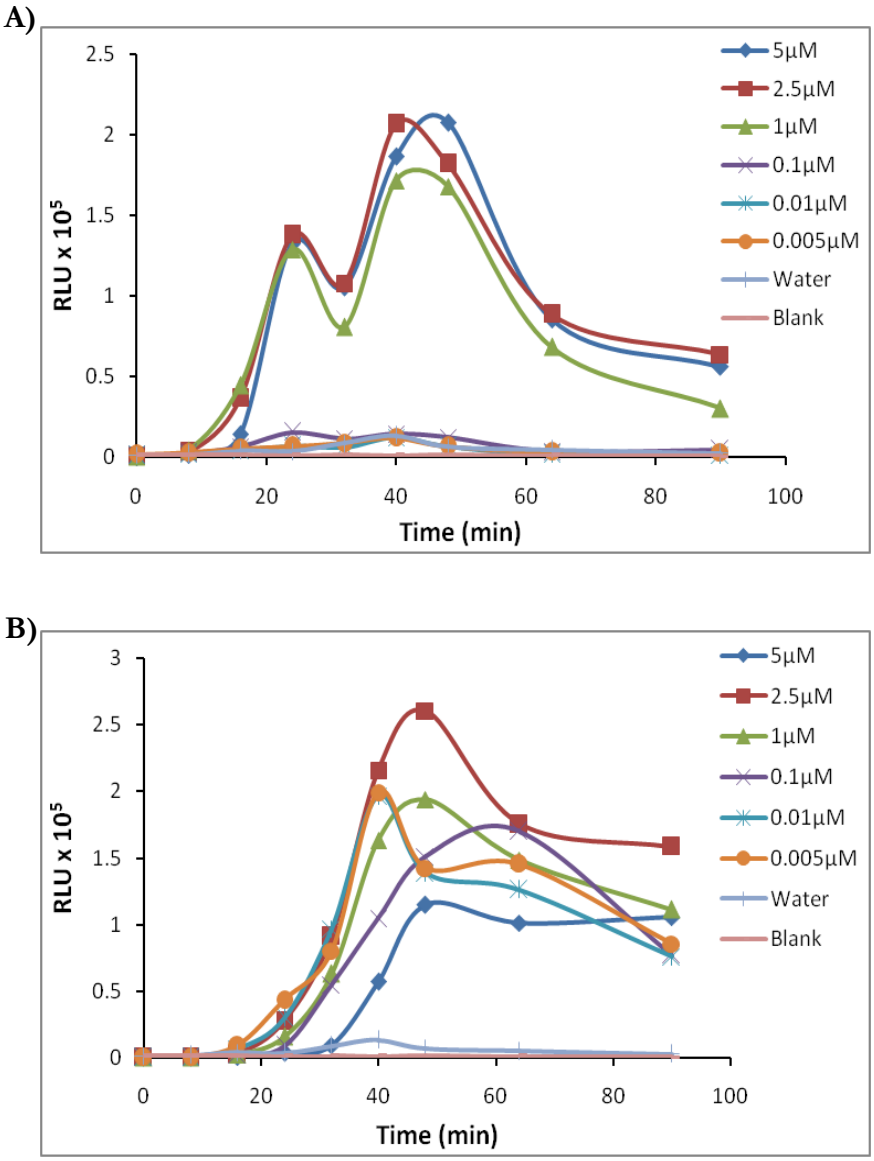

Fig. 6.8: Priming in rice cells with varying doses of purified COS. Purified DP4 **(A)** and DP12 **(B)** of different doses ranging from 0.005 µM to 5 µM were used for priming in suspension cultured rice cells. Sterilized MQ water was used as the control where as blank represents the basal level H_2O_2 mediated luminescence produced from untreated cells.

burst at 1, 2.5 and 5 µM, and the response was nearly similar at 2.5 and 5 µM. DP4 at 0.005, 0.01 and 0.1 µM didn't show oxidative burst response indicating dose-dependent priming in rice (Fig. 6.8A). DP12 COS induced strong priming activity at all the tested doses, and the maximum oxidative burst was observed at 2.5 µM. Although DP12 at 5 µM induced oxidative burst, the effect was quite less than the other tested doses. The priming-mediated oxidative burst was faster and started from 8 min onwards for DP4, whereas DP12 induced oxidative burst nearly at 16 min with stronger response in comparison to DP4 (Fig. 6.8).

6.3. Discussion

Plant diseases are an important constraint on worldwide crop production, accounting for losses of 10–30% of the global harvest each year (Strange & Scott, 2005). As a consequence, crop diseases represent a significant threat to ensure global food security. So, there is a pressing need for efficient, reliable and affordable disease control measures in order to deliver as much of the current productivity of crops as possible. Equally important from the modern perspective is the need to ensure that new disease control measures maintain crop yield and quality, without harming our fragile and long-suffering environment. In this context, exploitation of induced resistance, by application of novel bioactive elicitors, is an attractive alternative for crop protection.

COS released during plant-fungal interactions, induce plant defences upon recognition. Detailed analyses of structure/function relationships of bioactive chitosans as well as recent progress towards understanding the mechanism of COS sensing in plants through the identification and characterization of their cognate receptors have generated fresh impetus for approaches that would induce innate immunity in plants (Das et al., 2015). In the absence of an efficient process for the large-scale manufacturing of high DP COS, topical applications of COS for plant protection have not been realized currently. Enzyme-based technologies may provide an opportunity to produce COS with specific DP and DA and, thus, desired bio-activity.

In the present study, the ability of *Pe*Csn (an endo-acting non-processive

enzyme) for generating longer chain COS with plant strengthening activity was investigated. A great diversity of chitin and chitosan degrading enzymes exist, including endo- and exo-acting chitinases, endo-chitosanases, and glycosidases, such as GlcNase and GlcNAcase (El Gueddari et al., 2007). An important issue is processivity, which drastically decreases the enzyme efficiency for soluble substrates (Eijsink et al., 2008). Further, chitobiose is the major product of processive chitinases acting on chitin, and low DP COS are typically produced from chitosans. MALDI-ToF analysis of *Pe*Csn-generated hydrolysate and subsequent separation by HP-SEC using Superdex™ column revealed the generation of COS up to DP15 or more. Thus, our results suggested that the use of a non-processive endo-enzyme has an advantage for generation of higher DP COS suitable for plant protection.

The crude chitosan hydrolysate obtained by *Pe*Csn was tested for both priming and elicitor activities in suspension-cultured cells of tobacco (Fig. 6.5). The release of H_2O_2, a sensitive indicator of plant defence induction, was measured during an oxidative burst after treatment of the cells with the hydrolysates either as priming agent or as elicitor. When applied as an elicitor, the crude hydrolysate of the chitosan DA35% triggered a considerable oxidative burst (Fig. 6.5A) and no detectable priming response in tobacco cell lines (Fig. 6.5B). These results indicated that the COS with reasonably higher DA were good at eliciting oxidative burst in tobacco. The DA of COS was shown to affect the elicitor activity. For instance, spray or seed treatment with COS of higher DA proved better to protect tobacco against *Phytophthora parasitica* by systemic induction of plant resistance (Falcón et al., 2008).

Since the ability of well-defined COS to sensitise plant cells might be highly relevant for the development of reliable plant protection products, the purified COS obtained after HP-SEC were characterised by UHPLC-ELSD-ESI-MS analyses and tested for elicitor and priming activity in both tobacco and rice cell suspension models. When applied as elicitors, COS with different DP triggered a considerable oxidative burst in tobacco cells (Fig. 6.6A) and no oxidative response in rice cell lines (Fig. 6.7A). In contrary, when rice cells were primed with the same COS, the oxidative burst was

considerably enhanced (Fig. 6.7B) and no detectable priming effect in tobacco cells (Fig. 6.6B). It might be due to the difference in plant defence response between monocotyledons and dicotyledons. For example, it has been reported that tobacco and parsley cells are elicited by a bacterial exopolysaccharide, whereas rice and wheat cells are primed by the same compound (Ortmann & Moerschbacher, 2006). Taken together, it points out the difference of cellular recognition mechanisms between monocot and dicot plants.

Both the crude hydrolysate and COS obtained from chitosanase had elicitor activity in tobacco and MS analysis of the oligomers obtained from *Pe*Csn showed longer chain COS with higher DA (Table 6.1), in contrast to the lower DA oligomers generated previously using chitinases (Madhuprakash et al., 2015). The elicitor activity could be explained by the fact that the higher acetylated COS may be mimicked easily as a kind of fungal attack by plant. The cells immediately respond to this attack by a hypersensitive response that causes high costs of energy. Many fungi convert chitin to chitosan to hide themselves from the plant defence (El Gueddari et al., 2002). Hence, COS with a low DA are not perceived by the plant as a real threat. In fact, previous studies have demonstrated that fully deacetylated COS were elicitor-inactive in different plants whereas fully and partially COS showed elicitation (Vander et al., 1998; dos Santos et al., 2008). However, experiments on *Arabidopsis thaliana* cell suspension cultures, fully deacetylated oligomers maintain their elicitor activity and progressive reacetylation impaired their ability to enhance H_2O_2 accumulation (Cabrera et al., 2006).Receptors for the recognition of chitin oligomers have been already described (Miya et al., 2007; Shimizu et. al., 2010). It might be possible that COS with higher DA can also bind to these receptors and the affinity of COS receptors also may vary depending on plant species. However, it still remains unclear how COS with low DA are recognized.

In general, the biological activity of COS increases with an increase in DP and the highest activity was reported for hexamers to nonamers (DP=6–9) and little or no activity for small oligomers (DP<5) in suspension-cultured Arabidopsis cells (Cabrera

et al., 2006). Interestingly, purified DP4 showed both elicitor and priming activity in tobacco and rice suspension cells, respectively. This observation was further confirmed by the dose-dependent priming study performed by DP4, which was comparable to DP12 priming activity in rice suspension cells. UHPLC-ELSD-ESI-MS analyses revealed that the DP4 fraction composed of oligomer species D4 and D3A1. However, pure D4 didn't show priming in rice (results from Prof. Moerschbacher's lab, unpublished) and, therefore, the biological active molecule in DP4 fraction was D3A1. In future, it would be interesting to uncover and link the PA of D3A1 towards its priming activity. To put in a nutshell, our study projects the necessity to know the PA of COS, in addition to its DP and DA, giving rise to the third generation COS of a particular biological function.

Chapter VII

Summary and conclusions

7. Summary and conclusions

Chitin, an unbranched homopolymer of β-(1→4) linked *N*-acetyl-D-glucosamine is the second most abundant and renewable polysaccharide (after cellulose) on Earth. Irrespective of its abundance, the major difficulties in using chitin, chitosan and COS for large scale applications has been the variations in their biological activity, mostly due to poorly characterized molecules with the differences in their DP, DA and PA. Therefore, it is highly desirable to generate COS molecules with defined DP, DA, and if possible, also the defined PA using enzymatic approaches. Furthermore, higher DP COS are suitable for plant protection and other biological applications, which can be produced by a nonprocessive endo-enzyme of known specificity or an enzyme having transglycosylation (TG) ability. The availability of COS with defined DP, DA, and PA would also facilitate understanding molecular structure/function relationships and cellular modes of action of COS towards plant and animal cells. Therefore, the aim of the present work was to search for efficient chitinolytic bacteria with novel enzymes for generation of bioactive COS. We identified *Paenibacillus elgii* as an efficient chitin-degrading Gram-positive bacterium, and characterized its chitin/chitosan degrading enzymes with emphasis to understand their mode of action and substrate specificity.

7.1 Search for efficient chitinolytic bacteria with potential PGP activity

To search for efficient chitinolytic bacteria, we assessed the chitinolytic bacterial diversity of soils from two industries having 10 years of chitin production history. A total of 27 chitinolytic isolates were isolated and identified as *Bacillus*, *Paenibacillus*, *Stenotrophomonas* and *Pseudomonas* using morphological, biochemical and 16S rDNA analysis. Molecular phylogenetic analysis revealed that *Gammaproteobacteria* and *Bacilli* were found to be the predominant classes in these chitin-enriched soils. Among the isolated chitinolytic bacteria, the isolate SMA-1-SDCH02 was an efficient chitin degrader and was identified as *Paenibacillus elgii*. Selected isolates were also screened for their plant growth promoting traits such as antifungal and mineral phosphate solubilization abilities in addition to their chitinolytic activity. The isolate *P. elgii* SMA-

1-SDCH02 enhanced the growth of groundnut in terms of shoot height, root length, total chlorophyll, and fresh and dry weight when applied alone or in combination with chitosan. The plant growth promoting activity of *P. elgii* was also seen in tobacco in a specially designed gnotobiotic setup indicating its capability to promote the growth of at least groundnut and tobacco.

Although *P. elgii* SMA-1-SDCH02 was not isolated from plant parts, it had tremendous potential in plant growth promotion and antifungal activities similar to other reported PGPR strains. The efficiency of *P. elgii* in this study demonstrated that the unconventional sources could be a source for potential PGP bacteria for the development of bioformulations to increase crop yields and reduce disease.

7.2 Identification of a TG enzyme and mutagenesis to improve TG in *Pe*Chi1

P. elgii SMA-1-SDCH02 possessed five different chitinases belonging to two GH families i.e. GH18 and 19 along with one chitosanase (GH8) and a CBP (AA10). Multiple chitinases in combination with diverse domain arrangements indicated that the chitinolytic machinery of *P. elgii* is complex with the ability to degrade chitin efficiently. We cloned, expressed and characterized four GH18 chitinases (*Pe*Chi1, *Pe*Chi3, *Pe*Chi4, *Pe*Chi5) by determining their mode of action, and screened these chitinases for TG ability for longer chain COS synthesis.

All the four *Pe* chitinases were optimally active in mildly acidic to neutral pH (5.0-7.0). Chitinases of *P. elgii* displayed different temperature optima –40°C for *Pe*Chi1, 50°C for *Pe*Chi5, and 60°C for *Pe*Chi3 and *Pe*Chi4. Overall, we observed a great difference in kinetic parameters among the four chitinases. *Pe*Chi4 displayed the highest (412.887) overall catalytic efficiency (k_{cat}/K_m) when compared to *Pe*Chi1 (0.109), *Pe*Chi3 (15.003) and *Pe*Chi5 (0.045). The difference in the kinetic parameters among these chitinases could be due to difference in the sequence of catalytic domains in combination with different auxiliary domains. It is conceivable that the primary role of the auxiliary domains (CBMs, PKD and FN3) is to potentiate catalytic activity by disrupting the substrate, without even promoting the enzyme-substrate binding. All the four chitinases of *P. elgii* showed a diverse mode of action on chitin substrates.

Hydrolysis of colloidal chitin and chitin oligomers indicated that *Pe*Chi1 and *Pe*Chi5 are endo-acting chitinases, whereas *Pe*Chi3 and *Pe*Chi4 are exo-acting chitinases.

Among the four chitinases, *Pe*Chi1 showed a weak TG activity with a potential to synthesise DP7 COS from DP5 substrate. The inherent feeble TG activity by *Pe*Chi1 remained only up to 10 min, enticing the scope to improve TG by the mutational approach. We employed a mutation-based approach to alter the substrate interaction in the catalytic cleft of *Pe*Chi1 for improving TG. Out of many single and double mutants targeted in the catalytic triad, catalytic groove and solvent accessible region of *Pe*Chi1, only two mutants (Y105W and F62W/Y105W) showed increased TG activity. The mutant Y105W resulted in the formation of nearly 2 fold DP7 as a TG product, when DP5 was used as the substrate. The mutant Y105W was also unique in showing higher TG activity irrespective of increased hydrolysis in comparison to the wild type, suggesting the faster deglycosylation step in *Pe*Chi1-Y105W due to the higher rate of formation of TG products. The double mutant, F62W/Y105W displayed TG similar to the Y105W single mutant but increased the duration of formation of TG products. Thus, the introduction of bulkier aromatic amino acid at -2 and +1 subsite in F62W/Y105W resulted in increased TG both in quantity and duration of accumulation of TG products.

7.3 Degradation of chitosan by *Pe*Csn and role of its auxiliary CBM32 domain in chitosan binding

Chitosanases often have a single catalytic domain without any auxiliary domains, unlike chitinases and cellulases which are frequently associated with CBMs. The chitosanase of *P. elgii* (*Pe*Csn) is a multi-domain protein with an N-terminal GH8 catalytic domain and a C-terminal CBM32 (*Pe*CBM32) linked by an FN3 domain. Because of the multi-domain structure, we have investigated the subsite specificity of *Pe*Csn by using well-defined chitosan polymers and oligomers. The role of *Pe*CBM32 was also investigated by making truncated mutants (GH8 and GH8FN3) of *Pe*Csn. The specificities and affinities of *Pe*CBM32 towards chitosan polymers and oligomers were also studied by biophysical methods.

*Pe*Csn is a 69 kDa nonprocessive endo-acting enzyme and requires a minimum chain length of 4 (tetramer) for its activity at optimum pH 6 and 60°C. Subsite mapping by using defined PA chitosan tetramers revealed that *Pe*Csn accepts only GlcN (D unit) at both positions -1 and -2 subsites. *Pe*Csn can productively bind (though not preferred) acetylated unit at +2 subsite but not at -2. *Pe*Csn had very low hydrolytic activity on D-D-D-A tetramer cleaving into D-D and D-A, indicating that A unit could bind productively in +2 subsite in addition to D units. Due to lack of D-D-A-D tetramer, we couldn't get information in +1 subsite. Therefore, using MS, we sequenced and quantified the hydrolytic products generated from chitosan polymer to gain insight about the reducing end of oligomers. At the initial phase of degradation (2 min), an absolute preference for D units was observed in +1 subsite. Quantification of hydrolytic products generated 720 min showed near to 60% of COS had GlcNAc (A unit) in their reducing end, indicating productive binding of both D and A units in the +1 subsite at a later phase of degradation. Our data unequivocally revealed that *Pe*Csn is a type III chitosanase which can cleave GlcN-GlcNAc linkage in addition to GlcN-GlcN linkage of chitosan, though it prefers GlcN-GlcN linkage at initial degradation phase.

We also investigated the role and mechanism of specific binding of *Pe*CBM32, an auxiliary domain present in *Pe*Csn, to chitosan. Both activity and mode of action of *Pe*Csn towards soluble chitosan polymers were not different with/without the *Pe*CBM32. The decreased activity of *Pe*Csn without *Pe*CBM32 towards insoluble chitosan suggested the possible involvement of a penetration mechanism in the degradation of amorphous chitosan. *Pe*CBM32 specifically bound to both chitosan polymers and oligomers, and showed very weak binding to chitin and cellulose. In ITC, the binding stoichiometry of 2 and 1 for chitosan monomer (GlcN) and dimer (GlcN-GlcN), respectively, was indicative of two primary binding subsites in *Pe*CBM32. Molecular docking and site-directed mutagenesis (SDM) also showed the participation of an extended part of longer oligomers, beyond the primary binding subsites, in the interaction with the protein. A 3D-model-guided SDM and the use of chemically

synthesized defined dimers varying in the pattern of acetylation suggested that the amino groups of chitosan, and the polar residues E16 and E38 of *Pe*CBM32 play a crucial role for the observed selective binding. The specificity of CBM32 was further elucidated by generating a fusion protein composed of *Pe*CBM32 and eGFP for staining infection structures of *Puccinia graminis* f. sp. *tritici*.The fusion protein*Pe*CBM32-GFP specifically bound to the chitosan exposing endophytic infection structures. Our results describe the identification and characterization of a chitosan-specific CBM32 useful for *in situ* staining of chitosans in the fungal cell wall during the plant-fungus interaction.

7.4 Plant strengthening activities of chitosan oligosaccharides generated by *Pe*Csn

The ability of an endo-acting non-processive enzyme like *Pe*Csn to generate long chain COS was studied. The COS, thus generated, could be tested for plant strengthening activity. MALDI-ToF analysis of *Pe*Csn-generated hydrolysate and subsequent separation by HP-SEC using Superdex™ column revealed the generation of COS up to DP15 or more. The purified COS (based on their DP) obtained after HP-SEC were characterized by UHPLC-ELSD-ESI-MS and tested for elicitor and priming activity on suspension cultures of tobacco and rice cells. When applied as elicitors, COS with different DP triggered a considerable oxidative burst in tobacco cells and no oxidative response in rice cell lines. In contrast, when rice cells were primed with the same COS, the oxidative burst was considerably enhanced and no detectable priming effect in tobacco cells, suggesting the difference in plant defence response between monocots and dicots. It also indicates the apparent difference of cellular recognition mechanisms between monocot and dicot plants. Interestingly, a shorter COS (with DP4) had both elicitor and priming activity in tobacco and rice suspension cells, respectively. UHPLC-ELSD-ESI-MS analyses revealed that the DP4 fraction composed of oligomer species D4 and D3A1. In future, it would be interesting to uncover and link the PA of D3A1 towards its priming activity. In a nutshell, this work highlighted the necessity to know

the PA of COS, in addition to its DP and DA, giving rise to the third generation COS for specific biological function(s).

7.5 Conclusions

- Soils dumped with chitin wastes were dominated by chitinolytic bacteria belonging to classes *Gammaproteobacteria* and *Bacilli*.
- Chitinolytic bacterial diversity and plant growth promotion studies led to the identification of *Paenibacillus elgii* SMA-1-SDCH02 with the ability to promote plant growth in both groundnut and tobacco.
- The chitinolytic machinery of *P. elgii* was found to be complex with chitinases of diverse domain architecture and mode of action required for efficient chitin degradation.
- Among the four chitinases characterized, *Pe*Chi1 showed TG and the TG activity was further improved by two mutants Y105W and F62W/Y105W useful for longer chain synthesis of COS.
- Subsite specificity study on both oligomers and polymer revealed that *Pe*Csn is a type III chitosanase which can cleave GlcN-GlcNAc linkage in addition to GlcN-GlcN linkage of chitosan.
- The *Pe*CBM32 had two primary binding sites, and the amino groups of chitosan and the polar residues E16 and E38 of *Pe*CBM32 were crucial for interaction owing to the well-ordered substrate binding site topology specific for chitosan.
- *In situ* staining of the cell wall of *Puccinia graminis* f. sp. *tritici* established that CBM32 of *Pe*Csn would be useful for localisation of chitosan in biological tissues.
- Use of an endo non-processive chitosanase (*Pe*Csn) generated longer chain bioactive COS showing the oxidative burst in both rice and tobacco suspension cells.

References

Biochemical characterization of chitinoloytic enzymes and evaluation of

ORIGINALITY REPORT

5%	2%	5%	1%
SIMILARITY INDEX	INTERNET SOURCES	PUBLICATIONS	STUDENT PAPERS

PRIMARY SOURCES

1	Das, Subha Narayan, Jogi Madhuprakash, P. V. S. R. N. Sarma, Pallinti Purushotham, Katta Suma, Kaur Manjeet, Samudrala Rambabu, Nour Eddine El Gueddari, Bruno M. Moerschbacher, and Appa Rao Podile. "Biotechnological approaches for field applications of chitooligosaccharides (COS) to induce innate immunity in plants", Critical Reviews in Biotechnology, 2015. Publication	3%
2	www.mdpi.com Internet Source	1%
3	davapc1.bioch.dundee.ac.uk Internet Source	<1%
4	Hiroaki Tsuji. "Kinetic and crystallographic analyses of the catalytic domain of chitinase from Pyrococcus furiosus- the role of conserved residues in the active site : Archaeal chitinase complexed with substrate", FEBS Journal, 05/2010 Publication	<1%

5	Bjornar Synstad. "Mutational and computational analysis of the role of conserved residues in the active site of a family 18 chitinase", European Journal of Biochemistry, 1/2004 Publication	<1%
6	Submitted to Institute of Chemical Technnology, Mumbai Student Paper	<1%
7	Svein Jarle Horn. "Endo/exo mechanism and processivity of family 18 chitinases produced by Serratia marcescens", FEBS Journal, 2/2006 Publication	<1%
8	www.researchgate.net Internet Source	<1%
9	Subha Narayan Das. "Members of Gammaproteobacteria and Bacilli represent the culturable diversity of chitinolytic bacteria in chitin-enriched soils", World Journal of Microbiology and Biotechnology, 03/19/2010 Publication	<1%
10	Purushotham, P., and A. R. Podile. "Synthesis of Higher Chain Chitooligosaccharides by a Hyper Transglycosylating Processive Endo-Chitinase of Serratia proteamaculans 568", Journal of Bacteriology, 2012. Publication	<1%

11	Thermophilic Microbes in Environmental and Industrial Biotechnology, 2013. Publication	<1%
12	www.biochemj.org Internet Source	<1%
13	www.ncbi.nlm.nih.gov Internet Source	<1%
14	Madhuprakash, Jogi, Nour Eddine El Gueddari, Bruno M. Moerschbacher, and Appa Rao Podile. "Catalytic Efficiency of Chitinase-D on Insoluble Chitinous Substrates Was Improved by Fusing Auxiliary Domains", PLoS ONE, 2015. Publication	<1%
15	Perugino, Giuseppe, Pierpaolo Falcicchio, Maria Michela Corsaro, Ikuo Matsui, Michelangelo Parrilli, Mose' Rossi, and Marco Moracci. "Preparation of a glycosynthase from the β-glycosidase of the Archaeon Pyrococcus horikoshii", Biocatalysis and Biotransformation, 2006. Publication	<1%
16	Y. Honda. "Kinetic Studies on the Hydrolysis of N-Acetylated and N-Deacetylated Derivatives of 4-Methylumbelliferyl Chitobioside by the Family 18 Chitinases ChiA and ChiB from Serratia marcescens", Journal of Biochemistry, 02/01/2003 Publication	<1%

17	repositorium.sdum.uminho.pt Internet Source	<1%
18	203.158.6.22:8080 Internet Source	<1%
19	www.riceworld.org Internet Source	<1%
20	Heggset, Ellinor B., Ingunn A. Hoell, Marius Kristoffersen, Vincent G. H. Eijsink, and Kjell M. Vårum. "Degradation of Chitosans with Chitinase G from Streptomyces coelicolor A3(2): Production of Chito-oligosaccharides and Insight into Subsite Specificities", Biomacromolecules, 2009. Publication	<1%
21	Aam, Berit B., Ellinor B. Heggset, Anne Line Norberg, Morten SÃ¸rlie, Kjell M. VÃ¥rum, and Vincent G. H. Eijsink. "Production of Chitooligosaccharides and Their Potential Applications in Medicine", Marine Drugs, 2010. Publication	<1%
22	Arakane, Yasuyuki, Toki Taira, Takayuki Ohnuma, and Tamo Fukamizo. "Chitin-Related Enzymes in Agro-Biosciences", Current Drug Targets, 2012. Publication	<1%
23	Ingunn A. Hoell. "Crystal structure and enzymatic properties of a bacterial family 19	<1%

chitinase reveal differences from plant enzymes", FEBS Journal, 11/2006
Publication

---

24 Horn, S. J., M. Sørlie, G. Vaaje-Kolstad, A. L. Norberg, B. Synstad, K. M. Vårum, and V. G. H. Eijsink. "Comparative studies of chitinases A, B and C from Serratia marcescens", Biocatalysis and Biotransformation, 2006.
Publication

<1%

---

25 Submitted to University of Hyderabad, Hyderabad
Student Paper

<1%

---

26 Shinya, S., A. Urasaki, T. Ohnuma, T. Taira, A. Suzuki, M. Ogata, T. Usui, O. Lampela, A. H. Juffer, and T. Fukamizo. "Interaction of di-N-acetylchitobiosyl moranoline with a family GH19 chitinase from moss, Bryum coronatum", Glycobiology, 2014.
Publication

<1%

---

27 M. Kojima. "Family 19 Chitinase from Aeromonas sp. No.10S-24: Role of Chitin-Binding Domain in the Enzymatic Activity", Journal of Biochemistry, 02/01/2005
Publication

<1%

---

28 Ohnuma, Takayuki, and Tamo Fukamizo. "Chitin/Chitosan Oligosaccharides : Effective Substrates for Functional Analysis of Chitinases/Chitosanases", Chitin Chitosan Oligosaccharides and Their Derivatives

<1%

Biological Activities and Applications, 2010.
Publication

29 Sikorski, Pawel, Audun Sørbotten, Svein J. Horn, Vincent G. H. Eijsink, and Kjell M. Vårum. "*Serratia marcescens* Chitinases with Tunnel-Shaped Substrate-Binding Grooves Show Endo Activity and Different Degrees of Processivity during Enzymatic Hydrolysis of Chitosan†", Biochemistry, 2006. <1%
Publication

30 Microorganisms in Environmental Management, 2012. <1%
Publication

EXCLUDE QUOTES ON
EXCLUDE BIBLIOGRAPHY ON
EXCLUDE MATCHES < 5 WORDS